



Universidad de Concepción
Dirección de Postgrado
Facultad de Ciencias Naturales y Oceanográficas
Programa de Doctorado en Oceanografía

**CARACTERIZACIÓN DE LA MATERIA ORGÁNICA
PARTICULADA DE LA FOSA DE ATACAMA
MEDIANTE LÍPIDOS POLARES INTACTOS E
ISÓTOPOS ESTABLES**

**(CHARACTERIZATION OF THE PARTICULATE ORGANIC
MATTER FROM THE ATACAMA TRENCH THROUGH
INTACT POLAR LIPIDS AND STABLE ISOTOPES)**

Tesis para optar al grado de Doctor en Oceanografía

EDGART ELVIS FLORES RAFAEL
CONCEPCIÓN-CHILE
Marzo de 2023

Profesor Guía: Dr. Osvaldo Ulloa Quijada
Dpto. Oceanografía, Facultad de Ciencias Naturales y Oceanográficas
Universidad de Concepción

© 2022 Edgart Elvis Flores Rafael

Se autoriza la reproducción total o parcial, con fines académicos, por cualquier medio o procedimiento, incluyendo la cita bibliográfica del documento.

Universidad de Concepción
Dirección de Postgrado

La Tesis de *Doctorado en Oceanografía* titulada “*Caracterización de la materia orgánica particulada de la fosa de Atacama mediante lípidos polares intactos e isotopos estables*”, del Sr. Edgart Elvis Flores Rafael y realizada bajo la Facultad de Ciencias Naturales y Oceanográficas, Universidad de Concepción, ha sido aprobada por la siguiente Comisión de Evaluación:

Dr. Osvaldo Ulloa
Profesor Guía
Universidad de Concepción

Dr. Julio Sepúlveda
Profesor Co-guía
University of Colorado, Boulder

Dr. Marcelo Gutiérrez
Miembro Comité de Tesis
Universidad de Concepción

Dr. Marcos Moreno
Miembro Comité de Tesis
Universidad de Concepción

Dr. Humberto González
Evaluador Externo
Universidad Austral de Chile

Dra. Pamela Hidalgo
Director
Programa de Doctorado en Oceanografía
Universidad de Concepción

*Agradezco a todas y todos quienes me han
acompañado en este proceso.*

Curriculum Vitae

Edgart Elvis Flores Rafael

Nacido el 27 de agosto, 1988, en Chiclayo, Perú

2007-2012: Título profesional de Biólogo, Universidad Nacional Pedro Ruiz Gallo, Perú.

2014-2016: Magister en Ciencias del Mar, Universidad Peruana Cayetano Heredia, Perú.

2017-2023: Doctor en Oceanografía, Universidad de Concepción, Chile.

ÁREAS DE INVESTIGACIÓN

Principal: Oceanografía biológica

Secundaria: Biogeoquímica, Geoquímica orgánica

Otras: Ecología microbiana y Lipidómica.

PUBLICACIONES

Edgart Flores, Sebastian I. Cantarero, Paula Ruiz-Fernández, Nadia Dildar, Matthias Zabel, Osvaldo Ulloa, Julio Sepúlveda, 2022. Bacterial and eukaryotic intact polar lipids point to in situ production as a key source of labile organic matter in hadal surface sediment of the Atacama Trench. *Biogeosciences*, 19, 1395–1420. <https://doi.org/10.5194/bg-19-1395-2022>.

Jonathan Raberg, **Edgart Flores**, Sarah Crump, Greg de Wet, Nadia Dildar, Gifford Miller, Áslaug Geirsdóttir, Julio Sepúlveda, 2022. Intact Polar brGDGTs in Arctic Lake Catchments: Implications for Lipid Sources and Paleoclimate Applications. *Journal of Geophysical Research: Biogeosciences*, 2022, p. e2022JG006969. <https://doi.org/10.1029/2022JG006969>.

Sebastian I. Cantarero, Paulina Aguayo, **Edgart Flores**, Cristian A. Vargas, John E. Tamanaha Jr., Bentley C. Scholz, Lennart T. Bach, Carolin R. Löscher, Ulf Riebesell, Balaji Rajagopalan, Nadia Dildar, Julio Sepúlveda, 2023. Evidence for intact polar lipid remodeling among phytoplankton communities in response to multi-environmental drivers in mesocosm experiments. En preparación para *Biogeosciences*.

Edgart Flores, Igor Fernández-Urruzola, Sebastian I. Cantarero, Matías Pizarro-Koch, Matthias Zabel, Julio Sepúlveda, Osvaldo Ulloa, 2023. Particulate organic matter in the Atacama Trench: Tracing sources and possible transport mechanisms to the hadal seafloor. En revisión en *Journal of Geophysical Research: Biogeosciences*.

Edgart Flores, Ursula Mendoza, Cameron Callbeck, Rut Díaz, Arturo Aguirre-Velarde, Michael E. Böttcher, Lander Merma-Mora, Manuel Moreira, Maritza S. Saldarriaga, Emmanoel V. Silva-Filho, Ana L. Albuquerque, Matias Pizarro-Koch, and Michelle Graco, 2023. Attenuation of wind intensities exacerbate anoxic conditions leading to sulfur plume development off the coast of Peru. En revisión en *Plos One*.

BECAS Y PREMIOS

- Beca del Consejo Nacional de Ciencia y Tecnología (CONCYTEC) para estudios de maestría en Ciencias del Mar, 2014 – 2016.
- Beca de movilidad estudiantil, proyecto Paleotracas (IRD, Francia), 2015.
- Beca de Doctorado del Proyecto del Fondo Nacional de Desarrollo Científico y Tecnológico (FONDECYT) N° 1191360: Dr. Osvaldo Ulloa, 2019-2021.
- Beca de Doctorado Instituto Milenio de Oceanografía (IMO), IC 120019, 2018-2022.
- Beca de movilidad estudiantil, proyecto UCO 1865 postgrado de la Universidad de Concepción para pasantías Doctorales, 2020 y 2022.

EXPERIENCIA DOCENTE

- 2011: Ayudante de Cátedra en la asignatura de pregrado “Oceanografía” a cargo de la Dr. Wilmer Carbajal, Universidad Nacional Pedro Ruiz Gallo.
- 2018: Ayudante de Cátedra en la asignatura de pregrado “Técnicas de comunicación científica” a cargo de la Dra. Pamela Hidalgo y Marcelo Gutiérrez, Universidad de Concepción.

- 2021: Instructor en el curso “Nuevos métodos y herramientas para el análisis integral de datos biológicos”, organizado por el Instituto Milenio de Oceanografía (Chile) e INVEMAR (Colombia) en el marco del proyecto BIOMACC.

CRUCEROS OCEANOGRÁFICOS

- 2014: Crucero oceanográfico CRIO-IMARPE, R/V Flores Portugal, Lima-Pisco, Perú. Colaboración con la Dra. Michelle Graco.
- 2015: Crucero Oceanográfico CRIO-IMARPE, R/V Olaya, Lima-Pisco, Perú. Colaboración con la Dra. Michelle Graco.
- 2018: Crucero Oceanográfico Internacional "HADES" SO261 R/V SONNE, San Antonio, Chile- Guayaquil, Ecuador. Colaboración con el Dr. Osvaldo Ulloa.

ESTADÍAS DE INVESTIGACIÓN O ENTRENAMIENTO

- Pasantía en el laboratorio de Oceanografía Observacional y Paleoceanografía (LOOP) de la Universidad Federal Fluminense de Brasil, 2015. Investigador patrocinante: Dra. Rut Diaz. Actividad principal: técnicas de destilación secuencial para el análisis de azufre inorgánico en sedimentos marinos y análisis de sulfuro de hidrógeno en agua intersticial.
- Entrenamiento en el análisis de series de tiempo y estadística multivariada, impartido por el laboratorio de Ecología Marina Cuantitativa del Ecosistema de Afloramiento Peruano “EMACEP” en colaboración con el JEAI (Jeunes équipes associées à l’IRD), 2015.
- Entrenamiento en el curso: Ecology and Diversity of marine Microorganisms (ECODIM-IX), Universidad de Concepción, Chile, 2016.
- Entrenamiento analítico en el laboratorio de Geología Marina del Instituto del Mar del Perú, durante el proyecto KOSMOS-2016 en colaboración con GEOMAR. Investigador patrocinante: Dra. Maricarmen Igarza. Actividad principal: Extracción y análisis de DOC y DOM.
- Course: Extending linear model with R, Universidad de Concepcion, Chile, 2017.
- Assistant to the 11th International Conference on Applications of Stable Isotope Techniques to Ecological (IsoEcol). Andrés Bello University, Chile, 2018.

- Pasantía Doctoral en University of Colorado, Boulder, USA, desde octubre de 2019 a febrero de 2021. Investigador patrocinante: Dr. Julio Sepúlveda, del Organic Geochemistry Group (“Sepúlveda Lab”) del Geological Sciences department. Actividad principal: extracción y análisis de lípidos intactos polares en sedimentos marinos de la Fosa de Atacama.
- Course: Advanced Isotopic Geochemistry, Universidad de Concepcion, Chile, 2020.
- Course: R Fundamentals and Best Practices for Mass Spectrometry Data Analysis, USA, 2020 (online).
- Pasantía Doctoral en University of Colorado, Boulder, USA, desde junio a agosto de 2022. Investigador patrocinante: Dr. Julio Sepúlveda, del Organic Geochemistry Group (“Sepúlveda Lab”) del Geological Sciences department. Actividad principal: análisis de isótopos estables en sedimentos hadales de la Fosa de Atacama.

PRESENTACIONES EN CONGRESOS

Presentaciones de resultados de la presente tesis:

- Febrero, 2020: Presentación oral en el Grupo de Geoquímica Orgánica de la University of Colorado, Boulder.
- Noviembre, 2020: Presentación oral en el VIII Encuentro de estudiantes de postgrado de la Universidad del Bío-Bío.
- Diciembre, 2021: Presentación en póster en el AGU Fall Meeting, New Orleans, LA and online everywhere, USA.
- Agosto, 2022: Participación en la Gordon Research Seminar (GRS) y presentación en póster en la Gordon Research Conference (GRC) de geoquímica orgánica en New Hampshire, USA.
- Septiembre, 2022: Presentación oral en la sesión #17 Shedding light in the darkness: New insights into the deep ocean ecosystems of the major EBUS. Session proposed and presented by the Millennium Institute of Oceanography at the Conference on Eastern Boundary Upwelling Systems (EBUS): Past, Present, and Future and the Second International Conference on the Humboldt Current System.

Índice de Contenidos

RESUMEN.....	v
ABSTRACT.....	viii
1. INTRODUCCIÓN	1
1.1 Tectónica de placas y fosas oceánicas.....	1
1.2 La fosa de Atacama.....	2
1.3 Rol de la materia orgánica en la zona hadal.....	4
1.4 Biomarcadores lipídicos y análisis de isótopos estables en la materia orgánica particulada.	7
2. HIPÓTESIS Y OBJETIVOS ESPECÍFICOS.....	11
3. MATERIAL Y MÉTODOS.....	13
3.1 Área de estudio.....	13
3.2 Diseño de muestreo y adquisición de datos	13
3.3 Objetivo específico 1.....	16
3.4 Objetivo específico 2.....	18
3.5 Objetivo específico 3.....	20
4. RESULTADOS.....	21
Resumen.....	21
5. DISCUSIÓN	115
5.1 Lípidos intactos polares autóctonos y alóctonos en la Fosa de Atacama.....	115
5.2 IPLs característicos de los sedimentos hadales y batiales.....	117
5.3 ¿Las IPL revelan una adaptación homeoviscosa al medio marino profundo?	118
5.4 Procedencia de la materia orgánica en los sedimentos superficiales de la Fosa de Atacama.....	119
5.5 ¿Cuál es la contribución relativa de las fuentes alóctonas a los sedimentos de la Fosa de Atacama?	122
5.6 Implicaciones.....	125
6. CONCLUSIONES	126
7. REFERENCIAS.....	127

Índice de Figuras

- Figura 1. Esquema presentado por Belyaev (1989) con las principales fosas alrededor del planeta: HD1: Aleutian-Japan, HD2: Filipinas, HD3: Marianas, HD4: Bougainville-New Hebrides, HD5: Tonga–Kermadec, HD6: Atacama, HD7: Java, HD8: Puerto Rico, HD9: Romanche y HD10: Antillas del sur (Tomado de Watling et al., 2013). 2
- Figura 2. Representación de las principales fuentes de aporte de material orgánico hacia el ecosistema hadal (Tomado de Yunping Xu et al., 2018). 7
- Figura 3. Clases más abundante de IPL en el océano. Fosfolípidos: PG-(Fosfatidilglicerol), PE-(Fosfatidiletanolamina), PC-(Fosfatidilcolina). Glicolípidos: MG (Monoglicósil), DG (Diglicósil), SQ (Sulfo-quinovosil). Lípidos de Betaína: DGTS-(Diacilglicerilhidroximetiltrimetilhomoserina), DGTA-(Diacilglicerilhidroximetiltrimetil- β -alanina), DGCC-(Diacilglicerilcarboxihidroximetilcolina). Los subíndices numerados indican las referencias de las fuentes biológicas de las distintas clases de lípidos: (1) Wada y Murata, 2007), (2) Barridge y Shively, 1968; Imhoff y Bias-Imhoff, 1995, (3) Goldfine y Hagen, 1968) (4) Makula, 1978; Fang et al., 2000), (5) Rütters et al., 2001; Sturt et al., 2004, (6) Van Mooy et al., 2000 Van Mooy et al., 2006, (7) Popendorf et al., 2011, (8) Oguz y Merico, 2006, (9) Benning et al., 1995, (10) Schubotz et al., 2018. Tomado de Cantarero et al., 2020. 11
- Figura 4. Mapa tridimensional de la Fosa de Atacama que muestra las ubicaciones de muestreo de este estudio. Los cuadrados negros indican las estaciones de muestreo de sedimentos hadales, los círculos negros indican las estaciones de muestreo de sedimentos batiales de Matys et al. (2017), y los triángulos negros indican las estaciones de muestreo de la columna de agua de Cantarero et al. (2020). 14
- Figura 5. The potential temperature–salinity (θ –s) diagrams from CTD data coupled to an AUV (autonomous underwater vehicle). The color scale is related to depth (m) and oxygen concentration (μ M). 49
- Figura 6. IPL chemical structures from the LIPID MAPS database (Sud et al., 2007). R1 and R2 represent acyl groups, whereas the charges are those expected at seawater pH. 50
- Figura 7. Relative abundances of IPLs distinctive (red color; Cantarero et al. 2020) and non-distinctive (turquoise; total IPLs minus IPLs from Chlorophyll maximum) of the Chlorophyll maximum for all samples. 51
- Figura 8. Total concentration of IPL by class, in (a) bathyal and (b) hadal sediment samples. 52
- Figura 9. TOC-normalized IPL concentration (μ g IPL/g TOC) in hadal sediments. 53
- Figura 10. Cumulative bar chart of PC phospholipid fractional abundances. The number of carbon atoms and unsaturation in core fatty acids follows the order shown in the legend. The right panel depicts a cluster analysis with AU and BP shown in red and

green, respectively, and p-values shown at branching points. The number of bootstrap replicates is 10000. Clusters with AU \geq 95% confidence are highlighted in red boxes on the left-hand side. 56

Figura 11. Cumulative bar chart of SGDG glycolipid fractional abundances. The number of carbon atoms and unsaturation in core fatty acids follows the order shown in the legend. The right panel depicts a cluster analysis with AU and BP in red and green, respectively, and p-values shown at branching points. The number of bootstrap replicates is 10000. Clusters with AU \geq 95% confidence are highlighted in red boxes on the left-hand side. 60

Figura 12. Cumulative bar chart of DGTA betaine fractional abundances. The number of carbon atoms and unsaturation in core fatty acids follows the order shown in the legend. The right panel depicts a cluster analysis with AU and BP in red and green, respectively, and p-values shown at branching points. The number of bootstrap replicates is 10000. Clusters with AU \geq 95% confidence are highlighted in red boxes on the left-hand side. 62

Figura 13. Cumulative bar chart of DGCC betaine fractional abundances. The number of carbon atoms and unsaturation in core fatty acids follows the order shown in the legend. The right panel depicts a cluster analysis with AU and BP in red and green, respectively, and p-values shown at branching points. The number of bootstrap replicates is 10000. Clusters with AU \geq 95% confidence are highlighted in red boxes on the left-hand side. 63

Figura 14. Water column depth profiles of (A) $\delta^{13}\text{C}_{\text{POC}}$, (B) $\delta^{15}\text{N}_{\text{PON}}$, and (C) C/N ratio over the Atacama Trench. The gray area represents the pelagic hadal zone (>6000 m depth). 80

Figura 15. Biplots of (A) $\delta^{15}\text{N}_{\text{PON}}$ and $\delta^{13}\text{C}_{\text{POC}}$, and (B) C/N ratios and $\delta^{13}\text{C}_{\text{POC}}$. The water column was divided by depth into the epipelagic (200-1000 m), mesopelagic (200-1000 m), bathypelagic (3500-6000 m), and hadopelagic (>6000 m) zones following Jamieson (2015 and references therein). Panels C, D and E describe the 95% family-wise confidence intervals for the differences in the mean values of $\delta^{13}\text{C}_{\text{POC}}$, $\delta^{15}\text{N}_{\text{PON}}$ and C/N, respectively. Red lines indicate the occurrence of statistically significant differences (pairwise comparison by Tukey's test, $p < 0.05$). 81

Figura 16. Biplots showing the relationship between (A) $\delta^{15}\text{N}_{\text{PON}}$ and $\delta^{13}\text{C}_{\text{POC}}$, and (B) C/N ratios and $\delta^{13}\text{C}_{\text{POC}}$ in bathyal and hadal sediments. Plots C, D, and E display the 95% family-wise confidence intervals of the difference in means between $\delta^{13}\text{C}_{\text{POC}}$, $\delta^{15}\text{N}_{\text{PON}}$, and C/N ratios, respectively. The red line indicates means that are significantly different (pairwise comparison by Tukey's test). 82

Figura 17. Boxplot showing the (A) $\delta^{13}\text{C}$, (B) $\delta^{15}\text{N}$, and (C) C/N values of the different depth regions of the water column and the bathyal and hadal sediments. We use the same depth zonation as in figure 3. The same combinations of letters over boxplots do not differ significantly ($p < 0.05$, Tukey's test). 84

Figura 18. (A, C) Spatio-temporal variability of POCsat calculated for mean weekly observations ~90 days prior to the Hades expedition (January-March 2018) in surface (0 m) and subsurface (1000 m) waters, and (B, D) their respective \pm standard deviations. 86

Figura 19. POC fluxes and concentration in the water column overlying the Atacama Trench. (A) Empirical estimates of POC fluxes ($\text{mg C m}^{-2} \text{d}^{-1}$) obtained from (i) the Martin curve using 0.36, 0.78, and 1.33 as attenuation coefficients (blue lines), (ii) an exponential curve (black line), (iii) depth-attenuation rational (red dashed line), and (iv) double exponential curve (black dashed line). Solid circles indicate measured POC fluxes from deep-moored sediment traps (Hebbeln et al., 2002; González et al., 2004), free-drifting sediment traps (Wakeham et al., 1984), and ^{230}Th -normalized isotope-based samples (Pavia et al., 2019). (B) *In situ* POC concentrations measured at stations A1, A2, A4, and A6 during the Hades expedition. The inset highlights the depth region between 5,000 and 8,000 m. 88

Figura 20. Isotopic signatures of organic matter and their mixing in surface hadal sediments. (A) Biplot showing $\delta^{13}\text{C}$ and $\delta^{15}\text{N}$ of POM in the water column and surface hadal sediments ("mixture"). (B) Biplot showing $\delta^{13}\text{C}$ and $\delta^{15}\text{N}$ of POM in the water column and surface hadal sediments ("mixture"), in addition to bathyal sediments as an additional source of POM. (C, D) Relative fractional contribution of POM from the different pelagic zones as well as from bathyal and hadal sediments using the MixSIAR (Stable Isotope Analysis in R) mixing model. 95

Figura 21. Spatio-temporal variability of POCsat over the Atacama Trench region (18°S-30°S) calculated for seasonal mean from 1998 to 2022 in surface (0 m) and subsurface (1000 m) waters, and their respective \pm standard deviations (STD). 112

Figura 22. Spatio-temporal variability of POCsat over the Atacama Trench region (18°S-30°S) calculated for annual mean from 1998 to 2022 in surface (0 m) and subsurface (1000 m) waters, and their respective \pm standard deviations (STD). 113

Figura 23. Biplot showing in panel A, the $\delta^{15}\text{N}_{\text{PON}}$ and $\delta^{13}\text{C}_{\text{POC}}$, and panel B the C/N ratio and $\delta^{13}\text{C}_{\text{POC}}$ to compare our hadal versus non-hadal sediment samples published for the Atacama region (Hebbeln et al., 2000). 114

Figura 24. Biplot showing the C/N ratio and $\delta^{13}\text{C}_{\text{POC}}$ for all data in our study reflect the presence of a particular signature in hadal sediments of the Atacama Trench. 114

Índice de Tablas

Tabla 1. Isótopos estables de la materia orgánica y los grupos principales de IPLs en ambientes marinos.	10
Tabla 2. Estaciones de muestreo de las expediciones HADES, ChiMeBo y LowpHOX-2.	15
Tabla 3. Similarity percentage (SIMPER) analysis showing the average abundance and contribution of IPLs that explained the main differences among the hierarchical clusters in Fig. 8, and that include the water column and sediment samples.....	65
Tabla 4. Sampling stations from the HADES and ChiMeBo cruises, and from published sediment-trap data.....	75
Tabla 5. Parameters calculated for four models used (see Figure 2) that predict the POC fluxes to Atacama Trench. The goodness of fit between the theoretical fluxes and the data collected in situ were added in the text.	111
Tabla 6. Linear correlations between theoretical POC fluxes and sediment trap-derived measurements.	111

RESUMEN

Los sedimentos superficiales de la zona hadal (>6000 m) presentan ~20% más de concentraciones de materia orgánica (MO) en comparación con el fondo marino abisal (3500-6000 m) circundante. Sin embargo, el origen de este material biológico sigue siendo incierto. En este trabajo, evaluamos las fuentes de MO lábil en el fondo marino hadal a través de la composición y distribución de los lípidos polares intactos (IPL) de las membranas celulares microbianas extraídas de los sedimentos superficiales de los puntos más profundos de la Fosa de Atacama y del margen batial adyacente. Además, investigamos las fuentes de MO en los sedimentos superficiales hadales utilizando un modelo de mezcla basado en las señales isotópicas del carbono orgánico y el nitrógeno total, tomando como fuentes de origen potenciales a las distintas zonas de la columna de agua y de los sedimentos batiales. Complementamos nuestros análisis con información satelital de carbono orgánico particulado (POC) superficial (0 m) y subsuperficial (1000 m), y flujos teóricos de POC desde la superficie hasta la zona hadal.

En este estudio, se analizaron nueve sedimentos superficiales hadales (0-1 cm) y subsuperficiales (1-2 y 2-3 cm) en tres sitios entre 7,734 y 8,063 m de profundidad colectados durante el crucero HADES-SO261 (marzo a abril de 2018) a bordo del R.V. Sonne (Wenzhöfer, 2019) y siete sedimentos superficiales batiales (siete sitios; entre 529-1,200 m de profundidad) colectados durante el crucero ChiMeBo-SO211 (2-29 de noviembre de 2010) a bordo del R.V. Sonne (Matys et al., 2017). Además, comparamos nuestros resultados de IPLs en sedimentos con los resultados de IPL de la columna de agua suprayacente (0-700 m) reportados en Cantarero et al. (2020). Esto incluye MO en suspensión fraccionada por tamaño (0,3-2,7 y 2. 7-53 μm) en dos estaciones y desde seis profundidades de agua que son representativas de la zonación biogeoquímica dominante asociada con la zona deficiente de oxígeno (ODZ) de esta región: el máximo de clorofila (~ 10 m), la quimioclina superior (~ 25 m), la quimioclina inferior (~ 45 m), ODZ superior (~ 60 m), el núcleo de ODZ (~ 250 m), y la zona mesopelágica (~ 750 m). Además, las muestras de sedimentos colectadas en ambos cruceros (i.e. HADES-SO261 y ChiMeBo-SO211) también fueron utilizadas para análisis de isótopos estables y comparadas con data disponible de trampas de sedimento profundas de la región de Atacama a 2,300 y 3700 m de profundidad, reportadas previamente en Hebbeln et al. (2000) y González et al. (2004), respectivamente.

En el Capítulo 1 investigamos la diversidad química y la abundancia de IPL microbianas como marcadores de una de las fracciones moleculares más lábiles de la MO en los sedimentos más profundos de la Fosa de Atacama. Más concretamente, evaluamos la posible procedencia de IPLs de origen de producción *in situ* vs. transporte alóctono y la presencia de señales únicas de IPL de la comunidad microbiana, así como la evidencia de adaptaciones moleculares (i.e., cambios en la estructura química de los IPLs) a las condiciones extremas de la región hadal. Los resultados sugieren que los IPLs bacterianos y eucariotas en los sedimentos hadales superficiales de los puntos más profundos de la Fosa de Atacama comparten características con los presentes en sedimentos batiales y difieren de los encontrados en las partículas suspendidas de los 750 m superiores de la columna de agua, incluyendo la ODZ. Esto indica que (a) la mayoría de los IPLs abundantes en la columna de agua superior se degradan casi por completo durante su descenso al fondo marino hadal y (b) los IPLs encontrados en los sedimentos hadales se derivan predominantemente de comunidades microbianas *in situ*. Además, las elevadas proporciones de ácidos grasos insaturados/saturados en los sedimentos hadales son probablemente indicativos de la adaptación homeoviscosa de estos organismos a la alta presión y las bajas temperaturas presentes en este ambiente, lo que les permiten mantener la fluidez de sus membranas celulares.

En el Capítulo 2 realizamos un análisis exhaustivo de los isótopos estables de la MO para rastrear las fuentes de carbono y nitrógeno en la columna de agua y en los sedimentos superficiales batiales y hadales. Además, evaluamos las contribuciones relativas de la POM y la exportación de partículas que conectan la productividad del océano superficial iluminado por el sol con la zona crepuscular y el fondo marino hadal. Utilizando un modelo de mezcla basado en la señal isotópica del carbono orgánico y el nitrógeno total en la POM pelágica y la MO sedimentaria, calculamos que ~75% de la POM presente en los sedimentos superficiales de la Fosa de Atacama podría derivar de los sedimentos batiales. Cuando se excluye el sedimento batial del modelo, calculamos que ~68% de la MO en los sedimentos hadales podría derivar de la región epipelágica (<200 m). En particular, los flujos verticales de POC que mejor se ajustan a los datos existentes de trampas de sedimentos profundos (~2300 y 3700 m) sugieren que ~3,3% del flujo total de POC que llega a los sedimentos superficiales hadales deriva de las aguas superficiales.

Por lo tanto, concluimos que el transporte de sedimento a lo largo del talud continental y las laderas abisales hacia la zona hadal bentónica contribuye con un mayor aporte de carbono orgánico comprado con lo que llega por hundimiento desde la columna de agua. Sin embargo, dado que se espera que los flujos de estas distintas fuentes varíen tanto espacial como temporalmente, y por el hecho de que la geoquímica del sedimento incluye escalas temporales mayores que la columna de agua, no podemos descartar una mayor contribución de las zonas epipelágicas superficiales durante ciertas épocas del año.

ABSTRACT

The surface sediments from the hadal zone (>6000 m water depth) have high concentrations of organic matter (OM) compared to the surrounding abyssal seabed (3500-6000 m). However, the origin of this biological material remains uncertain. In this work, we evaluate the sources of labile organic matter in the hadal seafloor through the composition and distribution of intact polar lipids (IPLs) from microbial cell membranes extracted from surface sediments at the deepest points of the Atacama Trench and adjacent bathyal margin. In addition, we investigated the sources of OM in Atacama Trench sediments using a mixing model based on the isotopic signal of organic carbon and total nitrogen from different zones of the water column and bathyal sediments. We complemented our analyses with satellite particulate organic carbon (POC) in surface (0 m) and subsurface (1000 m), and theoretical models to estimate vertical POC export fluxes from the surface to hadalpelagic depths.

In this study, we investigated the diversity and abundance of bacterial and eukaryotic IPLs in a total of nine hadal surface (0–1 cm) and subsurface (1–2, and 2–3 cm) sediments on three sites between 7,734 and 8,063 m water depth collected during the HADES-SO261 cruise (March to April 2018) aboard the RV Sonne (Wenzhöfer, 2019) and seven bathyal surface sediments (seven sites; 529–1200 m water depth) collected during the ChiMeBo-SO211 cruise (2–29 November 2010) aboard the RV Sonne (Matys et al., 2017). In addition, we compare our IPL results from surface sediment in the hadal and bathyal regions against samples from the overlying water column from the LowpHOX-2 cruise recently reported by Cantarero et al. (2020). This includes size-fractionated suspended OM (0.3–2.7 and 2.7–53 μm) at two stations and from six water depths that are representative of the dominant biogeochemical

zonation associated with the ODZ of this region: chlorophyll maximum (~ 10 m), upper chemocline (~ 25 m), lower chemocline (~ 45 m), upper ODZ (~ 60 m), core ODZ (~ 250 m), and mesopelagic zone (~ 750 m). Additionally, we compare our results with stable isotope data from nonhadal sediments (<6000 m) and deep sediment traps from the Atacama region (2,300 and 3700 m).

In Chapter 1 we investigated the chemical diversity and abundance of microbial IPL as markers of one of the most labile molecular fractions of MO in sediments of the deepest points of the Atacama Trench. More specifically, we evaluate the possible origin of IPLs from *in situ* production versus allochthonous transport and the presence of unique IPL signatures of the *in situ* microbial community, as well as evidence for molecular adaptations (i.e., changes in the chemical structure of the IPLs) to the extreme conditions of the hadal region. The results suggest that bacterial and eukaryotic IPLs in surface hadal sediments of the deepest points of the Atacama Trench share characteristics with those in bathyal sediments and differ from those found in suspended particles from the upper 750 m of the water column, including the ODZ. This indicates that (a) most IPLs abundant in the upper water column are almost entirely degraded during their descent to the hadal seafloor and (b) IPLs found in the hadal sediments are predominantly derived from *in situ* microbial communities. In addition, the high ratios of unsaturated/saturated fatty acids in hadal sediments are likely indicative of the homeoviscous adaptation of these organisms to the high pressure and low temperatures present in this environment, allowing them to maintain the fluidity of their cell membranes.

In Chapter 2 we perform a comprehensive analysis of stable isotope of bulk OM to trace carbon and nitrogen sources over the overlying water column as well as in bathyal-hadal surface sediment. We assess the relative contributions of OM and particle export connecting sunlit ocean surface productivity to the twilight zone and hadal seafloor. Using a mixing model based on the isotopic signals of organic carbon and total nitrogen in pelagic particulate organic matter (POM) and sedimentary OM, we estimate that ~75% of the POM present in surface sediments of the Atacama Trench could be derived from bathyal sediments. When the bathyal sediment is excluded from the model, we calculate that ~68% of sedimentary OM in the hadal sediments could derive from the epipelagic region (<200 m). Notably, the vertical POC fluxes

that best fit with the existing data from deep sediment traps (~2300 and 3700 m) suggest that ~3.3% of the total POC flux that reaches hadal surface sediments derives from surface waters.

Therefore, we conclude that sediment transport along the continental slope and abyssal slopes to the benthic hadal zone contributes to a greater input of organic carbon compared to that which arrives by sinking from the water column. However, since the fluxes of these sources are expected to vary both spatially and temporally and the fact that the bulk geochemistry of sediment includes time scales larger than the water column, we cannot rule out a greater contribution from the surface epipelagic zones at certain times of the year.

1. INTRODUCCIÓN

1.1 Tectónica de placas y fosas oceánicas

La corteza exterior de la Tierra consiste en placas rígidas en movimiento (McKenzie & Parker, 1967; Morgan 1968; Chen, 2010). De acuerdo al tipo de movimiento, éstas han sido clasificadas como placas convergentes, divergentes y transformantes. La expresión morfológica de las placas divergentes son las dorsales oceánicas y están caracterizadas por presentar mayor actividad volcánica, mientras que las placas convergentes colisionan entre sí, posicionándose una debajo de la otra (Lallemand et al., 1990, 1992), proceso denominado “subducción” por Amstutz (1951). La subducción permite que la litosfera oceánica se recicle en el manto y forme un cinturón orogénico del cual emergen las cadenas de montañas (p.ej. Los Andes en Sudamérica o Los Alpes en Europa), siendo su principal característica, la actividad sísmica (Ewing & Heezen, 1956). Los márgenes actuales bajo los que subduce una placa se denomina bordes activos, y su expresión morfológica es una gran depresión denominada trinchera o fosa oceánica.

En el planeta existen un total de 33 fosas oceánicas y 13 valles oceánicos (Jamieson, 2015). Ambos ecosistemas se encuentran bajo los 6,500 m de profundidad (Menzies et al., 1973; Vinogradova 1979; Belyaev 1989; Briones et al., 2009), sin embargo, difieren en su origen. Las fosas se originan en los límites convergentes, mientras los valles oceánicos se encuentran dentro de una planicie abisal. Al interior de las fosas oceánicas se pueden distinguir dos ecosistemas: (1) el hadal-bentónico asociado al piso marino y (2) el hadal-pelágico asociado a la columna de agua que ocupa la fosa (Wolff, 1959). Watling (2013), usando información batimétrica de ETOPO2, caracterizó la distribución geográfica de esos sistemas ultra- profundos (fosas y valles oceánicos), y demostró que el Océano Pacífico es la cuenca que alberga la mayor cantidad de estos ecosistemas (Figura 1). Además, se ha observado que estos sistemas hadales reciben materia orgánica de una gran variedad de regímenes de producción primaria generada en la superficie. Por ejemplo, la Fosa de las Marianas (~11.000 m, la más profunda del planeta) se encuentra bajo una región oligotrófica en el Océano Pacífico noroccidental, mientras las Fosas de Japón e Izu-Bonin (~9,000 m) se ubican en una región mesotrófica. Por otra parte, la Fosa de Atacama ubicada en el Océano Pacífico sudeste se encuentra bajo en una de las regiones más productivas del océano (Wenzhöfer *et al.*, 2016).

Por otra parte, a pesar de los esfuerzos realizados por la comunidad científica en comprender los procesos biogeoquímicos que ocurren en estos ambientes extremos, la zona hadal sigue siendo parte de la biosfera menos investigada en la Tierra, principalmente debido al gran desafío tecnológico que implica obtener muestras a altas profundidades (Liu et al., 2017). En la actualidad, estos ecosistemas probablemente son menos explorados que la Luna y Marte, por lo cual sus procesos geológicos, fisicoquímicos y biológicos siguen siendo desconocidos en gran medida.

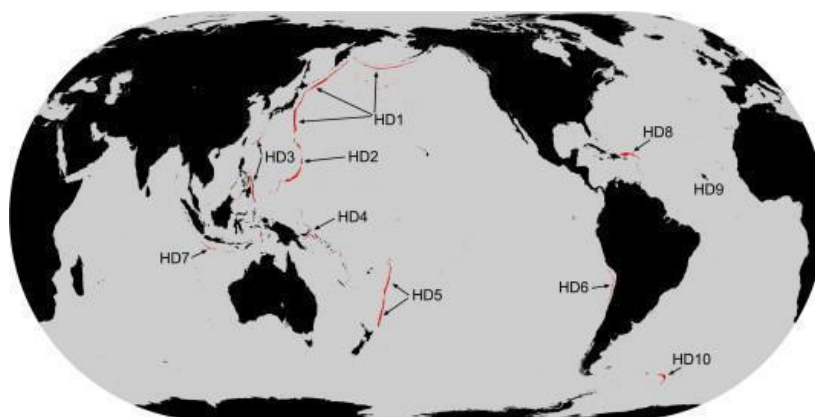


Figura 1. Esquema presentado por Belyaev (1989) con las principales fosas alrededor del planeta: HD1: Aleutian-Japan, HD2: Filipinas, HD3: Marianas, HD4: Bougainville-New Hebrides, HD5: Tonga–Kermadec, HD6: Atacama, HD7: Java, HD8: Puerto Rico, HD9: Romanche y HD10: Antillas del sur (Tomado de Watling et al., 2013).

1.2 La fosa de Atacama

Frente a las costas del Océano Pacífico suroriental se encuentra la Fosa de Atacama, conocida también como Fosa de Perú-Chile, la cual se origina debido a la subducción de la Placa Oceánica de Nazca bajo la Placa Continental Sudamericana, con una tasa aproximada de 7 cm/año (Vigny et al., 2009; Argus et al., 2011). La Fosa de Atacama es la más extensa del mundo, con ~5900 km de longitud, extendiéndose desde el Ecuador hasta Chiloé y un ancho promedio de ~100 km (Fisher & Raitt, 1962; Angel, 1982). La profundidad máxima reportada para la Fosa de Atacama fue de 8074 m de profundidad en el 2003 entre los 23°-24 °S (Danovaro et al., 2003). Sin

embargo, a inicios del año 2018 este récord fue reemplazado por 8081 m de profundidad durante el crucero ATACAMEX, realizado por del Instituto Milenio de Oceanografía (IMO).

En general, la mayoría de las trincheras en su forma moderna, particularmente en el Océano Pacífico, se formaron hace 65.5 millones de años durante el período Cenozoico (Belyaev, 1989). La edad del fondo marino de la Fosa de Atacama es <40 millones de años (Stern, 2002), siendo más joven que las fosas de las Marianas, Tonga y Kermadec. La Fosa de Atacama, está asociada a un área con importantes eventos de surgencia y consecuentemente con altos valores de producción primaria en aguas superficiales (Fossing et al., 1995). En la zona norte de Chile, no hay grandes ríos en el desierto continental adyacente, por lo cual los vientos cumplen un rol importante en la transferencia de material terrígeno del continente adyacente hacia el océano (Ángel, 1982, Perrone et al., 2003).

Desde un punto de vista latitudinal (Norte-Sur), la Fosa de Atacama presenta una intercepción a $\sim 15^\circ$ S asociada a la Dorsal de Nazca que la divide en un sector norte y sur respectivamente, de manera similar a lo que ocurre entre las fosas de Tonga y Kermadec (Jamieson, 2015). Algunos autores han denominado al sector norte de la fosa Perú-Chile cómo: "Milne-Edwards Trench" (Menzies & George, 1967), cuya profundidad máxima alcanza los $\sim 6,000$ m (Fisher & Raitt, 1962) y al sector sur como: "Atacama Trench" cuya zona más profunda supera los 8,000 m de profundidad y se ubica entre los 20-30°S (Danovaro et al., 2002). En este trabajo nos referimos a la Fosa de Atacama para referirnos a todo el sistema. Diversas expediciones se han llevado a cabo con el fin de explorar la Fosa de Atacama, principalmente orientados al estudio batimétrico. La Expedición Galathea realizada en 1957, logró identificar diversos crustáceos de profundidad. De forma similar, expediciones estadounidenses hicieron exitosos arrastres bentónicos en profundidades entre 6,000 y 6,328 m (Menzies et al., 1959; Menzies, 1963a). Posteriormente, la expedición a bordo del Anton Bruun en 1965 alcanzó profundidades de 6,500 m, (Menzies & Barbilla, 1966). Profundidades similares se alcanzaron durante la expedición "Downwind" en 1957, donde se realizaron estudios de eco-resonancia y refracción sísmica (Fisher, 1958). Estudios batimétricos realizados a finales de los 50's (Zeigler et al., 1957) empleando la embarcación soviética Akademik Kurchatov, tomó muestras de arrastre a una profundidad de 7,720 m (Zenkevitch, 1969 b; Zenkevitch, 1971). En 1997, durante una expedición Italiana-chilena (ATIE), se colectaron muestras de sedimento a 7,800 m de profundidad a bordo del AGOR 60

Vidal-Gormaz (Donavaro et al., 2003, Perrone et al., 2003). En años más recientes, específicamente en enero de 2018, el “lander Audacia”, un vehículo no tripulado logró descender 8,081 metros en caída libre por la Fosa de Atacama durante la Expedición Chilena “ATACAMEX”. Durante Marzo del mismo año, como parte del proyecto HADES-ERC, se describió una nueva especie de anfípodo que habita las profundidades de la Fosa de Atacama, *Eurythenes atacamensis* sp. nov. (Weston et al., 2021). Finalmente durante enero de 2022 a bordo del buque de investigación DSSV “Pressure Drop”, se utilizó el sumergible tripulado “Limiting Factor” que logró por primera vez que seres humanos desciendan a la Fosa de Atacama. De lo mencionado anteriormente se deduce un avance en la exploración del océano profundo, especialmente del conocimiento de la zona hadal-bentónica; sin embargo, la zona hadal-pelágica y el suministro de alimento y energía de las fosas oceánicas sigue siendo en gran medida desconocida.

1.3 Fuentes de materia orgánica en la zona hadal

El flujo vertical de materia orgánica (MO) se atenúa con la profundidad debido a la utilización directa por la biota o por la solubilización a través de la actividad enzimática extracelular por microbios heterótrofos (Delong et al., 1993, Herndl et al., 2013). Por lo tanto, sólo una fracción de la MO logra depositarse en los sedimentos profundos y consecuentemente las tasas de respiración de la MO tienden a ser bajas (Wakeham et al., 1984, 1997a, 1997b, Hedges et al., 2001, Armstrong et al., 2001). Sin embargo, Glud et al., (2013) demostró que la tasa de respiración en los sedimentos hadales de la Fosa de las Marianas, es el doble de lo que existe en las planicies abisales adyacentes, evidenciando que la actividad biológica/microbiana en el ambiente hadobentónico es mayor de lo esperado. Este reciente cambio de paradigma en el funcionamiento de los ecosistemas hadales ha llevado a replantearse los mecanismos de distribución de la MO. Sin embargo, los mecanismos que explican estas observaciones aún no están claros.

La evidencia circunstancial indica que especialmente los microbios heterótrofos del océano profundo dependen de la materia orgánica presente en partículas que se hunden a través de la columna de agua (Bergauer et al., 2017). En efecto, un estudio reciente, utilizando estimaciones empíricas de la fracción de exportación y la atenuación del flujo en la columna de agua que recubre

la Fosa de Atacama ha demostrado que la producción de exportación puede sustentar la mayor parte de la demanda de carbono respiratorio de la comunidad de plancton en la zona hadopelágica (Fernández-Urruzola et al., 2021).

En general, las fosas oceánicas, son consideradas como áreas dentro de la cuenca sedimentaria caracterizadas por altas tasas de deposición de material orgánico, denominadas depocentros (Jahnke & Jahnke, 2000) distribuido a lo largo de su eje de extensión, caracterizados por comunidades bentónicas distintas a las planicies abisales adyacentes (Tietjen et al., 1989; Danovaro et al., 2003; Leduc et al., 2016b). Diversos estudios, sugieren que la disponibilidad de alimentos probablemente sea un factor clave para la distribución de las comunidades bentónicas (Danovaro et al., 2003; Turnewitsch et al., 2014; Ichino et al., 2015; Leduc et al., 2016). Así mismo, estudios realizados en los sedimentos superficiales de las fosas de Izu-Bonin y Tonga, en el Pacífico occidental, indican una mayor actividad diagenética concomitante con la productividad de aguas superficiales (mesotróficas > oligotróficas) (Wenzhöfer et al., 2016). Sin embargo, a pesar que los sedimentos de las fosas en general parecen estar enriquecidos en materia fresca (lábil), lo mismo no ocurre con las zonas abisales (Danovaro et al., 2003; Glud et al., 2013; Leduc et al., 2016; Wenzhöfer et al., 2016). Por lo tanto, se puede inferir que otros aportes, además de la zona superficial, podrían estar incrementando el material orgánico a estos ecosistemas. Un mecanismo plausible, sería el transporte lateral desde la pendiente oceánica (Jahnke et al., 1990), aunque no se refleje necesariamente en el mayor contenido de carbono orgánico lábil, ya que la materia orgánica sedimentaria se compone en gran parte de material relativamente refractario (Wenzhöfer et al., 2016). Por otro lado, Tamburini (2013), sugiere que el aumento de la presión hidrostática puede inhibir la remineralización y así el material fito-detrital, relativamente lábil, puede alcanzar las profundidades hadales. Sin embargo, esto último no explica una mayor concentración de fito-pigmentos en las profundidades hadales versus las abisales, lo que requeriría un enfoque descendente preferencial (preservación selectiva) del material fito-detrital hacia el sistema hadal (Turnewitsch et al., 2014).

Otro mecanismo plausible para el transporte de material orgánico sería a través de la actividad sísmica ocasional, facilitado por la topografía del fondo marino (Itou, 2000; Rathburn et al., 2009). Este efecto no sería posible sobre el plano abisal (Jamieson, 2015), por lo que nos haría pensar que los ecosistemas hadal-pelágicos, dependen principalmente de factores externos

(alóctonos, para más detalles de factores alóctonos y autóctonos ver Jamison et al., 2015). Por otra parte, la actividad quimiosintética, se presenta como un factor interno (autóctono) de aporte de materia orgánica (Fujikura, 1999). Yunping Xu et al., (2018), proponen 5 fuentes principales de materia orgánica para las zonas hadales: (1) el flujo vertical de la materia orgánica particulada (POM) que se produce principalmente por la fotosíntesis en la zona eufótica (Jamieson et al., 2010; Stockton & Delaca, 1982), (2) el material de carroña, producto de mamíferos marinos, peces y grandes invertebrados (Britton & Morton, 1994), (3) la entradas de materia orgánica terrestre, ya que muchas fosas están adyacentes a los continentes (George & Higgins, 1979), (4) el transporte lateral de materia orgánica desde pendientes continentales bajo los efectos combinados de topografía y gravedad (Ichino et al., 2015) y finalmente (5) la producción quimiosintética *in situ* asociada con los respiraderos hidrotermales o “cold seeps” (Fujikura, 1999), tal como se puede observar en la Figura 2.

Desde la superficie del océano el transporte vertical de partículas, como material fecal de zooplancton, aportan entre el 20-30 % del carbono orgánico por ingesta de fitoplancton (Eppley & Peterson, 1979), así como exudados, restos de fitoplancton y agregados macroscópicos (Urrère & Knaves, 1981). En este contexto, se ha comprobado experimentalmente que las partículas orgánicas pueden recorrer la columna de agua a una velocidad de entre 50 y 300 m/día (Eppley & Peterson, 1979), esto contribuye al flujo de material orgánico al interior del océano.

A medida que las partículas se hunden a través de la columna de agua, su composición se altera constantemente, debido a que los componentes más lábiles se remineralizan preferentemente, dando lugar a un cambio progresivo hacia una composición más refractaria con la profundidad (Romankevich, 1984). El material que sobrevive al transporte a través de la columna de agua se somete luego a una mayor alteración y descomposición por parte de los heterótrofos bentónicos (Emerson & Hedges, 1988), dando lugar a la diagénesis temprana, que puede llegar incluso a alterar las señales isotópicas de carbono y nitrógeno. Durante este tránsito, la composición química y el flujo de la POM son afectados por la estructura de la comunidad biológica que controla las reacciones de transformación (Wakeham et al., 1984). Sin embargo, el material relativamente fresco (lábil) encontrado por Danovaro (2013) en los sedimentos de la Fosa de Atacama y altos valores en la tasa de respiración encontrados en los sedimentos de la Fosa de

las Marianas por Glud (2013), nos estarían indicando que existe un mecanismo que transporta MO hacia los sedimentos mucho más rápido de lo que se esperaba.

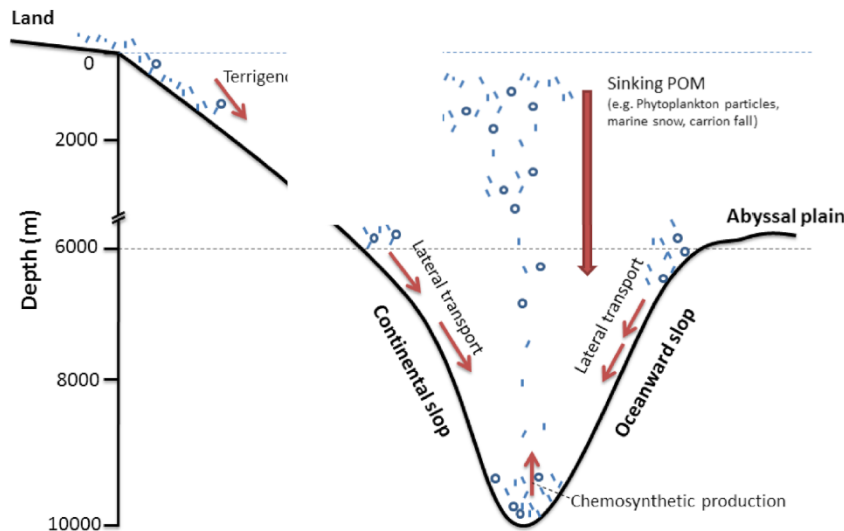


Figura 2. Representación de las principales fuentes de aporte de material orgánico hacia el ecosistema hadal (Tomado de Yunping Xu et al., 2018).

En tal sentido, la actividad sísmica podría tener un papel preponderante en el rápido transporte de material lábil hacia los sedimentos de la zona hadal. Oguri (2013), empleando muestras de sedimento de la trinchera de Japón, reportó perturbaciones sucesivas que transportaban material hacia los sedimentos superficiales, afirmando que el impacto de la actividad sísmica podría involucrar cambios en la biogeoquímica de los sedimentos superficiales por varios años. Además, mediante el registro de video-cámara *in situ* reporta una capa densa nefeloide que permaneció 4 meses después del gran terremoto de Tohoku – Oki en el 2011.

1.4 Biomarcadores lipídicos y análisis de isótopos estables en la materia orgánica particulada.

La POM en el océano ha sido descrita principalmente mediante el uso de moléculas orgánicas como lípidos, carbohidratos y aminoácidos (Wakeham & Lee, 1989), componentes fundamentales de organismos (Handa & Tominaga, 1969), y que son utilizados a menudo como

biomarcadores orgánicos para investigar la fuente, la composición y la degradación de la OM (Wakeham & Lee, 1989, Arts et al., 2001; Lee et al., 2004, Rontani et al., 2011). La composición de la MO es diversa, sin embargo los lípidos se encuentran entre las estructuras biológicas más estables a altas presiones y bajas temperaturas (Oger & Jebbar, 2010), por lo tanto son ideales para el estudio de los ecosistemas hadales.

En este estudio nos enfocamos en los lípidos polares intactos (IPL), que son los componentes básicos de todas las membranas celulares, y se utilizan como un indicador de células vivas, ya que sus grupos de cabeza polar se hidrolizan rápidamente tras la muerte celular (White et al., 1979, Petersen et al., 1991), lo que significa que las abundancias de IPL pueden ser relacionadas con las abundancias celulares. Muchas clases diferentes de IPL se han atribuido a grupos funcionales microbianos específicos y se pueden utilizar para determinar la abundancia relativa y absoluta *in situ* de diferentes vías metabólicas presentes en el océano (Wakeham et al., 2012; Schubotz et al., 2009, Van Mooy et al., 2012; Schubotz et al., 2018, Van Mooy y Fredericks, 2010). Es importante destacar que, en comparación con los análisis genéticos, los IPL proporcionan estimaciones semicuantitativas de la biomasa microbiana *in situ*, ya que suelen representar entre el 10 y el 20 % del contenido de carbono celular en los organismos planctónicos (Cantarero et al., 2020).

Aproximadamente, 9 clases principales de IPL dominan el conjunto de lípidos intactos (Figura 3) presentes en los ambientes marinos (Van Mooy y Fredericks, 2010). Su diversidad estructural proporciona un grado variable de especificidad en las fuentes biológicas preservadas en la heterogeneidad de los grupos de cabeza polares, el número de átomos de carbono en los lípidos del núcleo de diacilglicéridos y el grado de insaturación y metilación dentro de la estructura del lípido del núcleo. Por ejemplo: el predominio de ácidos grasos poli-insaturados en células eucariotas (Volkman et al., 1989), la síntesis preferencial de ácidos grasos de cadena impar en membranas bacterianas (Schubotz et al., 2009, Van Mooy y Fredericks, 2010), la presencia de lípidos isoprenoides en las arqueas (Pearson, 2013) y las diferencias estereoquímicas en los enlaces éter y éster entre los lípidos bacterianos, eucarióticos y de arqueas (Weijers et al., 2006) suelen evocarse para evaluar fuentes biológicas distintas en la columna de agua.

Por otra parte, la composiciones de isótopos estables de carbono y nitrógeno de la MO se han utilizado ampliamente para dilucidar la contribución relativa de las fuentes de MO (Meyers &

Eadie, 1993; Middelburg & Nieuwenhuize, 1998; Gao et al., 2012), incluidos los sedimentos hadales de la Fosa de las Marianas (Luo et al., 2019), la Fosa de Nueva Bretaña (Xiao et al., 2020), y las Fosas de Atacama y Kermadec (Xu., et al., 2021). Sin embargo, pocos estudios han evaluado la composición isotópica de la POM desde las aguas superficiales hasta la región hadopelágica, incluidos los sedimentos superficiales hadales y batiales. En la tabla 1, mostramos un resumen las aproximaciones geoquímicas que permiten inferir las distintas fuentes de materia orgánica y los grupos típicamente clasificadas y más representativos de lípidos intactos polares (IPLs).

Considerando estos antecedentes, en esta tesis doctoral, evaluamos la presencia de señales únicas de IPL de la comunidad microbiana, y su posible procedencia (producción *in situ* vs. alóctona), así como evidencia de adaptaciones moleculares a las condiciones extremas de la región hadal. Además, analizamos la composición isotópica de la POM desde las aguas superficiales hasta la región hadopelágica, incluidos los sedimentos superficiales hadales y así evaluar la procedencia y el destino de las partículas que se hunden a través de las regiones mesopelágico (200-1,000 m), batipelágico (1,000-3,500 m), abisopelágico (3,500-6,000 m) y hadalpelágico (>6,000 m), y el material sedimentario en los puntos más profundos de la Fosa de Atacama (7,734-8,063 m).

Tabla 1. Isótopos estables de la materia orgánica y los grupos principales de IPLs en ambientes marinos.

	Biomarcadores orgánicos	Indicador o fuente de materia orgánica	Referencias	
Carbono (C) y nitrógeno (N) orgánico	Carbono orgánico particulado (POC)	Indicador de productividad primaria superficial	Turnewitsch et al., 2007; Prentice et al., 2001	
	C/N	Indicador de fuentes de materia orgánica marina y terrestre	Meyers et al., 1997; Sampei and Matsumoto, 2001	
Isótopos estables	$\delta^{13}C_{POC}$	Indicador de fuentes de carbono y nitrógeno, así como de comunidades específicas	Jeffrey et al., 1982; Druffel et al., 1992	
	$\delta^{15}N_{PON}$	através de la su fraccionamiento isotópico.	Sigman et al., 1999	
Lípidos intactos polares (IPLs)	Fosfolípidos	Fosfatidilglicerol (PG)	Membranas de cloroplasto, bacterias verdes del azufre, nitrificantes y metanotróficas	Wada and Murata, 2007; Goldfine and Hagen, 1968
		Fosfatidiletalona (PE)	Bacterias nitrificantes/denitrificantes, metanotróficas, oxidantes de azufre, reductoras de sulfato.	Barridge and Shively, 1968; Imhoff and Bias-Imhoff, 1995; Goldfine and Hagen, 1968; Makula, 1978; Fang et al., 2000
		Fosfatidilcolina (PC)	Fitoplancton eucariota, bacterias heterotróficas.	Van Mooy et al., 2010; Van Mooy et al., 2006; Popenoerf et al., 2011
	Lípido betaina	Diacilgliceril trimetilhomoserina (DGTS)	Fitoplancton eucariota, bacteria púrpura sin azufre, bacterias reductoras de sulfato.	Kato et al., 1996; Benning et al., 1995; Schubotz et al., 2018
		Diacilgliceril hidroximetil-trimetil- β -alanina (DGTA)		Kato et al., 1996; Schubotz et al., 2018
		Diacilgliceril carboxihidroximetilcolina (DGCC)	Fitoplancton eucariota, bacterias reductoras de sulfato.	Kato et al., 1996; Schubotz et al., 2018
	Glicolípidos	Monogalactosyldiacilglicerol (MGDG)	Membranas de cloroplasto, bacterias heterotróficas.	Wada and Muarata, 2007; Popenoerf et al., 2011
		Digalactosyldiacilglicerol (DGDG)	Membranas de cloroplastos.	
		Sulfoquinovosyldiacilglicerol (SQDG)	Membranas de cloroplasto particularmente abundantes en cianobacterias.	Wada and Muarata, 2007

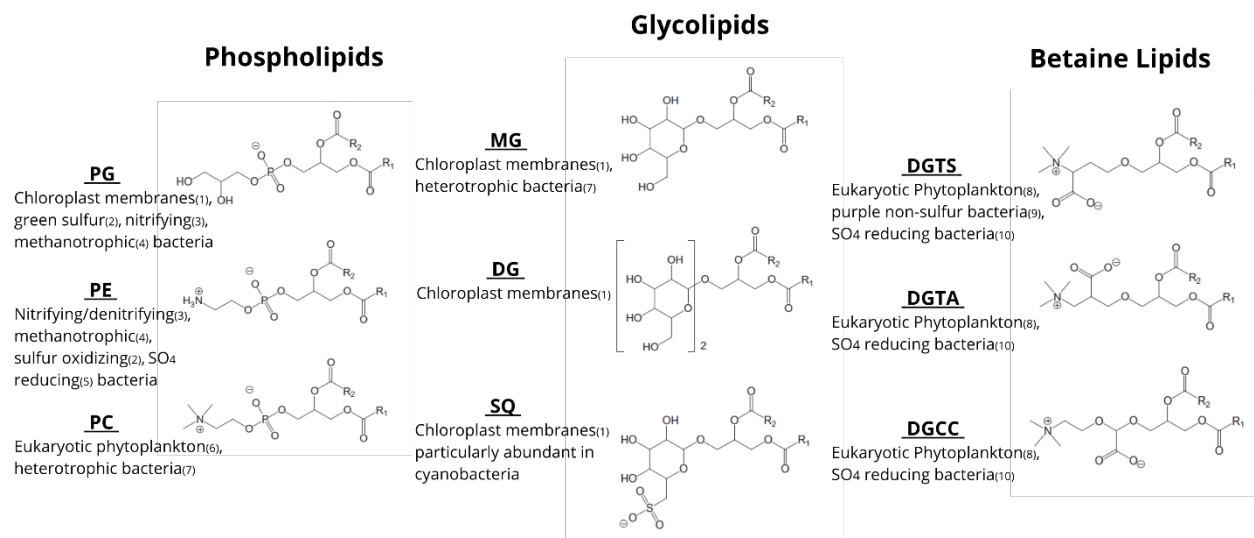


Figura 3. Clases más abundante de IPL en el océano. Fosfolípidos: PG-(Fosfatidilglicerol), PE-(Fosfatidiletanolamina), PC-(Fosfatidilcolina). Glicolípidos: MG (Monoglicósil), DG (Diglicósil), SQ (Sulfo-quinovosil). Lípidos de Betaína: DGTS-(Diacilglicerilhidroximetiltrimetilhomoserina), DGTA-(Diacilglicerilhidroxi-metiltrimetil-β-alanina), DGCC-(Diacilglicerilcarboxihidroxi-metilcolina). Los subíndices numerados indican las referencias de las fuentes biológicas de las distintas clases de lípidos: (1) Wada y Murata, 2007), (2) Barridge y Shively, 1968; Imhoff y Bias-Imhoff, 1995, (3) Goldfine y Hagen, 1968) (4) Makula, 1978; Fang et al., 2000), (5) Rütters et al., 2001; Sturt et al., 2004, (6) Van Mooy et al., 2000 Van Mooy et al., 2006, (7) Pependorf et al., 2011, (8) Oguz y Merico, 2006, (9) Benning et al., 1995, (10) Schubotz et al., 2018. Tomado de Cantarero et al., 2020.

2. HIPÓTESIS Y OBJETIVOS ESPECÍFICOS

El flujo de MO hacia los sedimentos representa una de las fuentes principales de alimento para los organismos bentónicos y conecta la superficie con el océano profundo (Tortell et al., 2000; Schippers et al., 2004; Lovenduski et al., 2008). El hundimiento de carbono orgánico particulado ha sido estudiado a partir de un modelo geoquímico clásico de 2 capas, calculando que el flujo de material particulado al océano profundo (> 200 m) es del ~10% de la producción del océano superficial, ~100 mg C m² día⁻¹ en sistemas oligotróficos y ~2000 mg C m² día⁻¹ en áreas de surgencia (Eppley & Peterson, 1979) y sólo ~1% llega al sedimento. Por lo que, en última instancia, comprende el suministro primario de alimento hacia los ecosistemas de aguas profundas

(Smith et al., 2009), además es la vía principal para el almacenamiento de carbono en los sedimentos superficiales. Sin embargo, la mayor parte (~90%) de la MO es reciclada en zona epipelágica (< 200 m) (Suess, 1980; Wakeham et al., 1984; Lee & Cronin, 1984) y sólo una pequeña fracción (<10%) logra llegar hasta la zona mesopelágica y en menor medida a profundidades hadales. Esta observación, apoyó el paradigma tradicional de un ambiente hadal pobre en alimento, sin embargo aunque la oligotrofia aparentemente caracteriza a los ecosistemas abisales y hadales, estudios recientes (Donavaro et al., 2003; Glud et al., 2013, Leduc et al., 2016; Wenzhöfer et al., 2016), muestran altos contenidos de carbono orgánico en sedimentos hadales superficiales, alta biomasa bentónica y una actividad microbiana más intensa que en los ecosistemas abisales, reflejando altas tasas de depositación en los ecosistemas hadal-bentónicos.

A partir de lo antes planteado, se proponen las siguientes hipótesis:

Hipótesis 1: La MO lábil de los sedimentos superficiales de la Fosa de Atacama reflejan principalmente un transporte lateral desde la pendiente continental y en menor medida un transporte vertical desde aguas superficiales.

Hipótesis 2: La señal isotópica de la materia orgánica en la zona epipelágica no difiere significativamente de la zona hadalpelágica, lo que reflejaría un rápido hundimiento de partículas desde el océano superficial altamente productivo.

Hipótesis 3: La señal isotópica del sedimento superficial de la Fosa de Atacama difiere significativamente de toda la columna de agua porque está dominada por diferentes fuentes de materia orgánica y actividad microbiana *in situ*.

Los objetivos específicos de esta tesis son:

Objetivo específico 1: Caracterizar la materia orgánica particulada en función de marcadores lipídicos (IPLs) e inferir su origen en los sedimentos superficiales de la Fosa de Atacama.

Objetivo específico 2: Analizar la composición isotópica de carbono y nitrógeno orgánico particulado las distintas zonas pelágicas y de los sedimentos superficiales hadales y batiales de la Fosa de Atacama.

Objetivo específico 3: Utilizar modelos de flujos de POC para inferir el exporte de carbono y utilizar un modelo de mezcla isotópico para de las distintas fuentes de MO que contribuyen a los sedimentos hadales de la Fosa de Atacama.

3. MATERIAL Y MÉTODOS

3.1 Área de estudio

La zona más profunda de la Fosa de Atacama está ubicada frente a la costa oeste de América del Sur en el Océano Pacífico entre los 19 y 25 °S. Esta zona está asociada a aguas altamente productivas en superficie, mediciones de clorofila-a realizadas *in situ* muestran una concentración media de $15.12 \pm 8.86 \text{ mg m}^{-3}$ (Dávila et al., 2014) y un flujo total de POC de $997.24 \text{ g C año}^{-1}$ estimados a profundidades máximas de 6,000 m (Lutz et al., 2007, Jamieson 2015). La temperatura registrada en superficie es de $\sim 17 \text{ °C}$ y por debajo de los 1,500 m es $\sim 2 \text{ °C}$ (Sievers et al., 1999) y entre los 2,000 y 5,000 m, la temperatura disminuye lentamente ($\Delta T 0.4 \text{ °C}$) a 1.75 °C (Danovaro et al., 2003).

La Fosa de Atacama está situada en el Pacífico Sur Tropical Oriental (ETSP) a lo largo del margen Perú-Chile, y subyace al Sistema de la Corriente de Humboldt, eutrófico y altamente productivo (Ángel, 1982; Ahumada, 1989), que incluye la cuarta zona mínima de oxígeno (ZMO) más grande (por volumen) del mundo (Schneider et al., 2006). En esta zona, si bien la escorrentía fluvial es mínima (Houston, 2006), los vientos pueden transferir polvo desde el desierto continental adyacente (Angel, 1982). La Fosa de Atacama es la más extensa en longitud del mundo (Sabbatini et al., 2002) con $\sim 5,900 \text{ km}$, y está geográficamente aislada de otras fosas del Océano Pacífico.

3.2 Diseño de muestreo y adquisición de datos

En este estudio, investigamos la diversidad y abundancia de IPLs bacterianos y eucariotas en un total de nueve sedimentos superficiales hadales (0-1 cm) y subsuperficiales (1-2 y 2-3 cm) (tres sitios entre 7,734 y 8,063 m de profundidad de agua) colectados durante el crucero HADES-SO261 (marzo a abril de 2018) a bordo del RV Sonne (Wenzhöfer, 2019) y siete sedimentos superficiales batiales (siete sitios; 529-1200 m de profundidad de agua) colectados durante el

crucero ChiMeBo-SO211 (2-29 de noviembre de 2010) a bordo del R.V. Sonne (Matys et al. , 2017) (Tabla 1; Figura 4). Comparamos nuestros resultados con los resultados de la IPL de la columna de agua suprayacente (0-700 m) recientemente reportados en Cantarero et al. (2020).

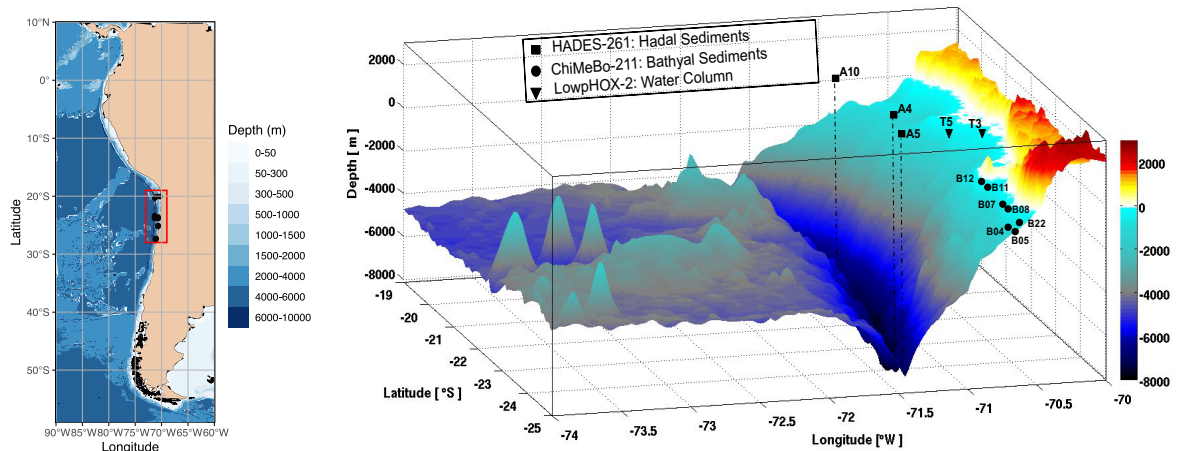


Figura 4. Mapa tridimensional de la Fosa de Atacama que muestra las ubicaciones de muestreo de este estudio. Los cuadrados negros indican las estaciones de muestreo de sedimentos hadales, los círculos negros indican las estaciones de muestreo de sedimentos batiales de Matys et al. (2017), y los triángulos negros indican las estaciones de muestreo de la columna de agua de Cantarero et al. (2020).

Las muestras de sedimentos se colectaron con un multicore (MUC) equipado con doce tubos acrílicos de 60 cm de longitud (de 6 a 10 cm de diámetro para los sedimentos batiales y de 9,5 cm de diámetro para los sedimentos hadales). Durante la expedición HADES, se utilizó un lander autónomo “Audacia” equipado con un CTD Sea-Bird SBE-19 plus y dos botellas Niskin (30 L) para obtener datos hidrográficos hasta $\sim 7,850$ m. Los sedimentos hadales del crucero HADES-SO261 se almacenaron a 4 °C hasta que fueron extruidos y submuestreados a bordo, con una resolución de 1 cm y luego se mantuvieron congelados a -20 °C hasta su procesamiento en el laboratorio. Se puede encontrar más información sobre la colecta de muestras de sedimentos batiales y hadales durante los cruceros ChiMeBo-SO211 y HADES-SO261 en Matys et al. (2017) y Wenzhöfer et al. (2019), respectivamente. Estas muestras de sedimento también fueron utilizadas para el análisis elemental y de isótopos estables e incluimos datos publicados sobre el material de

las trampas de sedimentos de la región que recubre la Fosa de Atacama (Hebbeln et al., 2000; González et al., 2004).

Adicionalmente, comparamos nuestros resultados de IPL de los sedimentos superficiales en las regiones hadal y batial con las muestras de la columna de agua suprayacente del crucero LowpHOX-2 recientemente reportado por Cantarero et al. (2020). Esto incluye la MO suspendida fraccionada por tamaño (0.3-2.7 y 2.7-53 μm) en dos estaciones y desde seis profundidades de agua que son representativas de la zonación biogeoquímica dominante asociada a la OMZ de esta región. (ver Tabla 2 y Cantarero et al. , 2020, para más detalles).

Tabla 2. Estaciones de muestreo de las expediciones HADES, ChiMeBo y LowpHOX-2.

Cruise-RV	Device	Environment	Station	Environmental samples	Sampling depth (m)	Latitude (°S)	Longitude (°W)	Date	Reference
HADES SONNE SO-261	Multi-corer (MUC)	Hadal sediments	A10	Hadal sediments (0-1, 1-2 and 2-3 cm)	7734	20.32	71.29	26/03/2018	This study
			A5	Hadal sediments (0-1, 1-2 and 2-3 cm)	7890	23.81	71.37	11/03/2018	
			A4	Hadal sediments (0-1, 1-2 and 2-3 cm)	8063	23.36	71.34	14/03/2018	
ChiMeBo SONNE SO-211	Multi-corer (MUC)	Bathyal Sediments	B12	Upper bathyal sediment (0-1 cm)	529	23.59	70.67	02-29/11/2010	This study
			B08	Upper bathyal sediment (0-1 cm)	539	25.2	70.68	02-29/11/2010	
			B22	Upper bathyal sediment (0-1 cm)	545	27.29	71.05	02-29/11/2010	
			B07	Lower bathyal sediment (0-1 cm)	920	25.07	70.66	02-29/11/2010	
			B05	Lower bathyal sediment (0-1 cm)	957	27.5	71.13	02-29/11/2010	
			B11	Lower bathyal sediment (0-1 cm)	1113	23.85	70.65	02-29/11/2010	
LowpHOX-2 Cabo de Hornos	Rosette (Niskin bottles)	Water column	T3/T5	Chlorophyll maximum (0.3-2.7 μm)	9-10	20.07/20.03	70.36/70.89	04-06/02/2018	Cantarero et al., 2020
			T3/T5	Upper chemocline (0.3-2.7 μm)	25-28	20.07/20.03	70.36/70.89	04-06/02/2018	
			T3/T5	Lower chemocline (0.3-2.7 μm)	35-45	20.07/20.03	70.36/70.89	04-06/02/2018	
			T3/T5	Upper OMZ (0.3-2.7 μm)	55-60	20.07/20.03	70.36/70.89	04-06/02/2018	
			T3/T5	Core OMZ (0.3-2.7 μm)	250	20.07/20.03	70.36/70.89	04-06/02/2018	
			T3/T5	Mesopelagic zone (0.3-2.7 μm)	750	20.07/20.03	70.36/70.89	04-06/02/2018	

Para analizar el carbono orgánico particulado (POC) y los isótopos estable de carbono y nitrógeno en la columna de agua, se colectaron muestras en 4 sitios entre 21 y 24 °S sobre la Fosa de Atacama durante el crucero SO261 (Tabla 2). Obtuvimos agua de mar de ocho profundidades discretas hasta 6,000 m usando un roseta con 24 botellas 12L-Niskin, y de 1,5 m por encima del fondo marino usando un vehículo autónomo equipado con 2 botellas 10L-Niskin. Tamizamos entre ~0,5 y 60 L de agua de mar a través de una malla de nailon de 20 μm y luego filtramos las muestras usando filtros Whatman GFFs pre-combustionados (450 °C, 24 h) (0,7 μm de tamaño de poro nominal) utilizando contenedores presurizados para el análisis elemental y de isótopos estables. Los filtros se secaron inmediatamente a 60 °C durante 24 h y se mantuvieron secos en la oscuridad hasta su análisis en el laboratorio.

3.3 Objetivo específico 1

Para cumplir con este objetivo se analizaron las muestras de sedimento superficial colectadas dentro del eje latitudinal de la Fosa de Atacama durante el crucero Hades y ChiMeBo. Para la extracción de lípidos, se extrajeron y analizaron en el Laboratorio de Geoquímica Orgánica de la Universidad de Colorado Boulder. Las muestras de sedimento se liofilizaron antes de la extracción. Aproximadamente 1-2 g de sedimento seco, se colocaron en un tubo de centrifuga de vidrio comburente y se extrajeron utilizando una versión modificada (Wörmer et al., 2013) del método de extracción de Bligh y Dyer (Bligh y Dyer, 1959). Brevemente, antes de la extracción, añadimos 1 µg de C16 PAF (C₂₆H₅₄NO₇P) a cada muestra como estándar interno. Las muestras se extrajeron secuencialmente utilizando diclorometano/MeOH/ buffer fosfato/ (1:2:0.8 v:v:v; 2×), diclorometano/MeOH/ buffer tricloroacético (1:2:0.8 v:v;; 2×), y diclorometano/MeOH (1:5 v:v; 1×). Después de cada adición, las muestras se agitaron en vórtex durante 30 s, se sonicaron durante 10 min y, a continuación, se centrifugaron durante 5 min a 2,000 rpm. A continuación, cada extracción se transfirió a un embudo separador donde se combinó un extracto lipídico total (TLE) y luego se concentró bajo una suave flujo de N₂. Antes del análisis, los TLE se resuspendieron en diclorometano/MeOH (9:1) v:v y se filtraron a través de un filtro de jeringa de politetrafluoroetileno (PTFE) de 0,45 µm. El procesamiento y la extracción de sedimentos batiales del crucero ChiMeBo-SO211 y de muestras de columna de agua del crucero LowpHOX-2 han sido reportados por Matys et al. (2017) y Cantarero et al. (2020), respectivamente. Los TLEs se transfirieron a viales de 2 mL con insertos de 200 µL y se disolvieron en 100 µL de diclorometano/MeOH (9:1, v:v).

Los IPL se analizaron según Wörmer et al. (2013) utilizando un cromatógrafo líquido de alta resolución (HPLC) Thermo Scientific UltiMate 3000 acoplado a un espectrómetro de masas de alta resolución cuadrupolar Q Exactive Focus Orbitrap (HPLC-HRMS) mediante ionización por electrospray (ESI). El programa de HPLC comprendía un caudal de 0,4 mL min⁻¹ utilizando una mezcla de dos fases móviles: la mezcla A consistía en acetonitrilo/diclorometano (75:25, v:v) con 0,01 % de ácido fórmico y 0,01 % de NH₄OH; la mezcla B consistía en metanol/agua (50:50, v:v) con 0,4 % de ácido fórmico y 0,4 % de NH₄OH. Se utilizó un gradiente lineal como sigue 1 % de mezcla B (0-2,5 min), 5 % (4 min), 25 % de mezcla B (22,5 min), 40 % de mezcla B (26,5-27,5 min), y la columna de HPLC se mantuvo a 40 °C. Se inyectaron muestras (10 µl) y se

disolvieron en diclorometano/metanol (9:1, v:v). Los IPL se separaron utilizando una columna Waters Acquity BEH Amide (2,1×150 mm; tamaño de partícula de 1.7 μm) que permite una separación específica de clase basada en su grupo de cabeza hidrófilo (Wörmer et al., 2013). Los ajustes de ESI comprendían la presión del gas de cubierta (N_2) 35 (unidades arbitrarias), la presión del gas auxiliar (N_2) 13 (unidades arbitrarias), el voltaje de pulverización 3,5 kV (ESI de iones positivos), la temperatura capilar 265 °C y lente S nivel RF 55 (unidades arbitrarias). Se calibró la resolución de masa y la precisión del instrumento utilizando la solución de calibración de iones positivos Thermo Scientific Pierce LTQ Velos ESI (que contiene una mezcla de cafeína, MRFA, Ultramark 1,621 y N-butilamina en una solución de acetonitrilo, metanol y ácido acético).

Los IPLs se identificaron en modo de ionización positiva, tanto en barrido completo como en MS^2 dependiente de datos, basándose en sus pesos moleculares de compuestos protonados ($\text{M} + \text{H}^+$) o de amonio ($\text{M} + \text{NH}_4^+$), los patrones de fragmentación y los tiempos de retención, fueron comparados con la literatura relevante (Sturt et al., 2004; Schubotz et al., 2009; Wakeham et al., 2012) y la base de datos interna del Laboratorio de Geoquímica Orgánica de la Universidad de Colorado Boulder, USA. Las áreas bajo la curva de los IPL individuales se integraron utilizando el software Trace-Finder de Thermo Fisher Scientific utilizando cromatogramas iónicos extraídos de sus iones moleculares característicos. Las abundancias de IPL se determinaron con una combinación de un estándar interno (C16PAF, Avanti Polar Lipids) y una calibración externa a una regresión lineal entre áreas bajo la curva y concentraciones conocidas de un cóctel de IPL compuesto de 17 clases diferentes de IPL a través de una serie de dilución de cinco puntos (0.001-2.5 ng μL) (véase Cantarero et al., 2020). Se utilizaron estándares deuterados (Avanti Polar Lipids: d7-PC, d7-PG, d7-PE, y DGTS-d9) para corregir los efectos potenciales de la matriz en la eficiencia de ionización. A pesar del número limitado de estándares deuterados disponibles, en promedio, observamos que el efecto matriz representa una pérdida de $\sim 7 \pm 0,6 \%$ en la eficiencia de ionización. Por lo tanto, es razonable suponer una pérdida similar para otras clases de IPL, aunque esto queda por comprobar en futuros estudios. Destacamos la importancia de utilizar tantas clases de IPL como sea posible para tener en cuenta tanto las diferencias en la eficiencia de ionización como el efecto de matriz al realizar la cuantificación de IPL en muestras ambientales. Los factores de respuesta relativos siguieron el orden $\text{MGDG} > \text{DGTS} > \text{DGTA} > \text{PDME} > \text{PME} > \text{PG} > \text{PC} > \text{PE} > \text{SQDG} > \text{DGCC} > \text{DGDG}$. Las clases de lípidos se agruparon en fosfolípidos

(PG, fosfatidilglicerol; PE, fosfatidiletanolamina; PC, fosfatidilcolina; y PME/PDME, fosfatidil(di)metiletanolamina), glicolípidos (MGDG, monoglicosildiactilglicerol; DGDG, diglicosildiactilglicerol; y SQDG, sulfoquinovosildiactilglicerol), lípidos de betaína (DGTA, diactilgliceril hidroximetil-trimetil- β -alanina; DGTS, diactilgliceril trimetilhomoserina; y DGCC, diactilglicerilcarboxi-N-hidroximetilcolina), y otros lípidos (ceramidas glicosídicas, Gly-Cer; PI, fosfatidilinositol; y OL, lípidos de ornitina). Además, utilizamos DAG para designar un diactilglicerol y AEG para designar un aciloterglicerol, y describimos cadenas cortas y largas para referirnos a cadenas alquílicas combinadas de C₂₈₋₃₆ y C₃₆₋₄₄, respectivamente (Rêzanka y Sigler, 2009; Schubotz et al., 2009; Brandsma., et al., 2012).

Utilizamos el coeficiente de similitud de Bray-Curtis (Mirzaei et al., 2008) para producir una agrupación jerárquica de la abundancia de clases y moléculas de IPLs; se disponía de dos tipos de valores p: valor p aproximadamente insesgado (AU) y valor de probabilidad bootstrap (BP) con el número de réplicas bootstrap de 10,000 (Suzuki y Shimodaira, 2006). Realizamos un escalado multidimensional no métrico (NMDS) (Warton et al., 2012) para examinar la disimilitud entre los IPL de cada muestra. Las distancias calculadas a los centroides de grupo se basaron en la disimilitud de Bray-Curtis a partir de la matriz de abundancia de IPL, y la significación de las asociaciones se determinó mediante 999 permutaciones aleatorias. Las pruebas de significación de la disimilitud multivariante entre grupos se realizaron utilizando el análisis de similitud (ANOSIM), donde la separación completa y la no separación entre grupos se sugiere con R=1 y R=0, respectivamente (Clarke y Gorley, 2015). Las diferencias estadísticas en el número de átomos de carbono y dobles enlaces se identificaron mediante ANOVA y la prueba post hoc HSD (diferencia honestamente significativa) de Tukey. Se utilizó el análisis de similitud de porcentajes (SIMPER) para identificar las contribuciones porcentuales de los IPL que representaban > 90 % de la similitud dentro de cada clúster. Los análisis estadísticos multivariantes, así como otros análisis estadísticos, se calcularon utilizando el paquete vegan (Oksanen et al., 2013) del software de código abierto R versión 3.6.2 dentro del paquete ggplots (Warnes et al., 2015).

3.4 Objetivo específico 2

Para cumplir con este objetivo, realizamos análisis elemental y de isótopos estables de carbono y nitrógeno en masa. El carbono orgánico particulado (POC) y el nitrógeno orgánico particulado (PON), así como sus respectivos isótopos estables a granel ($\delta^{13}\text{C}_{\text{POC}}$ y $\delta^{15}\text{N}_{\text{PON}}$) se midieron en el

Laboratorio de Biogeoquímica e Isótopos Estables Aplicados de la Pontificia Universidad Católica de Chile. Antes del análisis, se eliminaron los carbonatos inorgánicos acidificando las muestras durante una noche con vapores de HCl. A continuación, se envasaron en cápsulas de estaño y se introdujeron mediante combustión flash (1,020 °C) en un analizador elemental (EA) Thermo Scientific Flash 2000 CHN acoplado a un espectrómetro de masas de relación isotópica (IRMS) Thermo DeltaV Advantage. Las relaciones isotópicas se notifican utilizando la notación estándar (δ) y se expresan por mil (‰) con respecto al material de referencia estándar:

$$X (\text{‰}) = [(R_{\text{sample}} / R_{\text{standard}}) - 1] \times 1000 \text{ (Ecuación 1)}$$

Donde X es el $^{13}\text{C}_{\text{POC}}$ o $^{15}\text{N}_{\text{PON}}$, R es la relación correspondiente de $^{13}\text{C}/^{12}\text{C}$ o $^{15}\text{N}/^{14}\text{N}$ en una muestra o estándar (PDB para carbono y N_2 atmosférico para nitrógeno). La precisión analítica se calculó en $\pm 0,215\%$ y $\pm 0,33\%$ para el nitrógeno y el carbono, respectivamente, basándose en cuatro estándares analizados por triplicado (acetanilida, atropina, cafeína y ácido glutámico). La precisión analítica en el análisis elemental fue de $\pm 0,003$ mg y $\pm 0,007$ mg para el nitrógeno y el carbono, respectivamente. El patrón utilizado para este cálculo fue la acetanilida (71,10% C y 10,36% N).

Las muestras de sedimentos se analizaron con un espectrómetro de masas de relación isotópica Thermo Scientific Elemental Analyzer-Delta V en el Laboratorio de Isótopos Estables de Sistemas Terrestres de CU Boulder. Se midieron acetanilida y ácido etilendiaminotetraacético purificados como patrones para la calibración externa y las correcciones de deriva. La precisión analítica para el carbono orgánico total y el nitrógeno total fue de $\pm 0,2\%$ y $\pm 0,11\%$, respectivamente, mientras que la precisión analítica fue de $\pm 0,2\%$ y $\pm 0,15\%$ para $\delta^{13}\text{C}_{\text{POC}}$ y $^{15}\text{N}_{\text{PON}}$, respectivamente.

Las diferencias estadísticas con respecto a $\delta^{13}\text{C}_{\text{POC}}$ o $^{15}\text{N}_{\text{PON}}$ en cada ambiente se identificaron mediante ANOVA y la prueba post hoc HSD (diferencia honestamente significativa) de Tukey. Las pruebas estadísticas se calcularon utilizando el paquete *vegan* (Oksanen et al., 2013) del software de código abierto R versión 3.6.2 con el paquete *ggplots* (Warnes et al., 2015).

3.5 Objetivo específico 3

Para cumplir con este objetivo, realizamos una parametrización del flujo de partículas, utilizando modelos teóricos para estimar los flujos verticales de exportación de POC desde la superficie hasta las profundidades hadalpelágicas. El modelo más común es la función de potencia normalizada conocida como "Curva de Martin" (Martin et al., 1987), que iguala el flujo de POC $f_p(z)$ [$\text{mg m}^{-2} \text{d}^{-1}$] a cualquier profundidad z [m] con el flujo de exportación (C) a la profundidad de referencia, es decir, en la base de la zona eufótica (E_z) según Buesseler et al. (2020):

$$f_p(z) := C(z/E_z)^{-b} \text{ (Ecuación 2)}$$

Utilizamos una E_z de 84,7 m (de entre 63 a 118 m de profundidad) según lo informado por Pizarro et al. (2002) para esta región. El coeficiente de atenuación (b), depende del equilibrio entre la velocidad de hundimiento de la POC w [m/día] y la tasa de remineralización k [1/día] (Middelburg, 2019). El valor de b sugerido para el océano Pacífico abierto es de 0,858 (Martin et al., 1987), mientras que se han sugerido valores similares para aguas oceánicas abiertas frente a Antofagasta (0,834; González et al., 2009). Sin embargo, también se han sugerido valores b más bajos (0,319) para la región de Perú y el Pacífico Norte tropical oriental debido al impacto de la deficiencia de oxígeno en la exportación de partículas (Van Mooy et al., 2002). En este estudio, utilizamos un rango de valores de b (0,36 a 1,33, $\bar{x} = 0,78$, $n = 13$) para calcular la atenuación del flujo como ha sugerido previamente Fernández-Urruzola et al. (2021). Dadas las incertidumbres inherentes a los modelos biogeoquímicos, probamos una serie de parametrizaciones, como el modelo exponencial básico (Banse, 1990), el modelo racional original de atenuación en profundidad (Suess, 1980) y el modelo exponencial doble (Lutz et al., 2002) para estimar un rango de valores de flujo de POC que alcanzan profundidades hadales. A continuación, comparamos estas estimaciones con los flujos de POC publicados en la región derivados de trampas de sedimentos ancladas (Hebbeln et al., 2002; González et al., 2004), trampas de sedimentos a la deriva (Wakeham et al., 1984), y muestras de partículas basadas en isótopos normalizados de ^{230}Th (Pavia et al., 2019).

Finalmente para evaluar la contribución relativa de las fuentes potenciales de MO hacia los sedimentos superficiales de la Fosa de Atacama utilizamos un modelo de mezcla isotópico, MixSIAR (Versión 3.2.0) según Stock et al. (2018).

4. RESULTADOS

4.1. **Capítulo 1:** “Los lípidos polares intactos de bacterias y eucariotas apuntan a la producción *in situ* como fuente clave de materia orgánica lábil en el sedimento superficial hadal de la Fosa de Atacama”. Artículo científico publicado en la revista “*Biogeosciences*” 19, 1395–1420, 2022. <https://doi.org/10.5194/bg-19-1395-2022>

Resumen

Los sedimentos superficiales del entorno hadal presentan elevadas concentraciones de materia orgánica (MO) en comparación con la zona abisal circundante. Sin embargo, el origen de este material biológico sigue siendo incierto. En este trabajo se estudia la composición y distribución de los lípidos polares intactos (IPL) de las membranas celulares extraídos de los sedimentos superficiales de los puntos más profundos de la Fosa de Atacama y del margen batial adyacente, con el fin de evaluar y restringir las fuentes de MO lábil en el fondo marino hadal. El análisis bootstrap de la diversidad estructural y abundancia de IPLs indica distintas señales lipídicas en los sedimentos de la Fosa de Atacama que están más estrechamente relacionadas con las encontradas en los sedimentos batiales que con las reportadas previamente para la columna de agua oceánica superior en la región. Mientras que el número total de estructuras IPL únicas en los sedimentos hadales contribuye en una pequeña fracción a la reserva total de IPL, también reportamos una alta contribución de fosfolípidos con ácidos grasos mono- y di-insaturados que no están asociados con fuentes fotoautotróficas y que se asemejan a rasgos de adaptación fisiológica a alta presión y baja temperatura. Nuestros resultados indican que los IPLs en los sedimentos hadales superficiales de la Fosa de Atacama provienen predominantemente de la producción microbiana *in situ* y de la biomasa, mientras que la exportación del componente lipídico más lábil de la reserva de MO de la zona eufótica y de la zona deficiente de oxígeno suprayacente es despreciable. Aunque no se pueden descartar otras fuentes de MO, como el transporte descendente y/o lateral de la MO lábil, que quedan por estudiar, es probable que sean menos importantes en vista de la labilidad de los IPL con enlaces éster. Nuestros resultados contribuyen a la comprensión de los mecanismos que controlan el transporte de MO lábil a este ecosistema extremo de aguas profundas. Además, proporcionan información sobre la posible adaptación fisiológica de la

comunidad microbiana *in situ* a la alta presión y la baja temperatura mediante la remodelación lipídica.



Bacterial and eukaryotic intact polar lipids point to in situ production as a key source of labile organic matter in hadal surface sediment of the Atacama Trench

Edgart Flores^{1,2,3}, Sebastian I. Cantarero⁴, Paula Ruiz-Fernández^{1,2,3}, Nadia Dildar⁴, Matthias Zabel⁵, Osvaldo Ulloa^{2,3}, and Julio Sepúlveda^{3,4}

¹Programa de Postgrado en Oceanografía, Departamento de Oceanografía, Facultad de Ciencias Naturales y Oceanográficas, Universidad de Concepción, Concepción, Chile

²Departamento de Oceanografía, Universidad de Concepción, Casilla 160-C, Concepción, Chile

³Millennium Institute of Oceanography, Universidad de Concepción, Concepción, Chile

⁴Department of Geological Sciences and Institute of Arctic and Alpine Research, University of Colorado Boulder, Boulder, CO 80309, USA

⁵MARUM – Center for Marine Environmental Sciences and Department of Geosciences, University of Bremen, 28334 Bremen, Germany

Correspondence: Edgart Flores (edgart.flores@imo-chile.cl) and Julio Sepúlveda (jsepulveda@colorado.edu)

Received: 30 August 2021 – Discussion started: 3 September 2021

Revised: 27 December 2021 – Accepted: 8 January 2022 – Published: 8 March 2022

Abstract. Elevated organic matter (OM) concentrations are found in hadal surface sediments relative to the surrounding abyssal seabed. However, the origin of this biological material remains elusive. Here, we report on the composition and distribution of cellular membrane intact polar lipids (IPLs) extracted from surface sediments around the deepest points of the Atacama Trench and adjacent bathyal margin to assess and constrain the sources of labile OM in the hadal seabed. Multiscale bootstrap resampling of IPLs' structural diversity and abundance indicates distinct lipid signatures in the sediments of the Atacama Trench that are more closely related to those found in bathyal sediments than to those previously reported for the upper ocean water column in the region. Whereas the overall number of unique IPL structures in hadal sediments contributes a small fraction of the total IPL pool, we also report a high contribution of phospholipids with mono- and di-unsaturated fatty acids that are not associated with photoautotrophic sources and that resemble traits of physiological adaptation to high pressure and low temperature. Our results indicate that IPLs in hadal sediments of the Atacama Trench predominantly derive from in situ microbial production and biomass, whereas the export of the most labile lipid component of the OM pool from the euphotic zone and the overlying oxygen minimum zone is ne-

glectable. While other OM sources such as the downslope and/or lateral transport of labile OM cannot be ruled out and remain to be studied, they are likely less important in view of the lability of ester-bond IPLs. Our results contribute to the understanding of the mechanisms that control the delivery of labile OM to this extreme deep-sea ecosystem. Furthermore, they provide insights into some potential physiological adaptation of the in situ microbial community to high pressure and low temperature through lipid remodeling.

1 Introduction

The deep ocean has been classically considered a vast “biological desert” (Danovaro et al., 2003) due to the attenuation of organic matter (OM) fluxes with increasing depth (Wakeham et al., 1984; Martin et al., 1987; Hedges et al., 2001; Rex et al., 2006). However, hadal trenches (~6000–11 000 m below sea level) contradict this paradigm (Danovaro et al., 2003; Glud et al., 2013; Leduc et al., 2016; Wenzhöfer et al., 2016; Luo et al., 2017), as they act as depocenters of OM (Jahnke and Jahnke, 2000) and hotspots for microbial activity (Glud et al., 2013; Wenzhöfer et al., 2016; Liu et

al., 2019). Indeed, OM availability is considered the major factor controlling the abundance, biomass, and diversity of life in the deep ocean (Danovaro et al., 2003; Ichino et al., 2015), whereas hydrostatic pressure appears to be an important and additional factor controlling biological activity in hadal trench systems (Jamieson et al., 2010; Tamburini et al., 2013). However, our understanding of the composition, sources, and lability of OM in marine trenches remains limited. According to Xu et al. (2018), the main sources of OM to the hadal zone include (1) the vertical sinking of particulate OM (POM), (2) the carrion falls of dead bodies, (3) inputs of terrestrial OM, (4) downslope transport of OM from continental slopes, and (5) *in situ* chemosynthetic production associated with cold seeps or hydrothermal vents. Several studies have highlighted the importance of POM sinking mainly from the euphotic zone (Stockton and DeLaca, 1982; Angel, 1984; Gooday et al., 2010). In fact, POM fluxes measured at 4000 m in the North Pacific Subtropical Gyre reveal that a seasonal export pulse can exceed the mean annual flux by ~ 150 % (Poff et al., 2021). However, it is unknown whether such pulses reach the hadal sediments (6000–11 000 m). Downslope transport, on the other hand, can be facilitated by trench topography and gravity (Jahnke et al., 1990; Fischer et al., 2009; Inthorn et al., 2006; Ichino et al., 2015) and/or by earthquakes (Glud et al., 2013; Kioka et al., 2019), as recently reported in the Japan Trench (Schwestermann et al., 2021). Independent of the main sources of OM, which are spatially and temporally variable, the channeling of allochthonous OM to the hadal zone should be facilitated by the characteristic V-shape cross-section of trenches, unique tectonic position in the ocean, and the physiography of the canyons that connect to coast systems (Itou et al., 2000, 2011; Bao et al., 2018). Additionally, autochthonous OM sources include *in situ* microbial biomass production (Smith, 2012; Nunoura et al., 2016; Ta et al., 2019; Hand et al., 2020), although their overall contribution as a secondary input to carbon budgets and energy flow in these systems remains poorly constrained (Grabowski et al., 2019). The spatial variations in community structure seen in benthic prokaryotic populations in hadal regions such as the Mariana, Japan, and Izu-Ogasawara trenches have been attributed to the variability of biogeochemical conditions, mainly nitrate and oxygen availability (Hiraoka et al., 2020), with benthic oxygen consumption exhibiting heterogeneity (Glud et al., 2021). Recent metagenomic data have revealed the presence of abundant heterotrophic microorganisms in sediments of the Challenger Deep (Nunoura et al., 2018), which are likely fueled by the endogenous recycling of available OM (Nunoura et al., 2015; Tarn et al., 2016). Furthermore, the abundance of prokaryotes in hadal depths can be influenced by dynamic depositional conditions (Schauberger et al., 2021), which in turn may be influenced by the intensity of propagating internal tides (Turnewitsch et al., 2014). All these factors likely alter the deposition, distribution, and composition of OM present in trench sediments.

An alternative approach to study microbial processes and the contribution of autochthonous OM is the use of cell membrane intact polar lipids (IPLs), which although less specific than genomic markers, allow for more quantitative estimates of microbial biomass in nature (e.g., Lipp et al., 2008; Schubotz et al., 2009; Cantarero et al., 2020). IPLs are composed of a polar head group typically attached to a glycerol backbone from which aliphatic chains are attached via ester and/or ether bonds (Sturt et al., 2004). Their structural diversity is given by the modifications found in the different components of their chemical structure (e.g., polar head groups can be comprised of phosphorous, nitrogen, sulfur, sugars, and amino acids), whereas aliphatic chains (alkyl or isoprenoidal) can vary in their length (number of carbon atoms) and their degree of unsaturation, methylation, hydroxylation, and cyclization (Van Mooy and Fredricks, 2010; Brandsma et al., 2012; Schubotz et al., 2013). In bacteria and eukaryotes, alkyl chains are most commonly linked via an ester bond to the *sn*-glycerol-3-phosphate backbone (Koga and Morii, 2007), although some bacteria are known to produce di- and tetraether lipids (Weijers et al., 2007). The variability of membrane chemical structures underlies the adaptability of microbial lifestyles to changing environmental conditions such as nutrients, temperature, oxygen, pH, and pressure (DeLong and Yayanos, 1985; Somero, 1992; Van Mooy et al., 2009; Carini et al., 2015; Sebastián et al., 2016; Siliakus et al., 2017; Boyer et al., 2020). Furthermore, since eukaryotic and bacterial ester-bond IPLs are more labile than ether-bond counterparts (Logemann et al., 2011), they are suitable biomarkers to evaluate sources of labile OM in marine environments.

IPLs have been previously used as microbial markers in diverse marine settings, such as along strong redox gradients in the Black Sea (Schubotz et al., 2009) and the oxygen minimum zones (OMZs) of the eastern tropical Pacific (Schubotz et al., 2018; Cantarero et al., 2020) and the Arabian Sea (Pitcher et al., 2011), as well as in surface open-ocean waters of the eastern South Pacific (Van Mooy and Fredricks, 2010), the northwestern Atlantic (Popendorf et al., 2011b), and the Mediterranean Sea (Popendorf et al., 2011a), to name a few. Their utility as markers of microbial diversity and processes has also been tested in marine sediments (Liu et al., 2011, 2012; Sturt et al., 2004), such as along the Peru margin, equatorial Pacific, Hydrate Ridge, and Juan de Fuca Ridge (Lipp and Hinrichs, 2009a), and in subsurface sediment layers from the Peru margin (Biddle et al., 2006). However, to the best of our knowledge, no IPL studies have been reported for sediments of hadal trenches.

In this study, we investigate the chemical diversity and abundance of microbial IPLs as markers of one of the most labile molecular fractions of OM in sediments of the deepest points of the Atacama Trench and compare them to IPL stocks in bathyal surface sediments (~ 500–1200 m) and the overlying 700 m of the water column (Cantarero et al., 2020). More specifically, we evaluate possible IPL provenance (in

situ vs. allochthonous production) and the presence of unique IPL signatures of the in situ microbial community as well as evidence for molecular adaptations to the extreme conditions of the hadal region.

2 Material and methods

2.1 Study areas and sampling

The Atacama Trench is located in the eastern tropical South Pacific (ETSP) along the Peru–Chile margin, and it underlies the eutrophic and highly productive Humboldt Current System (Angel, 1982; Ahumada, 1989), which includes the fourth largest (by volume) oxygen minimum zone (OMZ) in the world (Schneider et al., 2006). In this area, while there is minimal river runoff (Houston, 2006), winds can transfer dust from the adjacent continental desert (Angel, 1982). With an extension of ~5900 km, the Atacama Trench is the world's largest trench (Sabbatini et al., 2002), whereas it is geographically isolated from other trenches in the Pacific Ocean.

In this study, we investigated the diversity and abundance of bacterial and eukaryotic IPLs in a total of nine hadal surface (0–1 cm) and subsurface (1–2 and 2–3 cm) sediments (three sites between 7734 and 8063 m water depth) collected during the HADES-SO261 cruise (March to April 2018) aboard the RV *Sonne* (Wenzhöfer, 2019) and seven bathyal surface sediments (seven sites; 529–1200 m water depth) collected during the ChiMeBo-SO211 cruise (2–29 November 2010) aboard the RV *Sonne* (Matys et al., 2017) (Table 1; Fig. 1). We compare our results against IPL results from the overlying water column (0–700 m) recently reported in Cantarero et al. (2020).

Sediment samples were collected using a multi-corer (MUC) equipped with twelve 60 cm long acrylic tubes (6–10 cm diameter for bathyal sediments and 9.5 cm diameter for hadal sediments). During the HADES expedition, an autonomous lander equipped with a Sea-Bird SBE-19 plus CTD and two Niskin bottles (30 L) was used to obtain hydrographic data down to ~7850 m. Hadal sediments from the HADES-SO261 cruise were stored at 4 °C until they were extruded and subsampled aboard at 1 cm resolution and then kept frozen at –20 °C until their processing in the laboratory. Further information about sample collection of bathyal and hadal sediments during the ChiMeBo-SO211 and HADES-SO261 cruises can be found in Matys et al. (2017) and Wenzhöfer et al. (2019), respectively.

We compare our IPL results from surface sediment in the hadal and bathyal regions against samples from the overlying water column from the LowpHOX-2 cruise recently reported by Cantarero et al. (2020). This includes size-fractionated suspended OM (0.3–2.7 and 2.7–53 µm) at two stations and from six water depths that are representative of the dominant biogeochemical zonation associated with the OMZ of this

Table 1. Sampling stations from the HADES, ChiMeBo, and LowpHOX-2 expeditions.

Cruise-RV	Device	Environment	Station	Environmental samples	Sampling depth (m)	Latitude (° S)	Longitude (° W)	Date (dd/mm/yyyy)	Reference
HADES <i>Sonne</i> SO261	Multi-corer (MUC)	Hadal sediments	A10	Hadal sediments (0–1, 1–2 and 2–3 cm)	7734	20.32	71.29	26/03/2018	This study
			A5	Hadal sediments (0–1, 1–2 and 2–3 cm)	7890	23.81	71.37	11/03/2018	
			A4	Hadal sediments (0–1, 1–2 and 2–3 cm)	8063	23.36	71.34	14/03/2018	
ChiMeBo <i>Sonne</i> SO211	Multi-corer (MUC)	Bathyal sediments	B12	Upper bathyal sediment (0–1 cm)	529	23.59	70.67	02–29/11/2010	This study
			B08	Upper bathyal sediment (0–1 cm)	539	25.2	70.68	02–29/11/2010	
			B22	Upper bathyal sediment (0–1 cm)	545	27.29	71.05	02–29/11/2010	
			B07	Lower bathyal sediment (0–1 cm)	920	25.07	70.66	02–29/11/2010	
			B05	Lower bathyal sediment (0–1 cm)	957	27.5	71.13	02–29/11/2010	
			B11	Lower bathyal sediment (0–1 cm)	1113	23.85	70.65	02–29/11/2010	
			B04	Lower bathyal sediment (0–1 cm)	1200	27.45	71.16	02–29/11/2010	
LowpHOX-2 <i>Cabo de Hornos</i>	Rosette (Niskin bottles)	Water column	T3/T5	Chlorophyll maximum (0.3–2.7 µm)	9–10	20.07/20.03	70.36/70.89	04–06/02/2018	Cantarero et al. (2020)
			T3/T5	Upper chemocline (0.3–2.7 µm)	25–28	20.07/20.03	70.36/70.89	04–06/02/2018	
			T3/T5	Lower chemocline (0.3–2.7 µm)	35–45	20.07/20.03	70.36/70.89	04–06/02/2018	
			T3/T5	Upper OMZ (0.3–2.7 µm)	55–60	20.07/20.03	70.36/70.89	04–06/02/2018	
			T3/T5	Core OMZ (0.3–2.7 µm)	250	20.07/20.03	70.36/70.89	04–06/02/2018	
			T3/T5	Mesopelagic zone (0.3–2.7 µm)	750	20.07/20.03	70.36/70.89	04–06/02/2018	

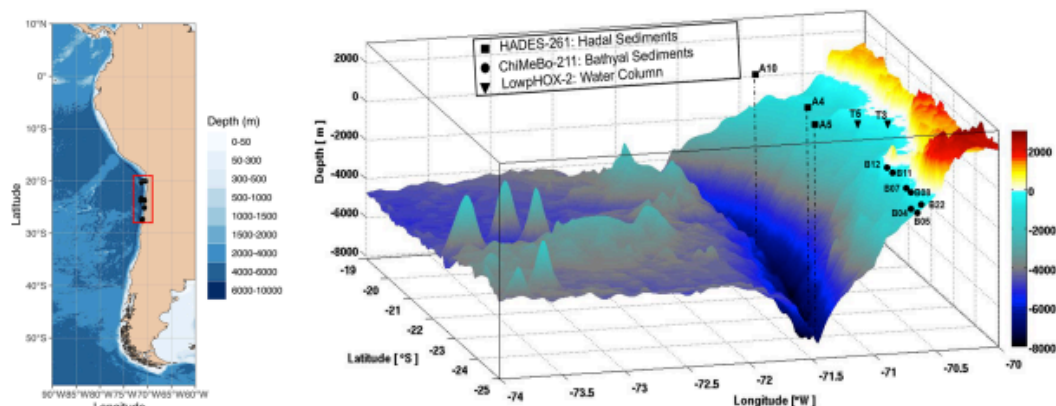


Figure 1. Three-dimensional map of the Atacama Trench showing the sampling locations of this study. The black squares indicate the hadal sediment sampling stations, the black circles indicate the bathyal sediment sampling stations from Matys et al. (2017), and the black triangles indicate water-column sampling stations from Cantarero et al. (2020).

region: chlorophyll maximum (~10 m), upper chemocline (~25 m), lower chemocline (~45 m), upper OMZ (~60 m), core OMZ (~250 m), and mesopelagic zone (~750 m) (see Table 1 and Cantarero et al., 2020, for further details).

2.2 Analytical methods

2.2.1 Lipid extraction

All samples were processed, extracted, and analyzed in the Organic Geochemistry Laboratory at the University of Colorado Boulder. Sediment samples were freeze-dried before extraction. Approximately 1–2 g of dry sediment was placed in a combusted glass centrifuge tube and extracted using a modified version (Wörmer et al., 2013) of the Bligh and Dyer extraction method (Bligh and Dyer, 1959) as detailed in Cantarero et al. (2020). Briefly, before extraction, we added 1 µg of C16 PAF (C₂₆H₅₄NO₇P) to each sample as an internal standard. Samples were sequentially extracted using dichloromethane/MeOH/phosphate buffer (1 : 2 : 0.8 v : v : v; 2×), dichloromethane/MeOH/trichloroacetic buffer (1 : 2 : 0.8 v : v : v; 2×), and dichloromethane/MeOH (1 : 5 v : v; 1×). After each addition, samples were vortexed for 30 s, sonicated for 10 min, and then centrifuged for 5 min at 2000 rpm. Each extraction was then transferred to a separatory funnel where a total lipid extract (TLE) was combined and then concentrated under a gentle N₂ stream. Before analysis, the TLEs were resuspended in dichloromethane/methanol (9 : 1) v : v and filtered through a 0.45 µm polytetrafluoroethylene (PTFE) syringe filter. The processing and extraction of bathyal sediments from the ChiMeBo-SO211 cruise and water-column samples from the LowPHOX-2 cruise has been reported by Matys et al. (2017)

and Cantarero et al. (2020), respectively. TLEs were transferred into 2 mL vials with 200 µL inserts and dissolved in 100 µL of dichloromethane/MeOH (9 : 1, v : v).

2.2.2 IPL analysis

IPL were analyzed according to Wörmer et al. (2013) and as described in Cantarero et al. (2020) using a Thermo Scientific UltiMate 3000 high-performance liquid chromatograph (HPLC) coupled to a Q Exactive Focus Orbitrap quadrupole high-resolution mass spectrometer (HPLC-HRMS) via electrospray ionization (ESI). The HPLC program comprised a flow rate of 0.4 mL min⁻¹ using a mixture of two mobile phases: mixture A consisted of acetonitrile/dichloromethane (75 : 25, v : v) with 0.01 % formic acid and 0.01 % NH₄OH; mixture B consisted of methanol/water (50 : 50, v : v) with 0.4 % formic acid and 0.4 % NH₄OH. We used a linear gradient as follows: 1 % mixture B (0–2.5 min), 5 % (4 min), 25 % mixture B (22.5 min), 40 % mixture B (26.5–27.5 min), and the HPLC column was kept at 40 °C. Samples were injected (10 µL) and dissolved in dichloromethane/methanol (9 : 1, v : v). IPLs were separated using a Waters Acquity BEH Amide column (2.1 × 150 mm; 1.7 µm particle size) that enables class-specific separation based on their hydrophilic head group (Wörmer et al., 2013).

ESI settings comprised sheath gas (N₂) pressure 35 (arbitrary units), auxiliary gas (N₂) pressure 13 (arbitrary units), spray voltage 3.5 kV (positive ion ESI), capillary temperature 265 °C, and S-lens RF level 55 (arbitrary units). The instrument was calibrated for mass resolution and accuracy using the Thermo Scientific Pierce LTQ Velos ESI Positive Ion Calibration Solution (containing a mixture of caffeine,

MRFA, Ultramark 1621, and N-butylamine in an acetonitrile / methanol / acetic acid solution).

IPLs were identified on positive ionization mode, on both full scan and data-dependent MS², based on their molecular weights as either protonated (M + H)⁺ or ammonium (M + NH₄)⁺ adducts compounds, fragmentation patterns, and retention times, and they were compared against relevant literature (Sturt et al., 2004; Schubotz et al., 2009; Wakeham et al., 2012) and the internal database of the Organic Geochemistry Laboratory at the University of Colorado Boulder.

The peak areas of individual IPLs were integrated using the Thermo Fisher Scientific TraceFinder software using extracted ion chromatograms of their characteristic molecular ions. IPL abundances were determined with a combination of an internal standard (C₁₆PAF, Avanti Polar Lipids) and an external calibration to a linear regression between peak areas and known concentrations of an IPL cocktail comprised of 17 different IPL classes across a five-point dilution series (0.001–2.5 ng μL) (see Cantarero et al., 2020). Deuterated standards (Avanti Polar Lipids: d7-PC, d7-PG, d7-PE, and DGTS-d9) were used to correct for potential matrix effects on ionization efficiency. Despite the limited number of available deuterated standards, on average, we observed that the matrix effect accounts for a loss of $7 \pm 0.6\%$ in ionization efficiency. Therefore, it is reasonable to assume a similar loss for other IPL classes, although this remains to be tested in future studies. We highlight the importance of using as many IPLs classes as possible to account for both differences in ionization efficiency and matrix effect when performing IPL quantification in environmental samples. The relative response factors followed the order MGDG > DGTS > DGTA > PDME > PME > PG > PC > PE > SQDG > DGCC > DGDG. Lipid classes were grouped into phospholipids (PG, phosphatidylglycerol; PE, phosphatidylethanolamine; PC, phosphatidylcholine; and PME/PDME, phosphatidyl(di)methylethanolamine), glycolipids (MGDG, monoglycosyldiacylglycerol; DGDG, diglycosyldiacylglycerol; and SQDG, sulfoquinovosyldiacylglycerol), betaine lipids (DGTA, diacylglyceryl hydroxymethyl-trimethyl-β-alanine; DGTS, diacylglyceryl trimethylhomoserine; and DGCC, diacylglycerylcarboxy-N-hydroxymethyl-choline), and other lipids (glycosidic ceramides, Gly-Cer; PI, phosphatidylinositol; and OL, ornithine lipids). In addition, we use DAG to designate a diacylglycerol and AEG to designate an acyletherglycerol, and we describe short and long chains to refer to combined alkyl chains of C_{28–36} and C_{36–44}, respectively (Rêzanka and Sigler, 2009; Schubotz et al., 2009; Brandsma, et al., 2012).

2.3 Statistical analyses

We used the Bray–Curtis similarity coefficient (Mirzaei et al., 2008) to produce hierarchical clustering of the abundance of classes and molecules of IPLs; two types of *p* val-

ues were available: approximately unbiased (AU) *p* value and bootstrap probability (BP) value with the number of bootstrap replications of 10 000 (Suzuki and Shimodaira, 2006). We performed non-metric multidimensional scaling (NMDS) (Warton et al., 2012) to examine the dissimilarity between the IPLs in each sample. The calculated distances to group centroids were based on the Bray–Curtis dissimilarity from the IPL abundance matrix, and the significance of the associations was determined by 999 random permutations. Significance tests of the multivariate dissimilarity between groups were made using analysis of similarity (ANOSIM), where complete separation and no separation among groups is suggested by *R* = 1 and *R* = 0, respectively (Clarke and Gorley, 2015). Statistical differences in the numbers of carbon atoms and double bonds were identified by ANOVA and Tukey's HSD (honestly significant difference) post hoc test. We used similarity of percentage (SIMPER) analysis to identify the percentage contributions of IPLs which accounted for > 90 % of the similarity within each cluster. The multivariate statistical analyses as well as other statistical analyses were calculated using the vegan package (Oksanen et al., 2013) of open-source software R version 3.6.2 within the ggplots package (Warnes et al., 2015).

3 Results

3.1 Hydrographic conditions

A physical–chemical characterization of the water column during the ChiMeBo-SO211, LowpHOX-2, and HADES-SO261 cruises has been reported in Matys et al. (2017), Cantarero et al. (2020) and Vargas et al. (2021), and Fernández-Urruzola et al. (2021), respectively. Briefly, the potential-temperature–salinity–dissolved oxygen (*θ-s-O₂*) diagrams revealed an oxygenated and well-mixed water mass occupying the deeper parts of the Atacama Trench (Fig. S1). However, the upper 1000 m shows variability in temperature (12–23 °C), salinity (34.4–34.8 psu), and oxygen (0.5–267 μM). More stable physical–chemical conditions are apparent in the mesopelagic and bathypelagic zone of the Atacama Trench between 1000 and 4000 m (temperature ~ 2.3 °C, salinity ~ 34.6 psu, oxygen ~ 120.6 μM). Below 4000 m, average conditions were characterized by a potential temperature ~ 1.8 °C, salinity ~ 34.7 psu, and oxygen ~ 143 μM (Fig. S1).

3.2 IPLs in surface sediments of the Atacama trench

3.2.1 Distribution of IPL classes by polar head groups

The 16 sediment samples from bathyal and hadal regions statistically grouped into four clusters based on their dominant polar head group classes (Fig. 2, chemical structures in Fig. S2). Clusters 1 and 2 had approximately unbiased (AU) *p* values of 91 % and 88 %, respectively. Cluster 3 had the

highest AU p value of $\geq 97\%$, whereas cluster 4 had the lowest AU p value of 61% . The cluster analysis revealed a degree of spatial heterogeneity between bathyal and hadal depths and between the top three centimeters of hadal sediments, which results in the lack of a clear separation between hadal and bathyal environments. In addition, the 0–1 cm hadal sediments at the A4 station were un-clustered, consistent with a distinct distribution pattern of IPL classes. Cluster 1, composed of only hadal samples from three different stations and depths, included phospholipids as the most abundant IPL class (Fig. 2). Clusters 2, 3, and 4, composed of mixed bathyal and hadal samples, were mostly differentiated by changes in the relative abundances of non-phosphorous IPLs including betaine classes. The un-clustered sample was characterized by the lowest relative abundance of phospholipids and the highest relative abundance of betaine lipids (especially DGCC).

3.2.2 Distribution of individual IPLs

An overview of the most important IPLs contributing to dissimilarity between samples was obtained through a SIMPER analysis based on the Bray–Curtis coefficient within each cluster (Fig. 3). Samples in cluster 1 were on average 59.5% similar, with 14 individual IPLs contributing 50.6% of the total similarity. This cluster exhibited a high contribution of PE-DAG (32 : 1, 33 : 1, and 34 : 2), PG-DAG (36 : 2), and DGCC (26 : 0, 27 : 0, and 28 : 0) molecules (Table 2). Additionally, this cluster exhibited a large diversity of PC molecules, although with a low relative abundance (Fig. 3). Samples in cluster 2, on the other hand, which includes mainly bathyal stations, were on average 58.8% similar and exhibited a high contribution of PC-DAG (35 : 0, 32 : 1, 36 : 2, 33 : 1, and 35 : 1) (Table 2). While this cluster shows a wide range of molecules, including PG, PE, and MGDG, their relative contributions are low (Fig. 3). Samples in cluster 3 were on average 57.3% similar and included three bathyal and one hadal stations. This cluster exhibited a high contribution of DGCC (42 : 6) and PC-DAG (35 : 0, 33 : 2, 30 : 1, and 29 : 2) molecules (Table 2). Samples in cluster 4 were on average 63.6% similar and exhibited a high contribution of PC-DAG (30 : 2, 33 : 2), DGCC (42 : 6), MGDG (28 : 0), and PE-DAG (33 : 2 and 31 : 2) molecules (Table 2). The un-cluster sample (hadal sediment of 0–1 cm at A4 station) is mainly composed by the DGCC 42 : 6 (Fig. 3). In general, phospholipids showed a wide distribution and were found across all sediment samples. The total dissimilarity between cluster 1 and 2 was 59.17% , with PC-DAG-35 : 0, PE-DAG-32 : 1, PI-AR, PG-DAG-36 : 2, DGCC 27 : 0, PC-DAG-36 : 2, PC-DAG-34 : 1, PC-DAG-32 : 1, DGCC 26 : 0, and PC-DAG-35 : 1 contributing 32.4% of it (Table 2). The total dissimilarity between cluster 1 and 3 was 60.7% , with DGCC 42 : 6, PC-DAG-35 : 0, PI-AR, PE 32 : 1, PG-DAG-36 : 2, DGCC 27 : 0 and 26 : 0, and PC-DAG-33 : 2 contributing 38.1% of it (Table 2). The total dissimilarity be-

tween cluster 1 and 4 was 62.5% , with DGCC 42 : 6, PC-DAG-30 : 2, PE 32 : 1, PC-DAG-35 : 0, PG-DAG-36 : 2, PC-DAG-33 : 2, and DGCC 27 : 0 contributing 37.62% of it (Table 2).

3.3 Distribution of alkyl chains based on length and degree of unsaturation

The difference in the total number of acyl carbon atoms in both alkyl chains, rather than in individual fatty acids, and in the number of acyl double bonds within each cluster is shown in Fig. 4. Statistical differences of IPLs classes within each cluster were obtained through a Tukey HSD post hoc test at a significant level of $p < 0.05$ (Fig. 4a, b). The average number of carbon atoms in the diglyceride moieties of IPLs in the cluster 1 presented that DGCC, MGDG, others, PC, and PG were all distinct from one another ($n = 283$; $P < 0.05$; Fig. 4a). PG and others were characterized by relatively long alkyl chains (35–36 C atoms, respectively) and DGCC for shorter alkyl chains (32 C atoms). In general, cluster 1 exhibited a wide range of chain lengths among DAGs (28–36 C atoms). Cluster 2 showed a narrower range than cluster 1 (30–36 C atoms). This cluster also displayed no statistical difference ($p > 0.05$) among IPL classes (Fig. 4a), following pairwise comparisons with Tukey's HSD post hoc test, despite the wide range of DGCC structures. For cluster 3, while it exhibited low variability in betaine lipids, it also revealed the highest number of carbon atoms in DGCCs (42). On the contrary, cluster 4 presented high variability in DGCCs, which did not exceed 42 carbon atoms. Within the phospholipid class, PG showed the highest number of carbon atoms in all clusters; the mean we observed was 34 carbon atoms and a range of 32–37 (Fig. 4a). The un-cluster sample (hadal sediment of 0–1 cm at A4 station) was characterized by relatively longer alkyl chains (up to 42 C atoms) than cluster 1 (Fig. 4a).

Overall, the degree of unsaturation (i.e., number of double bonds) within clusters was variable (Fig. 4b). Cluster 1 predominantly consisted of fully saturated and mono-unsaturated IPLs, except for PG that showed 2 double bonds on average. In cluster 2, the fatty acids of DGCCs were distinctly variable, although they exhibited 2 unsaturations on average. A similar pattern was observed in DGDGs with an average of 2.5 unsaturations (Fig. 4b). DGTS, MGDG, PC, and SQDG showed zero to 1 unsaturation, whereas DGTA, PE, and PG exhibited between 1 and 2.5 unsaturations. Cluster 3 showed more than 5 unsaturations on average for DGCC, unlike other IPL classes that did not exceed 2 unsaturations. In cluster 4, PG and DGCC presented ~ 3 and ~ 5 unsaturations on average. Also, on average, DGDG and SQDG exhibited 2 unsaturations, MGDG and others were mono-unsaturated, and DGTS was saturated (Fig. 4b). Additionally, the ratio of total unsaturated fatty acids to total saturated fatty acids in IPLs increased from (on average) ~ 0.9 in

Table 2. Similarity percentage (SIMPER) analysis. The average abundance and contribution of IPLs that explain the main differences among the sediment samples is based on the hierarchical clusters shown in Fig. 2.

Group cluster 1					
Cluster 1: average similarity = 59.53					
IPLs	Average cluster 1	Average similarity	Similarity/SD	Contribution (%)	Cumulative (%)
PI-AR	0.06	4.76	2.46	7.99	7.99
PE-DAG-32 : 1	0.06	4.37	1.45	7.34	15.33
PG-DAG-36 : 2	0.05	3.79	2	6.36	21.69
PE-DAG-33 : 1	0.03	2.06	33.49	3.45	25.14
PE-DAG-34 : 2	0.03	1.89	1.74	3.17	28.31
DGCC-26 : 0	0.04	1.84	2.04	3.09	31.4
PC-DAG-30 : 1	0.03	1.76	2.21	2.96	34.36
DGCC-27 : 0	0.04	1.74	1.8	2.93	37.3
PE-DAG-30 : 0	0.02	1.7	13.1	2.86	40.15
PE-DAG-32 : 2	0.02	1.39	1.07	2.34	42.49
PC-DAG-35 : 0	0.02	1.31	1.52	2.2	44.69
DGCC-28 : 0	0.02	1.22	1.96	2.05	46.74
PC-DAG-26 : 0	0.02	1.18	1.46	1.99	48.73
PC-DAG-28 : 0	0.02	1.14	1.59	1.91	50.63
Group cluster 2					
Cluster 2: average similarity = 58.79					
IPLs	Average cluster 2	Average similarity	Similarity/SD	Contribution (%)	Cumulative (%)
PC-DAG-35 : 0	0.08	5.63	7.54	9.58	9.58
PC-DAG-32 : 1	0.03	3.12	31.24	5.3	14.88
PC-DAG-36 : 2	0.05	2.74	1.13	4.67	19.55
PC-DAG-33 : 1	0.02	2.04	10.17	3.46	23.01
PC-DAG-35 : 1	0.03	1.63	4.48	2.77	25.78
PI-AR	0.02	1.61	3.9	2.74	28.53
MGDG-32 : 1	0.02	1.44	1.35	2.45	30.98
PE-DAG-32 : 1	0.02	1.38	5.03	2.35	33.33
PE-DAG-34 : 2	0.02	1.38	2.75	2.35	35.68
PE-DAG-32 : 2	0.02	1.22	2.79	2.08	37.76
PC-DAG-32 : 0	0.01	1.14	5.69	1.94	39.69
PG-DAG-36 : 2	0.02	1.1	3.23	1.87	41.57
PG-DAG-35 : 2	0.02	1.09	1.23	1.86	43.43
PC-DAG-34 : 1	0.04	1.06	0.41	1.8	45.23
PC-DAG-30 : 1	0.01	1.05	7.23	1.79	47.02
PC-DAG-32 : 2	0.01	0.95	11.7	1.61	48.64
PC-DAG-29 : 2	0.01	0.95	2.69	1.61	50.25
Group cluster 3					
Cluster 3: average similarity = 57.31					
IPLs	Average cluster 3	Average similarity	Similarity/SD	Contribution (%)	Cumulative (%)
DGCC-42 : 6	0.16	12.84	6.72	22.4	22.4
PC-DAG-35 : 0	0.08	4.78	1.14	8.33	30.74
PC-DAG-33 : 2	0.03	2.07	1.19	3.61	34.35
PC-DAG-30 : 1	0.03	1.96	1.82	3.42	37.77
PC-DAG-29 : 2	0.03	1.79	1.2	3.12	40.89
PI-AR	0.05	1.69	1.09	2.95	43.84
MGDG-32 : 1	0.01	1.22	7.66	2.14	45.98
PE-DAG-32 : 1	0.01	1.18	10.45	2.05	48.03
PC-DAG-30 : 0	0.02	1.13	1.22	1.97	50

Table 2. Continued.

Group cluster 1						
Cluster 1: average similarity = 59.53						
IPLs	Average cluster 1	Average similarity	Similarity/SD	Contribution (%)	Cumulative (%)	
Group cluster 4						
Cluster 4: average similarity = 63.64						
IPLs	Average cluster 2	Average similarity	Similarity/SD	Contribution (%)	Cumulative (%)	
PC-DAG-30 : 2	0.12	9.04		14.21	14.21	
DGCC-42 : 6	0.14	8.91		13.99	28.2	
PI-AR	0.05	4.14		6.5	34.71	
PC-DAG-33 : 2	0.04	3.71		5.83	40.54	
MGDG-28 : 0	0.04	3.44		5.41	45.95	
PE-DAG-33 : 2	0.03	2.52		3.97	49.92	
PE-DAG-31 : 2	0.03	2.14		3.37	53.28	
Groups cluster 1 and cluster 2						
Average dissimilarity = 59.17						
IPLs	Average cluster 1	Average cluster 2	Average dissimilarity	Dissimilarity/SD	Contribution (%)	Cumulative (%)
PC-DAG-35 : 0	0.02	0.08	3.18	1.34	5.37	5.37
PE-DAG-32 : 1	0.06	0.02	2.35	1.73	3.98	9.35
PI-AR	0.06	0.02	2.21	1.74	3.73	13.08
PG-DAG-36 : 2	0.05	0.02	1.98	1.64	3.35	16.43
DGCC-27 : 0	0.04	0	1.93	1	3.26	19.69
PC-DAG-36 : 2	0.01	0.05	1.79	1.57	3.02	22.71
PC-DAG-34 : 1	0	0.04	1.79	1.03	3.02	25.73
PC-DAG-32 : 1	0.01	0.03	1.36	5.58	2.3	28.03
DGCC-26 : 0	0.04	0.01	1.34	0.95	2.27	30.3
PC-DAG-35 : 1	0.01	0.03	1.27	0.9	2.15	32.45
PE-DAG-33 : 1	0.03	0.01	1.02	1.2	1.73	34.18
PC-DAG-33 : 1	0	0.02	0.96	7.61	1.63	35.8
DGCC-28 : 0	0.02	0	0.93	1.28	1.57	37.37
PC-AEG-34 : 3	0.02	0	0.9	1.03	1.52	38.89
PE-DAG-34 : 2	0.03	0.02	0.88	1.2	1.49	40.38
MGDG-32 : 1	0	0.02	0.83	1.81	1.4	41.78
PC-DAG-30 : 1	0.03	0.01	0.83	1.15	1.4	43.18
PG-DAG-34 : 2	0.02	0	0.77	1.05	1.3	44.48
PE-DAG-33 : 0	0.02	0	0.76	1.11	1.29	45.77
PG-DAG-35 : 1	0.02	0.01	0.74	1.22	1.26	47.03
PE-DAG-34 : 1	0.02	0	0.74	2.06	1.25	48.27
PC-DAG-26 : 0	0.02	0	0.72	1.74	1.21	49.48
DGCC-30 : 0	0	0.01	0.68	1.32	1.15	50.64

Table 2. Continued.

Groups cluster 1 and cluster 3 Average dissimilarity = 60.69						
IPLs	Average cluster 1	Average cluster 3	Average dissimilarity	Dissimilarity/SD	Contribution (%)	Cumulative (%)
DGCC-42 : 6	0	0.16	8.02	3.2	13.21	13.21
PC-DAG-35 : 0	0.02	0.08	3.05	1.87	5.02	18.23
PI-AR	0.06	0.05	2.66	1.6	4.39	22.62
PE-DAG-32 : 1	0.06	0.01	2.49	1.74	4.1	26.72
PG-DAG-36 : 2	0.05	0.02	1.9	1.49	3.14	29.86
DGCC-27 : 0	0.04	0.01	1.84	0.97	3.03	32.89
DGCC-26 : 0	0.04	0.01	1.59	1.12	2.62	35.52
PC-DAG-33 : 2	0	0.03	1.58	1.7	2.61	38.12
PE-DAG-34 : 2	0.03	0.01	1.13	1.35	1.86	39.98
PE-DAG-33 : 1	0.03	0.01	1.07	1.33	1.76	41.75
PC-AEG-34 : 3	0.02	0	0.95	1.08	1.57	43.31
PC-DAG-29 : 2	0.02	0.03	0.95	1.88	1.56	44.87
DGCC-28 : 0	0.02	0	0.9	1.25	1.49	46.36
PC-DAG-30 : 1	0.03	0.03	0.87	1.35	1.43	47.79
PE-DAG-33 : 0	0.02	0	0.76	1.07	1.26	49.05
PG-DAG-34 : 2	0.02	0.01	0.76	1.1	1.26	50.3
Groups cluster 1 and cluster 4 Average dissimilarity = 62.47						
IPLs	Average cluster 1	Average cluster 4	Average dissimilarity	Dissimilarity/SD	Contribution (%)	Cumulative (%)
DGCC-42 : 6	0	0.14	6.99	2.57	11.19	11.19
PC-DAG-30 : 2	0.01	0.12	5.66	3.64	9.06	20.24
PE-DAG-32 : 1	0.06	0	3.17	2.09	5.07	25.31
PC-DAG-35 : 0	0.02	0.04	2.22	1.6	3.55	28.86
PG-DAG-36 : 2	0.05	0.01	2.12	1.64	3.4	32.27
PC-DAG-33 : 2	0	0.04	1.9	15.16	3.04	35.3
DGCC-27 : 0	0.04	0.02	1.45	0.78	2.32	37.62
PE-DAG-34 : 2	0.03	0	1.35	1.44	2.16	39.78
PI-AR	0.06	0.05	1.3	1.6	2.08	41.86
DGCC-26 : 0	0.04	0.01	1.26	0.89	2.02	43.88
DGDG-34 : 2	0	0.03	1.25	1.17	2	45.88
PE-DAG-31 : 2	0	0.03	1.21	4.58	1.93	47.81
PE-DAG-33 : 1	0.03	0.01	1.2	1.46	1.92	49.73
PE-DAG-33 : 3	0	0.02	1.16	4.61	1.86	51.59

all water-column samples (2–76 bar) to ~2.7 in the bathyal (54–113 bar) and hadal sediments (777–810 bar) (Fig. 5).

3.4 Unique IPLs in hadal sediments of the Atacama Trench

Water-column particles and bathyal–hadal sediments shared 242 (96.1 %) IPL structures (Fig. 6a), while hadal sediments and water-column particles shared 14 (0.02 %), and hadal and bathyal sediments shared 55 (3.6 %). Of all the analyzed IPLs reported in this study, eight of them were unique to the Atacama Trench sediments and are not present in shallower sediments or the overlying water column. They include

five glycolipids (SQDG-42 : 11, SQDG-23 : 0, DGDG-35 : 1, DGDG-35 : 2 and DGDG-37 : 1), two phosphatidylinositols (PI-diOH-Ext-AR and PI-OH-AR), and one ornithine lipid (OL-37 : 6). While unique to hadal sediments, their total concentration was low (~53.32 ng per gram of sediment), and they contributed ~0.00012 % of the total IPL pool (Fig. 6a). We then performed a cluster analysis to compare IPLs in deep-sea surface sediments against IPLs reported in the overlying water column (Cantarero et al., 2020; Fig. 6b). Cluster 1 comprised samples from the core OMZ in the free-living fraction (AU *p* value of 100 %). Cluster 2 comprised samples from both the upper and lower oxyclines (~14–60 m) as well as from the chlorophyll maximum (AU

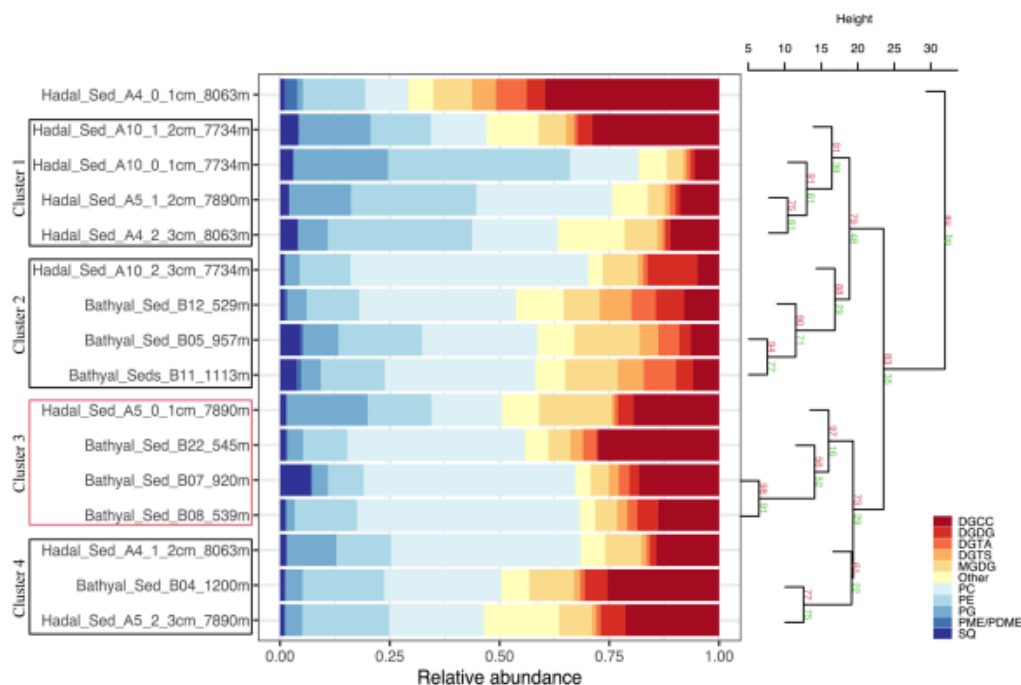


Figure 2. Cumulative bar charts of the fractional abundance of IPL classes in each surface sediment sample from the bathyal and hadal regions (left panel). Samples were grouped according to arithmetic mean (UPGMA) hierarchical clustering based on Euclidean distances. The p values are shown at branches, with AU in red and BP in green (right panel). Clusters 3 with an AU $\geq 95\%$ confidence are indicated by the red rectangles (left) and are considered to be strongly supported by the data.

p value of 99 %). Cluster 3 comprised bathyal and hadal samples (AU p value of 99 %). Cluster 4 mostly comprised the deepest water-column sample (mesopelagic region at 750 m) and hadal samples (AU p value of 98 %; Fig. 6b). We also compared IPLs in hadal and bathyal sediments against the pool of IPLs reported as diagnostic of the planktonic community inhabiting the chlorophyll maximum in the upper water column (Cantarero et al., 2020) and thus assess their export and stability through their transit to the deep sea. Notably, these IPLs from this region of the water column only represent $\sim 0.001\%$ – 0.005% and 0.002% – 0.03% of the total IPL pool in hadal and bathyal sediments, respectively (Fig. S3).

We found a high degree of heterogeneity in total IPL concentrations among sites and different sediment levels (0–1, 1–2, 2–3 cm) in the Atacama Trench, which were an order of magnitude higher than bathyal sediments (see Fig. S4a, b). Hadal sediments at station A10 (7734 m) showed a large range of phospholipid concentrations (~ 47 – 2698 ng per gram of sediment) (Fig. S4b). Although the highest total IPL abundances were observed at hadal station A10 (Fig. S4b), the greatest diversity in IPL composition was observed in the

0–1 cm of the hadal station A4, previously referred to as unclustered (see Fig. 2). The most abundant IPL class in hadal sediments was phospholipids, PCs (~ 41 – 2698 ng per gram of sediment), PEs (~ 26 – 1813 ng per gram of sediment), and PGs (5 – 937 ng per gram of sediment). The concentration of IPLs normalized by total organic carbon (TOC) (ng IPL per gram of TOC) showed maximum values in the hadal station A10 (~ 497 μg IPL per gram of TOC), followed by lower values in the hadal stations A5 and A4 of ~ 291 and ~ 75 μg IPL per gram of TOC, respectively (Fig. S5).

4 Discussion

4.1 Potential sources of phospholipids

PG (phosphatidylglycerol)

Phospholipids are common constituents of cellular membranes in most microorganisms (Ratledge and Wilkinson, 1988). Since PGs play an essential role in photosynthesis (Wada and Murata, 2007), they have therefore been mainly

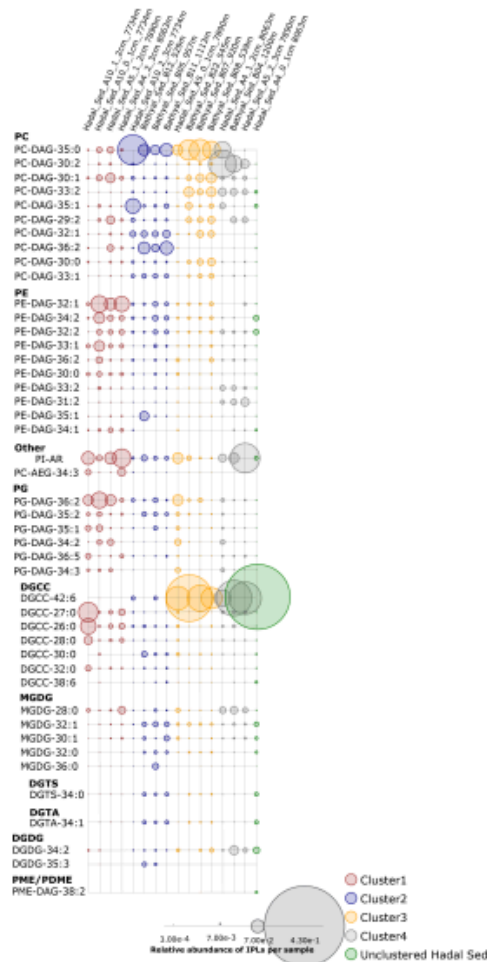


Figure 3. Relative abundance of individual IPLs contributing most of the dissimilarity between the four clusters shown in Fig. 2. Sampling stations are organized left to right and are shown using the same order from hierarchical clusters in Fig. 2, whereas IPL classes are organized from top to bottom. The circle size is proportional to the relative abundance of IPLs in each sample (bottom panel).

identified in algal and bacterial photoautotrophs (Dowhan, 1997; Sato et al., 2000; Gombos et al., 2002). However, their biological origin is highly diverse and also includes heterotrophic bacteria (Oliver and Colwell, 1973; Van Mooy et al., 2009; Pependorf et al., 2011b; Carini et al., 2015; Sebastián et al., 2016), methylotrophs (Batrakov and Nikitin, 1996), methanotrophic bacteria (Makula, 1978), *Pelagibacter ubique* (Van Mooy et al., 2009), and barophilic bacteria

(e.g., DB21MT-2 and DB21MT-5) isolated from sediments from the Mariana Trench (Fang et al., 2000).

The hierarchical cluster analysis on variations in the relative abundance of PGs suggests that several compounds maintained a similar proportion in bathyal and hadal sediments, which differs from the water column (Fig. S6). Most PGs in the bathyal and hadal sediments have long acyl carbon chains (C_{34} – C_{41}), and they show odd- and even-numbered polyunsaturated fatty acids (Fig. S6). The average chain lengths of even-numbered n - C_{18} , n - C_{20} , and n - C_{22} fatty acids, mostly in PCs and PGs, are indicative of algal inputs (Kaneda, 1991; Thompson, 1996; Bergé and Barnathan, 2005; Brandsma et al., 2012). However, since these PGs were not dominant in the water column, a source from deeper environments is likely. Specifically, PG-DAG-36 : 2, PG-DAG-35 : 2, PG-DAG-36 : 5, PG-DAG-37 : 2, and PG-DAG-41 : 4 are the dominant constituents of this IPL class in hadal–bathyal sediments (Figs. 7, S6). PG-DAG-36 : 2 has been described in surface waters of the North Sea and also detected in picoeukaryotes (Brandsma et al., 2012) and in heterotrophic bacteria in surface waters of the open South Pacific Ocean (Van Mooy and Fredricks, 2010). However, these PGs are not dominant in the water column near the Atacama Trench (Cantarero et al., 2020). On the other hand, PG-DAG-35 : 2, PG-DAG-36 : 5, PG-DAG-37 : 2, and PG-DAG-41 : 4 are not commonly reported in water-column studies. Thus, it is possible that PGs present in the Atacama Trench sediments derive from in situ microbial production, although downslope and lateral transport of labile OM cannot be ruled out. PG-DAG-36 : 2 (Fig. 3) is the PG contributing most to the dissimilarity within the cluster containing only hadal sediments (cluster 1 in Fig. 2). Thus, this lipid appears to be more representative of in situ microbial production in this environment.

PE (phosphatidylethanolamine)

PE and its methylated derivatives (PME, PDME) have been predominantly reported in membranes of diverse bacterial sources, including heterotrophic bacteria (Van Mooy and Fredricks, 2010; Schubotz et al., 2018), nitrifying/denitrifying bacteria (Goldfine and Hagen, 1968), sulfate-reducing bacteria (Rütters et al., 2001; Sturt et al., 2004), sulfur-oxidizing bacteria (Barridge and Shively, 1968; Imhoff, 1995; Wakeham et al., 2012), methanotrophic bacteria (Makula, 1978; Sturt et al., 2004), and barophilic bacteria (Fang et al., 2000).

PEs showed a similar distribution in bathyal and hadal sediments (Fig. S7), where they are dominated by long-chain (C_{36} – C_{44}) polyunsaturated fatty acids, contrary to the shorter chains (C_{28} – C_{36}) of saturated and monounsaturated fatty acids present in the water column. PE-DAG-32 : 1, PE-DAG-32 : 2, and PE-DAG-33 : 1 are the dominant PE compounds of bathyal and hadal sediments (Fig. 7). These IPLs have been previously reported in heterotrophic bacteria (Van Mooy and Fredricks, 2010; Brandsma et al., 2012). On the

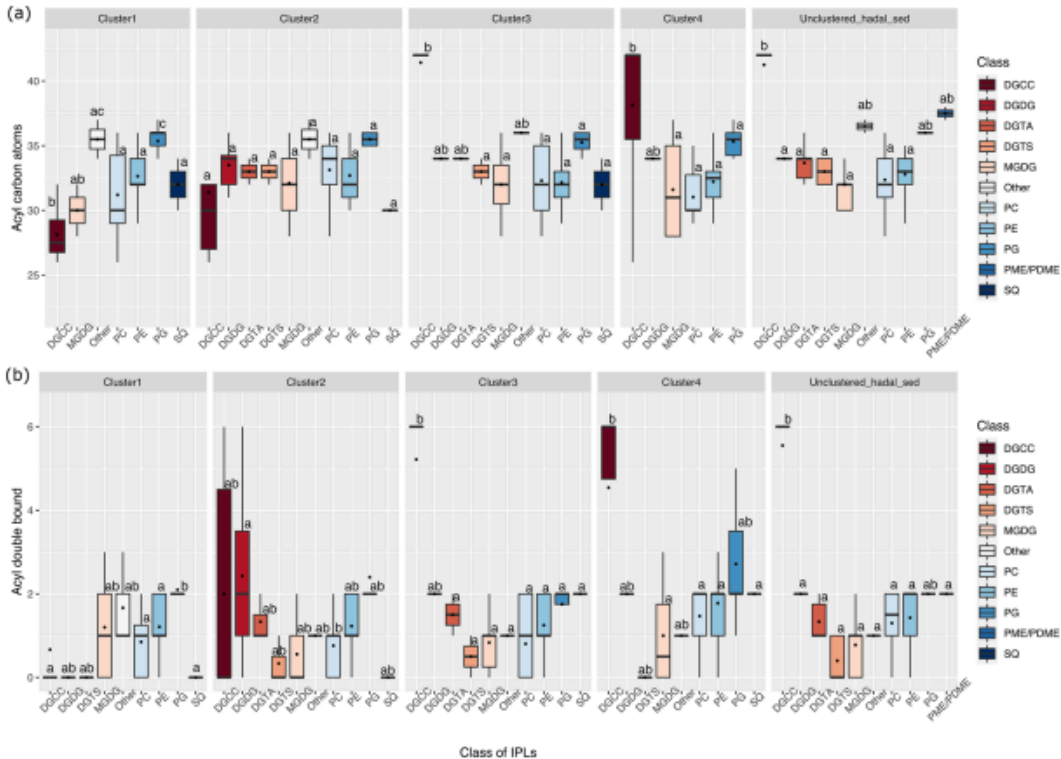


Figure 4. Total number of acyl carbon atoms (a) and acyl double bonds (b) in IPL classes across the distinct clusters shown in Fig. 2. The letters “a” and “b” indicate the presence of statistically distinct groups ($p < 0.05$) from both ANOVA and post hoc Tukey HSD tests, respectively.

other hand, fatty acids in PEs including monounsaturated and polyunsaturated (e.g., $C_{20:5}$ and $C_{22:6}$) have been reported in barophilic bacteria isolated from sediments from the Mariana Trench (Fang et al., 2000). Thus, although we cannot confidently rule out other sources, it is possible that PEs present in the AT sediments predominantly derive from in situ production by barophilic heterotrophic bacteria. PE-DAG-32 : 1, PE-DAG-32 : 2, and PE-DAG-33 : 1 (Fig. 3) are the PEs that contributed most to the dissimilarity within the cluster containing only hadal sediment samples (cluster 1 in Fig. 2). Thus, this cluster appears to be representative of in situ microbial production in this environment.

PC (phosphatidylcholine)

PCs were amongst the most diverse (43 structures; Fig. S8) and abundant phospholipid class in hadal sediments (Fig. S4). PC is the major membrane-forming phospholipid in eukaryotes (Lechevalier, 1988; Sohlenkamp et al., 2003;

Van Mooy et al., 2006; Van Mooy and Fredricks, 2010). Additionally, PC has been reported to be a major DAG in zooplankton, from protozoa to copepods and krill (Patton et al., 1972; Mayzaud et al., 1999; Lund and Chu, 2002). However, genomic data indicate that more than 10 % of all bacteria possess the genetic machinery for PC biosynthesis (Sohlenkamp et al., 2003). PC has also been reported in nitrifying bacteria (Lam et al., 2007), photoheterotrophic bacteria (Koblížek et al., 2006; Van Mooy et al., 2006), and barophilic bacteria (Fang et al., 2000). In surface sediments of the Black Sea (2000 m), PCs were related to algal material rapidly exported from surface waters (Schubotz et al., 2009).

Hadal and bathyal sediments, in addition to two OMZ core stations, were clustered in the PC class (AU p value of 97 %; Fig. S8). This cluster showed PCs with long (C_{33-38}) and polyunsaturated fatty acids (up to 10 unsaturations). The dominant constituents were PC-DAG-35 : 0, PC-DAG-30 : 2, PC-DAG-30 : 1, PC-DAG-33 : 2, PC-DAG-35 : 1, PC-DAG-29 : 2, PC-DAG-32 : 1, and PC-DAG-36 : 2 (Figs. 7, S8). PC-

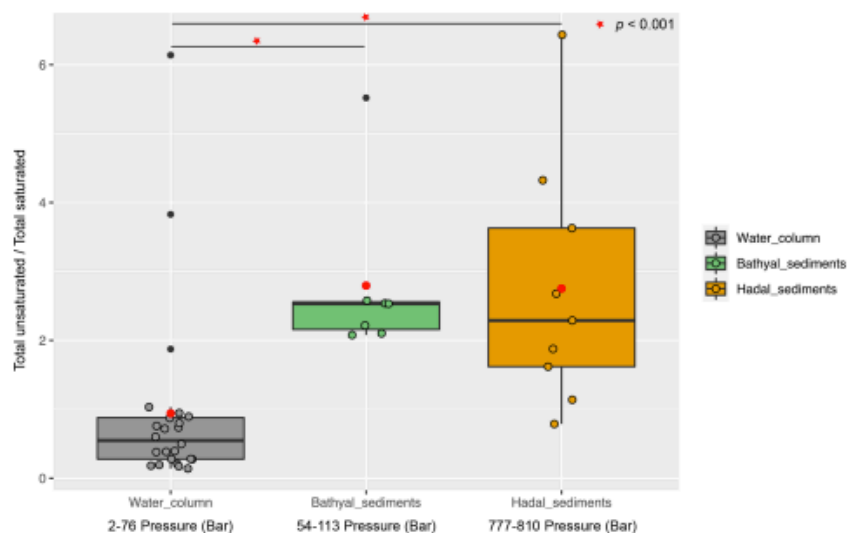


Figure 5. Boxplot showing the ratio of total unsaturated fatty acids to total saturated fatty acids derived from IPLs present in water-column samples (Cantarero et al., 2020) and sediments of the Atacama Trench (this study). Red circles indicate the average value in each environment. The Wilcoxon test (p value < 0.001) indicates that sediments have statistical ratios higher than the water column (horizontal lines and red stars).

DAG-36 : 2 and PC-DAG-30 : 1 have been associated with phytoplankton detritus (Schubotz et al., 2009) and bacteria (Brandsma et al., 2012), whereas PC-DAG-32 : 1 has been associated with picoeukaryotes (Brandsma et al., 2012).

Since the most abundant PCs in cluster 1 have not been reported as dominant structures in any specific environment before, they are possibly produced in situ, although downslope and/or lateral transport cannot be ruled out. Among bacteria, those membranes reported to contain PC belong to the alpha and gamma subgroups of the Proteobacteria (Sohlenkamp et al., 2003). Given that these bacterial groups are abundant in trench samples from Puerto Rico (Eloe et al., 2011), the Mariana Trench (Nunoura et al., 2015), and recently in the Atacama Trench (Schauberger et al., 2021), it is possible that PCs present in high abundance in the Atacama Trench are consistent with high abundance of Proteobacteria in these regions. Given their general known association and abundance in Atacama Trench sediments (Fig. S4), they likely derive primarily from bacterial but also possibly from fungi or metazoan sources that have not yet been studied and to a lesser extent from phytoplankton. Indeed, fungal strains isolated from the water column and sediment in the ESTP off Chile reported high levels of polyunsaturated fatty acids and PCs (Gutiérrez et al., 2020), whereas a high fungal diversity associated with denitrification potential was reported in the Yap Trench (Gao et al., 2020). The latter suggests that eu-

karyotic PCs in hadal sediments could be much more diverse in origin than previously thought.

PME/PDME (phosphatidyl(di)methylethanolamine)

PME/PDMEs have been observed in association with methanotrophic bacteria (Makula, 1978; Goldfine, 1984; Fang et al., 2000); sulfide-oxidizing bacteria (Barridge and Shively, 1968); sulfate-reducing bacteria, mainly *Desulfobulbus* spp. (Rossel et al., 2011), Proteobacteria (Oliver and Colwell, 1973; Goldfine, 1984); and barophilic bacteria from the Mariana Trench (Fang et al., 2000). Additionally, the occurrence of PME-DEG at some hadal stations suggests the presence of sulfate-reducing bacteria (Rütters et al., 2001; Sturt et al., 2004).

PME/PDMEs exhibited their lowest abundance (~ 10 ng per gram of sediment) in sediment samples compared to other phospholipids (Fig. S4b). In the bathyal and hadal sediments they were clustered (AU p value of 97 %) and dominated by PDME-DAG-33 : 1, PME-DAG-37 : 2, PME-DAG-34 : 2, PME-DAG-31 : 1, and PME-DEG-33 : 0 (Fig. S9a). PME-DEG-33 : 0 has been shown to correlate with high NO_2^- in the overlying water column of this area (Cantarero et al., 2020), which could suggest a potential association with denitrification processes. These structures have also been reported in the deep chemocline of the Cariaco Basin (Wakeham et al., 2012), suggesting a potential chemoautotrophic and/or heterotrophic source. The distribution of these com-

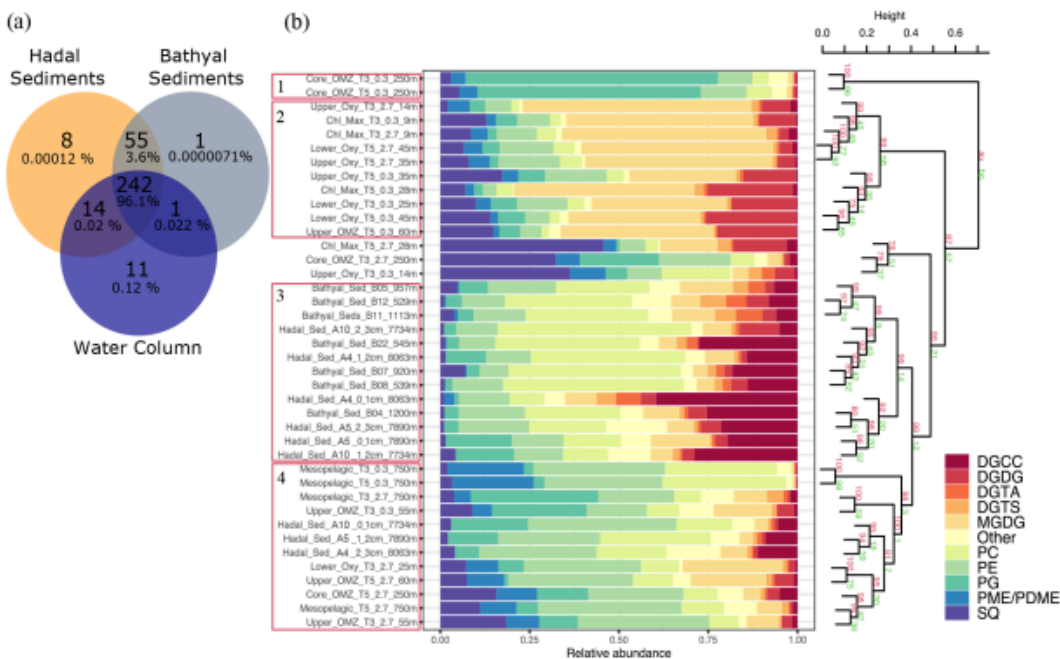


Figure 6. Comparison of IPLs in bathyal and hadal sediments (this study) and the overlying water column (Cantarero et al., 2020). (a) Venn diagram showing the number and percentage of unique and shared IPL molecules between these three environments. (b) Cumulative bar charts of IPL fractional abundances in each sample. Samples were grouped according to arithmetic mean (UPGMA) hierarchical clustering based on Euclidean distances. The cluster analysis on the right-hand side shows approximately unbiased (AU) and bootstrap probability (BP) in red and green numbers, respectively, whereas p values are shown at branching points. Clusters with $AU \geq 95\%$ confidence are highlighted in red on the left-hand side.

pounds is different from the water column, which is dominated by the saturated PME-32 : 0, PME-DAG-30 : 0, and PME-DAG-31 : 0 (Figs. S9a and S16; Cantarero et al., 2020). Thus, and similar to other lipid classes, they most likely derive from in situ production in hadal sediments rather than from the water column, although other sources such as downslope and/or lateral transport cannot be ruled out. No particular PME/PDMEs were found to contribute to the dissimilarity between the cluster containing only hadal sediment samples (cluster 1 in Fig. 2) and other sediment samples.

4.2 Potential sources of glycolipids

MGDG (monoglycosyldiacylglycerol)

Due to their dominant occurrence in chloroplast thylakoid membranes (Murata and Siegenthaler, 1998) and particularly in cyanobacteria (Heinz, 1977; Harwood, 1998; Wada and Murata, 2007; Van Mooy and Fredricks, 2010), but also in heterotrophic bacteria (Popendorf et al., 2011b), MGDGs are

probably the most abundant IPLs on earth (Gounaris and Barber, 1983).

The hierarchical cluster suggests that several MGDG compounds maintained a similar proportion in bathyal (AU p value of 90 %) and hadal (AU p value of 98 %) sediments (Fig. S10). The most abundant MGDGs in the bathyal and hadal sediments were MGDG-28 : 0, MGDG-32 : 1, MGDG-30 : 1, MGDG-32 : 0, and MGDG-37 : 3. MGDG-28 : 0 and MGDG-30 : 1 are ubiquitous along the oxycline of the overlying OMZ (Fig. 7; Cantarero et al., 2020). In addition, MGDG-32 : 1 has been previously reported in waters of the eastern South Pacific (Van Mooy and Fredricks, 2010). Thus, the occurrence of these MGDGs in sediment could indicate at least some export of labile OM from surface waters. On the other hand, MGDG-37 : 3 does not appear to be a dominant structure in any specific environment in the literature, which suggests a likely in situ production.

DGDG (diglycosyldiacylglycerol)

DGDGs are commonly found in membranes of eukaryotic algae and cyanobacteria (Wada and Murata, 1998; Sakurai et al., 2006; Kalisch et al., 2016). DGDGs clustered together in bathyal and hadal sediments (AU *p* value of 96 %), whereas their distribution differed from the water column (Fig. S11). The most abundant DGDGs in hadal and bathyal sediments of the Atacama Trench was DGDG-34 : 2 (Fig. 7), which has been previously reported in cyanobacterial strains isolated (da Costa et al., 2020) but has not been previously reported as abundant in the water column. In contrast, DGDG-30 : 0, which is widely distributed in the water column of this region (Cantarero et al., 2020), is consistently present in hadal and bathyal sediment samples although at very low abundances (Fig. 7). Thus, although DGDGs account for less than ~5 % of the total IPL pool (Fig. 6b), except for station A10 (2–3 cm) where they reach ~10 %, their presence in bathyal and hadal sediments is indicative of at least some export of labile OM from surface waters.

SQDG (sulfoquinovosyldiacylglycerol)

SQDGs are predominantly produced by photoautotrophs (Van Mooy et al., 2006; Popendorf et al., 2011b), including various groups of diatoms, brown and green algal chloroplast membranes (Harwood, 1998), and cyanobacteria (Siegenthaler, 1998; Wada and Murata, 1998). SQDGs have also been found in bacteria from the α - and γ -proteobacterial lineages (Benning, 1998). In the overlying water column of the Atacama Trench, Cantarero et al. (2020) suggested a higher contribution of SQDGs from cyanobacteria than algae. Also, SQDGs found in the deep Atlantic (down to ~4000–5000 m) appear to indicate a source and export from surface waters (Gašparović et al., 2018).

SQDGs showed a consistent distribution in bathyal and hadal sediments, where they are dominated by long-chain (C_{36–44}) fatty acids (Fig. S12). This is contrasting to their distribution in the overlying water column where they are dominated by shorter-chain (C_{28–36}) saturated fatty acids (Cantarero et al., 2020). SQDG-30 : 0, SQDG-32 : 0, SQDG-30 : 2, and SQDG-38 : 4 were the dominant SQDG constituents of bathyal and hadal sediments (Fig. 7). SQDG-30 : 0 and SQDG-30 : 2 have been reported in bacteria in North Sea surface waters (Brandsma et al., 2012), in cyanobacteria of the eastern subtropical South Pacific (Van Mooy and Fredricks, 2010), and in plankton detritus from surface sediments of the Black Sea (Schubotz et al., 2009). Furthermore, SQDG-30 : 0 is abundant in surface waters of our study area, and SQDG-38 : 4 has been correlated with NO₃⁻ (Cantarero et al., 2020). The observed differences in the distribution of SQDGs in deep sediments compared to the water column suggests an *in situ* production of previously poorly characterized compounds, in addition to at least some export from surface waters.

4.3 Potential biological sources of betaine lipids

DGTS (diacylglyceryl trimethylhomoserine)

DGTSs have diverse biological origins, being found in a wide range of eukaryotes (Sato, 1992; Dembitsky, 1996; Kato et al., 1997; Van Mooy et al., 2009), photoheterotrophic bacteria (Benning et al., 1995; Geiger et al., 1999), photoautotrophic bacteria (Popendorf et al., 2011b) including cyanobacteria (Řezanka et al., 2003), and members of the α -Proteobacteria subdivision (López-Lara et al., 2003). Schubotz et al. (2018) showed DGTS with varying fatty acid compositions in the OMZ system of the eastern tropical North Pacific, especially in OMZ waters, indicating that these compounds can be biosynthesized by a wider range of source organisms than previously thought.

Consistent with other IPL classes, DGTSs of the bathyal and hadal samples were grouped in the same cluster (AU *p* value of 98 %) and differed from the water column (Fig. S13). However, several DGTSs are shared between surface waters (9–60 m) and deep sediments. Indeed, the most abundant DGTSs in bathyal and hadal sediments (DGTS-34 : 0, DGTS-32 : 1, DGTS-26 : 0, DGTS-34 : 1, DGTS-32 : 0, and DGTS-25 : 0; Figs. 7, S13) are also prominent in the chlorophyll maximum in the eastern subtropical South Pacific (Van Mooy and Fredricks, 2010; Cantarero et al., 2020). Therefore, their presence in hadal sediments suggest the export of some labile OM from the euphotic zone, although we cannot rule out other sources.

DGTA (diacylglyceryl hydroxymethyl-trimethyl- β -alanine)

DGTAs have been widely reported in eukaryotic phytoplankton (Araki et al., 1991; Dembitsky, 1996; Cañavate et al., 2017), mainly in diatoms (Volkman et al., 1989; Zhukova, 2005; Gómez-Consarnau et al., 2007), and are also especially abundant in cultures of prymnesiophytes and cryptophytes (Kato et al., 1997). DGTAs have also been found in cyanobacteria (Brandsma et al., 2012) and heterotrophic bacteria (Popendorf et al., 2011a; Sebastián et al., 2016).

DGTAs in bathyal and hadal sediments are mainly composed of longer (C_{28–C₄₂}) and polyunsaturated (1–12) fatty acids compared to those present in the shallowest region of the overlying water column, composed of shorter and saturated fatty acids (Fig. S14). In the overlying water column, these compounds are associated with relatively high chlorophyll and O₂ concentrations (Cantarero et al., 2020), similar to North Sea surface waters (Brandsma et al., 2012). To the best of our knowledge, the dominant DGTAs in hadal and bathyal sediments (Figs. 7, S14) have not been previously reported as dominant IPLs in other environments. Whereas no specific biological sources in hadal sediments are known, the structures containing between 30 and 38 carbon atoms might be characteristic of this type of environment.

DGCC

(diacylglycerylcarboxy-N-hydroxymethyl-choline)

Our knowledge of DGCC sources is limited. They have been found in membranes of prymnesiophyte algae (Kato et al., 1994), mainly in *Pavlova lutheria* (Kato et al., 1994; Eichenberger and Gribi, 1997) and in *E. huxleyi* (Volkman et al., 1989; Pond and Harris, 1996; Van Mooy and Fredricks, 2010). Additionally, they have also been reported in the diatom *Thalassiosira pseudonana* (Van Mooy et al., 2009).

The most abundant IPL from the entire data set of bathyal and hadal sediments is DGCC-42 : 6 (Figs. 7, S15). This is the compound with the largest number of C atoms (42) and unsaturation (6) in all IPLs detected in this study. DGCCs with long-chain, polyunsaturated fatty acids (i.e., C_{38:6}, C_{40:10}, C_{42:11}, and C_{44:12}) have been previously reported in phytoplankton (Hunter, 2015; Van Mooy and Fredricks, 2010). However, the most abundant DGCCs in hadal sediments have, to the best of our knowledge, not been previously reported, which highlights their potential as biomarkers of deep-sea sediments. However, three hadal stations clustered in a separate group (see Fig. S15) were dominated by DGCC-27 : 0 and did not contain DGCC-42 : 6, indicating that this IPL probably derives from allochthonous sources.

4.4 Potential biological sources of other lipids

Glycosidic ceramides (Gly-Cer) have been reported in eukaryotic algae such as prymnesiophyte (Vardi et al., 2009) and have also been shown to be abundant in water columns of OMZ systems (Schubotz et al., 2009, 2018; Cantarero et al., 2020). In general, the overlying water column shows Gly-Cer with a ceramide chain and polyunsaturated fatty acids with C_{21–38}. However, these structures are scarce in the bathyal and hadal sediments (see Fig. S9b), which could reflect a deficient export from surface waters due to intense remineralization. On the other hand, ornithine lipids (OL), phosphatidylinositol (PI), PC-AEGs, and other unidentified phospholipids were also present in deep sediments (Fig. S9b). Some PIs and OLs have been reported in sulfate-reducing bacteria (Sturt et al., 2004; Bühring et al., 2014), whereas PC-AEGs have been reported in bacteria inhabiting water columns with reduced oxygen concentration (Schubotz et al., 2018). Thus, the high relative abundance of PC-AEG-34 : 3 in hadal and bathyal sediments (Figs. S9b and S16) could be indicative of anaerobic microbial processes. PC-AEG-34 : 3 contributed the most to the dissimilarity between the cluster containing only hadal sediment samples (cluster 1 in Figs. 2 and 3), thus suggesting an in situ microbial production, although we cannot confidentially rule out other sources.

4.5 Allochthonous versus autochthonous IPLs in the Atacama Trench

Given their rapid degradation after cell death (White et al., 1979; Harvey et al., 1986; Logemann et al., 2011; Schouten et al., 2010), IPLs are typically considered markers of living or recently dead cells (White et al., 1979; Harvey et al., 1986; Petersen et al., 1991; Lipp et al., 2008). The distribution of IPLs in bathyal and hadal sediments exhibits a high degree of similitude, as demonstrated by the hierarchical analysis (cluster 1 in Fig. 8a), the NMDS (Fig. 8b), and the SIMPER analysis (cluster 1 in Table S1). The deep-sea surface sediments showed weak clustering with the IPLs reported in the overlying water column by Cantarero et al. (2020) (Fig. 9a). Additionally, water-column samples exhibit a larger degree of separation than sediments (ANOSIM, $R = 0.78$; $P < 0.01$; Fig. 8b) and are broadly clustered by geochemical environments (Cantarero et al., 2020). The low abundance of IPLs characteristic of organisms inhabiting the chlorophyll maximum in deep-sea sediments of the Atacama Trench ($< 0.005\%$ of the total IPL pool; Fig. S3) suggests minimal export of labile organic compounds from the upper ocean. This result implies rapid IPL degradation during sinking in the water column, which is consistent with experimental degradation rates (Westrich and Berner, 1984; Logemann et al., 2011) and first-order POM sinking rates. Indeed, by using the experimentally calculated kinetic degradation rate constants (k') of ester-bound IPLs by Logemann et al. (2011) and the sinking rate of particles from surface waters to 4000 m ($20\text{--}100\text{ m d}^{-1}$; Billett et al., 1983; Danovaro et al., 2014), we calculated that $\sim 86\%$ – 98% ($k'_{t=80} = 0.033$ and $k'_{t=400} = 0.011$) of IPLs from surface waters should degrade by the time that particles reach depths of ~ 8000 m. These results are also in accord with studies indicating elevated benthic oxygen consumption rates resulting from intense microbial respiration of sinking OM reaching the sediment (Glud et al., 2013; Wenzhöfer et al., 2016). Thus, the pool of IPLs in hadal sediments appears to predominantly represent in situ microbial production, whereas the deep-sea microbial community in both bathyal and hadal sediments is similar despite their bathymetric zonation ($\sim 1000\text{--}8000$ m). Alternatively, we cannot rule out the possibility of new IPL production, particularly from heterotrophic and chemoautotrophic bacteria in micro niches of sinking particles reaching the deep sea and/or downslope and lateral sediment transport.

Marine trenches receive organic carbon from a variety of sources and transport mechanisms. These include canyons and river systems that channel OM from land to coastal regions, aeolian transport, surface water productivity, and in situ production, to name a few (Wenzhöfer et al., 2016; Tarn et al., 2016; Luo et al., 2017; Xu et al., 2018; Guan et al., 2019; Xu et al., 2021). Carbon flux events can increase the delivery of particulate carbon from surface waters to the seafloor (Poff et al., 2021), whereas river discharge and ae-

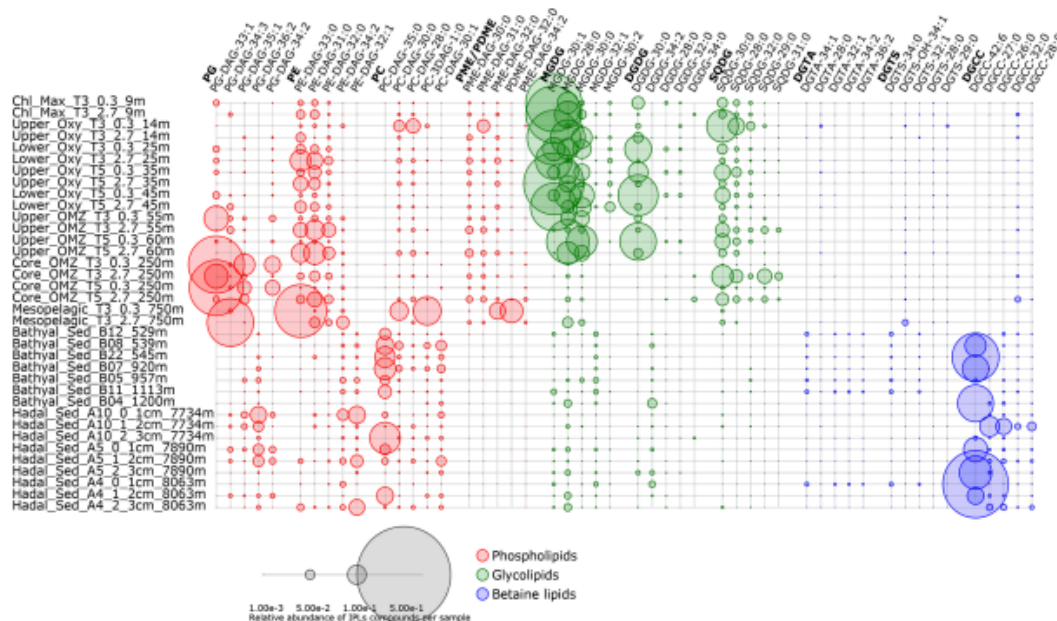


Figure 7. Relative abundance of the five most abundant individual IPLs contributing to each IPL class. Circle size is proportional to the relative abundance of IPL compounds per sample. Samples are organized along the vertical axis by depth, whereas phospholipids, glycolipids, and betaine lipids are shown in colors. The legend provides a scale for circumference size.

olian transport can result in enhanced terrestrial carbon (Xu et al., 2021). Mass wasting events are also known to create dynamic depositional conditions and strong spatial heterogeneity in OM distribution in marine trenches (Schauberger et al., 2021; Xu et al., 2021). While marine organic carbon appears to dominate sediments in the Japan (Schwestermann et al., 2021), Massau (Xu et al., 2020a), and New Britain (Xu et al., 2020b) trenches, the Atacama and Kermadec trenches, on the other hand, have been reported to be dominated by terrigenous OM. Since our study only focuses on the most labile component of the total lipid pool, it predominantly traces labile and indigenous OM and not recalcitrant fractions of the lipid pool. The latter warrants further investigation.

In regions like the Japan Trench, downslope sediment transport has been linked to earthquake-driven remobilization (Bao et al., 2018; Schwestermann et al., 2021). Whereas we lack sedimentological/geochemical data to discriminate whether the top 3 cm of our hadal stations represent debris flows, turbidite, or mass wasting events, ongoing work in the Atacama Trench indicates heterogenic sediment deposition along the hadal zone (Matthias Zabel, personal communication, 2021). Thus, the role of downslope transport as a mechanism to explain the high statistical similarity between bathyal and hadal sediments remains to be tested.

4.6 Characteristic IPLs of hadal and bathyal sediments

The IPLs that contribute most to the dissimilarity between the hierarchical cluster containing samples from the hadal and bathyal sediments (cluster 1 of Fig. 8) and the water column (cluster 2, 3, 4, and 5 of Fig. 8) are represented in Fig. 9. The most characteristic IPLs of hadal and bathyal sediments are DGCC-42 : 6, DGCC-27 : 0, DGCC-26 : 0, PC-DAG-35 : 0, PC-DAG-30 : 1, PC-DAG-30 : 2, PC-DAG-33 : 2, PC-DAG-32 : 1, PC-DAG-29 : 2, PE-DAG-32 : 1, PE-DAG-32 : 2, PE-DAG-33 : 1, PG-DAG-36 : 2, and DGDG-34 : 2, which we propose as potential markers for these environments. Even though DGCCs have been mainly related to algae membranes (Kato et al., 1994; Van Mooy et al., 2009), they are minor components of the water column in this area, suggesting the occurrence of an alternative source. In addition to DGCCs, the two other betaine lipids, DGTA and DGTS, exhibited five IPLs that were almost exclusively present in sediment samples (DGTA-34 : 1, DGTA-32 : 1, DGTA-34 : 2, DGTS-34 : 0, and DGTS-32 : 1; see Fig. 11). We note that almost all the PC phospholipids in our study have not, to the best of our knowledge, been previously reported in the literature, which reinforces their use as markers of sedimentary in situ bathyal and hadal production.

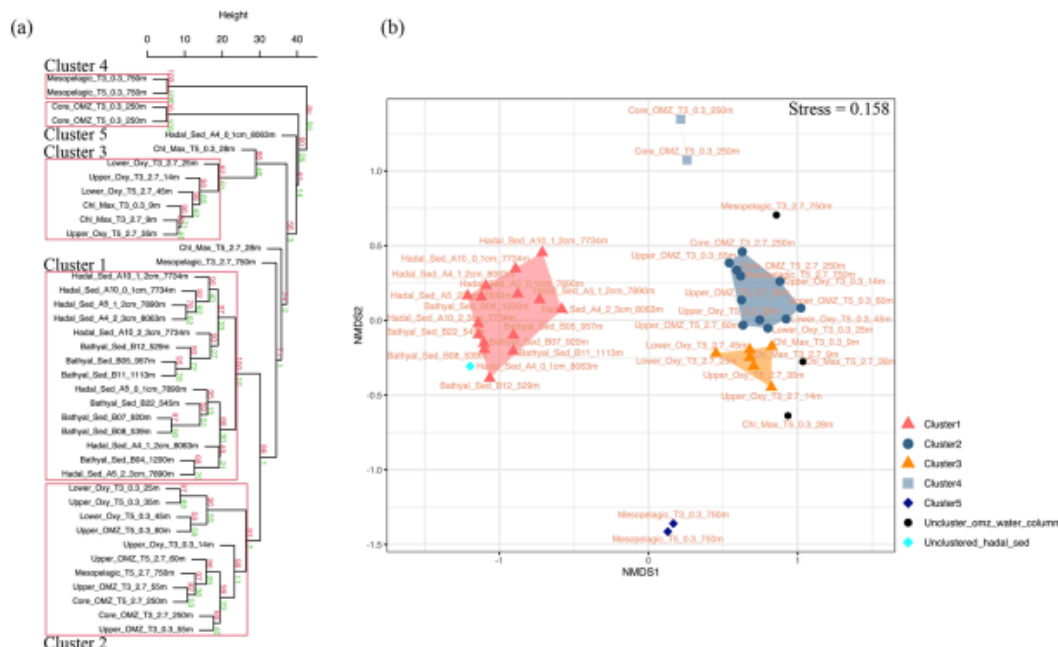


Figure 8. (a) Arithmetic mean (UPGMA) hierarchical clustering based on Euclidean distances calculated from IPLs in each sampling station. Red values are approximately unbiased (AU) p values, and green values are bootstrap probability (BP) for each node. Red boxes highlight clusters with 95 % confidence. The number of bootstrap replicates is 10000. (b) Non-metric multidimensional scaling (NMDS) analysis of IPLs at each sampling station. The distance matrix was calculated based on the Bray–Curtis dissimilarity. The stress value of the final configuration was 15.8 %. Different symbols and colors represent the sample grouping from hierarchical clusters shown in panel (a).

The presence of a few MGDGs and SQDGs in hadal and bathyal sediments ($\sim 7\%$ of the total IPL pool) indicates that at least some labile OM could derive from the shallow water column (see Sect. 4.2). However, the most abundant IPLs in our sediment samples, DGCC-42 : 6, PC-DAG-35 : 0, PE-DAG-32 : 1, and PG-DAG-36 : 2 (19.8 % of the total IPL pool; Fig. S16), are almost completely absent in the overlying water column (Fig. 9). This reinforces the idea that these IPLs most likely originate from in situ microbial production in sediments. The single most abundant IPL in sediments, DGCC-42 : 6, was not present in cluster 1, which only contains hadal sediments (Figs. 2 and 3). Instead, this compound is prominent in cluster 3, 4, and 5, containing both hadal and bathyal samples. Thus, DGCC-42 : 6 and PC-DAG-35 : 0, which has the lowest relative abundance in the cluster with only hadal sediments, could be indicators of downslope transport from bathyal to hadal regions.

We acknowledge that temporal variability in IPL production in the water column and sediment and the lack of data on the largely uncharacterized hadal endemic microbial community could complicate some of the phylogenetic and source associations of IPLs and warrant further investigation. De-

spite this, our study represents a step forward on the characterization of labile sources of OM sustaining hadal ecosystems.

4.7 Do IPLs reveal homeoviscous adaptation to the deep-sea environment?

Environmental factors such as pH, conductivity, temperature, and pressure impact the permeability and fluidity of cell membranes (Shaw, 1974; Macdonald, 1984; DeLong and Yayanos, 1985; Somero, 1992; Komatsu and Chong, 1998; Van Mooy et al., 2009; Carini et al., 2015; Sebastián et al., 2016; Siliakus et al., 2017; Boyer et al., 2020; Allen et al., 1999). Thus, organisms adapt to changes in environmental factors to maintain physiological homeostasis by altering their fatty acid composition (DeLong and Yayanos, 1985; Fang et al., 2000; Nichols et al., 2004; Siliakus et al., 2017). For instance, the combined physiological effects of high hydrostatic pressure and low temperature on prokaryotic membranes in laboratory cultures leads to the production of unsaturated lipids (DeLong and Yayanos 1985; Fang et al., 2000; Nichols et al., 2004; Zheng et al., 2020). However, few



Figure 9. Relative abundance of individual IPLs that contribute most to the dissimilarity between clusters of Fig. 8 derived from the SIMPER analysis (Table S1). Circle size is proportional to the relative abundance of IPL compounds per sample. Samples are organized along the vertical axis and shown in colors that match the hierarchical cluster analysis in Fig. 8. The legend shows the scale for circumference size.

studies have been conducted using culture-independent techniques in search for potential adaptation mechanisms in organisms inhabiting the deep ocean (i.e., Zhong et al., 2020). We sought to understand whether the chemical composition of core fatty acids within different IPL classes (i.e., carbon length and unsaturation degree) reflects the combined effects of the low temperature and high pressure typical of hadal settings. We show that PGs are abundant in hadal sediments of the Atacama Trench (Fig. S4). Bacterial strains isolated from Mariana Trench sediments contain PG as the most abundant class of phospholipids (Fang et al., 2000), which these authors presumed could represent a physiological response to high pressure and low temperature. This has been confirmed by subsequent studies (Winter et al., 2009; Periasamy et al., 2009; Jebbar et al., 2015; Allemann et al., 2021). Cluster 1 in the boxplot analysis (Fig. 4) likely contains the most characteristic IPL classes of the hadal zone. In general, the phospholipids in this cluster exhibited fatty acid chains that are monounsaturated and saturated compared to other environments (Fig. 4a, b). Additionally, we observed an increase in the ratio of total unsaturated to saturated fatty acids in deep sediments compared to the water column (Fig. 5), which could reflect physiological adaptations of their biological producers. These results are in accord with studies indicating biosynthesis and incorporation of polyunsaturated fatty acids into phospholipid membranes of piezophilic bac-

teria (DeLong and Yayanos, 1985; Baird et al., 1985; Yano et al., 1998; Winter, 2002; Mangelsdorf et al., 2005; Winter and Jeworrek, 2009; Allemann et al., 2021). Thus, the chemical characteristics (C length and degree of unsaturation) of the most abundant IPLs in sediments of the Atacama Trench suggest homeoviscous adaptation to this type of environment by their source organisms, in addition to potentially indicating the occurrence of compounds that are unique to the endogenous community.

5 Conclusions

Bacterial and eukaryotic IPLs in surface hadal sediments from the deepest points of the Atacama Trench share characteristics with those in bathyal sediments and differ from those found in suspended particles from the upper 750 m of the water column, including the oxygen minimum zone. This indicates that (a) most IPLs abundant in the upper water column are almost entirely degraded during their descent to the hadal seafloor and (b) IPLs found in hadal sediments are predominantly derived from in situ microbial communities.

The most dominant ester-bound IPL structures found in bathyal and hadal sediments show a great variety of phospholipids with varying degrees of unsaturation, most of them yet to be described, that are likely derived from as of yet poorly characterized bacterial and/or eukaryotes sources. Hadal sed-

iments also exhibit unique glycolipid structures, such as SQDG-42 : 11, SQDG-23 : 0, DGDG-35 : 1, DGDG-35 : 2, and DGDG-37 : 1, that to the best of our knowledge have not been reported in other environments. However, these lipids are present in low abundance and represent a small fraction (~0.00012 %) of the total IPL pool. Furthermore, elevated ratios of unsaturated/saturated fatty acids in hadal sediments are likely indicative of homeoviscous adaptation to the high pressure and low temperatures characteristic of this extreme deep-sea environment.

An improved understanding of the phylogenetic, ecological, and metabolic association of IPLs present in the Atacama Trench could be achieved in future studies by the pairing of lipidomics with genomic techniques (e.g., microbial community composition, functional groups, lipid biosynthesis), in addition to a detailed sedimentological and biogeochemical characterization of sediments.

Data availability. Biomarkers metadata that generates and supports the findings of this study and R code are available in: <https://github.com/EdgarteFlores/IPLs-Atacama-Trench->, last access: 3 March 2022 (<https://doi.org/10.5281/zenodo.6325647>, Flores, 2022).

Supplement. The supplement related to this article is available online at: <https://doi.org/10.5194/bg-19-1395-2022-supplement>.

Author contributions. EF, OU, and JS designed the study. MZ contributed with the hadal samples from the HADES-ERC cruise. EF prepared, extracted, and analyzed samples from the HADES-ERC cruise with help from SIC and ND under the supervision of JS. EF and SIC processed results. EF, SIC, and JS interpreted results. EF and PRF performed statistical analyses. EF wrote the manuscript with contributions from SIC, JS, and OU. All authors provided feedback on the manuscript. OU and JS funded the research.

Competing interests. The contact author has declared that neither they nor their co-authors have any competing interests.

Disclaimer. Publisher's note: Copernicus Publications remains neutral with regard to jurisdictional claims in published maps and institutional affiliations.

Acknowledgements. This work was supported by the European Research Council (HADES-ERC, grant agreement number 669947 to Ronnie N. Glud) and the Max Planck Society. Additional support was provided by the Department of Geological Sciences and INSTAAR at the University of Colorado Boulder (to Julio Sepúlveda). Edgarte Flores was also partially supported by the Universidad de Concepción. We are thankful to the captains, crews, and scientists of the German RV *Sonne* cruises SO261 (HADES-

ERC) and SO211 (ChiMeBo). In particular, we thank the chief scientists Ronnie N. Glud and Frank Wenzhöfer (HADES-ERC) and Dierk Hebbeln (ChiMeBo). The HADES-ERC and ChiMeBo cruises were funded by the European Research Council and the German Bundesministerium für Bildung und Forschung (BMBF), respectively. We also wish to thank Carina Lange and Silvio Pantoja for access to samples from the ChiMeBo cruise and Matias Pizarro-Koch for the preparation of the three-dimensional map. We also thank Lilian Nuñez, Benjamín Srain, Rodrigo Castro, Alejandro Ávila, Mahyar Mohtadi, Ricardo De Pol-Holz, and Gema Martínez-Méndez for sample collection during the ChiMeBo cruise and/or laboratory assistance.

Financial support. This research has been supported by the Instituto Milenio de Oceanografía (grant no. ICN12_019-IMO), the Fondo Nacional de Desarrollo Científico y Tecnológico (grant no. 1191360), and the Universidad de Concepción (UCO 1866 student scholarship 2019).

Review statement. This paper was edited by Sebastian Naeher and reviewed by two anonymous referees.

References

- Ahumada, R.: Producción y destino de la biomasa fitoplanctónica en un sistema de bahías en Chile central: una hipótesis, *Biol. Pesq. Chile*, 18, 53–66, 1989.
- Allemann, M. N. and Allen, E. E.: Genetic suppression of lethal mutations in fatty acid biosynthesis mediated by a secondary lipid synthase, *Appl. Environ. Microbiol.*, 87, e00035-21, <https://doi.org/10.1128/AEM.00035-21>, 2021.
- Allen, E. E., Facciotti, D., and Bartlett, D. H.: Monounsaturated but not polyunsaturated fatty acids are required for growth of the deep-sea bacterium *Photobacterium profundum* SS9 at high pressure and low temperature, *Appl. Environ. Microbiol.*, 65, 1710–1720, 1999.
- Angel, M.: Detrital organic fluxes through pelagic ecosystems, in: *Flows of energy and materials in marine ecosystems*, Springer, Boston, MA, 475–516, https://doi.org/10.1007/978-1-4757-0387-0_19, 1984.
- Angel, M. V.: Ocean trench conservation, *Environmentalist*, 2, 1–17, 1982.
- Araki, S., Eichenberger, W., Sakurai, T., and Sato, N.: Distribution of diacylglycerolhydroxymethyltrimethyl- β -alanine (DGTA) and phosphatidylcholine in brown algae, *Plant Cell Physiol.*, 32, 623–628, 1991.
- Baird, B.: Biomass and community structure of the abyssal microbiota determined from basin and Puerto Rico trench sediments, *Benthic Ecol. Sediment. Process. Venezuela Basin – Past Present*, 61, 217–213, 1985.
- Bao, R., Strasser, M., McNichol, A. P., Haghipour, N., McIntyre, C., Wefer, G., and Eglinton, T. I.: Tectonically-triggered sediment and carbon export to the Hadal zone, *Nat. Commun.*, 9, 1–8, 2018.
- Barridge, J. K. and Shively, J.: Phospholipids of the Thiobacilli, *J. Bacteriol.*, 95, 2182–2185, 1968.

- Batrakov, S. G. and Nikitin, D. I.: Lipid composition of the phosphatidylcholine-producing bacterium *Hyphomicrobium vulgare* NP-160, *Biochim. Biophys. Acta BBA-Lipids Lipid Metab.*, 1302, 129–137, 1996.
- Benning, C., Huang, Z.-H., and Gage, D. A.: Accumulation of a novel glycolipid and a betaine lipid in cells of *Rhodobacter sphaeroides* grown under phosphate limitation, *Arch. Biochem. Biophys.*, 317, 103–111, 1995.
- Bergé, J.-P. and Barnathan, G.: Fatty acids from lipids of marine organisms: molecular biodiversity, roles as biomarkers, biologically active compounds, and economical aspects, *Mar. Biotechnol.* 1, 96, 49–125, 2005.
- Biddle, J. F., Lipp, J. S., Lever, M. A., Lloyd, K. G., Sørensen, K. B., Anderson, R., Fredricks, H. F., Elvert, M., Kelly, T. J., Schrag, D. P., Sogin, M. L., Brenchley, J. E., Teske, A., House, C. H., and Hinrichs, K.-U.: Heterotrophic Archaea dominate sedimentary subsurface ecosystems off Peru, *P. Natl. Acad. Sci. USA*, 103, 3846–3851, 2006.
- Billett, D., Lampitt, R., Rice, A., and Mantoura, R.: Seasonal sedimentation of phytoplankton to the deep-sea benthos, *Nature*, 302, 520–522, 1983.
- Bligh, E. G. and Dyer, W. J.: A rapid method of total lipid extraction and purification, *Can. J. Biochem. Physiol.*, 37, 911–917, 1959.
- Boyer, G. M., Schubotz, F., Summons, R. E., Woods, J., and Shock, E. L.: Carbon oxidation state in microbial polar lipids suggests adaptation to hot spring temperature and redox gradients, *Front. Microbiol.*, 11, 229, <https://doi.org/10.3389/fmicb.2020.00229>, 2020.
- Brandsma, J., Hopmans, E. C., Philippart, C. J. M., Veldhuis, M. J. W., Schouten, S., and Sinnighe Damsté, J. S.: Low temporal variation in the intact polar lipid composition of North Sea coastal marine water reveals limited chemotaxonomic value, *Biogeosciences*, 9, 1073–1084, <https://doi.org/10.5194/bg-9-1073-2012>, 2012.
- Bühning, S. I., Kamp, A., Wörmer, L., Ho, S., and Hinrichs, K.-U.: Functional structure of laminated microbial sediments from a supratidal sandy beach of the German Wadden Sea (St. Peter-Ording), *J. Sea Res.*, 85, 463–473, 2014.
- Cañavate, J. P., Armada, I., and Hachero-Cruzado, I.: Interspecific variability in phosphorus-induced lipid remodelling among marine eukaryotic phytoplankton, *New Phytol.*, 213, 700–713, 2017.
- Cantarero, S. I., Henríquez-Castillo, C., Dildar, N., Vargas, C. A., Von Dassow, P., Cornejo-D’Ottone, M., and Sepúlveda, J.: Size-fractionated contribution of microbial biomass to suspended organic matter in the eastern Tropical South Pacific oxygen minimum zone, *Front. Mar. Sci.*, 7, 745 pp., 2020.
- Carini, P., Van Mooy, B. A., Thrash, J. C., White, A., Zhao, Y., Campbell, E. O., Fredricks, H. F., and Giovannoni, S. J.: SAR11 lipid renovation in response to phosphate starvation, *P. Natl. Acad. Sci. USA*, 112, 7767–7772, 2015.
- Clarke, K. and Gorley, R.: Getting started with PRIMER v7, *PRIMER-E Plymouth Plymouth Mar. Lab.*, 20, 1–18, 2015.
- da Costa, E., Amaro, H. M., Melo, T., Guedes, A. C., and Domingues, M. R.: Screening for polar lipids, antioxidant, and anti-inflammatory activities of *Gloeotheca* sp. lipid extracts pursuing new phytochemicals from cyanobacteria, *J. Appl. Phycol.*, 32, 3015–3030, 2020.
- Danovaro, R., Della Croce, N., Dell’Anno, A., and Pusceddu, A.: A depocenter of organic matter at 7800 m depth in the SE Pacific Ocean, *Deep-Sea Res. Pt. I*, 50, 1411–1420, 2003.
- Danovaro, R., Snelgrove, P. V., and Tyler, P.: Challenging the paradigms of deep-sea ecology, *Trends Ecol. Evol.*, 29, 465–475, 2014.
- DeLong, E. F. and Yayanos, A. A.: Adaptation of the membrane lipids of a deep-sea bacterium to changes in hydrostatic pressure, *Science*, 228, 1101–1103, 1985.
- Dembitsky, V. M.: Betaine ether-linked glycerolipids: chemistry and biology, *Prog. Lipid Res.*, 35, 1–51, 1996.
- Dowhan, W.: Molecular basis for membrane phospholipid diversity: why are there so many lipids?, *Annu. Rev. Biochem.*, 66, 199–232, 1997.
- Eichenberger, W. and Gribi, C.: Lipids of *Pavlova lutheri*: cellular site and metabolic role of DGCC, *Phytochemistry*, 45, 1561–1567, 1997.
- Eloe, E. A., Shulse, C. N., Fadrosch, D. W., Williamson, S. J., Allen, E. E., and Bartlett, D. H.: Compositional differences in particle-associated and free-living microbial assemblages from an extreme deep-ocean environment, *Environ. Microbiol. Rep.*, 3, 449–458, 2011.
- Fang, J., Barcelona, M. J., Nogi, Y., and Kato, C.: Biochemical implications and geochemical significance of novel phospholipids of the extremely barophilic bacteria from the Marianas Trench at 11,000 m, *Deep-Sea Res. Pt. I*, 47, 1173–1182, 2000.
- Fernández-Urruzola, I., Ulloa, O., Glud, R., Pinkerton, M., Schneider W., Wenzhöfer, F., and Escribano, R.: Plankton respiration in the Atacama Trench region: Implications for particulate organic carbon flux into the hadal realm, *Limnol. Oceanogr.*, 66, 3134–3148, <https://doi.org/10.1002/lno.11866>, 2021.
- Fischer, J. P., Ferdelman, T. G., D’Hondt, S., Røy, H., and Wenzhöfer, F.: Oxygen penetration deep into the sediment of the South Pacific gyre, *Biogeosciences*, 6, 1467–1478, <https://doi.org/10.5194/bg-6-1467-2009>, 2009.
- Flores, E.: *EdgartFlores/IPLs-Atacama-Trench*, v1.0.0, Zenodo [data set], <https://doi.org/10.5281/zenodo.6325647>, 2022.
- Gao, Y., Du, X. Xu, W., Fan, R., Zhang, X., Yang, S., Chen, X., Lv, J., and Luo, Z.: Fungal diversity in deep sea sediments from east yap trench and their denitrification potential, *Geomicrobiol. J.*, 37, 848–858, 2020.
- Gašparović, B., Penezić, A., Frka, S., Kazazić, S., Lampitt, R. S., Holguin, F. O., Sudasinghe, N., and Schaub, T.: Particulate sulfur-containing lipids: Production and cycling from the epipelagic to the abyssopelagic zone, *Deep-Sea Res. Pt. I*, 134, 12–22, 2018.
- Geiger, O., Röhrs, V., Weissenmayer, B., Finan, T. M., and Thomas-Oates, J. E.: The regulator gene *phoB* mediates phosphate stress-controlled synthesis of the membrane lipid diacylglycerol-N, N, N-trimethylhomoserine in *Rhizobium* (*Sinorhizobium*) *melioloti*, *Mol. Microbiol.*, 32, 63–73, 1999.
- Glud, R. N., Wenzhöfer, F., Middelboe, M., Oguri, K., Turnewitsch, R., Canfield, D. E., and Kitazato, H.: High rates of microbial carbon turnover in sediments in the deepest oceanic trench on Earth, *Nat. Geosci.*, 6, 284–288, 2013.
- Glud, R. N., Berg, P., Thandrup, B., Larsen, M., Stewart, H. A., Jamieson, A. J., Glud, A., Oguri, K., Sanci, H., Rowden, A. A., and Wenzhöfer, F.: Hadal trenches are dynamic hotspots for early

- diagenesis in the deep sea, *Commun. Earth Environ.*, 2, 1–8, 2021.
- Goldfine, H.: Bacterial membranes and lipid packing theory, *J. Lipid Res.*, 25, 1501–1507, 1984.
- Goldfine, H. and Hagen, P.-O.: N-Methyl groups in bacterial lipids III. phospholipids of hyphomicrobia, *J. Bacteriol.*, 95, 367–375, 1968.
- Gombos, Z., Várkonyi, Z., Hagio, M., Iwaki, M., Kovács, L., Masamoto, K., Itoh, S., and Wada, H.: Phosphatidylglycerol requirement for the function of electron acceptor plastoquinone QB in the photosystem II reaction center, *Biochemistry*, 41, 3796–3802, 2002.
- Gómez-Consarnau, L., González, J. M., Coll-Lladó, M., Gourdon, P., Pascher, T., Neutze, R., Pedrós-Alió, C., and Pinhassi, J.: Light stimulates growth of proteorhodopsin-containing marine Flavobacteria, *Nature*, 445, 210–213, 2007.
- Gooday, A. J., Bett, B. J., Escobar, E., Ingole, B., Levin, L. A., Neira, C., Raman, A. V., and Sellanes, J.: Habitat heterogeneity and its influence on benthic biodiversity in oxygen minimum zones, *Mar. Ecol.*, 31, 125–147, 2010.
- Goumaris, K. and Barber, J.: Monogalactosyldiacylglycerol: the most abundant polar lipid in nature, *Trends Biochem. Sci.*, 8, 378–381, 1983.
- Gutiérrez, M. H., Vera J., Srain B., Quiñones, R. A., Wörmer L., Hinrichs K.-U., and Pantoja, S.: Biochemical fingerprints of marine fungi: implications for trophic and biogeochemical studies, *Aquat. Microb. Ecol.*, 84, 75–90, <https://doi.org/10.3354/ame01927>, 2020.
- Guan, H., Chen, L., Luo, M., Liu, L., Mao, S., Ge, H., Zhang, M., Fang, J., and Chen, D.: Composition and origin of lipid biomarkers in the surface sediments from the southern Challenger Deep, Mariana Trench, *Geosci. Front.*, 10, 351–360, 2019.
- Grabowski, E., Letelier, R. M., Laws, E. A., and Karl, D. M.: Coupling carbon and energy fluxes in the North Pacific Subtropical Gyre, *Nat. Commun.*, 10, 1895, <https://doi.org/10.1038/s41467-019-09772-z>, 2019.
- Hand, K., Bartlett, D., Fryer, P., Peoples, L., Williford, K., Hofmann, A., and Cameron, J.: Discovery of novel structures at 10.7 km depth in the Mariana Trench may reveal chemolithoautotrophic microbial communities, *Deep-Sea Res. Pt. I*, 160, 103238, <https://doi.org/10.1016/j.dsr.2020.103238>, 2020.
- Harvey, H. R., Fallon, R. D., and Patton, J. S.: The effect of organic matter and oxygen on the degradation of bacterial membrane lipids in marine sediments, *Geochim. Cosmochim. Ac.*, 50, 795–804, 1986.
- Harwood, J. L.: Membrane lipids in algae, in: *Lipids in photosynthesis: structure, function and genetics*, Springer, Dordrecht, 53–64, https://doi.org/10.1007/0-306-48087-5_3, 1998.
- Hedges, J. I., Baldock, J. A., Gélinas, Y., Lee, C., Peterson, M., and Wakeham, S. G.: Evidence for non-selective preservation of organic matter in sinking marine particles, *Nature*, 409, 801–804, 2001.
- Heinz, E.: Enzymatic reactions in galactolipid biosynthesis, in: *Lipids and lipid polymers in higher plants*, Springer, Berlin, Heidelberg, 102–120, https://doi.org/10.1007/978-3-642-66632-2_6, 1977.
- Hiraoka, S., Hirai, M., Matsui, Y., Makabe, A., Minegishi, H., Tsuda, M., Rastelli, E., Danovaro, R., Corinaldesi, C., Kitahashi, T., Tasumi, E., Nishizawa, M., Takai, K., Nomaki, H., and Nunoura, T.: Microbial community and geochemical analyses of trans-trench sediments for understanding the roles of hadal environments, *ISME J.*, 14, 740–756, 2020.
- Houston, J.: Variability of precipitation in the Atacama Desert: its causes and hydrological impact, *Int. J. Climatol. J. R. Meteorol. Soc.*, 26, 2181–2198, 2006.
- Hunter, J. E.: Phytoplankton lipidomics: lipid dynamics in response to microalgal stressors, PhD Thesis, University of Southampton, <https://ethos.bl.uk/OrderDetails.do?uin=uk.bl.ethos.675198> (last access: 3 March 2022), 2015.
- Ichino, M. C., Clark, M. R., Drazen, J. C., Jamieson, A., Jones, D. O., Martin, A. P., Rowden, A. A., Shank, T. M., Yancey, P. H., and Ruhl, H. A.: The distribution of benthic biomass in hadal trenches: a modelling approach to investigate the effect of vertical and lateral organic matter transport to the seafloor, *Deep-Sea Res. Pt. I*, 100, 21–33, 2015.
- Imhoff, J. F.: Taxonomy and physiology of phototrophic purple bacteria and green sulfur bacteria, in: *Anoxygenic photosynthetic bacteria*, Springer, Dordrecht, 1–15, https://doi.org/10.1007/0-306-47954-0_1, 1995.
- Inthorn, M., Wagner, T., Scheeder, G., and Zabel, M.: Lateral transport controls distribution, quality, and burial of organic matter along continental slopes in high-productivity areas, *Geology*, 34, 205–208, 2006.
- Itoh, M., Matsumura, I., and Noriki, S.: A large flux of particulate matter in the deep Japan Trench observed just after the 1994 Sanriku-Oki earthquake, *Deep-Sea Res. Pt. I*, 47, 1987–1998, 2000.
- Itoh, M., Kawamura, K., Kitahashi, T., Kojima, S., Katagiri, H., and Shimanaga, M.: Bathymetric patterns of meiofaunal abundance and biomass associated with the Kuril and Ryukyu trenches, western North Pacific Ocean, *Deep-Sea Res. Pt. I*, 58, 86–97, 2011.
- Jahnke, R. A. and Jahnke, D. B.: Rates of C, N, P and Si recycling and denitrification at the US Mid-Atlantic continental slope depocenter, *Deep-Sea Res. Pt. I*, 47, 1405–1428, 2000.
- Jahnke, R. A., Reimers, C. E., and Craven, D. B.: Intensification of recycling of organic matter at the sea floor near ocean margins, *Nature*, 348, 50–54, 1990.
- Jamieson, A. J., Fujii, T., Mayor, D. J., Solan, M., and Priede, I. G.: Hadal trenches: the ecology of the deepest places on Earth, *Trends Ecol. Evol.*, 25, 190–197, 2010.
- Jebbar, M., Franzetti, B., Girard, E., and Oger, P.: Microbial diversity and adaptation to high hydrostatic pressure in deep-sea hydrothermal vents prokaryotes, *Extremophiles*, 19, 721–740, 2015.
- Kalisch, B., Dörmann, P., and Hölzl, G.: DGDG and glycolipids in plants and algae, *Lipids Plant Algae Dev.*, 86, 51–83, 2016.
- Kaneda, T.: Iso- and anteiso-fatty acids in bacteria: biosynthesis, function, and taxonomic significance, *Microbiol. Mol. Biol. Rev.*, 55, 288–302, 1991.
- Kato, C., Masui, N., and Horikoshi, K.: Properties of obligately barophilic bacteria isolated from a sample of deep-sea sediment from the Izu-Bonin trench, *Oceanogr. Lit. Rev.*, 1, 53–54, 1997.
- Kato, M., Adachi, K., Hajiro-Nakanishi, K., Ishigaki, E., Sano, H., and Miyachi, S.: betaine lipid from Pavlova lutheri, *Phytochemistry*, 37, 279–280, [https://doi.org/10.1016/0031-9422\(94\)85041-0](https://doi.org/10.1016/0031-9422(94)85041-0), 1994.

- Kioka, A., Schwestermann, T., Moernaut, J., Ikehara, K., Kanamatsu, T., Eglinton, T. I., and Strasser, M.: Event stratigraphy in a hadal oceanic trench: The Japan trench as sedimentary archive recording recurrent giant subduction zone earthquakes and their role in organic carbon export to the deep sea, *Front. Earth Sci.*, 7, 319, <https://doi.org/10.3389/feart.2019.00319>, 2019.
- Koblížek, M., Falkowski, P. G., and Kolber, Z. S.: Diversity and distribution of photosynthetic bacteria in the Black Sea, *Deep-Sea Res. Pt. II*, 53, 1934–1944, 2006.
- Koga, Y. and Morii, H.: Biosynthesis of ether-type polar lipids in archaea and evolutionary considerations, *Microbiol. Mol. Biol. Rev.*, 71, 97–120, 2007.
- Komatsu, H. and Chong, P. L.-G.: Low permeability of liposomal membranes composed of bipolar tetraether lipids from thermoacidophilic archaeobacterium *Sulfolobus acidocaldarius*, *Biochemistry*, 37, 107–115, 1998.
- Lam, P., Jensen, M. M., Lavik, G., McGinnis, D. F., Müller, B., Schubert, C. J., Amann, R., Thamdrup, B., and Kuypers, M. M.: Linking crenarchaeal and bacterial nitrification to anammox in the Black Sea, *P. Natl. Acad. Sci. USA*, 104, 7104–7109, 2007.
- Lechevalier, H.: Chemotaxonomic use of lipids—an overview, *Microb. Lipids*, 1, 869–902, 1988.
- Leduc, D., Rowden, A. A., Glud, R. N., Wenzhöfer, F., Kitazato, H., and Clark, M. R.: Comparison between infaunal communities of the deep floor and edge of the Tonga Trench: possible effects of differences in organic matter supply, *Deep-Sea Res. Pt. I*, 116, 264–275, 2016.
- Lipp, J. S. and Hinrichs, K.-U.: Structural diversity and fate of intact polar lipids in marine sediments, *Geochim. Cosmochim. Ac.*, 73, 6816–6833, 2009a.
- Lipp, J. S., Morono, Y., Inagaki, F., and Hinrichs, K.-U.: Significant contribution of Archaea to extant biomass in marine subsurface sediments, *Nature*, 454, 991–994, 2008.
- Liu, J., Zheng, Y., Lin, H., Wang, X., Li, M., Liu, Y., Yu, M., Zhao, M., Pedentchouk, N., Lea-Smith, D. J., Todd, J. D., Magill, C. R., Zhang, W.-J., Zhou, S., Song, D., Zhong, H., Xin, Y., Min, Y., Tian, J., and Zhang, X.-H.: Proliferation of hydrocarbon-degrading microbes at the bottom of the Mariana Trench, *Microbiome*, 7, 1–13, 2019.
- Liu, X., Lipp, J. S., and Hinrichs, K.-U.: Distribution of intact and core GDGTs in marine sediments, *Org. Geochem.*, 42, 368–375, 2011.
- Liu, X.-L., Lipp, J. S., Simpson, J. H., Lin, Y.-S., Summons, R. E., and Hinrichs, K.-U.: Mono- and dihydroxyl glycerol dibiphytanyl glycerol tetraethers in marine sediments: Identification of both core and intact polar lipid forms, *Geochim. Cosmochim. Ac.*, 89, 102–115, 2012.
- Logemann, J., Graue, J., Köster, J., Engelen, B., Rullkötter, J., and Cypionka, H.: A laboratory experiment of intact polar lipid degradation in sandy sediments, *Biogeosciences*, 8, 2547–2560, <https://doi.org/10.5194/bg-8-2547-2011>, 2011.
- López-Lara, I. M., Sohlenkamp, C., and Geiger, O.: Membrane lipids in plant-associated bacteria: their biosyntheses and possible functions, *Mol. Plant. Microbe Interact.*, 16, 567–579, 2003.
- Lund, E. D. and Chu, F.-L. E.: Phospholipid biosynthesis in the oyster protozoan parasite, *Perkinsus marinus*, *Mol. Biochem. Parasitol.*, 121, 245–253, 2002.
- Luo, M., Gieskes, J., Chen, L., Shi, X., and Chen, D.: Provenances, distribution, and accumulation of organic matter in the southern Mariana Trench rim and slope: Implication for carbon cycle and burial in hadal trenches, *Mar. Geol.*, 386, 98–106, 2017.
- Macdonald, A.: The effects of pressure on the molecular structure and physiological functions of cell membranes, *Philos. T. R. Soc. Lond. B*, 304, 47–68, 1984.
- Makula, R.: Phospholipid composition of methane-utilizing bacteria, *J. Bacteriol.*, 134, 771–777, 1978.
- Mangelsdorf, K., Zink, K.-G., Birrien, J.-L., and Toffin, L.: A quantitative assessment of pressure dependent adaptive changes in the membrane lipids of a piezosensitive deep sub-seafloor bacterium, *Org. Geochem.*, 36, 1459–1479, 2005.
- Martin, J. H., Knauer, G. A., Karl, D. M., and Broenkow, W. W.: VERTEX: carbon cycling in the northeast Pacific, *Deep-Sea Res. Pt. I*, 34, 267–285, 1987.
- Matys, E., Sepúlveda, J., Pantoja, S., Lange, C., Caniupán, M., Lamy, F., and Summons, R. E.: Bacteriohopanepolyols along redox gradients in the Humboldt Current System off northern Chile, *Geobiology*, 15, 844–857, 2017.
- Mayzaud, P., Virtue, P., and Albessard, E.: Seasonal variations in the lipid and fatty acid composition of the euphausiid *Meganycitiphanes norvegica* from the Ligurian Sea, *Mar. Ecol. Prog. Ser.*, 186, 199–210, 1999.
- Mirzaei, A., Rahmati, M., and Ahmadi, M.: A new method for hierarchical clustering combination, *Intell. Data Anal.*, 12, 549–571, 2008.
- Murata, N. and Siegenthaler, P.-A.: Lipids in photosynthesis: an overview, *Lipids Photosynth. Struct. Funct. Genet.*, 6, 1–20, 1998.
- Nichols, D. S., Miller, M. R., Davies, N. W., Goodchild, A., Raftery, M., and Cavicchioli, R.: Cold adaptation in the Antarctic archaeon *Methanococcoides burtonii* involves membrane lipid unsaturation, *J. Bacteriol.*, 186, 8508–8515, 2004.
- Nunoura, T., Takaki, Y., Hirai, M., Shimamura, S., Makabe, A., Koide, O., Kikuchi, T., Miyazaki, J., Koba, K., Yoshida, N., Sunamura, M., and Takai, K.: Hadal biosphere: insight into the microbial ecosystem in the deepest ocean on Earth, *P. Natl. Acad. Sci. USA*, 112, E1230–E1236, 2015.
- Nunoura, T., Hirai, M., Yoshida-Takashima, Y., Nishizawa, M., Kawagucci, S., Yokokawa, T., Miyazaki, J., Koide, O., Makita, H., Takaki, Y., Sunamura, M., and Takai, K.: Distribution and niche separation of planktonic microbial communities in the water columns from the surface to the hadal waters of the Japan Trench under the Eutrophic Ocean, *Front. Microbiol.*, 7, 1261, <https://doi.org/10.3389/fmicb.2016.01261>, 2016.
- Nunoura, T., Nishizawa, M., Hirai, M., Shimamura, S., Harnvoravongchai, P., Koide, O., Morono, Y., Fukui, T., Inagaki, F., Miyazaki, J., Takaki, Y., and Takai, K.: Microbial Diversity in Sediments from the Bottom of the Challenger Deep, the Mariana Trench, *Microbes Environ.*, 33, 186–194, 2018.
- Oksanen, J., Blanchet, F. G., Kindt, R., Legendre, P., Minchin, P., O'hara, R., Simpson, G., Solymos, P., Stevens, M., and Wagner, H.: Community ecology package, R Package Version, 2, 2013.
- Oliver, J. D. and Colwell, R. R.: Extractable lipids of gram-negative marine bacteria: phospholipid composition, *J. Bacteriol.*, 114, 897–908, 1973.
- Patton, S., Lee, R. F., and Benson, A. A.: The presence of unusually high levels of lysophosphatidylethanolamine in a wax ester-synthesizing copepod (*Calanus plumchrus*), *Biochim. Biophys. Acta BBA-Lipids Lipid Metab.*, 270, 479–488, 1972.

- Periasamy, N., Teichert, H., Weise, K., Vogel, R. F., and Winter, R.: Effects of temperature and pressure on the lateral organization of model membranes with functionally reconstituted multidrug transporter LmrA, *Biochim. Biophys. Acta BBA-Biomembr.*, 1788, 390–401, 2009.
- Petersen, S. O., Henriksen, K., Blackburn, T. H., and King, G. M.: A comparison of phospholipid and chloroform fumigation analyses for biomass in soil: potentials and limitations, *FEMS Microbiol. Lett.*, 85, 257–267, 1991.
- Pitcher, A., Villanueva, L., Hopmans, E. C., Schouten, S., Reichart, G.-J., and Sinninghe Damsté, J. S.: Niche segregation of ammonia-oxidizing archaea and anammox bacteria in the Arabian Sea oxygen minimum zone, *ISME J.*, 5, 1896–1904, <https://doi.org/10.1038/ismej.2011.60>, 2011.
- Poff, K. E., Leu, A. O., Eppley, J. M., Karl, D. M., and DeLong, E. F.: Microbial dynamics of elevated carbon flux in the open ocean's abyss, *P. Natl. Acad. Sci. USA*, 118, 4, <https://doi.org/10.1073/pnas.2018269118>, 2021.
- Pond, D. and Harris, R.: The lipid composition of the coccolithophore *Emiliania huxleyi* and its possible ecophysiological significance, *J. Mar. Biol. Assoc. U. K.*, 76, 579–594, 1996.
- Popendorf, K. J., Tanaka, T., Pujo-Pay, M., Lagaria, A., Courties, C., Conan, P., Oriol, L., Sofen, L. E., Moutin, T., and Van Mooy, B. A. S.: Gradients in intact polar diacylglycerol lipids across the Mediterranean Sea are related to phosphate availability, *Biogeosciences*, 8, 3733–3745, <https://doi.org/10.5194/bg-8-3733-2011>, 2011a.
- Popendorf, K. J., Lomas, M. W., and Van Mooy, B. A.: Microbial sources of intact polar diacylglycerol lipids in the Western North Atlantic Ocean, *Org. Geochem.*, 42, 803–811, 2011b.
- Ratledge, C. and Wilkinson, S. G.: Microbial lipids, Academic press, <https://doi.org/10.1002/abio.370110506>, 1988.
- Rex, M. A., Etter, R. J., Morris, J. S., Crouse, J., McClain, C. R., Johnson, N. A., Stuart, C. T., Deming, J. W., Thies, R., and Avery, R.: Global bathymetric patterns of standing stock and body size in the deep-sea benthos, *Mar. Ecol. Prog. Ser.*, 317, 1–8, 2006.
- Řezanka, T. and Sigler, K.: Odd-numbered very-long-chain fatty acids from the microbial, animal and plant kingdoms, *Prog. Lipid Res.*, 48, 206–238, 2009.
- Řezanka, T., Viden, I., Go, J., Dor, I., and Dembitsky, V.: Polar lipids and fatty acids of three wild cyanobacterial strains of the genus *Chroococcidiopsis*, *Folia Microbiol.*, 48, 781–786, 2003.
- Rossel, P. E., Elvert, M., Ramette, A., Boetius, A., and Hinrichs, K.-U.: Factors controlling the distribution of anaerobic methanotrophic communities in marine environments: evidence from intact polar membrane lipids, *Geochim. Cosmochim. Ac.*, 75, 164–184, 2011.
- Rütters, H., Sass, H., Cypionka, H., and Rullkötter, J.: Monoalkylether phospholipids in the sulfate-reducing bacteria *Desulfosarcina variabilis* and *Desulforhabdus amnigenus*, *Arch. Microbiol.*, 176, 435–442, 2001.
- Sabbatini, A., Morigi, C., Negri, A., and Goody, A. J.: Soft-shelled benthic foraminifera from a hadal site (7800 m water depth) in the Atacama Trench (SE Pacific): preliminary observations, *J. Micropalaeontol.*, 21, 131–135, 2002.
- Sakurai, I., Shen, J.-R., Leng, J., Ohashi, S., Kobayashi, M., and Wada, H.: Lipids in oxygen-evolving photosystem II complexes of cyanobacteria and higher plants, *J. Biochem.*, 140, 201–209, 2006.
- Sato, N.: Betaine lipids, *Bot. Mag. Shokubutsu-Gaku-Zasshi*, 105, 185–197, 1992.
- Sato, N., Hagio, M., Wada, H., and Tsuzuki, M.: Requirement of phosphatidylglycerol for photosynthetic function in thylakoid membranes, *P. Natl. Acad. Sci. USA*, 97, 10655–10660, 2000.
- Schauberger, C., Middelboe, M., Larsen, M., Peoples, L. M., Bartlett, D. H., Kirpekar, F., Rowden, A. A., Wenzhöfer, F., Thamdrup, B., and Glud, R. N.: Spatial variability of prokaryotic and viral abundances in the Kermadec and Atacama Trench regions, *Limnol. Oceanogr.*, 66, 2095–2109, 2021.
- Schneider, W., Fuenzalida, R., Garcés-Vargas, J., Bravo, L., and Lange, C.: Extensión vertical y horizontal de la zona de mínima oxígeno en el Pacífico Sur Oriental, *Gayana Concepc.*, 70, 79–82, 2006.
- Schouten, S., Middelburg, J. J., Hopmans, E. C., and Damsté, J. S. S.: Fossilization and degradation of intact polar lipids in deep subsurface sediments: a theoretical approach, *Geochim. Cosmochim. Ac.*, 74, 3806–3814, 2010.
- Schubotz, F., Wakeham, S. G., Lipp, J. S., Fredricks, H. F., and Hinrichs, K.-U.: Detection of microbial biomass by intact polar membrane lipid analysis in the water column and surface sediments of the Black Sea, *Environ. Microbiol.*, 11, 2720–2734, 2009.
- Schubotz, F., Meyer-Dombard, D., Bradley, A. S., Fredricks, H. F., Hinrichs, K.-U., Shock, E., and Summons, R. E.: Spatial and temporal variability of biomarkers and microbial diversity reveal metabolic and community flexibility in Streamer Biofilm Communities in the Lower Geyser Basin, Yellowstone National Park, *Geobiology*, 11, 549–569, 2013.
- Schubotz, F., Xie, S., Lipp, J. S., Hinrichs, K.-U., and Wakeham, S. G.: Intact polar lipids in the water column of the eastern tropical North Pacific: abundance and structural variety of non-phosphorus lipids, *Biogeosciences*, 15, 6481–6501, <https://doi.org/10.5194/bg-15-6481-2018>, 2018.
- Schwestermann, T., Eglinton, T., Haghipour, N., McNichol, A., Ikehara, K., and Strasser, M.: Event-dominated transport, provenance, and burial of organic carbon in the Japan Trench, *Earth Planet. Sci. Lett.*, 563, 116870, <https://doi.org/10.1016/j.epsl.2021.116870>, 2021.
- Sebastián, M., Smith, A. F., González, J. M., Fredricks, H. F., Van Mooy, B., Koblížek, M., Brandsma, J., Koster, G., Mestre, M., Mostajir, B., Pitta, P., Postle, A. D., Sánchez, P., Gasol, J. M., Scanlan, D. J., and Chen, Y.: Lipid remodelling is a widespread strategy in marine heterotrophic bacteria upon phosphorus deficiency, *ISME J.*, 10, 968–978, 2016.
- Shaw, N.: Lipid composition as a guide to the classification of bacteria, *Adv. Appl. Microbiol.*, 17, 63–108, 1974.
- Siegenthaler, P.-A.: Molecular organization of acyl lipids in photosynthetic membranes of higher plants, in: *Lipids in photosynthesis: structure, function and genetics*, Springer, 119–144, https://doi.org/10.1007/0-306-48087-5_7, 1998.
- Siliakus, M. F., van der Oost, J., and Kengen, S. W.: Adaptations of archaeal and bacterial membranes to variations in temperature, pH and pressure, *Extremophiles*, 21, 651–670, 2017.
- Smith, C.: Chemosynthesis in the deep-sea: life without the sun, *Biogeosciences Discuss.*, 9, 17037–17052, <https://doi.org/10.5194/bgd-9-17037-2012>, 2012.

- Sohlenkamp, C., López-Lara, I. M., and Geiger, O.: Biosynthesis of phosphatidylcholine in bacteria, *Prog. Lipid Res.*, 42, 115–162, 2003.
- Somero, G. N.: Adaptations to high hydrostatic pressure, *Annu. Rev. Physiol.*, 54, 557–577, 1992.
- Stockton, W. L. and DeLaca, T. E.: Food falls in the deep sea: occurrence, quality, and significance, *Deep-Sea Res. Pt. I*, 29, 157–169, 1982.
- Sturt, H. F., Summons, R. E., Smith, K., Elvert, M., and Hinrichs, K.-U.: Intact polar membrane lipids in prokaryotes and sediments deciphered by high-performance liquid chromatography/electrospray ionization multistage mass spectrometry – new biomarkers for biogeochemistry and microbial ecology, *Rapid Commun. Mass Spectrom.*, 18, 617–628, 2004.
- Suzuki, R. and Shimodaira, H.: Pvcust: an R package for assessing the uncertainty in hierarchical clustering, *Bioinformatics*, 22, 1540–1542, 2006.
- Ta, K., Peng, X., Xu, H., Du, M., Chen, S., Li, J., and Zhang, C.: Distributions and sources of glycerol dialkyl glycerol tetraethers in sediment cores from the Mariana subduction zone, *J. Geophys. Res.-Biogeo.*, 124, 857–869, 2019.
- Tamburini, C., Boutrif, M., Garel, M., Colwell, R. R., and Deming, J. W.: Prokaryotic responses to hydrostatic pressure in the ocean – a review, *Environ. Microbiol.*, 15, 1262–1274, 2013.
- Tarn, J., Peoples, L. M., Hardy, K., Cameron, J., and Bartlett, D. H.: Identification of free-living and particle-associated microbial communities present in hadal regions of the Mariana Trench, *Front. Microbiol.*, 7, 665, <https://doi.org/10.3389/fmicb.2016.00665>, 2016.
- Thompson Jr., G. A.: Lipids and membrane function in green algae, *Biochim. Biophys. Acta BBA-Lipids Lipid Metab.*, 1302, 17–45, 1996.
- Turnewitsch, R., Falahat, S., Stehlikova, J., Oguri, K., Glud, R. N., Middelboe, M., Kitazato, H., Wenzhöfer, F., Ando, K., Fujio, S., and Yanagimoto, D.: Recent sediment dynamics in hadal trenches: evidence for the influence of higher-frequency (tidal, near-inertial) fluid dynamics, *Deep-Sea Res. Pt. I*, 90, 125–138, 2014.
- Van Mooy, B. A. and Fredricks, H. F.: Bacterial and eukaryotic intact polar lipids in the eastern subtropical South Pacific: water-column distribution, planktonic sources, and fatty acid composition, *Geochim. Cosmochim. Ac.*, 74, 6499–6516, 2010.
- Van Mooy, B. A., Rocap, G., Fredricks, H. F., Evans, C. T., and Devol, A. H.: Sulfolipids dramatically decrease phosphorus demand by picocyanobacteria in oligotrophic marine environments, *P. Natl. Acad. Sci. USA*, 103, 8607–8612, 2006.
- Van Mooy, B. A., Fredricks, H. F., Pedler, B. E., Dyhrman, S. T., Karl, D. M., Koblížek, M., Lomas, M. W., Mincer, T. J., Moore, L. R., Moutin, T., Rappé, M. S., and Webb, E. A.: Phytoplankton in the ocean use non-phosphorus lipids in response to phosphorus scarcity, *Nature*, 458, 69–72, 2009.
- Vardi, A., Van Mooy, B. A., Fredricks, H. F., Popendorf, K. J., Osolinski, J. E., Haramaty, L., and Bidle, K. D.: Viral glycosphingolipids induce lytic infection and cell death in marine phytoplankton, *Science*, 326, 861–865, 2009.
- Vargas, C. A., Cantarero, S. I., Sepúlveda, J., Galán, A., De Pol-Holz, R., Walker, B., Schneider, W., Fariás, L., D’Ottone, M. C., Walker, J., Xu, X., and Salisbury, J.: A source of isotopically light organic carbon in a low-pH anoxic marine zone, *Nat. Commun.*, 12, 1–11, 2021.
- Volkman, J., Jeffrey, S., Nichols, P., Rogers, G., and Garland, C.: Fatty acid and lipid composition of 10 species of microalgae used in mariculture, *J. Exp. Mar. Biol. Ecol.*, 128, 219–240, 1989.
- Wada, H. and Murata, N.: Membrane lipids in cyanobacteria, in: *Lipids in photosynthesis: structure, function and genetics*, Springer, 65–81, https://doi.org/10.1007/0-306-48087-5_4, 1998.
- Wada, H. and Murata, N.: The essential role of phosphatidylglycerol in photosynthesis, *Photosynth. Res.*, 92, 205–215, 2007.
- Wakeham, S. G., Lee, C., Farrington, J. W., and Gagosian, R. B.: Biogeochemistry of particulate organic matter in the oceans: results from sediment trap experiments, *Deep-Sea Res. Pt. I*, 31, 509–528, 1984.
- Wakeham, S. G., Turich, C., Schubotz, F., Podlaska, A., Li, X. N., Varela, R., Astor, Y., Saenz, J. P., Rush, D., Damste, J. S. S., Summons, R. E., Scranton, M. I., Taylor, G. T., and Hinrichs, K.-U.: Biomarkers, chemistry and microbiology show chemoautotrophy in a multilayer chemocline in the Cariaco Basin, *Deep-Sea Res. Pt. I*, 63, 133–156, 2012.
- Warnes, G., Bolker, B., Bonebakker, L., Gentleman, R., Liaw, W., Lumley, T., Maechler, M., Magnusson, A., Moeller, S., Schwartz, M., Venables, B., and Galili, T.: gplots: various R programming tools for plotting data, R package version 2.16.0.2015, <https://github.com/talgalili/gplots> (last access: 3 March 2022), 2015.
- Warton, D. I., Wright, S. T., and Wang, Y.: Distance-based multivariate analyses confound location and dispersion effects, *Methods Ecol. Evol.*, 3, 89–101, 2012.
- Weijers, J. W., Schouten, S., van den Donker, J. C., Hopmans, E. C., and Damsté, J. S. S.: Environmental controls on bacterial tetraether membrane lipid distribution in soils, *Geochim. Cosmochim. Ac.*, 71, 703–713, 2007.
- Wenzhöfer, F.: The Expedition SO261 of the Research Vessel SONNE to the Atacama Trench in the Pacific Ocean in 2018, *Rep. Polar Mar. Res.*, 729, 1–111, 2019.
- Wenzhöfer, F., Oguri, K., Middelboe, M., Turnewitsch, R., Toyofuku, T., Kitazato, H., and Glud, R. N.: Benthic carbon mineralization in hadal trenches: Assessment by in situ O₂ microprofile measurements, *Deep-Sea Res. Pt. I*, 116, 276–286, 2016.
- Wenzhöfer, F.: The Expedition SO261 of the Research Vessel SONNE to the Atacama Trench in the Pacific Ocean in 2018, *Rep. Polar Mar. Res.*, 729, 1–111, 2019.
- Westrich, J. T. and Berner, R. A.: The role of sedimentary organic matter in bacterial sulphate reduction – the G model tested, *Limnol. Oceanogr.*, 29, 236–249, 1984.
- White, D., Bobbie, R., King, J., Nickels, J., and Amoe, P.: Lipid analysis of sediments for microbial biomass and community structure, in: *Methodology for biomass determinations and microbial activities in sediments*, ASTM International, 673, 87–103, 1979.
- Winter, R.: Effect of lipid chain length, temperature, pressure and composition on the lateral organisation and phase behavior of lipid bilayer/gramicidin mixtures, *Biophys. J.*, 1, 153A–153A, 2002.
- Winter, R. and Jeworrek, C.: Effect of pressure on membranes, *Soft Matter*, 5, 3157–3173, 2009.
- Wörmer, L., Lipp, J. S., Schröder, J. M., and Hinrichs, K.-U.: Application of two new LC-ESI-MS methods for improved detec-

- tion of intact polar lipids (IPLs) in environmental samples, *Org. Geochem.*, 59, 10–21, 2013.
- Xu, Y., Ge, H., and Fang, J.: Biogeochemistry of hadal trenches: Recent developments and future perspectives, *Deep-Sea Res. Pt. II*, 155, 19–26, <https://doi.org/10.1016/j.dsr2.2018.10.006>, 2018.
- Xu, Y., Wu, W., Xiao, W., Ge, H., Wei, Y., Yin, X., Yao, H., Lipp, S. J., Pan, B., and Hinrichs, K. U.: Intact ether lipids in trench sediments related to archaeal community and environmental conditions in the deepest ocean, *J. Geophys. Res.-Biogeo.*, 125, e2019JG005431, <https://doi.org/10.1029/2019JG005431>, 2020a.
- Xu, Y., Jia, Z., Xiao, W., Fang, J., Wang, Y., Luo, M., Wenzhöfer, F., Rowden, A. A., and Glud, R. N.: Glycerol dialkyl glycerol tetraethers in surface sediments from three Pacific trenches: Distribution, source and environmental implications, *Org. Geochem.*, 147, 104079, <https://doi.org/10.1016/j.orggeochem.2020.104079>, 2020b.
- Xu, Y., Li, X., Luo, M., Xiao, W., Fang, J., Rashid, H., Peng, Y., Li, W., Wenzhöfer, F., Rowden, A. A., and Glud, R. N.: Distribution, Source, and Burial of Sedimentary Organic Carbon in Kermadec and Atacama Trenches, *J. Geophys. Res.-Biogeo.*, 126, e2020JG006189, <https://doi.org/10.1029/2020JG006189>, 2021.
- Yano, Y., Nakayama, A., Ishihara, K., and Saito, H.: Adaptive changes in membrane lipids of barophilic bacteria in response to changes in growth pressure, *Appl. Environ. Microbiol.*, 64, 479–485, 1998.
- Zheng, Y., Wang, J., Zhou, S., Zhang, Y., Liu, J., Xue, C. X., Williams, B. T., Zhao, X., Zhao, L., Zhu, X.-Y., Sun, C., Zhang, H.-H., Xiao, T., Yang, G.-P., Todd, J. D., and Zhang, X. H.: Bacteria are important dimethylsulfoniopropionate producers in marine aphotic and high-pressure environments, *Nat. Commun.*, 11, 1–12, <https://doi.org/10.1038/s41467-020-18434-4>, 2020.
- Zhong, H., Lehtovirta-Morley, L., Liu, J., Zheng, Y., Lin, H., Song, D., Todd, J. D., Tian, J., and Zhang, X.-H.: Novel insights into the Thaumarchaeota in the deepest oceans: their metabolism and potential adaptation mechanisms, *Microbiome*, 8, 1–16, 2020.
- Zhukova, N. V.: Variation in microbial biomass and community structure in sediments of Peter the Great Bay (Sea of Japan/East Sea), as estimated from fatty acid biomarkers, *Ocean Sci. J.*, 40, 34–42, 2005.

Supplement of

Flores et al. 'Bacterial and eukaryotic intact polar lipids point to in situ production as a key source of labile organic matter in hadal surface sediment of the Atacama Trench'

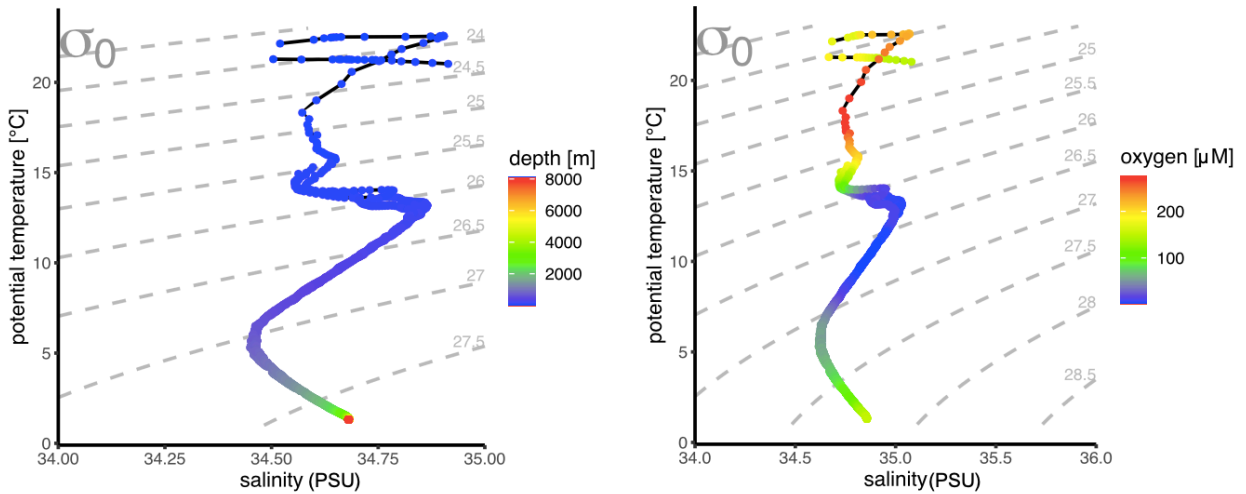
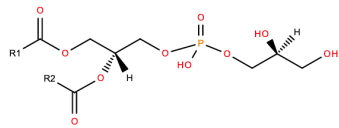
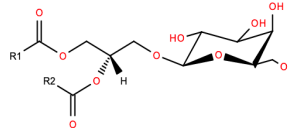


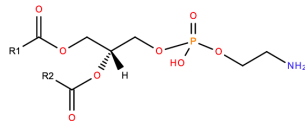
Figure 5. The potential temperature–salinity (θ – s) diagrams from CTD data coupled to an AUV (autonomous underwater vehicle). The color scale is related to depth (m) and oxygen concentration (μM).



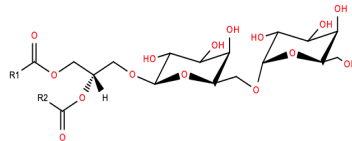
Phosphatidylglycerol Head group (PG)



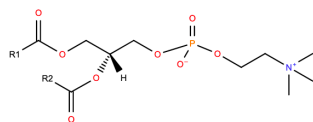
Monogalactosyl diacylglycerol Head group (MGDG)



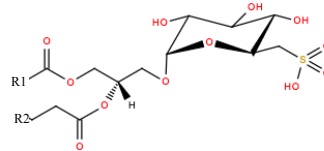
Phosphatidylethanolamine Head group (PE)



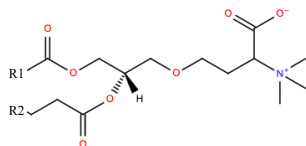
Digalactosyl diacylglycerol Head group (DGDG)



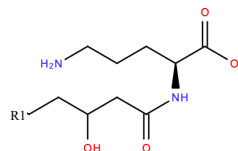
Phosphatidylcholine Head group (PC)



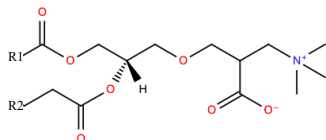
Sulfoquinovosyl diacylglycerol Head group (SQDG)



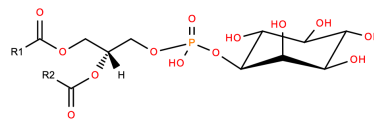
Diacylglyceryltrimethylhomoserine Head group (DGTS)



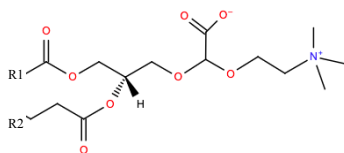
Ornithine lipid Head group (OL)



Diacylglyceryl-hydroxymethyltrimethyl- β -alanine Head group (DGTA)



Phosphatidylinositol Head group (PI)



Diacylglyceryl carboxyhydroxymethylcholine Head group (DGCC)

Figure 6. IPL chemical structures from the LIPID MAPS database (Sud et al., 2007). R1 and R2 represent acyl groups, whereas the charges are those expected at seawater pH.



Figure 7. Relative abundances of IPLs distinctive (red color; Cantarero et al. 2020) and non-distinctive (turquoise; total IPLs minus IPLs from Chlorophyll maximum) of the Chlorophyll maximum for all samples.

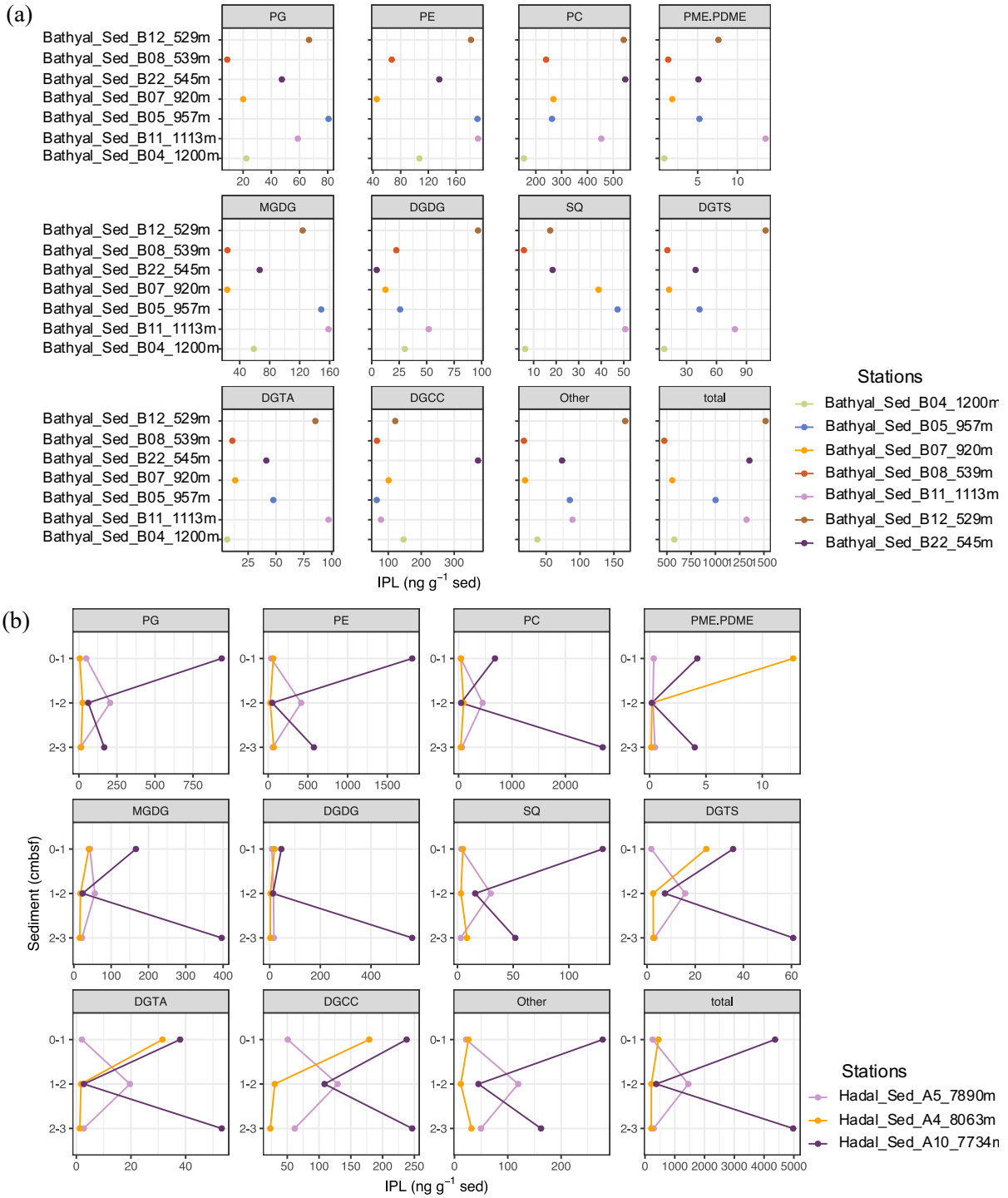


Figure 8. Total concentration of IPL by class, in (a) bathyal and (b) hadal sediment samples.

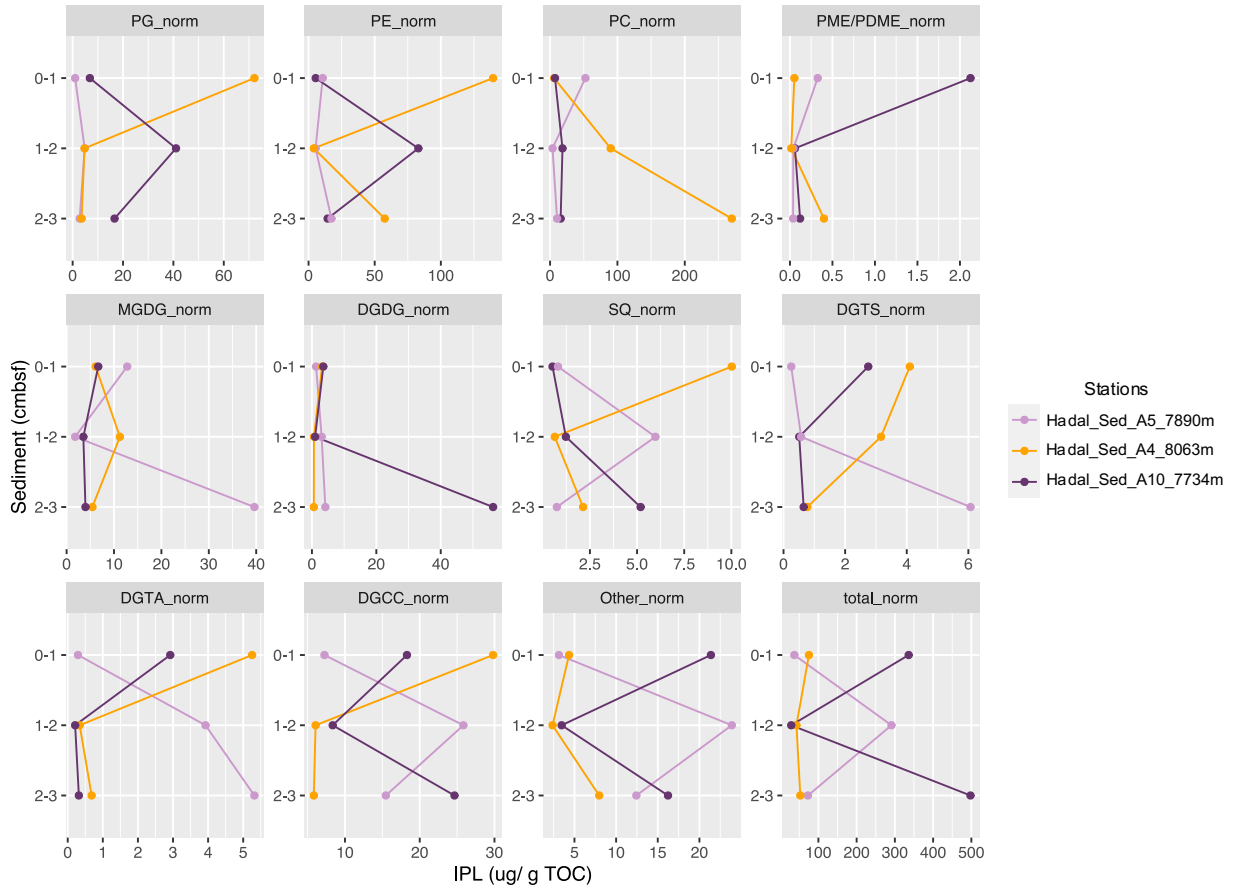


Figure 9. TOC-normalized IPL concentration (µg IPL/g TOC) in hadal sediments.

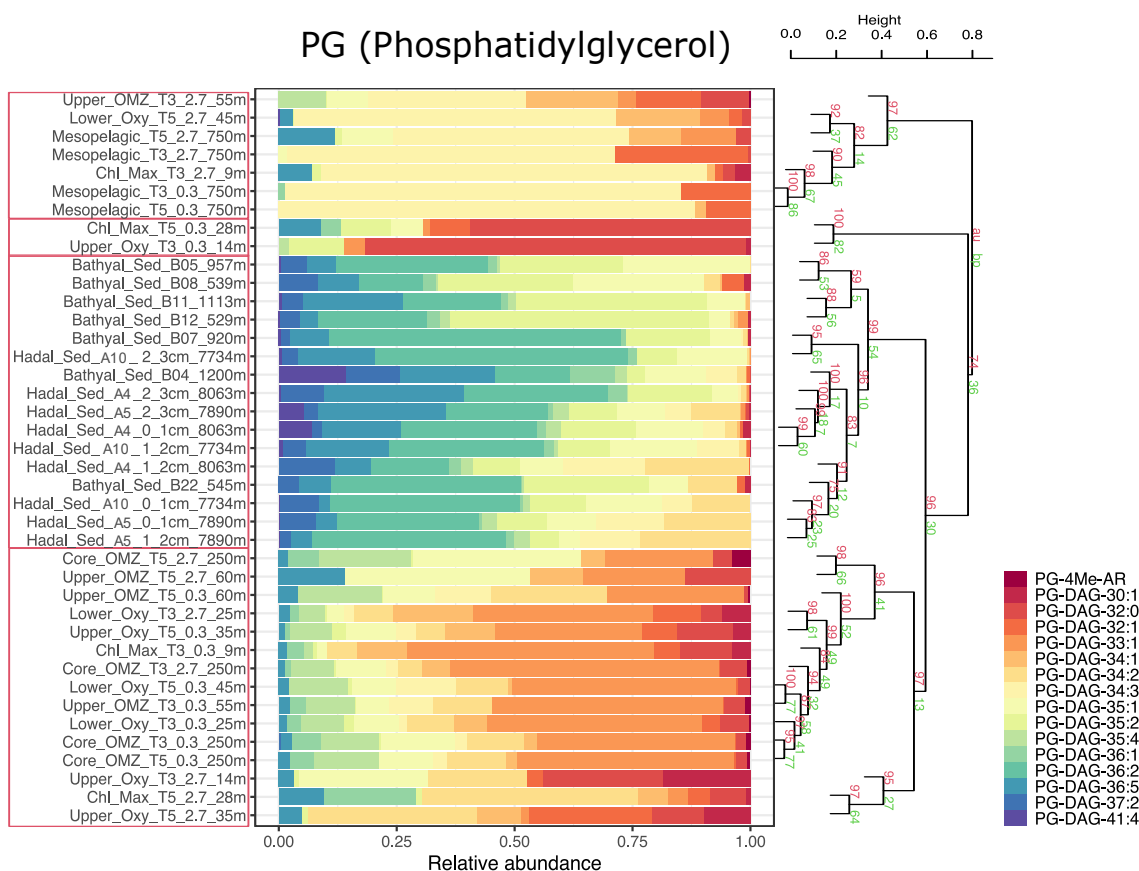


Figure 10. Cumulative bar chart of PG phospholipid fractional abundances. The number of carbon atoms and unsaturation in core fatty acids follows the order shown in the legend. The right panel depicts a cluster analysis with AU and BP shown in red and green, respectively, and p-values shown at branching points. The number of bootstrap replicates is 10000. Clusters with AU \geq 95% confidence are highlighted in red boxes on the left-hand side.

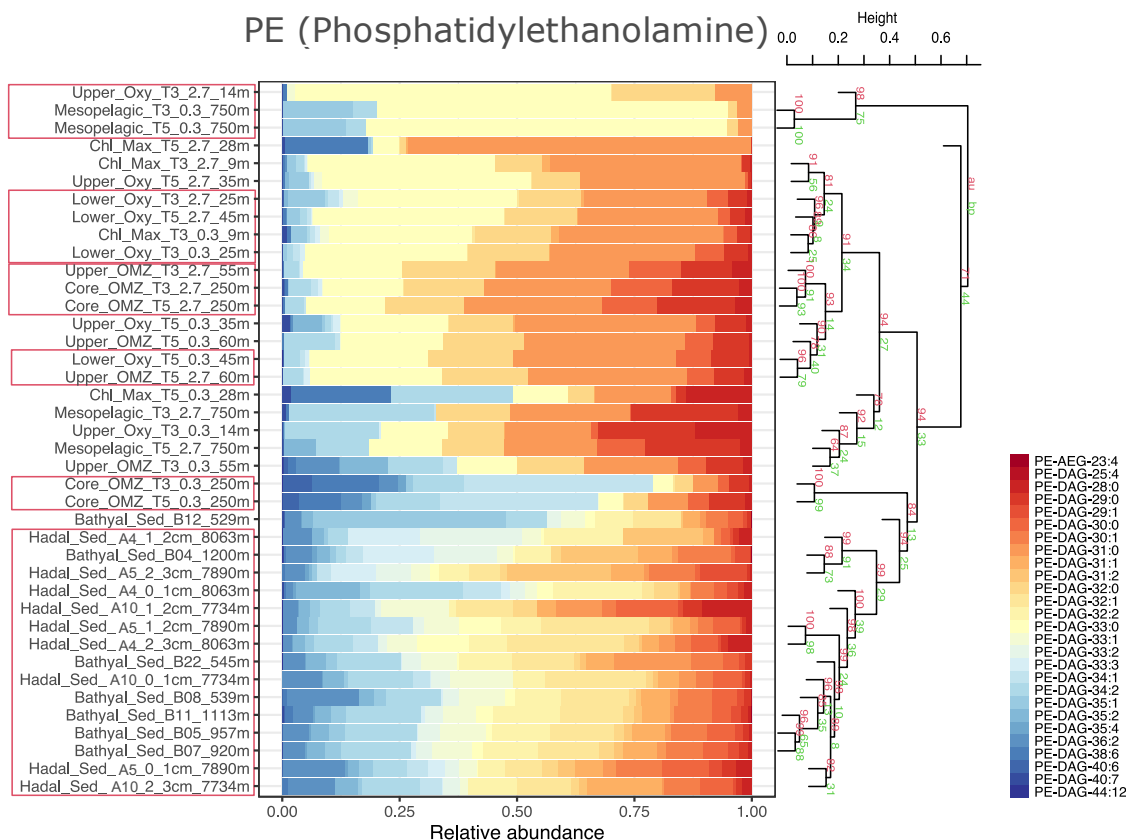


Figure 11. Cumulative bar chart of PE phospholipid fractional abundances. The number of carbon atoms and unsaturation in core fatty acids follows the order shown in the legend. The right panel depicts a cluster analysis with AU and BP shown in red and green, respectively, and p-values shown at branching points. The number of bootstrap replicates is 10000. Clusters with AU \geq 95% confidence are highlighted in red boxes on the left-hand side.

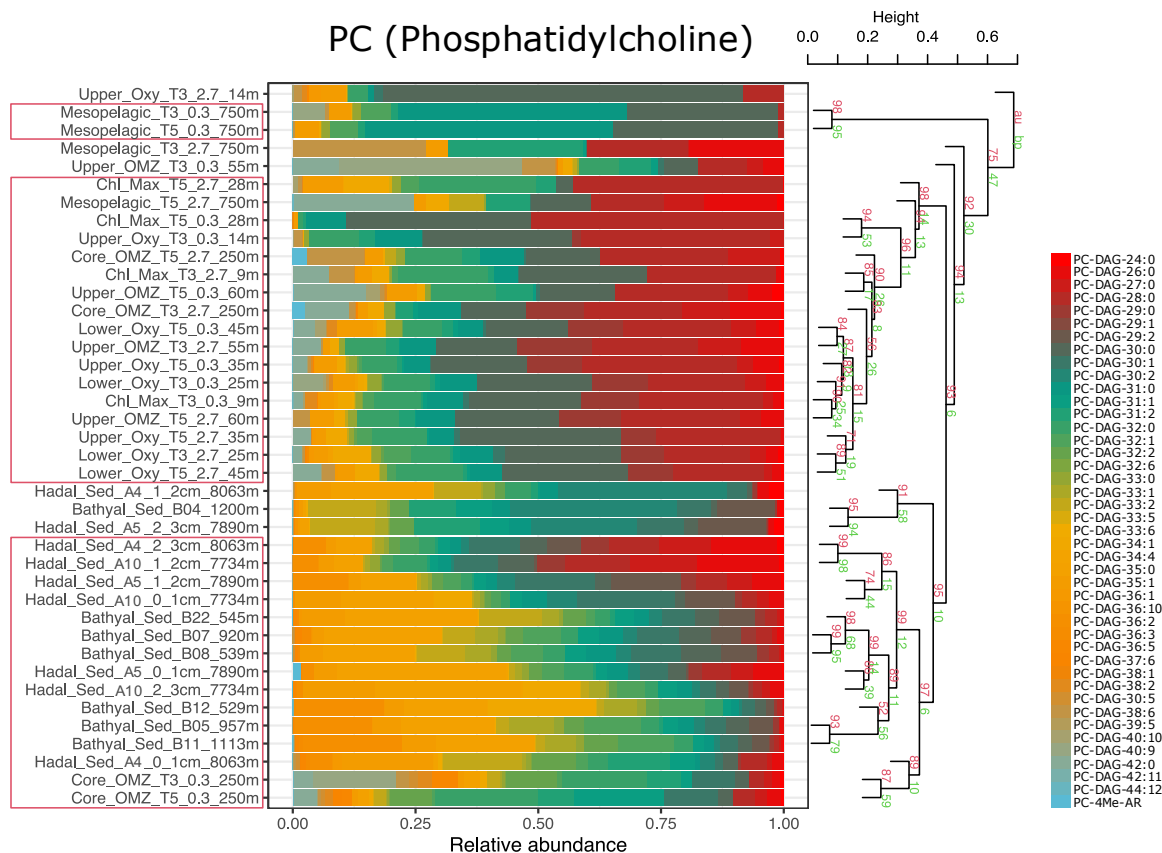


Figure 10. Cumulative bar chart of PC phospholipid fractional abundances. The number of carbon atoms and unsaturation in core fatty acids follows the order shown in the legend. The right panel depicts a cluster analysis with AU and BP shown in red and green, respectively, and p-values shown at branching points. The number of bootstrap replicates is 10000. Clusters with AU \geq 95% confidence are highlighted in red boxes on the left-hand side.

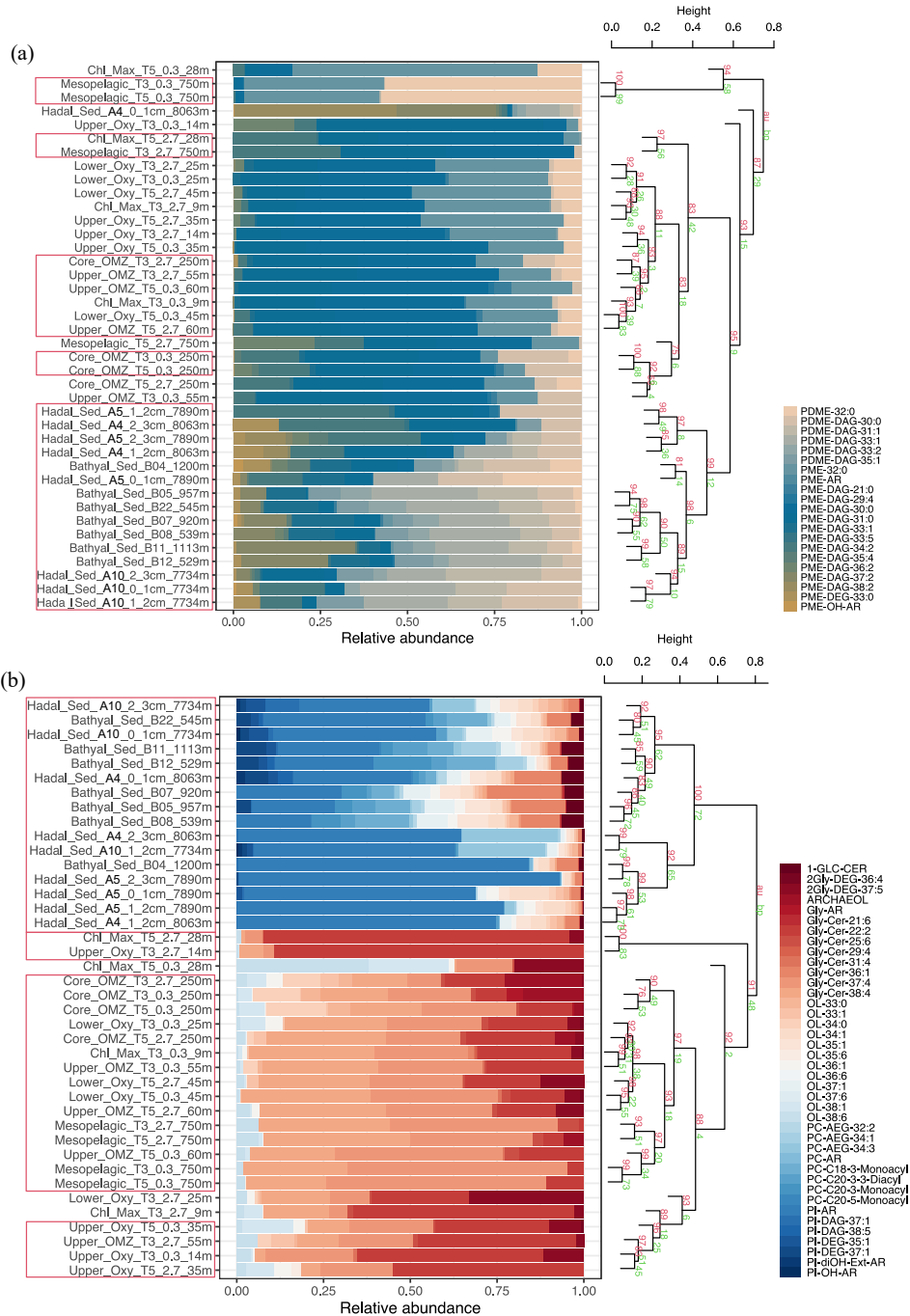


Figure 13. Cumulative bar chart of IPLs fractional abundances. a) PDME, PME; b) Other lipids. The number of carbon atoms and unsaturation in core fatty acids follows the order shown in the legend. The right panel depicts a cluster analysis with approximately unbiased (AU) and bootstrap probability (BP) shown in red and green, respectively, and p-values shown at branching points. The number of bootstrap replicates is 10000. Clusters with AU \geq 95% confidence are highlighted in red boxes on the left-hand side.

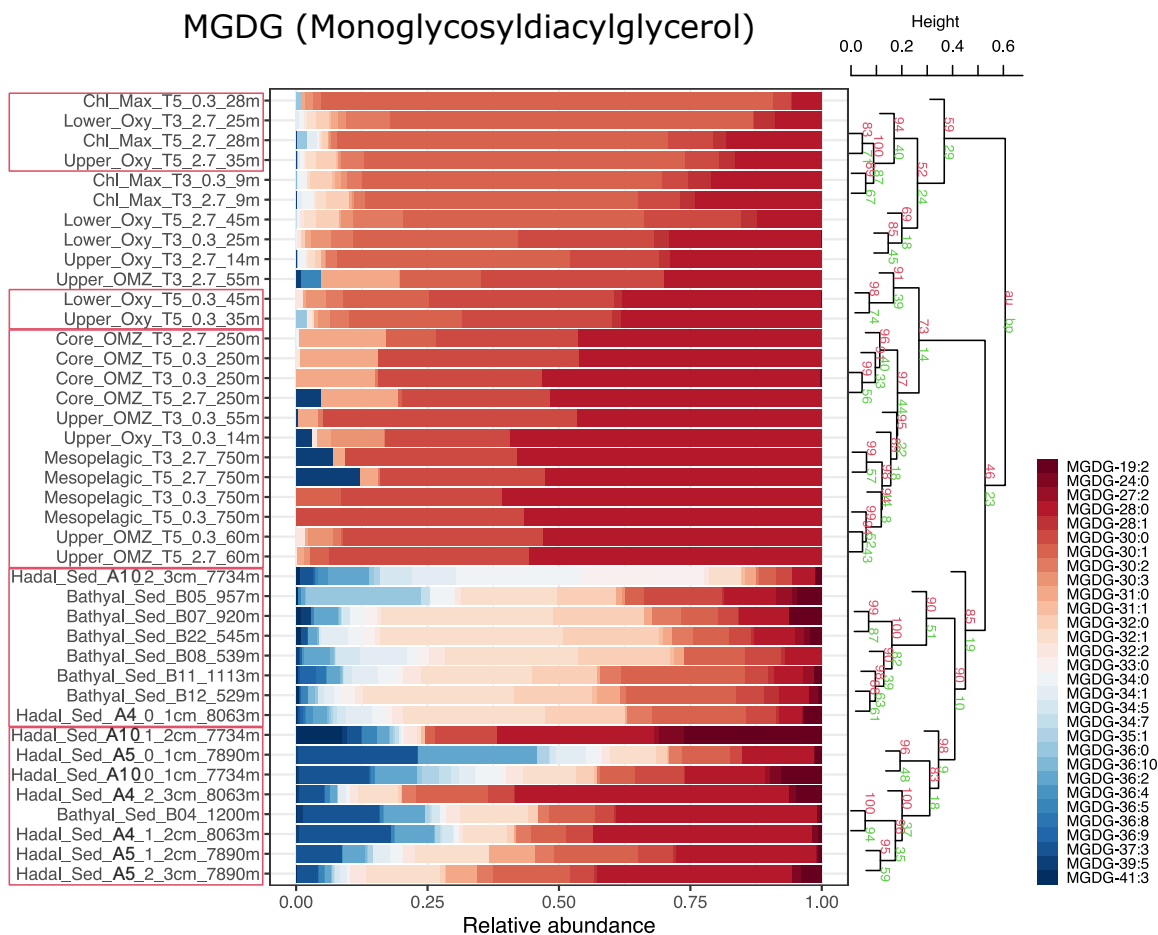


Figure 14. Cumulative bar chart of MGDG glycolipid fractional abundances. The number of carbon atoms and unsaturation in core fatty acids follows the order shown in the legend. The right panel depicts a cluster analysis with AU and BP in red and green, respectively, and p-values shown at branching points. The number of bootstrap replicates is 10000. Clusters with AU \geq 95% confidence are highlighted in red boxes on the left-hand side.

DGDG (Diglycosyldiacylglycerol)

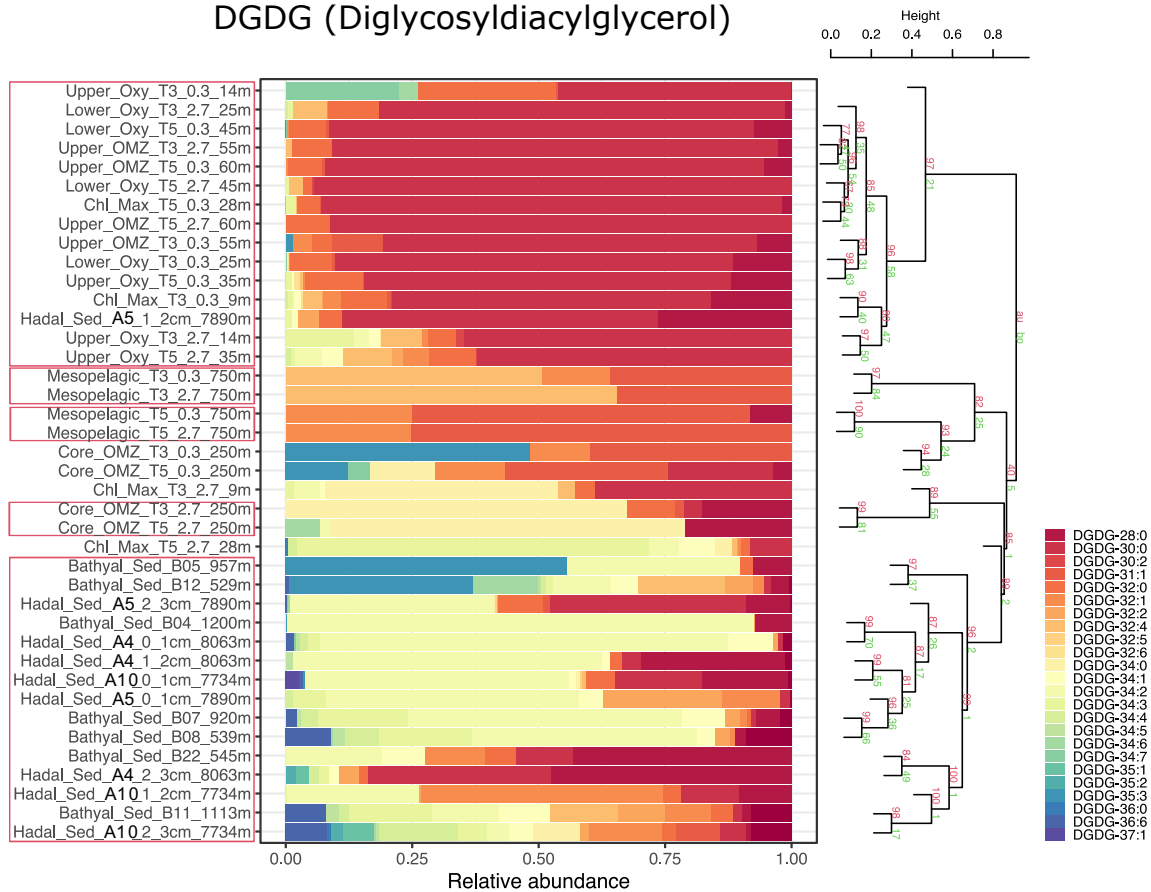


Figura 15. Cumulative bar chart of DGDG glycolipid fractional abundances. The number of carbon atoms and unsaturation in core fatty acids follows the order shown in the legend. The right panel depicts a cluster analysis with AU and BP in red and green, respectively, and p-values shown at branching points. The number of bootstrap replicates is 10000. Clusters with AU \geq 95% confidence are highlighted in red boxes on the left-hand side.

SQDG (Sulfoquinovosyldiacylglycerol)

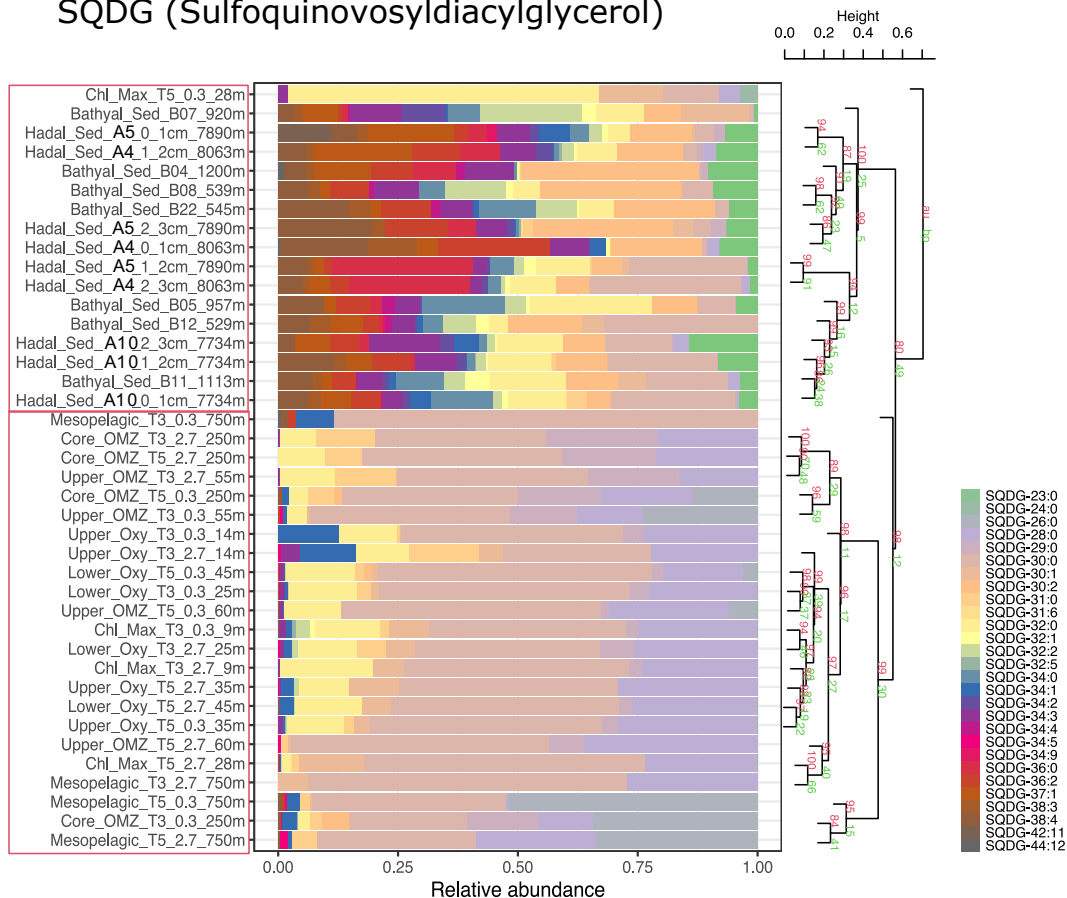


Figura 11. Cumulative bar chart of SQDG glycolipid fractional abundances. The number of carbon atoms and unsaturation in core fatty acids follows the order shown in the legend. The right panel depicts a cluster analysis with AU and BP in red and green, respectively, and p-values shown at branching points. The number of bootstrap replicates is 10000. Clusters with AU \geq 95% confidence are highlighted in red boxes on the left-hand side.

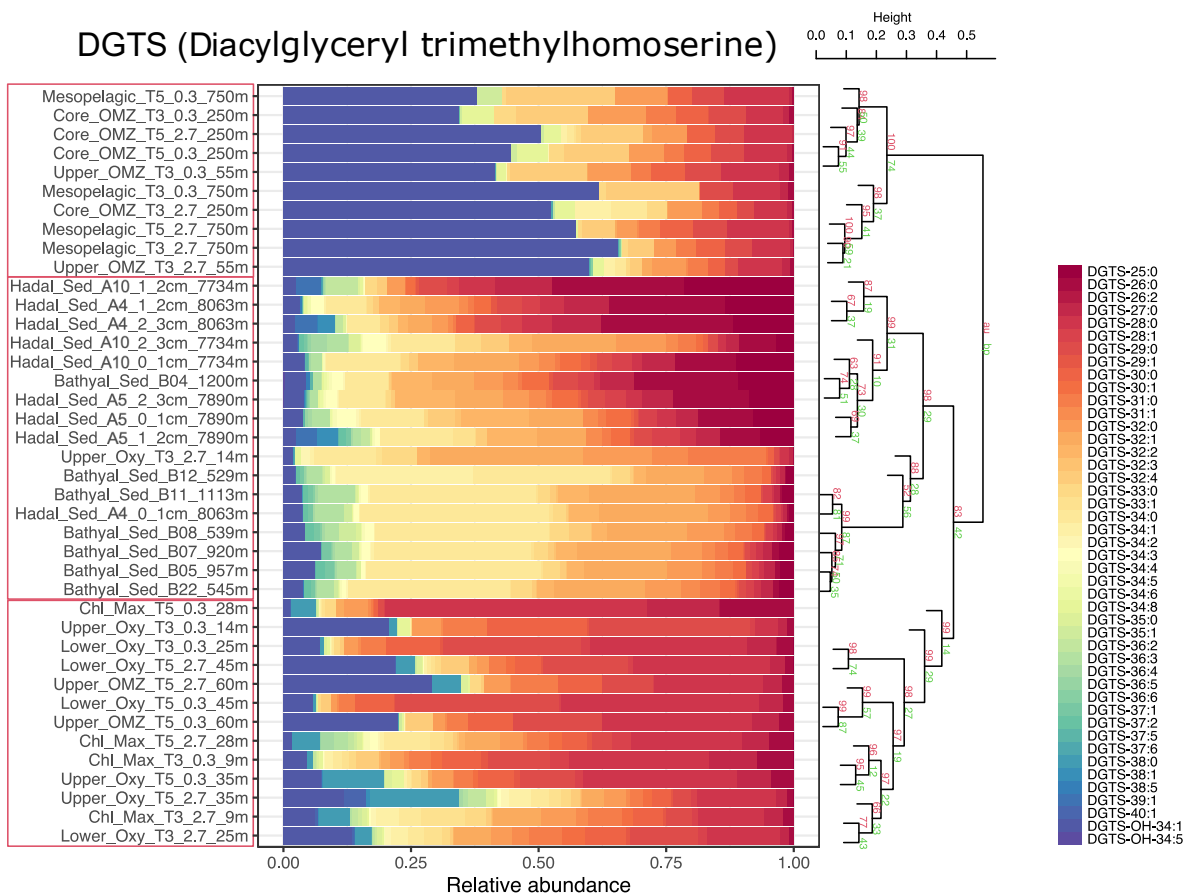


Figure 17. Cumulative bar chart of DGTS betaine fractional abundances. The number of carbon atoms and unsaturation in core fatty acids follows the order shown in the legend. The right panel depicts a cluster analysis with AU and BP in red and green, respectively, and p-values shown at branching points. The number of bootstrap replicates is 10000. Clusters with AU \geq 95% confidence are highlighted in red boxes on the left-hand side.

DGTA (Diacylglyceryl hydroxymethyl-trimethyl- β -alanine)

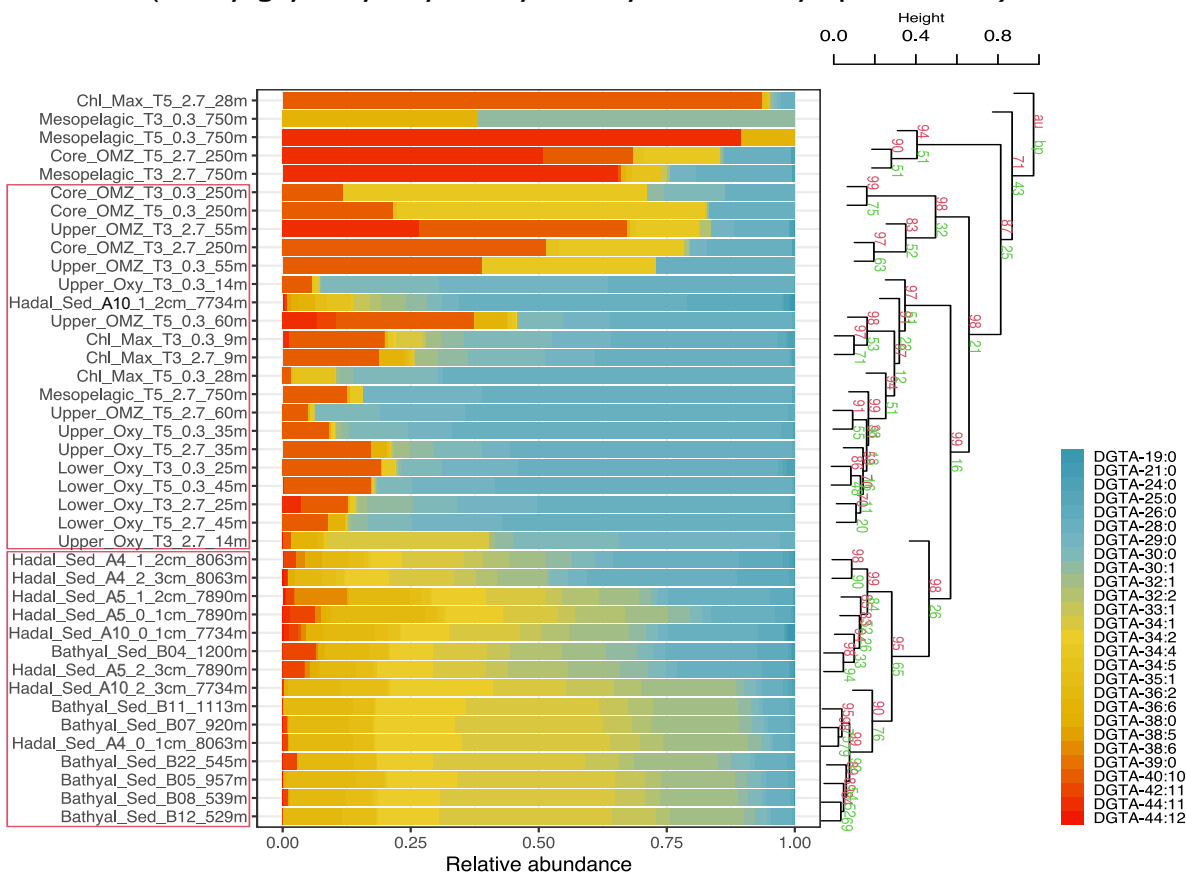


Figure 12. Cumulative bar chart of DGTA betaine fractional abundances. The number of carbon atoms and unsaturation in core fatty acids follows the order shown in the legend. The right panel depicts a cluster analysis with AU and BP in red and green, respectively, and p-values shown at branching points. The number of bootstrap replicates is 10000. Clusters with AU \geq 95% confidence are highlighted in red boxes on the left-hand side.

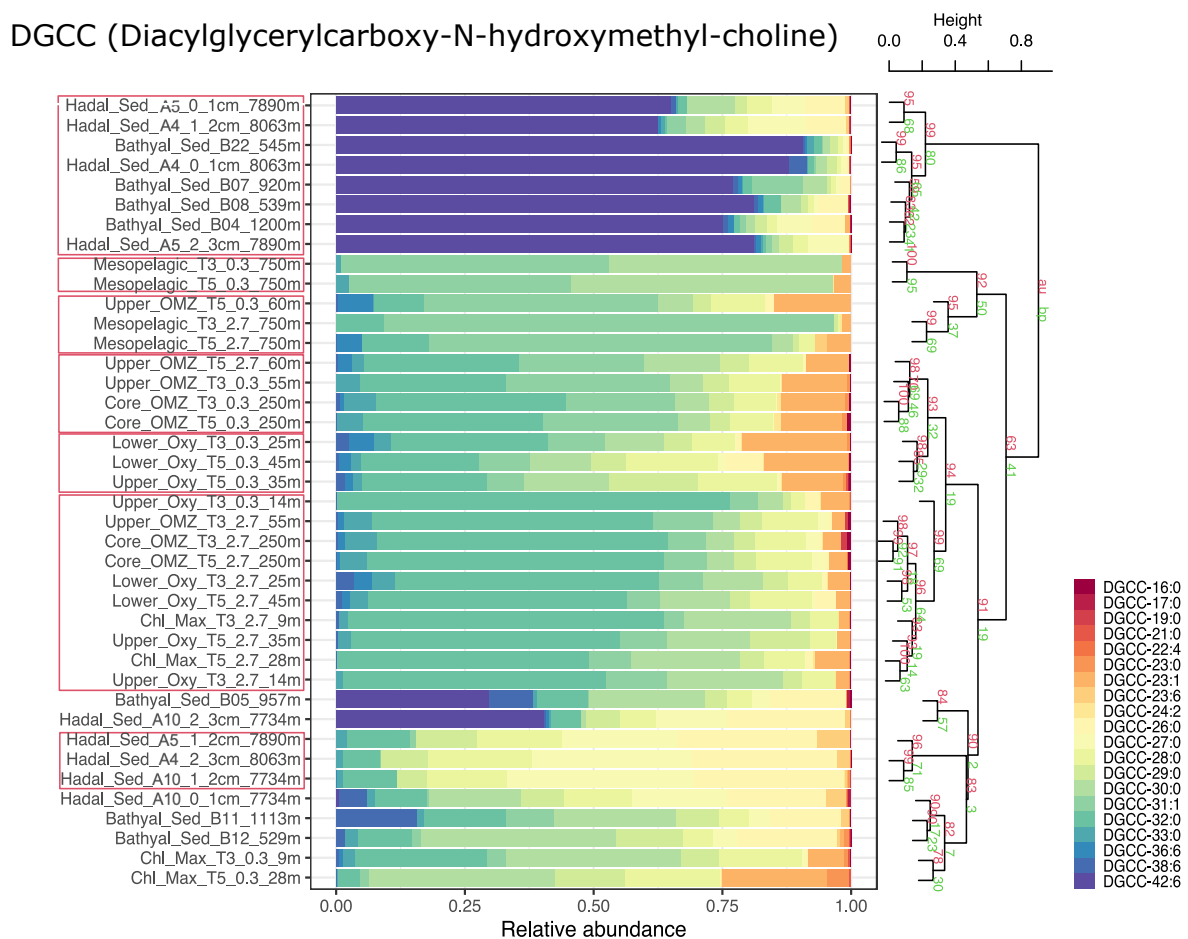


Figure 13. Cumulative bar chart of DGCC betaine fractional abundances. The number of carbon atoms and unsaturation in core fatty acids follows the order shown in the legend. The right panel depicts a cluster analysis with AU and BP in red and green, respectively, and p-values shown at branching points. The number of bootstrap replicates is 10000. Clusters with AU \geq 95% confidence are highlighted in red boxes on the left-hand side.

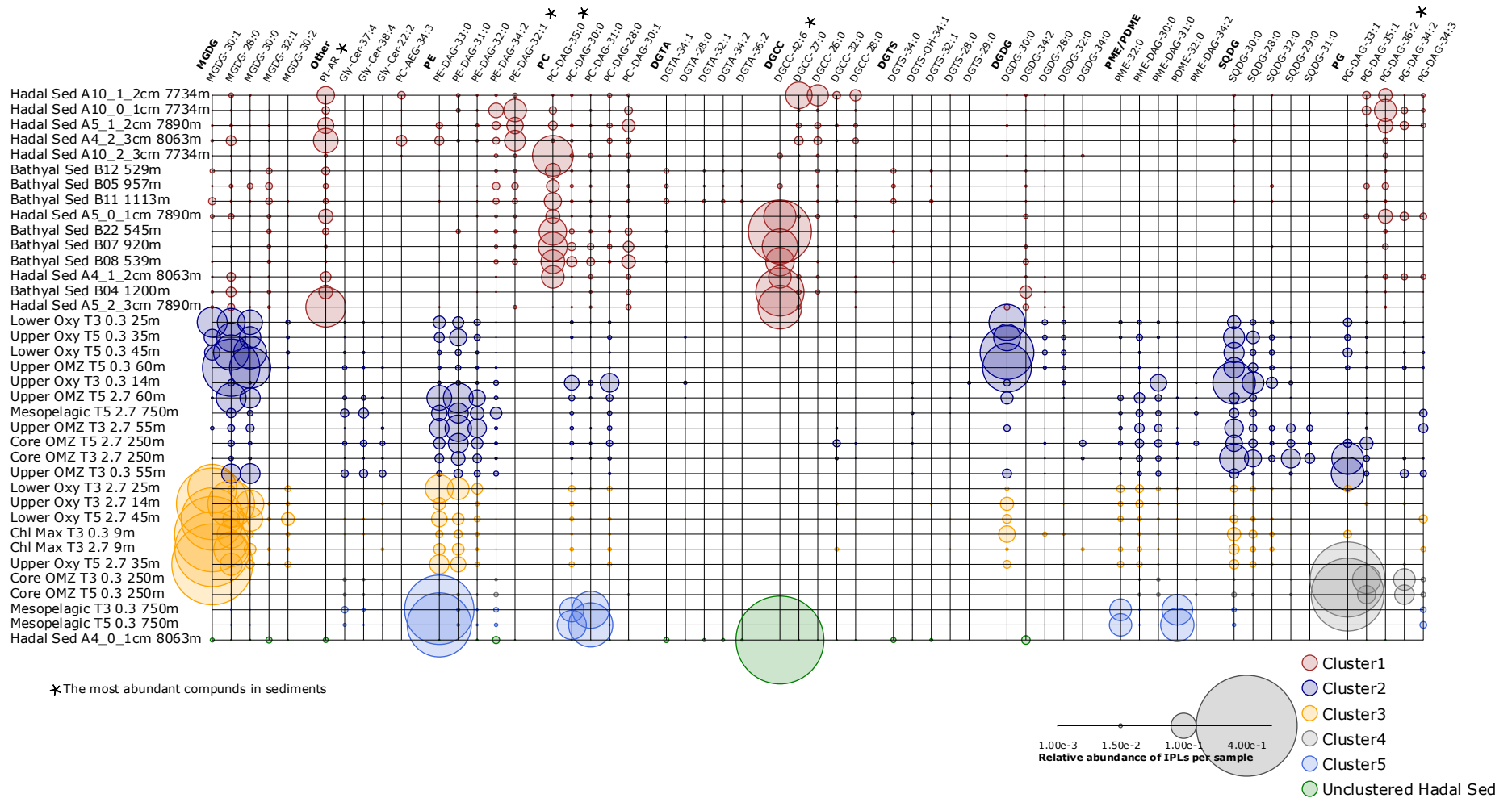


Figure 20. Relative abundance of the five most abundant IPL compounds per class in our study. Circle size is proportional to the relative abundance of IPL compounds per sample. Samples are organized along the Y axis and shown in colors that match the hierarchical cluster analysis in Fig. 8. The legend shows the scale for circumference size.

Tabla 3. Similarity percentage (SIMPER) analysis showing the average abundance and contribution of IPLs that explained the main differences among the hierarchical clusters in Fig. 8, and that include the water column and sediment samples.

Groups Cluster 1 & Cluster 2						
Average dissimilarity = 85.46						
IPLs	Average Cluster 1	Average Cluster 2	Average dissimilarity	Dissimilarit y/SD	Contribution (%)	Cumulative (%)
DGCC-42:6	0.07	0	3.74	0.9	4.37	4.37
SQDG-30:0	0	0.08	3.6	1.93	4.21	8.59
DGDG-30:0	0	0.07	3.52	0.95	4.12	12.71
MGDG-28:0	0.02	0.08	3.48	1.13	4.08	16.79
MGDG-30:0	0	0.07	3.06	1.23	3.58	20.37
PC-DAG-35:0	0.06	0	2.96	1.3	3.46	23.83
PE-DAG-31:0	0.01	0.06	2.64	1.59	3.09	26.92
PI-AR	0.05	0	2.32	1.2	2.72	29.64
PE-DAG-33:0	0.01	0.04	1.93	1.47	2.25	31.89
SQDG-28:0	0	0.04	1.89	1.81	2.21	34.1
PG-DAG-33:1	0	0.04	1.87	0.85	2.19	36.3
PE-DAG-32:0	0	0.03	1.5	1.42	1.76	38.05
PG-DAG-36:2	0.03	0	1.37	1.15	1.6	39.65
PE-DAG-32:1	0.03	0	1.31	0.95	1.53	41.19
MGDG-30:1	0.01	0.02	1.26	0.76	1.48	42.66
PC-DAG-30:2	0.02	0	1.24	0.62	1.45	44.11
PC-DAG-30:1	0.02	0	1.17	1.67	1.37	45.48
PE-DAG-29:0	0	0.03	1.15	1.06	1.35	46.83
PME-DAG-30:0	0	0.02	1.1	1.89	1.29	48.12
PME-DAG-31:0	0	0.02	1.09	1.32	1.28	49.39
PC-DAG-29:2	0.02	0	0.95	1.4	1.11	50.51
Groups Cluster 1 & Cluster 3						
Average dissimilarity = 84.70						
IPLs	Average Cluster 1	Average Cluster 3	Average dissimilarity	Dissimilarit y/SD	Contribution (%)	Cumulative (%)
MGDG-30:1	0.01	0.27	13.24	6.19	15.63	15.63
MGDG-28:0	0.02	0.1	4.35	1.68	5.14	20.77
DGCC-42:6	0.07	0	3.74	0.9	4.41	25.19
PC-DAG-35:0	0.06	0	2.95	1.29	3.49	28.67
PE-DAG-33:0	0.01	0.06	2.83	2.01	3.34	32.01
MGDG-30:0	0	0.05	2.44	1.3	2.88	34.89
PI-AR	0.05	0	2.32	1.2	2.74	37.63
PE-DAG-31:0	0.01	0.05	2.07	1.73	2.44	40.07
DGDG-30:0	0	0.03	1.6	1.64	1.89	41.97
SQDG-30:0	0	0.03	1.45	2.05	1.72	43.68
PG-DAG-36:2	0.03	0	1.37	1.14	1.61	45.3
PE-DAG-32:1	0.03	0	1.29	0.94	1.53	46.82
PC-DAG-30:2	0.02	0	1.24	0.62	1.46	48.29
PC-DAG-30:1	0.02	0	1.15	1.63	1.36	49.64
MGDG-30:2	0	0.02	1.08	1.6	1.27	50.92
Groups Cluster 1 & Cluster 4						
Average dissimilarity = 85.99						
IPLs	Average Cluster 1	Average Cluster 4	Average dissimilarity	Dissimilarit y/SD	Contribution (%)	Cumulative (%)
PG-DAG-33:1	0	0.29	14.63	66.25	17.02	17.02
PG-DAG-35:4	0	0.09	4.24	36.43	4.93	21.95
PG-DAG-35:1	0.01	0.09	4.05	3.59	4.71	26.67
DGCC-42:6	0.07	0	3.74	0.89	4.35	31.01
PG-DAG-34:2	0.01	0.08	3.63	5.35	4.22	35.23
PC-DAG-35:0	0.06	0	2.89	1.26	3.36	38.6
PI-AR	0.05	0	2.32	1.18	2.7	41.3
PG-DAG-36:1	0	0.04	1.8	6.37	2.09	43.39
PE-DAG-34:1	0.01	0.04	1.75	4.39	2.03	45.42
PG-DAG-36:2	0.03	0	1.37	1.13	1.59	47.01
PE-DAG-32:1	0.03	0	1.3	0.93	1.51	48.52
PC-DAG-30:2	0.02	0	1.24	0.61	1.44	49.96
Groups Cluster 1 & Cluster 5						
Average dissimilarity = 89.03						
IPLs	Average Cluster 1	Average Cluster 5	Average dissimilarity	Dissimilarit y/SD	Contribution (%)	Cumulative (%)
PE-DAG-33:0	0.01	0.26	12.94	17.5	14.54	14.54
PC-DAG-31:0	0.01	0.16	7.47	9.31	8.39	22.93
PDME-32:0	0	0.13	6.33	22.82	7.11	30.03
PC-DAG-30:0	0.01	0.11	4.66	6.45	5.24	35.27
PME-32:0	0	0.09	4.37	68.49	4.91	40.18
DGCC-42:6	0.07	0	3.74	0.89	4.2	44.38
PC-DAG-35:0	0.06	0	2.96	1.28	3.33	47.71
PI-AR	0.05	0	2.32	1.18	2.61	50.31

4.2 Capítulo 2: Materia orgánica particulada en la Fosa de Atacama: Rastreado su posible origen y transporte hasta el fondo marino hadal. Manuscrito científico sometido a la revista “*Journal of Geophysical Research: Biogeosciences*” el 20/01/2023.

The screenshot shows the AGU Publications author dashboard. At the top, there is a dark blue header with the text "AGU PUBLICATIONS" in white. Below this is a navigation bar with links for "Journal Home", "GEMS Desktop", "Author Instructions", "Reviewer Instructions", "Change Journal", and "Contact". On the right side of the navigation bar, there are links for "AGU.org" and "Join AGU".

Below the navigation bar, the text "JOURNAL OF GEOPHYSICAL RESEARCH" is displayed in a dark blue font, followed by "Biogeosciences" in a larger, bold, orange font. Underneath, it says "AN AGU JOURNAL". To the right of this text is a logo for "JGR" in white on a dark blue background.

The main content area of the dashboard includes the following elements:

- A status message: "Manuscript Approved (2023JG007401)."
- A link to the "Home Page for Edgart Elvis Flores".
- A "Use Modern Desktop" link.
- A section titled "Author Tasks" containing:
 - [Author Instructions](#)
 - [Submit Manuscript](#)
 - [Live Manuscripts \(1\)](#)
 - [Post Decision Manuscripts \(1\)](#)
- A section titled "General Tasks" containing:
 - [Modify Unavailability Dates](#)
 - [Modify Profile/Password](#)
 - [View/Modify My Policies](#)
 - [Download Copy of My Records](#)
 - [Log Out](#)

Resumen

En Las fosas oceánicas son un importante sumidero de materia orgánica (MO). Sin embargo, los conocimientos sobre las contribuciones relativas de la MO y la exportación de partículas que conectan la productividad del océano superficial iluminado por el sol con la zona crepuscular y el fondo marino hadal son limitados. Con el fin de comprender estas sinergias en la fosa de Atacama, realizamos un análisis exhaustivo de los isótopos estables de la materia orgánica para rastrear la dinámica del carbono y el nitrógeno en la columna de agua suprayacente, así como en los sedimentos superficiales del fondo marino, además de la concentración de carbono orgánico en partículas (POC) y los flujos derivados de datos de teledetección y mediciones in situ. Nuestros resultados, basados en análisis de varianza de dos vías, indican que no existen diferencias estadísticas en $\delta^{13}\text{C}_{\text{POC}}$ y la relación C/N entre la zona hadalpelágica y las zonas pelágicas menos profundas (excepto para $\delta^{13}\text{C}_{\text{POC}}$ en la Zona con Déficit de Oxígeno, ODZ). Además, los datos de teledetección indican que ~16-27% de la POC podría escapar a la remineralización superficial y ser potencialmente exportada a profundidades mayores que la región mesopelágica. También informamos de estimaciones de modelos de flujos de POC que indican que ~3,3% de la materia orgánica producida en la zona epipelágica puede potencialmente alcanzar profundidades hadales. Estos resultados son coherentes con las señales isotópicas de los sedimentos hadales que son distintos de toda la columna de agua y, en menor medida, de los sedimentos batiales. Así, nuestros resultados indican que los sedimentos batiales pueden aportar más MO a los sedimentos hadales que las distintas zonas de la columna de agua. Estos hallazgos arrojan nueva luz sobre los orígenes de la MO en el fondo marino hadal.

Particulate organic matter in the Atacama Trench: Tracing sources and possible transport mechanisms to the hadal seafloor

Edgart Flores^{1,2,*}, Igor Fernández-Urruzola², Sebastian I. Cantarero³, Matías Pizarro-Koch⁴, Matthias Zabel⁵, Julio Sepúlveda^{2,3}, and Osvaldo Ulloa^{1,2,*}

¹Programa de Postgrado en Oceanografía, Departamento de Oceanografía, Facultad de Ciencias Naturales y Oceanográficas, Universidad de Concepción, Concepción, Chile

²Millennium Institute of Oceanography, Universidad de Concepción, Concepción, Chile

³Department of Geological Sciences and Institute of Arctic and Alpine Research, University of Colorado Boulder, Boulder, CO, 80309, USA

⁴Millennium Nucleus Understanding Past Coastal Upwelling Systems and Environmental Local and Lasting Impacts, Coquimbo, 1780000, Chile

⁵MARUM – Center for Marine Environmental Sciences and Department of Geosciences, University of Bremen, 28334 Bremen, Germany

*Corresponding authors: Edgart Flores (edgart.flores@imo-chile.cl) and Osvaldo Ulloa (oulloa@udec.cl)

Key Points:

- The deep-sea waters of the Atacama Trench display bulk isotopic signatures similar to those in the epipelagic zone.
- The bulk and stable isotope composition of surficial bathyal and hadal sediments are distinguishable from the one in the water column.
- Results from a multi-source stable isotope model suggest that hadal sediments may receive more organic material from shallower sediments than from the water column.

Abstract

Oceanic trenches are an important sink for organic matter (OM). However, knowledge about the relative contributions of OM and particle export connecting the sunlit surface ocean productivity to the twilight zone and the hadal (>6000 m depth) seafloor is limited. In order to understand this connection in the Atacama Trench, we perform an analysis of carbon and nitrogen stable isotopes of bulk OM over the overlying water column, as well as in bathyal-hadal surficial sediments. Moreover, we estimated the particulate organic carbon (POC) concentration and downward carbon flux from remote-sensing data and *in situ* measurements. Our results based on two-way variance analyses show statistical differences in $\delta^{15}\text{N}_{\text{PON}}$ between the epipelagic zone and the deep zones. However, no statistical differences in $\delta^{13}\text{C}_{\text{POC}}$ and the C/N ratio between the hadopelagic zone and the shallower pelagic zone were displayed, except for $\delta^{13}\text{C}_{\text{POC}}$ in the Oxygen Deficient Zone. On the contrary, the isotopic signatures of hadal sediments are distinct from those in the entire water column but rather similar to the values in bathyal sediments. Thus, our results suggest that bathyal sediments can contribute more OM to hadal sediments than the different zones of the water column. In addition, flux estimates derived from remote sensing data indicate that ~16-27% of POC could escape surface remineralization and potentially be exported to depths greater than the mesopelagic (>200 m depth) region. Model estimates of POC fluxes suggest that ~3.3% of the organic matter produced in the epipelagic zone can potentially reach hadal depths.

1. Introduction

Most marine particulate organic matter (POM) produced at the ocean's surface is remineralized in its descent through the water column to the seafloor, resulting in a particle flux attenuation with increasing water depth (Wakeham et al., 1984; Hedges et al., 2001; Rex et al., 2006) that generally follows a simple power-law function (Martin et al., 1987). Both the magnitude of the export production and the remineralization depth of the sinking material determine the shape of the attenuation curve and, ultimately, the amount of POM that reaches the sediment surface and supplies energy to deep-sea communities. POM varies in size and composition, ranging from phytodetritus (Rice et al., 1986), mucilaginous aggregates (Martin & Miquel, 2010), larvacean houses (Robison et al., 2005), and faecal pellets (Turner, 2002). The downward flux of organic material is further affected by the regional and seasonal variability in export flux (Lutz et al., 2007; Poff et al., 2021; de Melo Virissimo et al., 2022), the size, shape, and composition of the POM (Kriest, 2002; De La Rocha & Passow, 2007; Omand et al., 2020), the interaction with microbes and/or zooplankton (Cavan et al., 2021; Neubauer et al., 2021), physical processes of aggregation/disaggregation of particles (Burd & Jackson, 2009; Iversen & Ploug, 2010), and ventilation/advection through deep-ocean circulation (Chunhui et al., 2020). According to biogeochemical models (e.g., Ichino et al., 2015), the export of sinking organic matter (MO) of photosynthetic origin to hadal depths (>6,000 m below sea level) is expected to be low. However, oceanic trenches have been described as depocenters of organic matter (MO; Danovaro et al., 2003) and hotspots for chemo-organo-heterotrophic microbial activity (Glud et al., 2013; Wenzhöfer et al., 2016; Liu et al., 2019). The coupling between microbial activity and MO availability is important for nutrient remineralization, which can in turn influence the rates and directions of biogeochemical fluxes (Azam et al., 1994). Thus, elevated concentrations of MO in trench sediments could be explained by more diverse sources of energy feeding the hadal environment. Besides the downward flux of POC from surface

waters, processes such as the carrion falls of dead bodies, terrestrial inputs from the adjacent continental margin, *in situ* chemosynthetic production, and the lateral transport of sediment along the continental slope may potentially provide MO to these remote ecosystems (Xu et al., 2018; Flores et al., 2022). However, their relative contribution to the total carbon supply to the hadal region remains poorly constrained. Whereas recent research has linked hadal microbiological in sediment activity to the regional productivity of the overlying surface waters (Glud et al., 2021), differences in calculated POM export from the productive sunlit surface ocean do not explain, by themselves, why hadal sediments consistently indicate greater biological activity than their shallower adjacent abyssal sites. Moreover, whether this ecological pattern in the trench sediments can also be extrapolated to the pelagic environment is unknown.

The Atacama Trench in the eastern tropical South Pacific (ETSP) is overlaid by a eutrophic water column compared to other trench ecosystems in the Pacific Ocean underling mesotrophic (e.g., Japan and Izu-Bonin Trenches) and oligotrophic waters (e.g., Mariana and Tonga Trenches) (Wenzhöfer et al., 2016). This trench underlies the Humboldt Current System (HCS), one of the world's most productive coastal upwelling ecosystems, and characterized by a permanent and intense oxygen deficient zone (ODZ; Daneri et al., 2000; Fuenzalida et al., 2009; Selden et al., 2021). Empirical estimates of export fraction and flux attenuation in the water column overlaying the Atacama Trench have demonstrated that the export production may sustain most of the respiratory carbon demand of the plankton community across the hadopelagic zone (Fernández-Urruzola et al., 2021). These authors hypothesized that fast-sinking particles represent an important mechanism for the injection of fresh POM into hadal depths, since large particles such as diatom aggregates and fecal pellets may more easily escape from remineralization in the upper ocean (González et al., 2000; Grabowski et al., 2019). Other physical and chemical processes would further play a role in the downward flux of POM to

hadal depths in the region; for instance, eddy-driven subduction events can rapidly transfer carbon in pulses below the mixed layer (Omand et al., 2015; Resplandy et al., 2019). Moreover, the presence of an ODZ can also impact carbon cycling and fluxes to the ocean's interior acting as a secondary biological pump, and providing an additional source of MO to the ocean's interior. (Pantoja et al., 2004; Devol & Hartnett, 2001; Van Mooy et al., 2002; Weber & Bianchi et al., 2020). A study of the distribution and abundance of intact polar lipids (IPLs) in POM of the ODZ system over the Atacama Trench suggested that chemosynthetic processes associated with dark carbon fixation provide additional sources of organic carbon to the mesopelagic region (Cantarero et al., 2020). These results were later confirmed by quantitative estimates using a stable isotope mass-balance (Vargas et al., 2021), which indicated that dark carbon fixation in ODZ waters contributes ~7–35% of the total POC exported to mesopelagic waters. While little is known about how much of this MO reaches the hadopelagic realm, the distribution and abundance of IPLs in hadal surface sediments of the Atacama Trench points to the importance of *in situ* microbial biomass production as a key source of labile MO in this hadal environment (Flores et al., 2022). These authors demonstrated that IPLs in hadal and bathyal sediments show close resemblance, and that they are distinguishable from the IPLs previously reported in the overlying water column (Cantarero et al., 2020). Thus, discrepancies remain among measurements of carbon accumulation in sediments, the vertical POC flux, and *in situ* production of hadal organic matter (Turnewitsch et al., 2014; Flores et al., 2022; Oguri et al., 2022), as well as between the dominant terrigenous versus marine carbon sources even within the same trench (e.g., Atacama Trench; Xu et al., 2021, Oguri et al., 2022).

The carbon and nitrogen stable isotope compositions of bulk MO have been widely used to elucidate the relative contribution of MO sources (Meyers & Eadie, 1993; Middelburg & Nieuwenhuize, 1998; Gao et al., 2012), including hadal sediments from the Mariana Trench (Luo et al., 2019), the New Britain Trench (Xiao et al., 2020), and the Atacama and Kermadec

Trenches (Xu., et al., 2021). However, few studies have evaluated the isotopic composition of POM from surface waters to the trench interior, including the hadopelagic region and the surface sediments. Here, we investigate the provenance and fate of sinking particles across the mesopelagic (200–1,000 m), bathypelagic (1,000–3,500 m), abyssopelagic (3,500–6,000 m) and hadalpelagic (>6,000 m) realms, and the sedimentary material at the deepest points of the Atacama Trench (7,734-8,063 m).

2. Materials and Methods

2.1 Study area and sample collection

Water column samples were collected at 4 sites between 21 and 24°S over the Atacama Trench during the SO261 cruise (March 05-25, 2018) on board the German RV *Sonne* (Fig. 1; Table 1). We obtained seawater from eight discrete depths down to 6,000 m using a rosette sampler with 24 12L-Niskin bottles, and from 1.5 m above the seafloor using an autonomous vehicle equipped with 2 10L-Niskin bottles (Table 1). We sieved between ~0.5 and 60 L of seawater through a 20 µm nylon mesh and then gently filtered sampled onto pre-combusted (450° C, 24 h) Whatman GFFs filters (0.7 µm nominal pore size) using pressurized canisters for bulk elemental and stable isotope analysis. Filters were immediately dried at 60 °C for 24 h and kept dry in the dark until their analysis in the laboratory.

Bathyal and hadal sediment samples were obtained during the German RV *Sonne* cruises SO211 (ChiMeBo, November 2–29, 2010; Matys et al., 2017) and SO261 (HADES, March 14-26, 2018, Wenzhöfer et al., 2019), respectively (Fig. 1). Samples were collected using a multi-corer (MUC) equipped with twelve 60 cm-long acrylic tubes (6–10 cm diameter for bathyal sediments and 9.5 cm diameter for hadal sediments). We used nine hadal surface (0–1 cm) and subsurface (1–2 and 2–3 cm) sediments (3 sites between 7,734 and 8,063 m) in

addition to seven bathyal surface sediments (7 sites between 529–1,200 m) for bulk elemental and stable isotope analysis (Table 1). We then compared our results against published data on sediment trap material for the region overlying the Atacama Trench (e.g., Hebbeln et al., 2000; González et al., 2004).

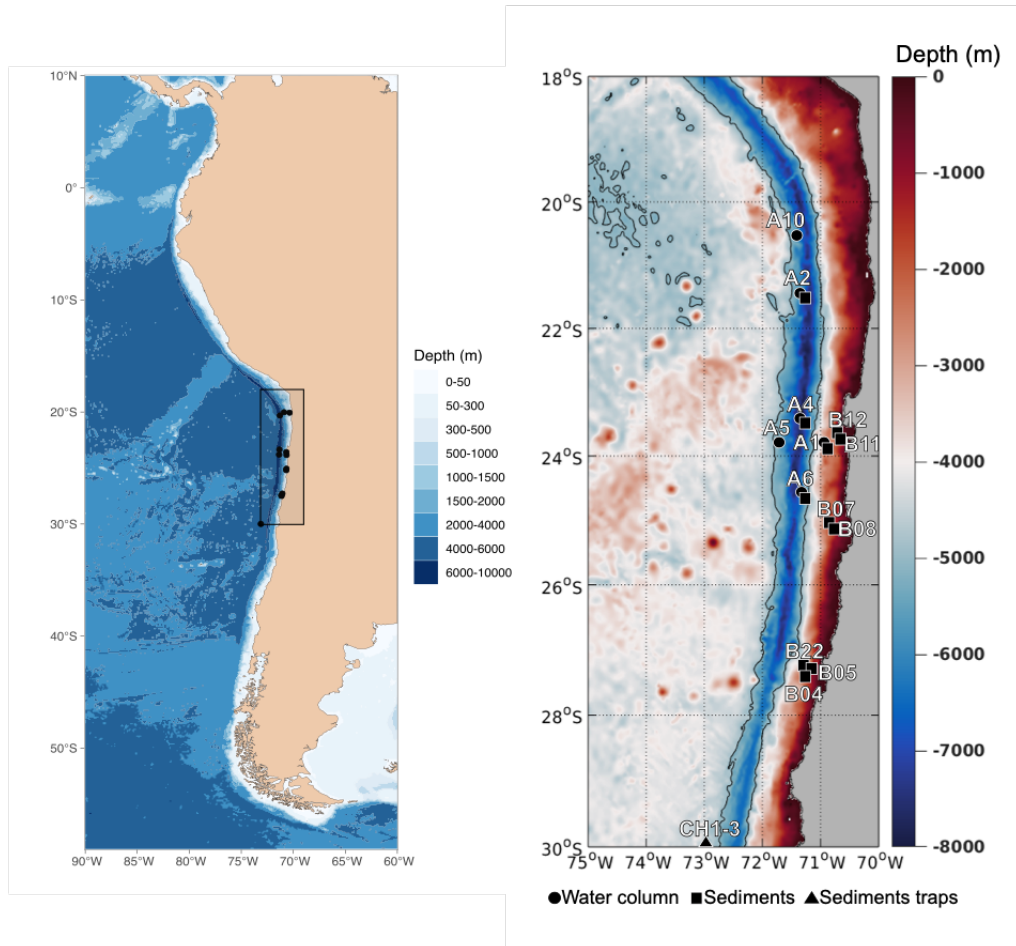


Figura 21. Bathymetric map of the Atacama Trench region off northern Chile showing the sampling locations.

Tabla 4. Sampling stations from the HADES and ChiMeBo cruises, and from published sediment-trap data.

Environment	Cruise-RV	Station	Samples type	Depth (m)	Latitude (°S)	Longitude (°W)	Date (dd/mm/yyyy)	Reference
Water column	HADES	A1	Epipelagic (5, 20, 60, 200 m); Mesopelagic (500, 1000 m)	2560	23.81	70.84	05/03/2018	This study
	<i>Sonne</i>	A2	Epipelagic (5, 20, 60, 200 m); Mesopelagic (500, 1000 m); Bathypelagic (2000, 3000, 4000 m); Abysopelagic (5000, 6000 m),	7994	21.78	71.21	25/03/2018	
	SO261	A4		8086	23.36	71.34	14/03/2018	
		A6		7720	24.27	71.42	09/03/2018	
		Vidal Gormaz	CH1-3	Bathypelagic depth sediment trap	2300, 3700	30	73.18	21/07/1993
	Abate Molina	-		2300	30	73.18	07/1993-05/1995	Gonzalez et al., 2000
Sediments	HADES	A10	Hadal sediments (0-1, 1-2 and 2-3 cm)	7734	20.32	71.29	26/03/2018	This study
	<i>Sonne</i>	A5	Hadal sediments (0-1, 1-2 and 2-3 cm)	7890	23.81	71.37	11/03/2018	
	SO261	A4	Hadal sediments (0-1, 1-2 and 2-3 cm)	8063	23.36	71.34	14/03/2018	
		B12	Upper bathyal sediment (0-1 cm)	529	23.59	70.67	02-29/11/2010	
		B08	Upper bathyal sediment (0-1 cm)	539	25.2	70.68	02-29/11/2010	
	ChiMeBo	B22	Upper bathyal sediment (0-1 cm)	545	27.29	71.05	02-29/11/2010	
	<i>Sonne</i>	B07	Lower bathyal sediment (0-1 cm)	920	25.07	70.66	02-29/11/2010	
	SO211	B05	Lower bathyal sediment (0-1 cm)	957	27.5	71.13	02-29/11/2010	
	B11	Lower bathyal sediment (0-1 cm)	1113	23.85	70.65	02-29/11/2010		
	B04	Lower bathyal sediment (0-1 cm)	1200	27.45	71.16	02-29/11/2010		

2.2 Bulk elemental and stable isotope analysis of carbon and nitrogen

Particulate organic carbon (POC) and particulate organic nitrogen (PON), as well as their respective bulk stable isotopes ($\delta^{13}\text{C}_{\text{POC}}$ and $\delta^{15}\text{N}_{\text{PON}}$) were measured in the Laboratory of Biogeochemistry and Applied Stable Isotopes at the Pontifical Catholic University of Chile. Prior to analysis, inorganic carbonates were removed by acidification of samples overnight with HCl fumes. Filters were then packed into tin capsules and fed via flash combustion (1,020 °C) into a Thermo Scientific Flash 2000 CHN elemental analyzer (EA) coupled to a Thermo DeltaV Advantage isotope ratio mass spectrometer (IRMS). Isotope ratios are reported using the standard (δ) notation and expressed as per mil (‰) with respect to standard reference material:

$$\delta X (\text{‰}) = [(R_{\text{sample}} / R_{\text{standard}}) - 1] \times 1000 \quad (\text{Eq. 1})$$

Where X is the $^{13}\text{C}_{\text{POC}}$ or $^{15}\text{N}_{\text{PON}}$, R is the corresponding ratio of $^{13}\text{C}/^{12}\text{C}$ or $^{15}\text{N}/^{14}\text{N}$ in a sample or standard (PDB for carbon and atmospheric N_2 for nitrogen). Analytical precision was calculated as $\pm 0.215\%$ and $\pm 0.33\%$ for nitrogen and carbon, respectively, based on four standards run in triplicate (acetanilide, atropine, caffeine, and glutamic acid). The analytical precision in the elemental analysis was ± 0.003 mg and ± 0.007 mg for nitrogen and carbon, respectively. The standard used for this calculation was Acetanilide (71.10% C and 10.36% N).

Sediment samples were analyzed using a Thermo Scientific Elemental Analyzer—Delta V Isotope Ratio Mass Spectrometer at the CU Boulder Earth Systems Stable Isotope Laboratory. Purified acetanilide and ethylenediaminetetraacetic acid were measured as standards for external calibration and drift corrections. The analytical precision for total organic carbon and

total nitrogen was $\pm 0.2\%$ and $\pm 0.11\%$, respectively, whereas the analytical precision was $\pm 0.2\text{‰}$ and $\pm 0.15\text{‰}$ for $\delta^{13}\text{C}_{\text{POC}}$ and $^{15}\text{N}_{\text{PON}}$, respectively.

2.3 Satellite POC estimates

We used the mean and standard deviation (\pm STD) from satellite POC (POCsat) data for a ~ 90 -days period (January-March 2018) prior to *in situ* POC sampling during the HADES expedition (March 2018) to evaluate the dynamics of POC in surface (0 m) and subsurface (1000 m) waters over the Atacama Trench (Fig. 6A-D). Our rationale assumes that particles found at 1,000 m must have originated in surface waters within that time. Additionally, POCsat values were averaged and binned into years for a 24 years period (1998–2022) to evaluate the seasonal (Fig. S1) and annual variability in this region (Fig. S2). POCsat was obtained from Copernicus Marine Service Information (<https://marine.copernicus.eu/es>) (MULTIOBS_GLO_BIO_BGC_3D_REP_015_010). This product merges satellite ocean color and Argo data using a neural network-based method and has shown strong potential to infer the global-scale vertical distribution of bio-optical properties with high space-time resolution, $0.25^\circ \times 0.25^\circ$ horizontal resolution, and over 36 depth levels from the surface to 1,000 m (Sauzede et al., 2016).

2.4 Particle Flux Parameterization

We used empirical models to estimate vertical POC export fluxes from the surface to hadalpelagic depths. The most common model is the normalized power function known as the “Martin Curve” (Martin et al., 1987), which equates the POC flux $f_p(z)$ [$\text{mg m}^{-2} \text{d}^{-1}$] at any depth z [m] with the export flux (C) at the reference depth, i.e., at the base of the euphotic zone (E_z) according to Buesseler et al. (2020):

$$f_p(z) := C(z/Ez)^{-b} \quad (\text{Eq. 2})$$

The Ez was assumed to be 84.7 m (from 63 to 118 m depth) as reported by Pizarro et al. (2002) for this region. The b is the attenuation coefficient, which depends on the balance between POC sinking speed w [m/day] and the rate of remineralization k [1/day] (Middelburg, 2019). The b value suggested for the open Pacific Ocean is 0.858 (Martin et al., 1987), whereas similar values have been suggested by open ocean waters off Antofagasta (0.834; González et al., 2009). However, lower b values (0.319) have also been suggested for the Peru region and the eastern tropical North Pacific due to the impact of oxygen deficiency on particle export (Van Mooy et al., 2002). In this study, we used a range of b values (0.36 to 1.33, $\bar{x} = 0.78$, $n = 13$) to calculate flux attenuation following Fernandez-Urruzola et al. (2021). Given the inherent uncertainties of biogeochemical models, we tested a series of parameterizations, such as the basic exponential model (Banse, 1990), the original depth-attenuation rational model (Suess, 1980), and the double exponential model (Lutz et al., 2002) to estimate a range of POC flux values reaching hadal depths (Fig. 7A, Table S1). We then compared these estimates to published POC fluxes in the region derived from moored sediment traps (Hebbeln et al., 2002; González et al., 2004), free-drifting sediment traps (Wakeham et al., 1984), and particulate ²³⁰Th-normalized isotope-based samples (Pavia et al., 2019) (Fig. 7A, Table S1).

2.5 Statistical analyses

We used averages and standard deviation for displaying the POCsat, and linear regressions to reveal significant correlations between theoretical models of vertical POC export fluxes and the available data derived from the sediment traps ($p < 0.001$). Statistical differences to ¹³C_{POC} or δ^{15} N_{POC} in each environment were identified by ANOVA and Tukey's HSD (honestly significant difference) post hoc test. We used the MixSIAR (Version 3.2.0) mixing model to

calculate the contribution of different OM sources according to Stock et al. (2018). Statistical tests were calculated using the vegan package (Oksanen et al., 2013) of the open-source software R version 3.6.2 with the ggplots package (Warnes et al., 2015).

3. Results

3.1 Elemental and stable isotope POM signatures from surface to hadalpelagic waters

The $\delta^{13}\text{C}_{\text{POC}}$ values in the epipelagic zone showed a relatively large range, from -29.2 to -20.5‰ (mean $-26.05 \pm 1.8\%$, $n=13$, Fig. 3A), and were statistically different from those in the ODZ (Tukey HSD post hoc test, $p < 0.05$, Fig. 2C). The differences in the $\delta^{13}\text{C}_{\text{POC}}$ values between the epipelagic and the deeper oxygenated layers, on the contrary, were not statistically significant at 0.05 as the critical significance level (Fig. 3C). The POC was isotopically enriched in ^{13}C at 5000 m (-25.4‰ at sites A2 and A4, and -21.6‰ at site 6) compared to other depths (see Fig. 2).

The $\delta^{15}\text{N}_{\text{PON}}$ values ranged between 5.4 and 11.2‰ throughout the water column (mean $8.41 \pm 1.37\%$) (Fig. 3A) and showed a statistical difference ($p < 0.05$) between the epipelagic zone and the deeper layers (i.e., mesopelagic, bathypelagic, abyssopelagic, and hadalpelagic zone) (see Fig. 2D). Overall, the $\delta^{15}\text{N}_{\text{PON}}$ values decreased with increasing water depth down to 5,000 m, with values of 9.4, 8.4, and 7.4‰ at sites A2, A4, and A6, respectively. Below 5,000 m, however, $\delta^{15}\text{N}_{\text{PON}}$ increased at sites A2 and A6. This pattern was the opposite at site A4, where $\delta^{15}\text{N}_{\text{PON}}$ reached the lowest value (5.4‰) in the pelagic zone (Fig. 2).

The C/N ratio varied between 7.0 and 23.6 (mean value of 11.2 ± 3.2 , Fig. 2B) throughout the water column. Despite this large overall range, we found a lack of significant difference ($p > 0.05$) between depth layers (Fig. 3E). Generally, the C/N ratios showed a consistent pattern

between sites A2, A4, and A6: A high variability at the surface, a tendency to decrease towards 5,000 m, and then a slight increase towards 8000 m (Fig. 2).

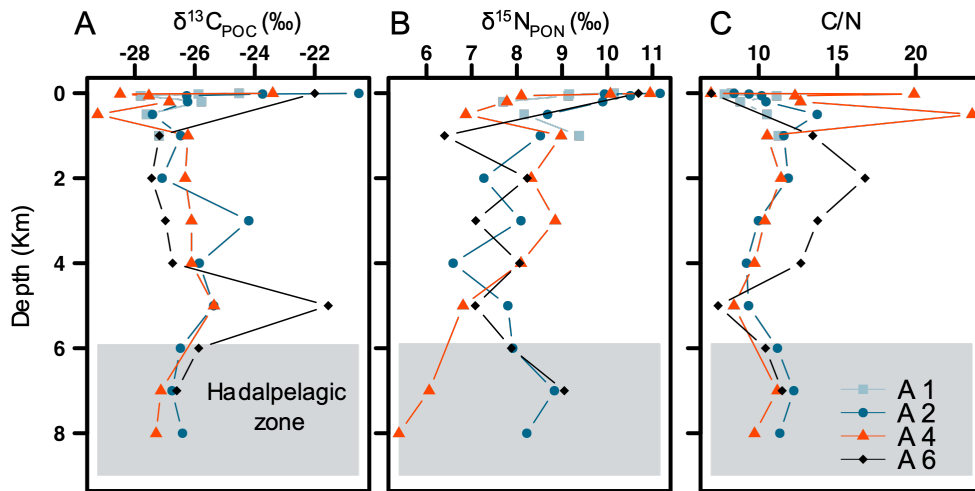


Figure 14. Water column depth profiles of (A) $\delta^{13}C_{POC}$, (B) $\delta^{15}N_{PON}$, and (C) C/N ratio over the Atacama Trench. The gray area represents the pelagic hadal zone (>6000 m depth).

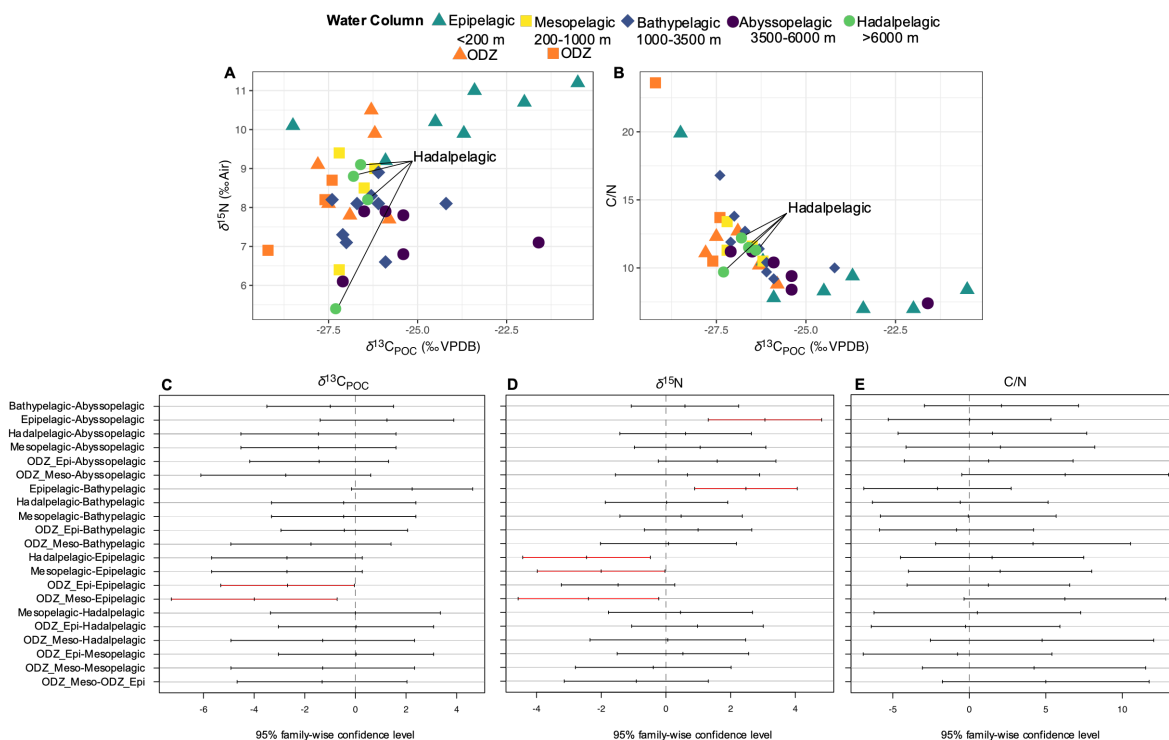


Figure 15. Biplots of (A) $\delta^{15}\text{N}_{\text{PON}}$ and $\delta^{13}\text{C}_{\text{POC}}$, and (B) C/N ratios and $\delta^{13}\text{C}_{\text{POC}}$. The water column was divided by depth into the epipelagic (200-1000 m), mesopelagic (200-1000 m), bathypelagic (3500-6000 m), and hadalpelagic (>6000 m) zones following Jamieson (2015 and references therein). Panels C, D and E describe the 95% family-wise confidence intervals for the differences in the mean values of $\delta^{13}\text{C}_{\text{POC}}$, $\delta^{15}\text{N}_{\text{PON}}$ and C/N, respectively. Red lines indicate the occurrence of statistically significant differences (pairwise comparison by Tukey's test, $p < 0.05$).

3.2 Differences in elemental and stable isotope signatures between bathyal and hadal sediments

In hadal and bathyal sediments, $\delta^{13}\text{C}_{\text{POC}}$ ranged from -23.6 to -22.7‰ (mean -23.2 ± 0.3 ‰) and from -22.9 to -21.8‰ (mean -22.2 ± 0.4 ‰), respectively (see Figs. 4A,B). The range of $\delta^{15}\text{N}_{\text{PON}}$ values in hadal and bathyal sediments was 9.6-12.4‰ (mean 10.7 ± 1.1 ‰) and 10.0-12.9‰ (mean 11.7 ± 1.0 ‰), respectively (Figs. 4A). The C/N ratio values were more homogeneous and significantly lower in hadal sediments (7.5 ± 0.2) compared to those found in bathyal sediments (8.5 ± 0.6) (Fig. 4B). A Tukey HSD post hoc test revealed statistical differences in the $\delta^{13}\text{C}_{\text{POC}}$ values ($p < 0.001$) and C/N ratios ($p < 0.05$) between bathyal and hadal

surface sediments. On the contrary, we found no significant differences in the $\delta^{15}\text{N}_{\text{PON}}$ values (see Figs. 4C, D, E).

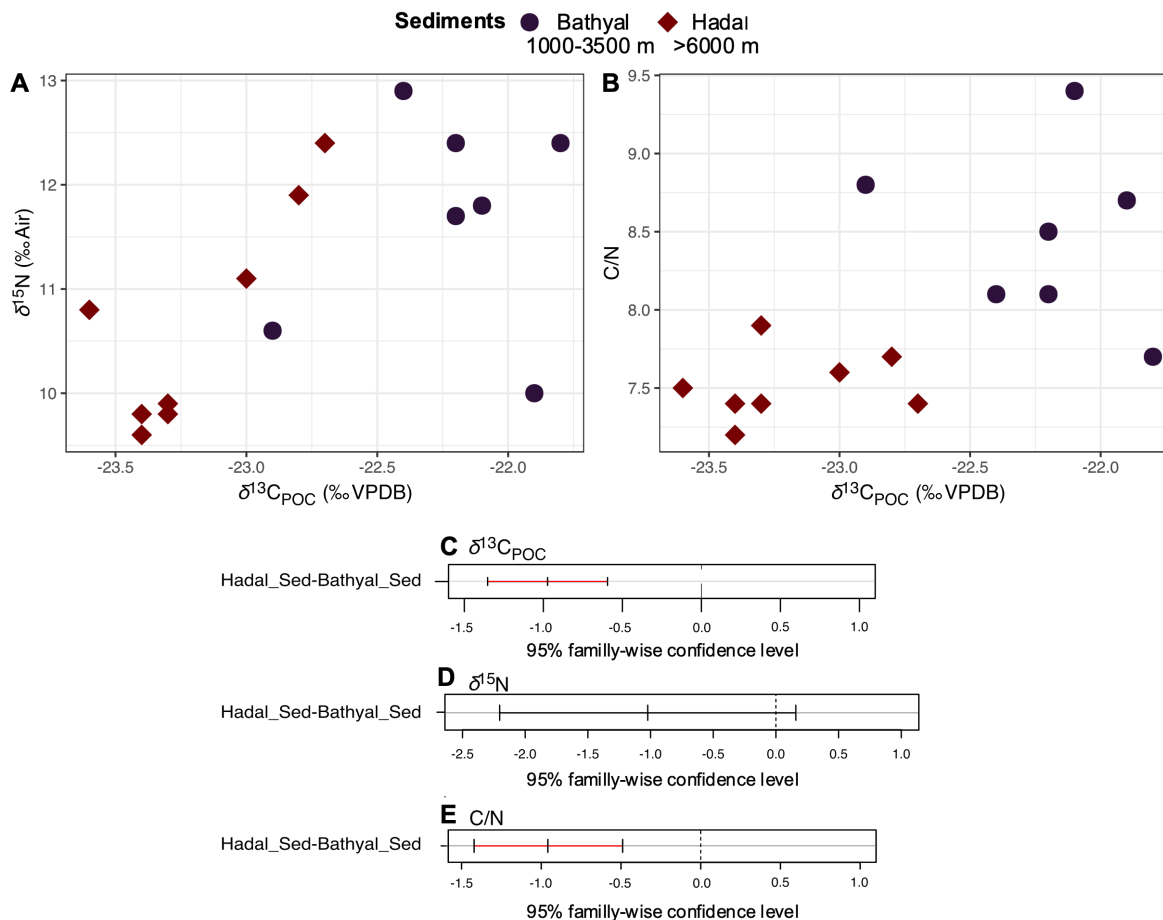


Figure 16. Biplots showing the relationship between (A) $\delta^{15}\text{N}_{\text{PON}}$ and $\delta^{13}\text{C}_{\text{POC}}$, and (B) C/N ratios and $\delta^{13}\text{C}_{\text{POC}}$ in bathyal and hadal sediments. Plots C, D, and E display the 95% family-wise confidence intervals of the difference in means between $\delta^{13}\text{C}_{\text{POC}}$, $\delta^{15}\text{N}_{\text{PON}}$, and C/N ratios, respectively. The red line indicates means that are significantly different (pairwise comparison by Tukey's test).

3.3 Differences in elemental and stable isotope signatures between the water column and trench sediments

We found that the $\delta^{13}\text{C}_{\text{POC}}$, $\delta^{15}\text{N}_{\text{PON}}$, and C/N values from the water column and bathyal and hadal surface sediments were statistically different among themselves (Box plots and Tukey's HSD post hoc test, $p < 0.05$, Fig. 5). Thus, the largely overlapping pelagic values tended to be

more depleted in ^{13}C and ^{15}N compared to bathyal and hadal surface sediments (Figs. 5A,B). The C/N ratio displayed lower values in hadal and bathyal surface sediments than in the pelagic zone (Fig. 5C).

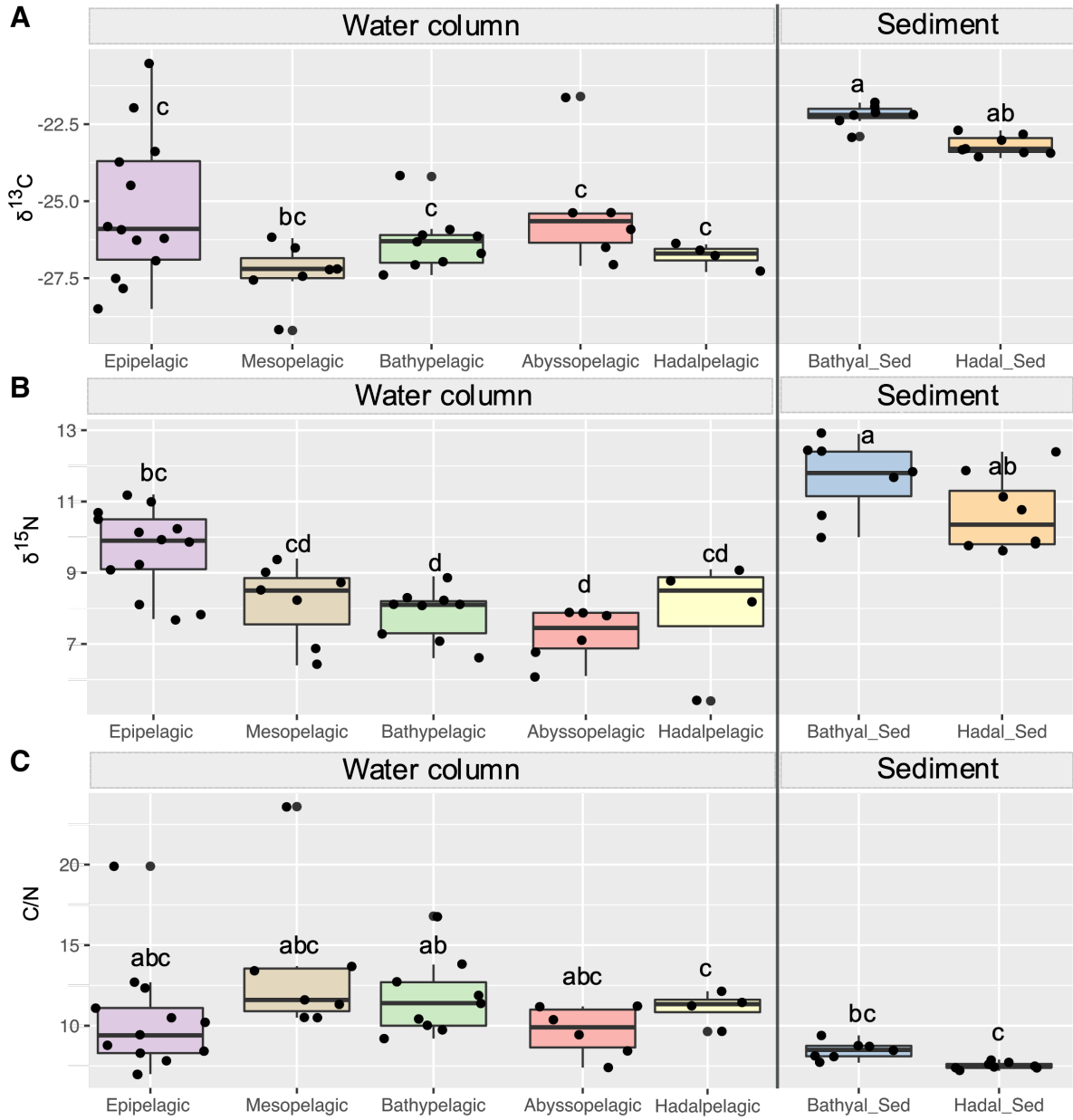


Figure 17. Boxplot showing the (A) $\delta^{13}\text{C}$, (B) $\delta^{15}\text{N}$, and (C) C/N values of the different depth regions of the water column and the bathyal and hadal sediments. We use the same depth zonation as in figure 3. The same combinations of letters over boxplots do not differ significantly ($p < 0.05$, Tukey's test).

3.4 POCsat in the water column overlying the Atacama Trench

POCsat between 18° and 30°S showed high variability during the summer of 2018, ranging ~50-110 (± 30 mg C m⁻³) in surface waters and ~15-30 (± 3 mg C m⁻³) in subsurface waters (1,000 m) (Fig. 6). The overall POCsat decrease throughout the upper 1,000 m of the water column was ~73-84% (Fig. 6A, C). The POC concentrations in surface and subsurface waters increased consistently southwards, especially between 28 and 30°S (Figs. 6A, C), peaking right above the deepest area of the Atacama Trench with surface values up to $\sim 110 \pm 30$ mg C m⁻³ (Figs. 6A,B). In surface waters of the northernmost region (~18°S -26°S), we observed higher monthly average POC values in winter ($\sim 80-90 \pm 10$ mg C m⁻³) and spring ($\sim 90-110 \pm 12$ mg C m⁻³) than in summer and autumn ($\sim 60-70 \pm 7$ mg C m⁻³) (Fig. S2). However, between 28°S and 30°S, the summer POC concentrations were as high as in spring, although more variable. These trends were similar in the more stable subsurface waters, where the highest POC values were observed in summer between 24°S and 30°S (Fig. S).

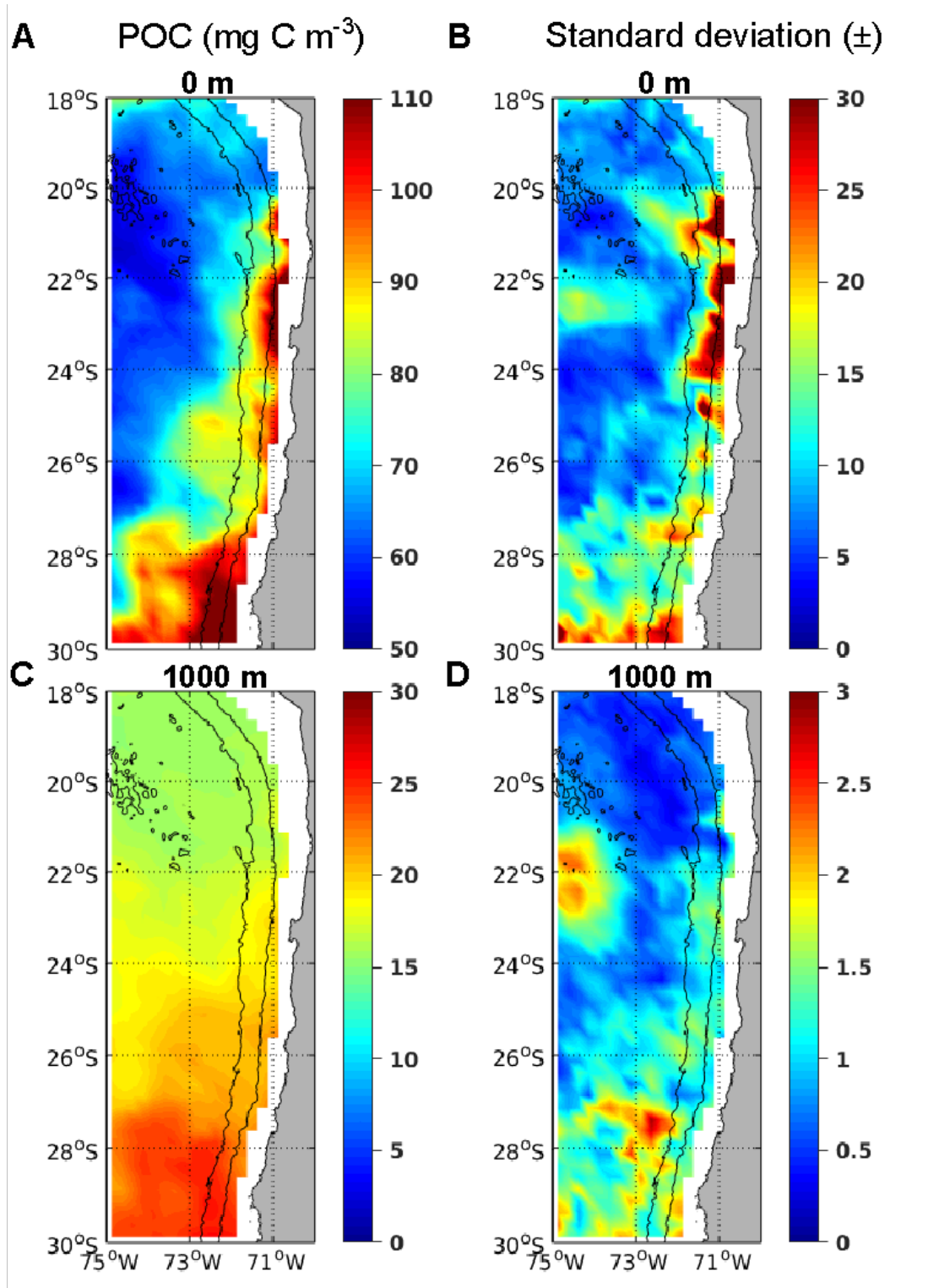


Figure 18. (A, C) Spatio-temporal variability of POCsat calculated for mean weekly observations ~90 days prior to the Hades expedition (January-March 2018) in surface (0 m) and subsurface (1000 m) waters, and (B, D) their respective \pm standard deviations.

3.5 Modelled versus observed POC fluxes

Model calculations that include a lower attenuation of POC flux in the upper part of the photic zone (i.e. exponential curve from Banse, 1990; depth-attenuation rational from Suess, 1980; and double exponential from Lutz et al., 2002) result in fluxes that decline dramatically from $\sim 120 \text{ mg C m}^{-2} \text{ d}^{-1}$ in surface waters to $\sim 1 \text{ mg C m}^{-2} \text{ d}^{-1}$ at 1,000 m depth (Fig. 7A). With this configuration, depth-attenuation rational and double exponential models display an enhanced fit (adjusted $R^2 = 0.6$) with mesopelagic and upper bathypelagic POC fluxes (<2000 m depth) derived from ^{230}Th off the coast of Peru (Pavia et al., 2019). The power-law model (Martin et al., 1987), on the other hand, displays an increase in the magnitude of POC fluxes, even though the attenuation is higher, concomitant with an increase in the attenuation coefficient. The average attenuation coefficient ($b=0.78$) shows the best fit with the power-law model of POC fluxes measured from sediment traps at 2,300 m and 3,700 m depth in this region (Hebbeln et al., 2000; González et al., 2004) (Fig. 7A).

On the other hand, *in situ* POC concentrations (Fig. 7B) decreased from $\sim 120 \text{ mg C m}^{-3}$ to $\sim 16.33 \text{ mg C m}^{-3}$ in the top 1,000 meters of the water column, which represents a degradation of 83.67%. Despite this trend, we observed an increase in the POC concentration up to $22.64 \text{ mg C m}^{-3}$ at 5,000 m followed by a decline to 5.55 mg C m^{-3} at 8,000 m at site A6 (see inside panel in Fig. 7B). Additionally, we observed a slight increase from 5000 m at sites A2 (10.6 mg C m^{-3}) and A4 (6.7 mg C m^{-3}) to 8,000 m (14.5 and 16.9 mg C m^{-3} , respectively) (see inside panel in Fig. 6B).

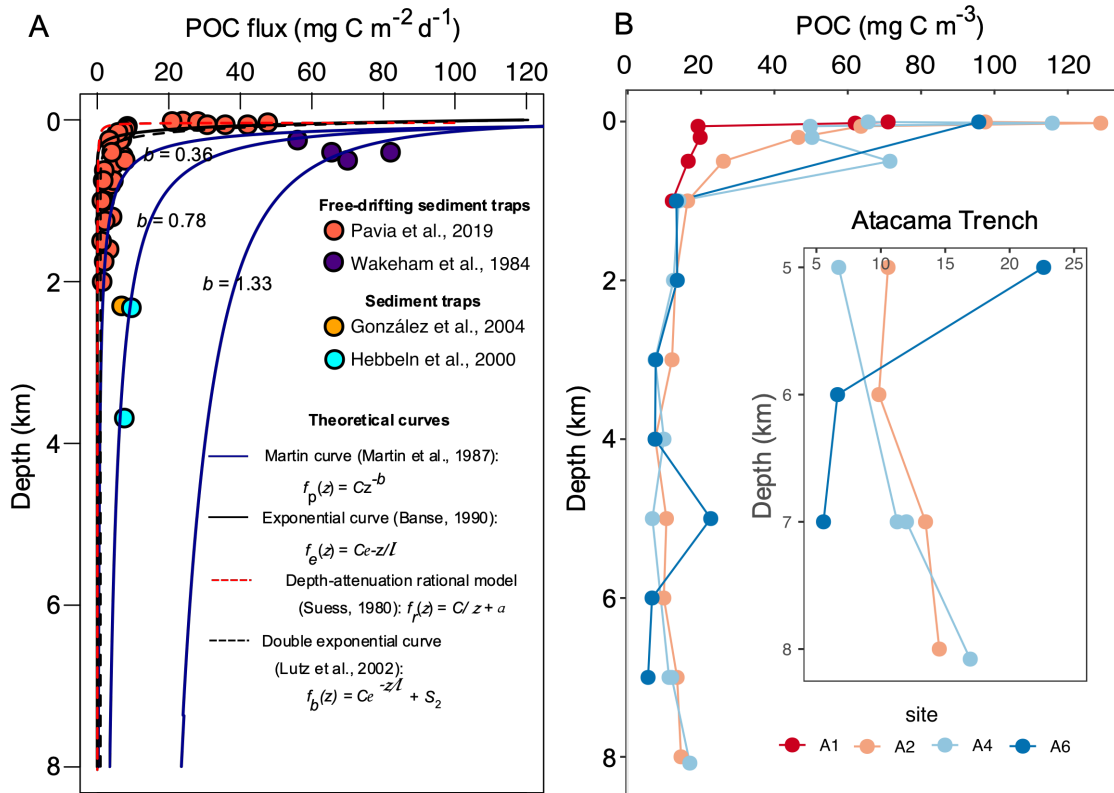


Figura 19. POC fluxes and concentration in the water column overlying the Atacama Trench. (A) Empirical estimates of POC fluxes ($\text{mg C m}^{-2} \text{d}^{-1}$) obtained from (i) the Martin curve using 0.36, 0.78, and 1.33 as attenuation coefficients (blue lines), (ii) an exponential curve (black line), (iii) depth-attenuation rational (red dashed line), and (iv) double exponential curve (black dashed line). Solid circles indicate measured POC fluxes from deep-moored sediment traps (Hebbeln et al., 2002; González et al., 2004), free-drifting sediment traps (Wakeham et al., 1984), and ^{230}Th -normalized isotope-based samples (Pavia et al., 2019). (B) *In situ* POC concentrations measured at stations A1, A2, A4, and A6 during the Hades expedition. The inset highlights the depth region between 5,000 and 8,000 m.

4. Discussion

4.1 Organic matter provenance

The stable carbon and nitrogen isotope signatures of phytoplankton, which constitute most of the organic matter (>80% of OC) produced in the euphotic zone (Lee et al., 2004), are influenced by: a) the isotopic composition of the source carbon and nitrogen, b) isotopic fractionation during carbon fixation and nutrient assimilation, and c) isotopic fractionation during catabolic processes (Goericke & Fry, 1994). Thus, several processes can impact the isotopic composition of carbon and nitrogen in surface waters, and consequently, the isotopic signature of bulk organic matter. These include the upwelling of subsurface waters, fluvial input, trophic interactions, and ecological successions (Peterson & Fry, 1987, and references therein), which are all dynamic in the euphotic zone. Our results show a large range in $\delta^{13}\text{C}_{\text{POC}}$ (-28.5 ‰ to -20.5 ‰, mean -25.30 ‰ \pm 2.36) and $\delta^{15}\text{N}_{\text{PON}}$ (7.7 to 11.2 ‰, mean 9.64 ‰ \pm 1.18) in the epipelagic zone (Figs. 2A,B and 3). These values are within the range of those previously reported in surface POM in the Atacama region (Barrios-Guzmán et al., 2019), and consistent with a predominantly marine planktonic origin (Williams & Gordon, 1990). We anticipate that POM from the ODZ influences the lower epipelagic and upper mesopelagic zones, where the POM is isotopically depleted in ^{13}C and ^{15}N compared to shallower depths (Figs 2A,B, and 3A). This isotopic depletion could be the result of dark autotrophic carbon fixation by chemolithoautotrophs in ODZ waters (Callbeck et al., 2018, Ruiz-Fernández et al., 2020; Vargas et al., 2021), in addition to widespread denitrification along the ETSP coastal margin (De Pol-Holz et al., 2009).

The bathypelagic zone displayed $\delta^{13}\text{C}_{\text{POC}}$ values between -27.4 ‰ and -24.2 ‰ (mean -26.31 ‰ \pm 0.94, n=9) and $\delta^{15}\text{N}_{\text{PON}}$ values between 6.6 and 8.9 ‰ (mean 7.85 ‰ \pm 0.7), whereas the abyssopelagic zone displayed similar values for $\delta^{13}\text{C}_{\text{POC}}$ between -27.1 ‰ and -25.4 ‰ (mean

-26.06 ‰ ±0.73, n=6) and for $\delta^{15}\text{N}_{\text{PON}}$ between 6.1 and 7.9 ‰ (mean 7.3 ‰ ±0.81) (Figs. 2A,B and 3A). However, compared to all other stations in the abyssopelagic zone, we detected ^{13}C -enriched POC at 5,000 m in station A6 (-21.6 ‰). This ^{13}C enrichment was associated with a decrease in the C/N ratio (7.4) (Fig. 2A,C) and a slight increase in POC concentration (~22 mg C m⁻³) (Fig. 7B), but with no isotopic change in $\delta^{15}\text{N}_{\text{PON}}$ (Fig. 2B). Whereas this ^{13}C enrichment at 5,000 m in station A6 is atypical for deep waters, it is in the range of values observed in the epipelagic zone. Since the $\delta^{13}\text{C}$ of POM is considered to be relatively uniform in the deep-sea (Menzel & Ryther, 1968; Follett et al., 2014), it is unlikely to be the cause for the ^{13}C enrichment in POM to be carried out *in situ*. Therefore, it is possible that the POM at this depth could be influenced by an epipelagic source, supported by the mechanism of the fast-sinking particle as suggested by Fernández-Urruzola et al. (2021) for this region. Although we cannot rule out other mechanisms such as the resuspension of particles through downslope sediment transport or deep nepheloid layers.

The hadalpelagic zone displays a low dispersion of $\delta^{13}\text{C}_{\text{POC}}$ values (from -27.3 ‰ to -26.4 ‰, mean -26.7‰ ±0.38, n=4), and a high dispersion in $\delta^{15}\text{N}_{\text{PON}}$ (from 5.4 to 9.1 ‰, mean 7.87 ‰ ±1.69) (shaded area in Figs. 2A,B; and 5A,B). Overall, the increase in $\delta^{15}\text{N}_{\text{PON}}$ values in the hadalpelagic zone coincides with an increase in the C/N ratio. This could indicate a degradation of the organic matter which is enriched in ^{15}N and increases its C/N ratio (Figs. 2A,B,C). This process does not affect C isotopes as much, which show a lower fractionation compared to N, and are more conservative with respect to their origin. In addition, in this deep region of the Atacama trench, we speculate that sediment resuspension may enhance the release of accumulated organic material at suboxic/anoxic sediments to oxic seawater. Thus, the resuspension probably influences both carbon and nitrogen isotopic signatures and is likely associated with the slight increase in POC (Fig. 7B). However, the lack of further hadalpelagic spatial and temporal resolution prevents us from contrasting these isotopic signatures at length.

Hadal surface sediments displayed low dispersion of $\delta^{13}\text{C}_{\text{POC}}$ (from -23.6 ‰ to -22.7 ‰, mean -23.18‰ \pm 0.31, n=9) and C/N ratios (from 7.2 to 7.9, mean 7.5 \pm 0.21), and high dispersion in $\delta^{15}\text{N}_{\text{PON}}$ (from: 9.6 ‰ to 12.4 ‰, mean 10.66 ‰ \pm 1.06) (Fig. 5A, B, C). Furthermore, bathyal surface sediments displayed low dispersion of $\delta^{13}\text{C}_{\text{POC}}$ (from -22.9 ‰ to -21.8 ‰, mean -22.21‰ \pm 0.36, n=7), and high dispersion of C/N values (from 7.7 to 9.4, mean 8.4 \pm 0.56) and $\delta^{15}\text{N}_{\text{PON}}$ (from 10 ‰ to 12.9 ‰, mean 11.68 ‰ \pm 1.04) (Fig. 5A, B, C). Despite the thousands of meters separating hadal and bathyal sediments, they exhibited small differences between their averages ($\delta^{13}\text{C}_{\text{POC}} \sim -0.97$ ‰; $\delta^{15}\text{N}_{\text{PON}} 0.9$ ‰; and C/N ratio 1.02). This similarity could be due to, a) a similar POM origin; b) downslope sediment transport from the bathyal to the hadal region; c) organisms involving a similar isotopic fractionation. It should be noted that the mechanisms behind post-depositional diagenesis could explain the slight isotopic differences between bathyal and hadal sediment (Gearing et al., 1984, Fenton & Ritz, 1988, Meyers, 1994; Liu et al., 2022). In addition, the bulk elemental and isotopic signatures of surface sediments previously collected from areas above the hadal realm (Hebbeln et al., 2000) displayed differences of $\delta^{13}\text{C}_{\text{POC}} \sim 3$ ‰ compared to the bathyal and hadal sediments of this study (see Fig. S3). Previous studies in the hadal realm suggest that the characteristic high pressures and low temperatures of this environment promote a higher carbon isotopic fractionation in heterotrophic piezophilic bacteria compared to shallower surface heterotrophic bacteria (Fang et al., 2006, Xu et al., 2018). These processes combined could partly explain why the hadal sediments are isotopically lighter in $\delta^{13}\text{C}$ and $\delta^{15}\text{N}$ than bathyal sediments. However, other modes of nutrition (e.g. chemoorganotrophs and/or chemolithoautotrophs) that may be performed for isotopic fractionation in these environments are less well known.

A recent geochemical study of Mariana Trench sediments concluded that marine algae is the primary OM source in this system, as reflected in bulk C/N and $\delta^{13}\text{C}$ values (Luo et al., 2017). This result is consistent with previous studies in the Japan and Atacama Trenches (Nakatsuka

et al., 1997; Danovaro et al., 2003). However, deeply buried sediment from the Atacama Trench has revealed phases of slow pelagic sedimentation in the past that alternate with rapid mass-wasting events, which fuel microbial carbon turnover at remarkably high rates (Glud et al., 2013; Zabel et al., 2022). Thus, we expect that the recycling by piezophilic bacteria in the hadal region of organic matter originated from primary production in the surface ocean and the downslope transport will alter the isotopic composition of sedimentary carbon and nitrogen (Xu et al., 2018 and references therein). Indeed, the biplot of C/N and $\delta^{13}\text{C}$ for all data in our study reflects the presence of a distinguishable signature in hadal sediments of the Atacama Trench that could represent a mixture of pelagic sources, downslope transport, and *in-situ*, sedimentary microbial activity (see Fig. S4).

4.2 What is the relative contribution of allochthonous sources to Atacama Trench sediments?

Marine trenches have been reported to receive diverse sources of organic matter (Glud et al., 2013; Luo et al., 2017; Xu et al., 2018). In general, intra- and inter-trench heterogeneity in the composition of the sedimentary organic matter, along with benthic hadal remineralization rates, have been ascribed to differences in regional surface ocean productivity (Jamieson, 2015; Wenzhöfer et al., 2016; Glud et al., 2021). Sinking particles, as transport mechanisms, are important in delivering carbon to the deep ocean where it can be stored and effectively removed from the modern carbon cycle (Williams & Giering, 2022). In fact, fresh phytodetrital material from surface waters has been observed in hadal regions (Danovaro et al., 2003; Oguri et al., 2013; Guo et al., 2018). Since the Atacama Trench underlies the highly productive waters of the HCS, it is reasonable to presume that this hadal system is more prone to receive particles synthesized in surface waters than other oligotrophic trenches. This could explain, for instance, why the Atacama Trench sediments contain higher organic carbon compared to the trenches

located in the western Pacific Ocean, which harbor less productive overlying surface waters (e.g. Kermadec Trench, Yunping Xu et al., 2021; Mariana Trench, Li et al., 2020; Japan Trench, Oguri et al., 2013). However, a recent study on sedimentary profiles of $^{210}\text{Pb}_{\text{ex}}$ and TOC in the Atacama Trench demonstrated no apparent relationship between the net primary productivity at the surface ocean and the carbon mass accumulation rate (Oguri et al., 2022). These observations suggest that depositional dynamics and local bathymetry are more important than how much OM is produced at the surface. However, high remineralization due to intense heterotrophic activity has also been demonstrated in the Atacama Trench (Glud et al., 2013, Glud et al., 2021). Therefore, although previous studies have suggested an important contribution of OM from material accumulated in sediments on the continental shelf, to hadal benthic zone (Flores et al., 2022; Oguri et al., 2022; Zabel et al., 2022), the contribution of OM from the euphotic zone to hadalpelagic zone could be more than expected.

We evaluated the changes in surface primary productivity through available POCsat data and modeled the POC fluxes in the Atacama Trench. POCsat exhibits high concentrations and a high degree of spatial heterogeneity in surface waters over the Atacama Trench region (Fig. 6A). This trend is modulated by offshore waters, where the chlorophyll maximum occurs in winter (Yuras et al., 2005) and is related to the propagation of mesoscale eddies that expand the area of high chlorophyll concentration beyond the coastal upwelling center (Correa-Ramirez et al., 2007). We observed similar patterns of seasonal increase in POCsat in autumn and winter in the study area (Fig. S1). Moreover, POCsat data below the epipelagic zone shows more attenuated spatial heterogeneity, which is maintained up to the lower limit of the mesopelagic zone (~16-27% POC; Fig. 6C). Our discrete measurements at the same depth (~16.3% POC; Fig. 7B) are consistent with the POCsat results. Similar POC percentages in the mesopelagic zone have been reported in other high-productivity systems, which has been

attributed to the presence of ODZ waters that could reduce the decomposition rate of POC and increase its sink into deeper waters (Weber & Bianchi, 2020; Ma et al., 2021).

Discrete measurements of organic matter composition from bathypelagic to hadalpelagic zones are scarce. Since POC concentrations in bathypelagic and upper abyssopelagic zones (i.e. 1,000-5,000 m; Fig. 7B) are low and stable, we speculate that this could reflect a well-mixed deep layer, such as previously suggested in the Izu–Ogasawara Trench (Kawagucci et al., 2018). However, the slight POC increase in the hadalpelagic zone at stations A2 and A4 (see Fig. 7B) may come from an additional POC input in this region. Potential sources include POC accumulation due to the resuspended sediment, or a lateral contribution through nepheloid layers from the shallower slope (Nakatsuka et al., 1997; Xu et al., 2018; Gardner et al., 2022). Studies in the open ocean and the Gulf of Mexico have found that areas of high surface eddy kinetic energy are often related to areas where nepheloid layers are common (Gardner et al., 2022). However, it is unknown whether nepheloid layer can reach hadal depths (6000–11 000 m). In order to investigate whether the production of POC in the epipelagic and mesopelagic zones affects its behavior in greater depths, we compared vertical POC fluxes calculated from theoretical models (see model parameters in table S1) against published, *in situ* POC flux measurements derived from sediment traps in the region (Fig. 7A). The theoretical calculations that best fit deep sediment trap data suggest a low POC flux ($3.96 \text{ mg C m}^{-2} \text{ d}^{-1}$, $\sim 3.3\%$, see Fig. 7A) from the euphotic zone to surface sediments of the Atacama Trench.

Given the multiple possible sources of OM to the deep ocean, we applied a multi-source percentage contribution model of Stock et al. (2018) to our isotope dataset. When only pelagic OM sources are used, we observed that the epipelagic zone is the dominant source of POM to hadal surface sediments (Figs. 8A, B). However, when we include bathyal sediments as an

additional source, the contribution to hadal sediments from the combined water column regions is <25% (Figs. 8C,D). Thus, these results suggest that OM can rapidly reach the hadal zone, likely through a combination of fast-sinking particulates and downslope and/or lateral transport that could be gain importance near the hadal seafloor, as has been suggested in previous studies for the Atacama Trench (Fernandez-Urruzola et al., 2021; Zabel et al., 2022; Oguri et al., 2022). We speculate that in addition to the processes described above, the slope of bathymetric relief ($\alpha = 6.5^\circ$) in the Atacama trench (computed from GEBCO 2020 Grid; Kioka & Strasser, 2021), may be an additional factor contributing to sedimentary organic matter through downslope transport in this region.

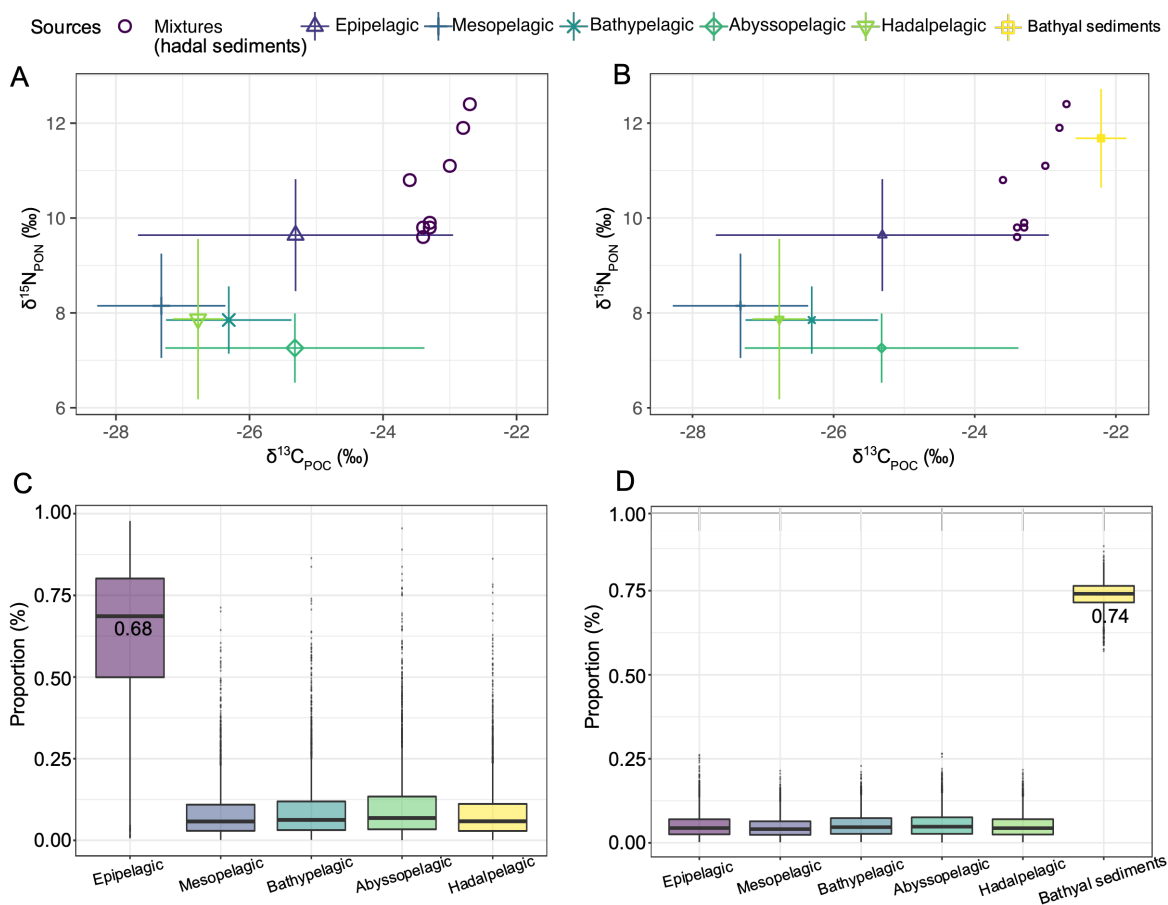


Figure 20. Isotopic signatures of organic matter and their mixing in surface hadal sediments. (A) Biplot showing $\delta^{13}\text{C}$ and $\delta^{15}\text{N}$ of POM in the water column and surface hadal sediments ("mixture"). (B) Biplot showing $\delta^{13}\text{C}$ and $\delta^{15}\text{N}$ of POM in the water column and surface hadal sediments ("mixture"), in addition to bathyal sediments as an additional source of POM. (C,

D) Relative fractional contribution of POM from the different pelagic zones as well as from bathyal and hadal sediments using the MixSIAR (Stable Isotope Analysis in R) mixing model.

Nonetheless, we acknowledge that we cannot infer biogeochemical or microbial processes in the hadalpelagic zone by simply extrapolating POC fluxes from surface waters through isotope models and without taking into account other allochthonous sources as well as autochthonous sources. As a consequence, we must delve into the complexity of processes influencing POC flux models, such as sinking velocity (Williams & Giering, 2022) and the “source funnel” effect proposed by Sigel et al. (2008) and widely discussed by Fernández-Urruzola et al. (2021). Future measurements of sediment trap fluxes from the bottom of the Atacama trench would allow us to quantify the contribution and composition of different OM sources, as well as understand its temporal variability.

5. Conclusions

We investigated the sources and mixing of organic matter in the hadal region of the Atacama trench using bulk elemental and stable isotope geochemical data. The $\delta^{13}\text{C}_{\text{POC}}$ and $\delta^{15}\text{N}_{\text{PON}}$ in surface sediments of the Atacama Trench indicate the presence of an isotopically heavier organic matter reservoir compared to the water column, which is more closely related to bathyal sediments. Using a mixing model based on the isotopic signatures of bulk organic carbon and total nitrogen in pelagic POM and sedimentary organic matter, we calculated that ~75% of the organic matter present in surface sediments from the Atacama Trench could derive from bathyal sediments. When bathyal sediment is excluded from the model, we computed that ~68% of sedimentary OM in the hadal sediments could derive from the epipelagic region. Additionally, we report evidence of high spatial heterogeneity in surface water POC from remote-sensing data in the highly productive region overlying the Atacama Trench. Notably,

the vertical POC fluxes that best fit with existing data from deep sediment traps (~2300 and 3700 m) suggest that ~3.3% of the total POC flux that reaches hadal surface sediments derives from surface waters. Thus, we conclude that the contribution from downslope sediment transport to the hadal benthic zone could be greater than the POM export from the water column. However, since the fluxes of these sources are expected to vary both spatially and temporally and the fact that the bulk geochemistry of sediment includes time scales larger than the water column, we cannot rule out a greater contribution from the surface epipelagic zones at times.

Acknowledgments

This work was supported by the Chilean National Agency for Research and Development through the Millenium Science Initiative-ANID Program (grant ICN12 019-IMO), grants FONDECYT 1191360 and 11221079 to O. Ulloa and I. Fernandez-Urruzola, respectively, and by the European Research Council (HADES-ERC, grant agreement number 669947 to R. Glud) and the Max Planck Society. J. Sepúlveda acknowledges partial support from NSF-CAREER award 2047057 and from the Department of Geological Sciences and INSTAAR at the University of Colorado Boulder. E. Flores was also partially supported by the Universidad de Concepción (UCO 1866 student scholarship 2022). We are thankful to the captains, crews, and scientists of the German RV Sonne cruises SO261 (HADES- ERC) and SO211 (ChiMeBo). In particular, we thank the chief scientists R. Glud and F. Wenzhöfer (HADES-ERC) and Dierk Hebbeln (ChiMeBo), and Nadin Ramirez for the deployment of the Lander "Audacia" during the HADES-ERC cruise. The HADES-ERC and ChiMeBo cruises were funded by the European Research Council and the German Bundesministerium für Bildung and Forschung (BMBF), respectively.

Open Research

Carbon and Nitrogen isotopic signatures of the bulk organic matter for all samples in this study are available at the PANGAEA data repository via [DOI to be inserted here] with [license, access conditions to be inserted here] [citation to be inserted here].

References

- Azam, F., Smith, D., Steward, G., & Hagström, Å. (1994). Bacteria-organic matter coupling and its significance for oceanic carbon cycling. *Microbial Ecology*, 28(2), 167–179.
- Banse, K. (1990). New views on the degradation and disposition of organic particles as collected by sediment traps in the open sea. *Deep Sea Research Part A. Oceanographic Research Papers*, 37(7), 1177–1195.
- Barrios-Guzmán, C., Sepúlveda, M., Docmac, F., Zarate, P., Reyes, H., & Harrod, C. (2019). Sample acidification has a predictable effect on isotopic ratios of particulate organic matter along the Chilean coast. *Rapid Communications in Mass Spectrometry*, 33(21), 1652–1659.
- Buesseler, K. O., Boyd, P. W., Black, E. E., & Siegel, D. A. (2020). Metrics that matter for assessing the ocean biological carbon pump. *Proceedings of the National Academy of Sciences*, 117(18), 9679–9687.
- Burd, A. B., & Jackson, G. A. (2009). Particle aggregation. *Annual Review of Marine Science*, 1, 65–90.
- Callbeck, C. M., Lavik, G., Ferdelman, T. G., Fuchs, B., Gruber-Vodicka, H. R., Hach, P. F., et al. (2018). Oxygen minimum zone cryptic sulfur cycling sustained by offshore transport of key sulfur oxidizing bacteria. *Nature Communications*, 9(1), 1–11.
- Cantarero, S. I., Henríquez-Castillo, C., Dildar, N., Vargas, C. A., Von Dassow, P., Cornejo-D’Ottone, M., & Sepúlveda, J. (2020). Size-fractionated contribution of microbial biomass to suspended organic matter in the eastern Tropical South Pacific oxygen minimum zone. *Frontiers in Marine Science*, 7, 745.

- Cavan, E. L., Kawaguchi, S., & Boyd, P. W. (2021). Implications for the mesopelagic microbial gardening hypothesis as determined by experimental fragmentation of Antarctic krill fecal pellets. *Ecology and Evolution*, *11*(2), 1023–1036.
- Chunhui, X., Yonghong, W., Jiwei, T., Xuchen, W., & Yu, X. (2020). Mineral composition and geochemical characteristics of sinking particles in the Challenger Deep, Mariana Trench: Implications for provenance and sedimentary environment. *Deep Sea Research Part I: Oceanographic Research Papers*, *157*, 103211.
- Correa-Ramirez, M. A., Hormazábal, S., & Yuras, G. (2007). Mesoscale eddies and high chlorophyll concentrations off central Chile (29–39 S). *Geophysical Research Letters*, *34*(12).
- Daneri, G., Dellarossa, V., Quiñones, R., Jacob, B., Montero, P., & Ulloa, O. (2000). Primary production and community respiration in the Humboldt Current System off Chile and associated oceanic areas. *Marine Ecology Progress Series*, *197*, 41–49.
- Danovaro, R., Della Croce, N., Dell'Anno, A., & Pusceddu, A. (2003). A depocenter of organic matter at 7800 m depth in the SE Pacific Ocean. *Deep Sea Research Part I: Oceanographic Research Papers*, *50*(12), 1411–1420.
- Danovaro, Roberto, Dell'Anno, A., & Pusceddu, A. (2004). Biodiversity response to climate change in a warm deep sea. *Ecology Letters*, *7*(9), 821–828.
- Danovaro, Roberto, Snelgrove, P. V., & Tyler, P. (2014). Challenging the paradigms of deep-sea ecology. *Trends in Ecology & Evolution*, *29*(8), 465–475.
- De La Rocha, C. L., Nowald, N., & Passow, U. (2008). Interactions between diatom aggregates, minerals, particulate organic carbon, and dissolved organic matter: Further implications for the ballast hypothesis. *Global Biogeochemical Cycles*, *22*(4).

De Pol-Holz, R., Robinson, R. S., Hebbeln, D., Sigman, D. M., & Ulloa, O. (2009). Controls on sedimentary nitrogen isotopes along the Chile margin. *Deep Sea Research Part II: Topical Studies in Oceanography*, 56(16), 1042–1054.

Devol, Allan H., Hartnett, Hilairy E., (2001), Role of the oxygen-deficient zone in transfer of organic carbon to the deep ocean, *Limnology and Oceanography*, 7, doi: 10.4319/lo.2001.46.7.1684.

Fang, J., Uhle, M., Billmark, K., Douglas, H., Bartlett, H., & Kato, C. (2006). Fractionation of carbon isotopes in biosynthesis of fatty acids by a piezophilic bacterium *Moritella japonica* strain DSK1. *Geochimica et Cosmochimica Acta*, 70(7), 1753-1760.

Fenton, G. E., & Ritz, D. A. (1988). Changes in carbon and hydrogen stable isotope ratios of macroalgae and seagrass during decomposition. *Estuarine, Coastal and Shelf Science*, 26(4), 429–436.

Fernández-Urruzola, I., Ulloa, O., Glud, R. N., Pinkerton, M. H., Schneider, W., Wenzhöfer, F., & Escribano, R. (2021). Plankton respiration in the Atacama Trench region: Implications for particulate organic carbon flux into the hadal realm. *Limnology and Oceanography*, 66(8), 3134–3148.

Follett, C. L., Repeta, D. J., Rothman, D. H., Xu, L., & Santinelli, C. (2014). Hidden cycle of dissolved organic carbon in the deep ocean. *Proceedings of the National Academy of Sciences*, 111(47), 16706– 16711. <https://doi.org/10.1073/pnas.1407445111>

Flores, E., Cantarero, S. I., Ruiz-Fernández, P., Dildar, N., Zabel, M., Ulloa, O., & Sepúlveda, J. (2022). Bacterial and eukaryotic intact polar lipids point to in situ production as a key source of labile organic matter in hadal surface sediment of the Atacama Trench. *Biogeosciences*, 19(5), 1395–1420.

Fuenzalida, R., Schneider, W., Garcés-Vargas, J., Bravo, L., & Lange, C. (2009). Vertical and horizontal extension of the oxygen minimum zone in the eastern South Pacific Ocean.

Deep Sea Res. Part II Top. Stud. Oceanogr., 56 (16), pp. 992-1003.

10.1016/j.dsr2.2008.11.001

Gao, X., Yanga, Y., & Wang, C. (2012). Geochemistry of organic carbon and nitrogen in surface sediments of coastal Bohai Bay inferred from their ratios and stable isotopic signatures. *Marine Pollution Bulletin*. Volume 64, Issue 6, June 2012, Pages 1148-1155

Gearing, J., Gearing, P., Rudnick, D., Requejo, A., & Hutchins, M. (1984). Isotopic variability of organic carbon in a phytoplankton-based, temperate estuary. *Geochimica et Cosmochimica Acta*, 48(5), 1089–1098.

Guo R, Liang Y, Xin Y, Wang L, Mou S, Cao C, Xie R, Zhang C, Tian J and Zhang Y (2018) Insight Into the Pico- and Nano-Phytoplankton Communities in the Deepest Biosphere, the Mariana Trench. *Front. Microbiol.* 9:2289. doi: 10.3389/fmicb.2018.02289.

Glud, R. N., Wenzhöfer, F., Middelboe, M., Oguri, K., Turnewitsch, R., Canfield, D. E., & Kitazato, H. (2013). High rates of microbial carbon turnover in sediments in the deepest oceanic trench on Earth. *Nature Geoscience*, 6(4), 284–288.

Glud, R. N., Berg, P., Thamdrup, B., Larsen, M., Stewart, H. A., Jamieson, A. J., et al. (2021). Hadal trenches are dynamic hotspots for early diagenesis in the deep sea. *Communications Earth & Environment*, 2(1), 1–8.

Goericke, R., & Fry, B. (1994). Variations of marine plankton $\delta^{13}\text{C}$ with latitude, temperature, and dissolved CO_2 in the world ocean. *Global Biogeochemical Cycles*, 8(1), 85–90.

González, H. E., Hebbeln, D., Iriarte, J. L., & Marchant, M. (2004). Downward fluxes of faecal material and microplankton at 2300 m depth in the oceanic area off Coquimbo (30 S), Chile, during 1993–1995. *Deep Sea Research Part II: Topical Studies in Oceanography*, 51(20–21), 2457–2474.

- González, H. E., Daneri, G., Iriarte, J. L., Yannicelli, B., Menschel, E., Barría, C., et al. (2009). Carbon fluxes within the epipelagic zone of the Humboldt Current System off Chile: The significance of euphausiids and diatoms as key functional groups for the biological pump. *Progress in Oceanography*, 83(1–4), 217–227.
- González, H.E., Ortiz, V., & Sobarzo, M. (2000). The role of faecal material in the particulate organic carbon flux in the northern Humboldt Current, Chile (23°S), before and during the 1997–98 El Niño *Journal of Plankton Research*, 22 (2000), pp. 499-529.
<https://doi.org/10.1093/plankt/22.3.499>
- Grabowski, E., Letelier, R. M., Laws, E. A., & Karl, D. M. (2019). Coupling carbon and energy fluxes in the North Pacific Subtropical Gyre. *Nature Communications*, 10(1), 1–9.
- Hebbeln, D., Marchant, M., & Wefer, G. (2000). Seasonal variations of the particle flux in the Peru-Chile current at 30 S under ‘normal’ and El Niño conditions. *Deep Sea Research Part II: Topical Studies in Oceanography*, 47(9–11), 2101–2128.
- Hedges, J. I., Baldock, J. A., Gélinas, Y., Lee, C., Peterson, M., & Wakeham, S. G. (2001). Evidence for non-selective preservation of organic matter in sinking marine particles. *Nature*, 409(6822), 801–804.
- Ichino, M. C., Clark, M. R., Drazen, J. C., Jamieson, A., Jones, D. O., Martin, A. P., et al. (2015). The distribution of benthic biomass in hadal trenches: a modelling approach to investigate the effect of vertical and lateral organic matter transport to the seafloor. *Deep Sea Research Part I: Oceanographic Research Papers*, 100, 21–33.
- Iversen, M. H., & Ploug, H. (2010). Ballast minerals and the sinking carbon flux in the ocean: carbon-specific respiration rates and sinking velocity of marine snow aggregates. *Biogeosciences*, 7(9), 2613–2624.
- Jamieson, A. (2015). *The hadal zone: life in the deepest oceans*. Cambridge University Press.

Kawagucci, S., Makabe, A., Kodama, T., Matsui, Y., Yoshikawa, C., Ono, E., et al. (2018). Hadal water biogeochemistry over the Izu–Ogasawara Trench observed with a full-depth CTD-CMS. *Ocean Science*, *14*(4), 575–588. <https://doi.org/10.5194/os-14-575-2018>

Kioka, A., & Strasser, M. (2022). Oceanic Trenches. In *Treatise on Geomorphology (Second Edition)* (pp. 882–900). Academic Press.

Kioka, A., Schwestermann, T., Moernaut, J., Ikehara, K., Kanamatsu, T., Eglinton, T. I., & Strasser, M. (2019). Event stratigraphy in a hadal oceanic trench: The Japan trench as sedimentary archive recording recurrent giant subduction zone earthquakes and their role in organic carbon export to the deep sea. *Frontiers in Earth Science*, *7*, 319.

Kriest, I. (2002). Different parameterizations of marine snow in a 1D-model and their influence on representation of marine snow, nitrogen budget and sedimentation. *Deep Sea Research Part I: Oceanographic Research Papers*, *49*(12), 2133–2162.

Lee, C., Wakeham, S., & Arnosti, C. (2004). Particulate organic matter in the sea: the composition conundrum. *AMBIO: A Journal of the Human Environment*, *33*(8), 565–575.

Li, D., Zhao, J., Yao, P., Liu, C., Sun, C., Chen, J., et al. (2020). Spatial heterogeneity of organic carbon cycling in sediments of the northern Yap Trench: Implications for organic carbon burial. *Marine Chemistry*, *223*, 103813.

Liu, J., Zheng, Y., Lin, H., Wang, X., Li, M., Liu, Y., et al. (2019). Proliferation of hydrocarbon-degrading microbes at the bottom of the Mariana Trench. *Microbiome*, *7*(1), 1–13.

Liu, X., Wendt-Potthoff, K., Barth, J.A.C. et al. Post-depositional alteration of stable isotope signals by preferential degradation of algae-derived organic matter in reservoir sediments. *Biogeochemistry* *159*, 315–336 (2022). <https://doi.org/10.1007/s10533-022-00930-y>

- Luo, M., Gieskes, J., Chen, L., Shi, X., & Chen, D. (2017). Provenances, distribution, and accumulation of organic matter in the southern Mariana Trench rim and slope: Implication for carbon cycle and burial in hadal trenches. *Marine Geology*, *386*, 98–106.
- Luo, M., Gieskes, J., Chen, L., Scholten, J., Pan, B., Lin, G., & Chen, D. (2019). Sources, degradation, and transport of organic matter in the New Britain Shelf-Trench continuum, Papua New Guinea. *Journal of Geophysical Research: Biogeosciences*, *124*(6), 1680–1695.
- Lutz, M., Dunbar, R., & Caldeira, K. (2002). Regional variability in the vertical flux of particulate organic carbon in the ocean interior. *Global Biogeochemical Cycles*, *16*(3), 11–1.
- Lutz, M. J., Caldeira, K., Dunbar, R. B., & Behrenfeld, M. J. (2007). Seasonal rhythms of net primary production and particulate organic carbon flux to depth describe the efficiency of biological pump in the global ocean. *Journal of Geophysical Research: Oceans*, *112*(C10).
- Ma, J., Song, J., Li, X., Wang, Q., Zhong, G., Yuan, H., et al. (2021). The OMZ and Its Influence on POC in the Tropical Western Pacific Ocean: Based on the Survey in March 2018. *Frontiers in Earth Science*, *9*. <https://doi.org/10.3389/feart.2021.632229>
- Martín, J., & Miquel, J.-C. (2010). High downward flux of mucilaginous aggregates in the Ligurian Sea during summer 2002: similarities with the mucilage phenomenon in the Adriatic Sea. *Marine Ecology*, *31*(3), 393–406.
- Martin, J. H., Knauer, G. A., Karl, D. M., & Broenkow, W. W. (1987). VERTEX: carbon cycling in the northeast Pacific. *Deep Sea Research Part A. Oceanographic Research Papers*, *34*(2), 267–285.
- Matys, E., Sepúlveda, J., Pantoja, S., Lange, C., Caniupán, M., Lamy, F., & Summons, R. E. (2017). Bacteriohopanepolyols along redox gradients in the Humboldt Current System off northern Chile. *Geobiology*, *15*(6), 844–857.

- de Melo Viríssimo, F., Martin, A. P., & Henson, S. A. (2022). Influence of seasonal variability in flux attenuation on global organic carbon fluxes and nutrient distributions. *Global Biogeochemical Cycles*, *36*(2), e2021GB007101.
- Menzel, D. W., & Ryther, J. H. (1968). Organic carbon and the oxygen minimum in the South Atlantic Ocean. In *Deep Sea Research and Oceanographic Abstracts* (Vol. 15, pp. 327–337). Elsevier.
- Meyers, P. A. (1994). Preservation of elemental and isotopic source identification of sedimentary organic matter. *Chemical Geology*, *114*(3–4), 289–302.
- Meyers, P.A. & Eadie, B.J. (1993). Sources, degradation and recycling of organic matter associated with sinking particles in Lake Michigan. *Org. Geochem.*, *20* (1) (1993), pp. 47-56.
- Middelburg, J. J. (2019). Carbon processing at the seafloor. In *Marine carbon biogeochemistry* (pp. 57–75). Springer.
- Middelburg J. & Nieuwenhuize, J. (1998). Carbon and nitrogen stable isotopes in suspended matter and sediments from the Schelde Estuary. *Marine Chemistry*. Volume 60, Issues 3–4, April 1998, Pages 217-225
- Nakatsuka, T., Handa, N., Harada, N., Sugimoto, T., & Imaizumi, S. (1997). Origin and decomposition of sinking particulate organic matter in the deep water column inferred from the vertical distributions of its $\delta^{15}\text{N}$, $\delta^{13}\text{C}$ and $\delta^{14}\text{C}$. *Deep Sea Research Part I: Oceanographic Research Papers*, *44*(12), 1957–1979. [https://doi.org/10.1016/S0967-0637\(97\)00051-4](https://doi.org/10.1016/S0967-0637(97)00051-4)
- Neubauer, D., Kolmakova, O., Woodhouse, J., Taube, R., Mangelsdorf, K., Gladyshev, M., et al. (2021). Zooplankton carcasses stimulate microbial turnover of allochthonous particulate organic matter. *The ISME Journal*, *15*(6), 1735–1750.

Nunoura, T., Nishizawa, M., Hirai, M., Shimamura, S., Harnvoravongchai, P., Koide, O., et al. (2018). Microbial diversity in sediments from the bottom of the Challenger Deep, the Mariana Trench. *Microbes and Environments*, ME17194.

Siegel, D. A., E. Fields, & K. O. Buesseler (2008). A bottom-up view of the biological pump: Modeling source funnels above ocean sediment traps. *Deep-Sea Res.* I55: 108–127.
doi:10.1016/j.dsr.2007.10.006

Oguri, K., Kawamura, K., Sakaguchi, A., Toyofuku, T., Kasaya, T., Murayama, M., et al. (2013). Hadal disturbance in the Japan Trench induced by the 2011 Tohoku–Oki Earthquake. *Scientific Reports*, 3(1), 1–6.

Oguri, K., Masqué, P., Zabel, M., Stewart, H. A., MacKinnon, G., Rowden, A. A., et al. (2022). Sediment accumulation and carbon burial in four hadal trench systems. *Journal of Geophysical Research: Biogeosciences*, 127(10), e2022JG006814.

Oksanen, J., Blanchet, F. G., Kindt, R., Legendre, P., Minchin, P., O’hara, R., et al. (2013). Community ecology package. *R Package Version*, 2(0).

Omand, M. M., D’Asaro, E. A., Lee, C. M., Perry, M. J., Briggs, N., Cetinić, I., & Mahadevan, A. (2015). Eddy-driven subduction exports particulate organic carbon from the spring bloom. *Science*, 348(6231), 222–225.

Omand, M. M., Govindarajan, R., He, J., & Mahadevan, A. (2020). Sinking flux of particulate organic matter in the oceans: Sensitivity to particle characteristics. *Scientific Reports*, 10(1), 1–16.

Pavia, F. J., Anderson, R. F., Lam, P. J., Cael, B., Vivancos, S. M., Fleisher, M. Q., et al. (2019). Shallow particulate organic carbon regeneration in the South Pacific Ocean. *Proceedings of the National Academy of Sciences*, 116(20), 9753–9758.

Peterson, B. J., & Fry, B. (1987). Stable isotopes in ecosystem studies. *Annual Review of Ecology and Systematics*, 293–320.

Pizarro, G., Iriarte, J. L., & Montecino, V. (2002). Mesoscale primary production and bio-optical variability off Antofagasta (23–24 S) during the transition to El Niño 1997–1998. *Revista Chilena de Historia Natural*, 75, 201–215.

Poff, K. E., Leu, A. O., Eppley, J. M., Karl, D. M., & DeLong, E. F. (2021). Microbial dynamics of elevated carbon flux in the open ocean's abyss. *Proceedings of the National Academy of Sciences*, 118(4).

Resplandy, L., Lévy, M., & McGillicuddy Jr, D. J. (2019). Effects of eddy-driven subduction on ocean biological carbon pump. *Global Biogeochemical Cycles*, 33(8), 1071–1084.

Rex, M. A., Etter, R. J., Morris, J. S., Crouse, J., McClain, C. R., Johnson, N. A., et al. (2006). Global bathymetric patterns of standing stock and body size in the deep-sea benthos. *Marine Ecology Progress Series*, 317, 1–8.

Rice, A., Billett, D., Fry, J., John, A., Lampitt, R., Mantoura, R., & Morris, R. (1986). Seasonal deposition of phytodetritus to the deep-sea floor. *Proceedings of the Royal Society of Edinburgh, Section B: Biological Sciences*, 88, 265–279.

Robison, B. H., Reisenbichler, K. R., & Sherlock, R. E. (2005). Giant larvacean houses: Rapid carbon transport to the deep sea floor. *Science*, 308(5728), 1609–1611.

Ruiz-Fernández, P., Ramírez-Flandes, S., Rodríguez-León, E., & Ulloa, O. (2020). Autotrophic carbon fixation pathways along the redox gradient in oxygen-depleted oceanic waters. *Environmental Microbiology Reports*, 12(3), 334–341.

Sauzède, R., Claustre, H., Uitz, J., Jamet, C., Dall'Olmo, G., d'Ortenzio, F., et al. (2016). A neural network-based method for merging ocean color and Argo data to extend surface bio-optical properties to depth: Retrieval of the particulate backscattering coefficient. *Journal of Geophysical Research: Oceans*, 121(4), 2552–2571.

Selden, C.R., Mulholland, M.R., Widner, B., Bernhardt, P. and Jayakumar, A. (2021), Toward resolving disparate accounts of the extent and magnitude of nitrogen fixation in the

Eastern Tropical South Pacific oxygen deficient zone. *Limnol Oceanogr*, 66: 1950-1960.

<https://doi.org/10.1002/lno.11735>

Stock, B. C., Jackson, A. L., Ward, E. J., Parnell, A. C., Phillips, D. L., & Semmens, B. X. (2018). Analyzing mixing systems using a new generation of Bayesian tracer mixing models. *PeerJ*, 6, e5096.

Suess, E. (1980). Particulate organic carbon flux in the oceans—surface productivity and oxygen utilization. *Nature*, 288(5788), 260–263.

Tokuda, A. K., Drazen, J. C., Geringer, M. E., Popp, B. N., Grammatopoulou, E., & Mayor, D. J. (2020). Trophic interactions of megafauna in the Mariana and Kermadec trenches inferred from stable isotope analysis. *Deep Sea Research Part I: Oceanographic Research Papers*, 164, 103360.

Turner, J. T. (2002). Zooplankton fecal pellets, marine snow and sinking phytoplankton blooms. *Aquatic Microbial Ecology*, 27(1), 57–102.

Turnewitsch, R., Falahat, S., Stehlikova, J., Oguri, K., Glud, R. N., Middelboe, M., et al. (2014). Recent sediment dynamics in hadal trenches: evidence for the influence of higher-frequency (tidal, near-inertial) fluid dynamics. *Deep Sea Research Part I: Oceanographic Research Papers*, 90, 125–138.

Van Mooy, B. A., Keil, R. G., & Devol, A. H. (2002). Impact of suboxia on sinking particulate organic carbon: Enhanced carbon flux and preferential degradation of amino acids via denitrification. *Geochimica et Cosmochimica Acta*, 66(3), 457–465.

Vargas, C. A., Cantarero, S. I., Sepúlveda, J., Galán, A., De Pol-Holz, R., Walker, B., et al. (2021). A source of isotopically light organic carbon in a low-pH anoxic marine zone. *Nature Communications*, 12(1), 1–11.

Wakeham, S. G., Lee, C., Farrington, J. W., & Gagosian, R. B. (1984). Biogeochemistry of particulate organic matter in the oceans: results from sediment trap experiments. *Deep Sea Research Part A. Oceanographic Research Papers*, 31(5), 509–528.

Warnes, G., Bolker, B., Bonebakker, L., Gentleman, R., Liaw, W., Lumley, T., & others. (2015). *gplots: various R programming tools for plotting data*. R package version 2.16.0. 2015.

Weber, T., & Bianchi, D. (2020). Efficient particle transfer to depth in oxygen minimum zones of the Pacific and Indian Oceans. *Frontiers in Earth Science*, 8, 376.

Wenzhöfer, F. (2019). The Expedition SO261 of the Research Vessel SONNE to the Atacama Trench in the Pacific Ocean in 2018. *Berichte Zur Polar-Und Meeresforschung= Reports on Polar and Marine Research*, 729.

Wenzhöfer, F., Oguri, K., Middelboe, M., Turnewitsch, R., Toyofuku, T., Kitazato, H., & Glud, R. N. (2016). Benthic carbon mineralization in hadal trenches: Assessment by in situ O₂ microprofile measurements. *Deep Sea Research Part I: Oceanographic Research Papers*, 116, 276–286.

Williams, J. R., & Giering, S. L. C. (2022). In situ particle measurements deemphasize the role of size in governing the sinking velocity of marine particles. *Geophysical Research Letters*, 49, e2022GL099563. <https://doi.org/10.1029/2022GL099563>

Williams, P. M., & Gordon, L. I. (1970). Carbon-13: carbon-12 ratios in dissolved and particulate organic matter in the sea. *Deep Sea Research and Oceanographic Abstracts*, 17(1), 19–27. [https://doi.org/10.1016/0011-7471\(70\)90085-9](https://doi.org/10.1016/0011-7471(70)90085-9)

Xiao, W., Xu, Y., Haghypour, N., Montluçon, D. B., Pan, B., Jia, Z., et al. (2020). Efficient sequestration of terrigenous organic carbon in the New Britain Trench. *Chemical Geology*, 533, 119446.

Xu, Y., Ge, H., & Fang, J. (2018). Biogeochemistry of hadal trenches: Recent developments and future perspectives. *Deep Sea Research Part II: Topical Studies in Oceanography*, 155, 19–26.

Xu, Y., Li, X., Luo, M., Xiao, W., Fang, J., Rashid, H., et al. (2021). Distribution, Source, and Burial of Sedimentary Organic Carbon in Kermadec and Atacama Trenches. *Journal of Geophysical Research: Biogeosciences*, 126(5), e2020JG006189.

Yuras, G., Ulloa, O., & Hormazábal, S. (2005). On the annual cycle of coastal and open ocean satellite chlorophyll off Chile (18–40 S). *Geophysical Research Letters*, 32(23).

Zabel, M., Glud, R. N., Sanei, H., Elvert, M., Pape, T., Chuang, P.-C., et al. (2022). High carbon mineralization rates in subseafloor hadal sediments—Result of frequent mass wasting. *Geochemistry, Geophysics, Geosystems*, 23(9), e2022GC010502.

Particulate organic matter transfer to the Atacama trench: Insights from bulk and stable isotope analyses

Edgart Flores *et al.*

Tabla 5. Parameters calculated for four models used (see Figure 2) that predict the POC fluxes to Atacama Trench. The goodness of fit between the theoretical fluxes and the data collected in situ were added in the text.

Theoretical calculations POC flux ($\text{mgC m}^{-2} \text{d}^{-1}$)								
Modeled POC flux	^I Ez (m)	^{II} C	z (m)	^{III} b	^{IV} l	^V α	^{VI} S ₂	Reference
Martin curve	83.4	123.48	8000	-0.36/-0.78/-1.33				Martin et al., 1987
Exponential curve	83.4	123.48	8000		0.0053			Banse, 1990
Depth-attenuation rational model	83.4	123.48	8000			0.212		Suess, 1980
Double exponential curve	83.4	123.48	8000		0.0053		0.0443	Lutz et al., 2002

^IThe depth euphotic zone (Ez) from ocean stations (28-100 nm) off Antofagasta (23-24° S) was averaged (see Pizarro et al., 2002); Ez = 83.4 m

^{II}The POC flux at Ez was interpolated from 65 m and 100 m depths measured in January 1997 off Antofagasta (23-24° S) (see Table 9 in González et al., 1998): 123.48 mg C m⁻² d⁻¹

^{III}The attenuation coefficients ("b") used were those suggested for the Atacama trench (Fernandez-Urruzula, et al., 2021)

^{IV}l := (D/w), D: is the instantaneous rate of decay and w: is the sinking rate (see Lutz et al., 2002; Banse et al., 1990)

^V α := Aw/k, where A is a constant dependent on initial conditions (see supplementary material from Cael et al., 2018)

^{VI}S₂: Value from equatorial Pacific (regional average) (see Table 6b. in Lutz et al., 2002)

Tabla 6. Linear correlations between theoretical POC fluxes and sediment trap-derived measurements.

Linear correlations	r ²	r ² adjusted	p-value	n
Pavia et al., 2019 - Double exponential curve (Lutz et al., 2002)	0.69	0.68222	0.001	34
Pavia et al., 2019 - Depth-attenuation rational model (Suess et al., 1980)	0.4308	0.413	0.001	34
González et al., 2002 and Hebbeln et al., 2000 data- Martin Curve (b=0.78)				3

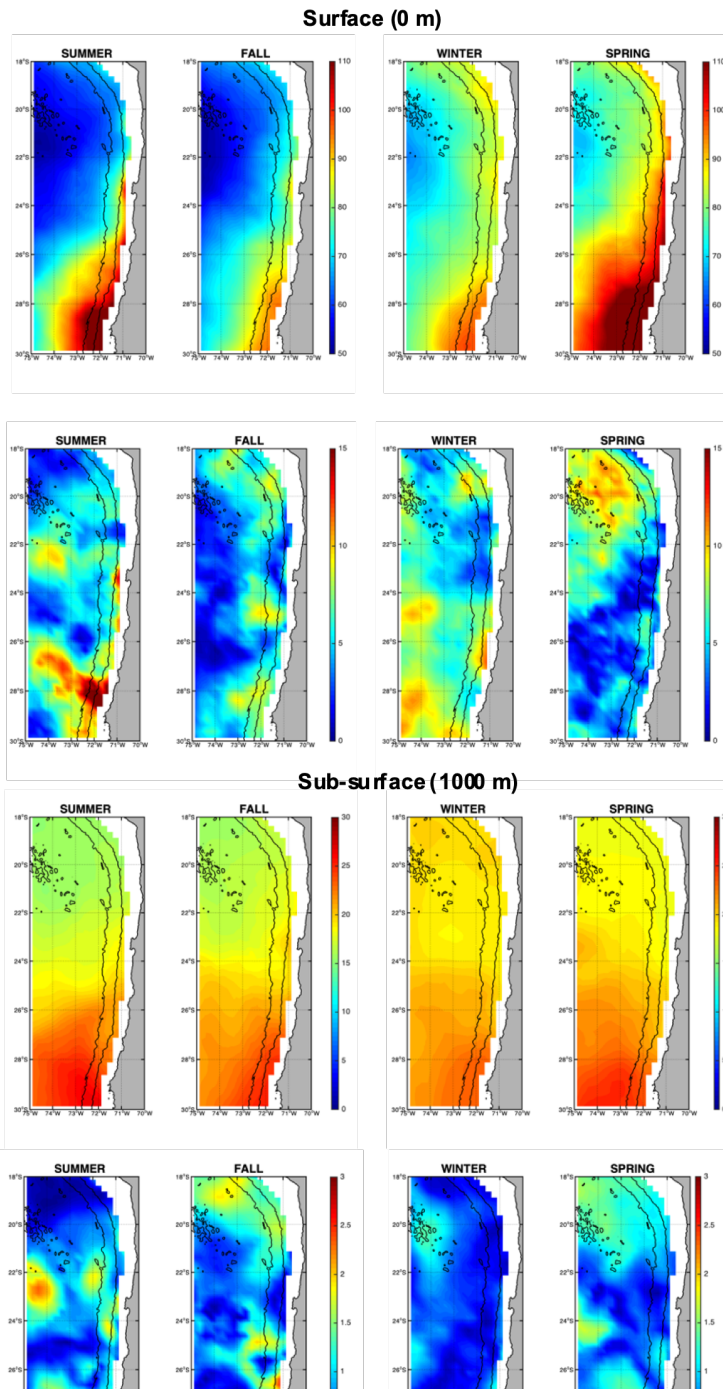


Figure 21. Spatio-temporal variability of POCsat over the Atacama Trench region (18°S-30°S) calculated for seasonal mean from 1998 to 2022 in surface (0 m) and subsurface (1000 m) waters, and their respective \pm standard deviations (STD).

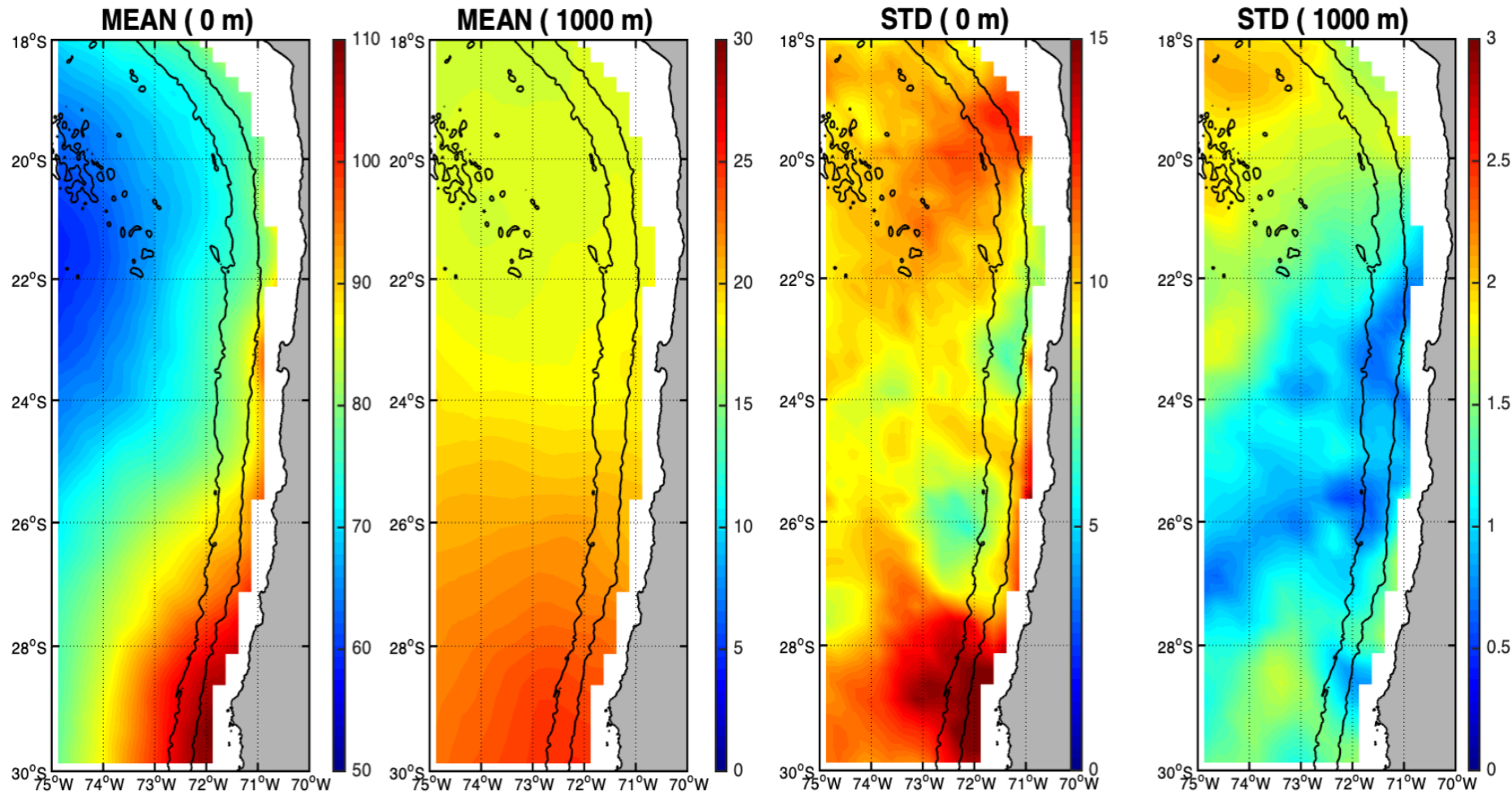


Figura 22. Spatio-temporal variability of POCsat over the Atacama Trench region (18°S-30°S) calculated for annual mean from 1998 to 2022 in surface (0 m) and subsurface (1000 m) waters, and their respective \pm standard deviations (STD).

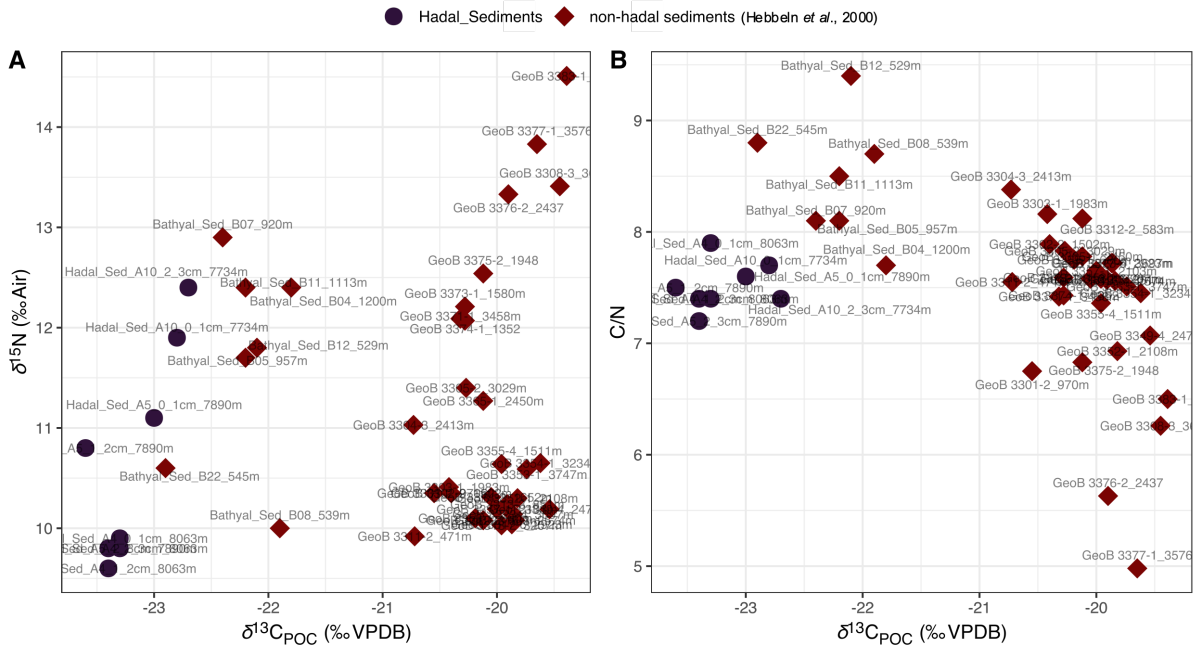


Figure 23. Biplot showing in panel A, the $\delta^{15}\text{N}_{\text{PON}}$ and $\delta^{13}\text{C}_{\text{POC}}$, and panel B the C/N ratio and $\delta^{13}\text{C}_{\text{POC}}$ to compare our hadal versus non-hadal sediment samples published for the Atacama region (Hebbeln et al., 2000).

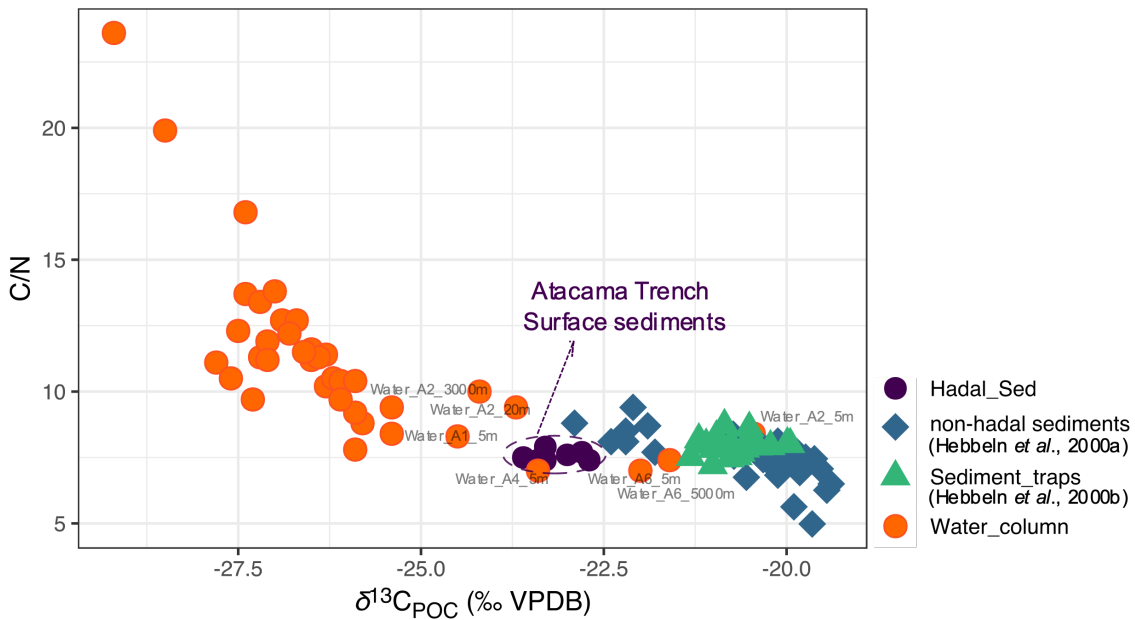


Figure 24. Biplot showing the C/N ratio and $\delta^{13}\text{C}_{\text{POC}}$ for all data in our study reflect the presence of a particular signature in hadal sediments of the Atacama Trench.

5. DISCUSIÓN

5.1 Lípidos intactos polares autóctonos y alóctonos en la Fosa de Atacama

La distribución de IPLs en los sedimentos batiales y hadales exhibe un alto grado de similitud, como lo demuestra el análisis jerárquico (cluster 1 en Fig. 8a manuscrito 1), el NMDS (Fig. 8b manuscrito 1), y el análisis SIMPER (cluster 1 en Tabla S1, manuscrito 1). Los sedimentos superficiales de aguas profundas mostraron un débil agrupamiento con los IPLs reportados en la columna de agua suprayacente por Cantarero et al. (2020) (Fig. 9^a, manuscrito 1). Adicionalmente, las muestras de la columna de agua exhiben un mayor grado de separación que los sedimentos (ANOSIM, $R = 0.78$; $P < 0.01$; Fig. 8b manuscrito 1) y están ampliamente agrupadas por ambientes geoquímicos (Cantarero et al., 2020). La baja abundancia de IPLs característicos de organismos que habitan el máximo de clorofila en sedimentos de aguas profundas de la Fosa de Atacama (< 0.005 % del total de IPLs; Fig. S3) sugiere una mínima exportación de compuestos orgánicos lábiles desde el océano superior. Este resultado implica una rápida degradación de IPL durante el hundimiento en la columna de agua, lo que es consistente con las tasas de degradación experimentales (Westrich y Berner, 1984; Logemann et al., 2011) y las tasas de hundimiento de primer orden de POM. De hecho, mediante el uso de las constantes de velocidad de degradación cinética (k') calculadas experimentalmente de POM unidas a ésteres por Logemann et al. (2011) y la tasa de hundimiento de partículas desde aguas superficiales hasta 4,000 m ($20\text{-}100$ m d^{-1} ; Billett et al., 1983; Danovaro et al., 2014), calculamos que $\sim 86\text{-}98$ % de los IPL procedentes de aguas superficiales deberían degradarse en el momento en que las partículas alcanzan profundidades de $\sim 8,000$ m. Estos resultados también concuerdan con estudios que indican elevadas tasas de consumo de oxígeno bentónico derivadas de la intensa respiración microbiana de la MO en hundimiento que llega al sedimento (Glud et al., 2013; Wenzhöfer et al., 2016). Por lo tanto, los de IPLs más abundantes en los sedimentos hadales parece representar predominantemente la producción microbiana *in situ*, mientras que la comunidad microbiana de aguas profundas tanto en sedimentos batiales como hadales es similar a pesar de su zonación batimétrica ($\sim 1,000\text{-}8,000$ m). Alternativamente, no podemos descartar la posibilidad de una nueva producción de IPLs, en particular a partir de bacterias

heterótrofas y quimioautótrofas en micro-nichos de partículas que se hundan y llegan a las profundidades marinas y/o del transporte descendente y lateral de sedimentos.

Las fosas marinas reciben carbono orgánico de diversas fuentes y mecanismos de transporte. Estos incluyen cañones y sistemas fluviales que canalizan la MO desde tierra hasta las regiones costeras, el transporte eólico, la productividad de las aguas superficiales y la producción *in situ*, por nombrar algunos (Wenzhöfer et al., 2016; Tarn et al., 2016; Luo et al., 2017; Xu et al., 2018; Guan et al., 2019; Xu et al., 2021). Los eventos de flujo de carbono pueden aumentar la entrega de carbono particulado de las aguas superficiales al fondo marino (Poff et al., 2021), mientras que la descarga fluvial y el transporte eólico pueden dar lugar a un aumento del carbono terrestre (Xu et al., 2021). También se sabe que los fenómenos de transporte masivo de sedimentos (por ejemplo durante los movimientos sísmicos) crean condiciones deposicionales dinámicas y una fuerte heterogeneidad espacial en la distribución de MO en fosas marinas (Schauberger et al., 2021; Xu et al., 2021). Mientras que el carbono orgánico marino parece dominar los sedimentos en las fosas de Japón (Schwestermann et al., 2021), Massau (Xu et al., 2020a) y Nueva Bretaña (Xu et al., 2020b), las fosas de Atacama y Kermadec, por otro lado, están dominadas por el carbono orgánico terrígeno. Dado que nuestro estudio sólo se centra en el componente más lábil del conjunto total de lípidos, rastrea predominantemente la MO lábil y no las fracciones recalcitrantes del conjunto de lípidos. Esto último merece una investigación subsecuente.

En regiones como la Fosa de Japón, el transporte de sedimentos pendiente abajo se ha relacionado con la removilización provocada por terremotos (Bao et al., 2018; Schwestermann et al., 2021). Mientras que carecemos de datos sedimentológicos/geoquímicos para discriminar si los 3 cm superiores de nuestras estaciones hadales representan flujos de escombros, turbiditas o eventos de pérdida masiva, un trabajo en curso en la Fosa de Atacama indica la deposición heterogénea de sedimentos a lo largo de la zona hadal (Matthias Zabel, comunicación personal, 2022). Por tanto, el papel del transporte ladera abajo como mecanismo para explicar la alta similitud estadística entre los sedimentos batiales y hadales está aún por probar.

5.2 IPLs característicos de los sedimentos hadales y batiales

Los IPLs que más contribuyen a la disimilitud entre los clusters jerárquicos que contiene muestras de los sedimentos hadales y batiales (cluster 1 de la Fig. 8) y la columna de agua (cluster 2, 3, 4, y 5 de la Fig. 8) están representados en la Fig. 9 (manuscrito 1). Los IPLs más característicos de los sedimentos hadales y batiales son DGCC-42:6, DGCC-27:0, DGCC-26:0, PC-DAG-35:0, PC-DAG-30:1, PC-DAG-30:2, PC-DAG-33:2, PC-DAG-32:1, PC-DAG-29:2, PE-DAG-32:1, PE-DAG-32:2, PE-DAG-33:1, PG-DAG-36:2, y DGDG-34:2, que proponemos como marcadores potenciales para estos ambientes. Aunque los DGCC se han relacionado principalmente con membranas de algas (Kato et al., 1994; Van Mooy et al., 2009), son componentes menores de la columna de agua en esta zona, lo que sugiere la existencia de una fuente alternativa. Además de los DGCCs, los otros dos lípidos de la clase betaína, DGTA y DGTS, mostraron cinco IPLs que estaban casi exclusivamente presentes en las muestras de sedimento (DGTA-34:1, DGTA-32:1, DGTA-34:2, DGTS-34:0, y DGTS-32:1; ver Fig. 11 manuscrito 1). Observamos que casi todos los fosfolípidos PC de nuestro estudio no han sido, hasta donde sabemos, descritos previamente en la literatura, lo que refuerza su uso como marcadores de la producción sedimentaria *in situ* de las zonas bathyal y hadal.

La presencia de unos pocos MGDGs y SQDGs en sedimentos hadales y batiales (~ 7 % del total de IPL) indica que al menos parte de la MO lábil podría derivar de la columna de agua poco profunda. Sin embargo, los IPLs más abundantes en nuestras muestras de sedimento, DGCC-42:6, PC-DAG-35:0, PE-DAG-32:1, y PG-DAG-36:2 (19,8 % del total de IPLs; Fig. S16 manuscrito 1), están casi completamente ausentes en la columna de agua suprayacente (Fig. 9, manuscrito 1). Esto refuerza la idea de que estos IPLs probablemente se originan de la producción microbiana *in situ* en los sedimentos. El único IPL más abundante en los sedimentos, DGCC-42:6, no estaba presente en el cluster 1, que sólo contiene sedimentos hadales (Figs. 2 y 3). En cambio, este compuesto es prominente en los grupos 3, 4 y 5, que contienen muestras hadales y batiales. Así, DGCC-42:6 y PC-DAG-35:0, que tiene la menor abundancia relativa en el cluster con sólo sedimentos hadales, podrían ser indicadores de transporte pendiente abajo desde las regiones batiales a las hadales.

Reconocemos que la variabilidad temporal en la producción de IPL en la columna de agua y los sedimentos y la falta de datos sobre la comunidad microbiana endémica hadal, en gran parte no caracterizada, podrían complicar algunas de las asociaciones filogenéticas y de origen de los IPL y justifican una investigación más profunda. A pesar de ello, nuestro estudio representa un paso hacia adelante en la caracterización de las fuentes lábiles de MO que sustentan los ecosistemas hadales.

5.3 ¿Revelan los IPLs una adaptación homeoviscosa al océano profundo?

Factores ambientales como el pH, la conductividad, la temperatura y la presión influyen en la permeabilidad y fluidez de las membranas celulares (Shaw, 1974; Macdonald, 1984; DeLong y Yayanos, 1985; Somero, 1992; Komatsu y Chong, 1998; Van Mooy et al., 2009; Carini et al., 2015; Sebastián et al., 2016; Siliakus et al., 2017; Boyer et al., 2020; Allen et al., 1999). Así, los organismos se adaptan a los cambios en los factores ambientales para mantener la homeostasis fisiológica, es decir la capacidad de mantener una condición estable frente a los cambios de su entorno, bajo condiciones de alta presión y bajas temperaturas puede alterar su composición de ácidos grasos (DeLong y Yayanos, 1985; Fang et al., 2000; Nichols et al., 2004; Siliakus et al., 2017). Por ejemplo, los efectos fisiológicos combinados de alta presión hidrostática y baja temperatura sobre las membranas procariotas en cultivos de laboratorio conducen a la producción de lípidos insaturados (DeLong y Yayanos 1985; Fang et al., 2000; Nichols et al., 2004; Zheng et al., 2020). Sin embargo, se han realizado pocos estudios utilizando técnicas independientes del cultivo en busca de posibles mecanismos de adaptación en organismos que habitan en las profundidades oceánicas (p. ej., Zhong et al., 2020). Intentamos comprender si la composición química de los ácidos grasos del núcleo dentro de las diferentes clases de IPL (es decir, la longitud del carbono y el grado de insaturación) refleja los efectos combinados de la baja temperatura y la alta presión típicas de los entornos hadales. Mostramos que los PGs son abundantes en los sedimentos hadales de la Fosa de Atacama (Fig. S4, ver manuscrito 1). Las cepas bacterianas aisladas de los sedimentos de la Fosa de las Marianas contienen PG como la clase más abundante de fosfolípidos (Fang et al., 2000), lo que estos autores presumieron que podría representar una respuesta fisiológica a la alta presión y baja temperatura. Esto ha sido confirmado por estudios posteriores (Winter et al., 2009; Periasamy et al., 2009; Jebbar et al., 2015, Allemann et al., 2021). El clúster 1 en el análisis boxplot (Fig.

4) probablemente contiene las clases de IPL más características de la zona hadal. En general, los fosfolípidos en este cluster exhibieron cadenas de ácidos grasos monoinsaturados y saturados en comparación con otros ambientes (Fig. 4a, b, manuscrito 1). Además, observamos un aumento en la proporción de ácidos grasos totales insaturados y saturados en los sedimentos profundos en comparación con la columna de agua (Fig. 5), lo que podría reflejar adaptaciones fisiológicas de sus productores biológicos. Estos resultados concuerdan con estudios que indican la biosíntesis e incorporación de ácidos grasos poliinsaturados en las membranas fosfolipídicas de bacterias piezófilas (DeLong y Yayanos, 1985; Baird et al., 1985; Yano et al., 1998; Winter, 2002; Mangelsdorf et al., 2005; Winter y Jeworrek, 2009; Allemann et al., 2021). Así, las características químicas (longitud del C y grado de insaturación) de los IPLs más abundantes en los sedimentos de la Fosa de Atacama sugieren una adaptación homeoviscosa a este tipo de ambiente por parte de sus organismos fuente, además de indicar potencialmente la ocurrencia de compuestos exclusivos de la comunidad endógena.

5.4 Procedencia de la materia orgánica en los sedimentos superficiales de la Fosa de Atacama mediante isótopos estables

Las señales isotópicas estables de carbono y nitrógeno del fitoplancton, que constituye la mayor parte de la materia orgánica (>80% de la OC) producida en la zona eufótica (Lee et al., 2004), están influidas por: a) la composición isotópica del carbono y el nitrógeno de origen, b) el fraccionamiento isotópico durante la fijación del carbono y la asimilación de nutrientes, y c) el fraccionamiento isotópico durante los procesos catabólicos (Goericke y Fry, 1994). Así, varios procesos pueden afectar a la composición isotópica del carbono y el nitrógeno en las aguas superficiales y, en consecuencia, a la firma isotópica de la materia orgánica en masa. Entre ellos se incluyen el afloramiento de aguas subsuperficiales, el aporte fluvial, las interacciones tróficas y las sucesiones ecológicas (Peterson & Fry, 1987, y sus referencias), todos ellos dinámicos en la zona eufótica. Nuestros resultados indican grandes variaciones en $\delta^{13}\text{C}_{\text{POC}}$ (-28,5 ‰ a -20,5 ‰, media -25,30 ‰ $\pm 2,36$) y $\delta^{15}\text{N}_{\text{PON}}$ (7,7 a 11,2 ‰, media 9,64 ‰ $\pm 1,18$) en la zona epipelágica (Figs. 2A,B y 3). Estos valores están dentro del rango de los reportados previamente en POM superficial en la región de Atacama (Barrios-Guzmán et al., 2019), y consistentes con un origen predominantemente planctónico marino (Williams & Gordon, 1990). Anticipamos que la POM de la ODZ influye en las zonas epipelágica inferior y mesopelágica

superior, donde la POM está isotópicamente agotada en ^{13}C y ^{15}N en comparación con profundidades menores (Figs 2A,B y 3A). Esta depleción isotópica podría ser el resultado de la fijación autótrofa oscura de carbono por quimiolitautótrofos en las aguas de la ODZ (Callbeck et al., 2018, Ruiz-Fernández et al., 2020; Vargas et al., 2021), además de la denitrificación generalizada a lo largo del margen costero de la ETSP (De Pol-Holz et al., 2009).

La zona batipelágica presenta valores de $\delta^{13}\text{C}_{\text{POC}}$ entre -27,4 ‰ y -24,2 ‰ (media -26,31 ‰ $\pm 0,94$) y de $\delta^{15}\text{N}_{\text{PON}}$ entre 6,6 y 8,9 ‰ (media 7,85 ‰ $\pm 0,7$), mientras que la zona abisopelágica muestra valores similares para $\delta^{13}\text{C}_{\text{POC}}$ entre -27,1 ‰ y -25,4 ‰ (media -26,06 ‰ $\pm 0,73$) y para $\delta^{15}\text{N}_{\text{PON}}$ entre 6,1 y 7,9 ‰ (media 7,3 ‰ $\pm 0,81$) (Figs. 2A,B y 3A). Sin embargo, en comparación con el resto de estaciones de la zona abisopelágica, detectamos POC enriquecido en ^{13}C a 5,000 m en la estación A6 (-21,6 ‰). Este enriquecimiento en ^{13}C está asociado a una disminución de la relación C/N (7,4) (Fig. 2A,C) y a un ligero aumento de la concentración de POC ($\sim 22 \text{ mg C m}^{-3}$) (Fig. 7B), pero sin cambios isotópicos en $\delta^{15}\text{N}_{\text{PON}}$ (Fig. 2B). Mientras que este enriquecimiento en ^{13}C a 5,000 m en la estación A6 es atípico para aguas profundas, está en el rango de valores observados en la zona epipelágica. Dado que se considera que el $\delta^{13}\text{C}$ de la POM es relativamente uniforme en aguas profundas (Menzel & Ryther, 1968; Follett et al., 2014), es poco probable que sea la causa del enriquecimiento en ^{13}C de la POM *in situ*. Por lo tanto, es posible que la POM a esta profundidad pueda estar influenciada por una fuente epipelágica, apoyada por el mecanismo de la partícula de hundimiento rápido sugerido por Fernández-Urruzola et al., (2021) para esta región. Aunque no podemos descartar otros mecanismos como la resuspensión de partículas a través del transporte de sedimentos ladera abajo o capas nefeloides profundas.

Por su parte, la zona hadalpelágica muestra una baja dispersión de los valores de $\delta^{13}\text{C}_{\text{POC}}$ (de -27,3 ‰ a -26,4 ‰, media -26,7 ‰ $\pm 0,38$), y una alta dispersión en $\delta^{15}\text{N}_{\text{PON}}$ (de 5,4 a 9,1 ‰, media 7,87 ‰ $\pm 1,69$) (zona sombreada en Figs. 2A,B; y 5A,B). En esta región profunda de la fosa de Atacama, especulamos que la resuspensión de sedimentos puede potenciar la liberación de materia orgánica acumulada en sedimentos subóxicos/anóxicos al agua de mar óxica. Así, la resuspensión probablemente influye tanto en las señales isotópicas de carbono como de nitrógeno y es probable que esté asociada con el ligero aumento de POC (Fig. 7B). Sin embargo,

la falta de una mayor resolución espacial y temporal hadalpelágica nos impide contrastar estas señales isotópicas en profundidad.

Los sedimentos superficiales del hadal muestran una baja dispersión de $\delta^{13}\text{C}_{\text{POC}}$ (de -23.6 ‰ a -22.7 ‰, media -23.18‰ \pm 0.31) y relaciones C/N (de 7.2 a 7.9, media 7.5 \pm 0.21), y una alta dispersión en $\delta^{15}\text{N}_{\text{PON}}$ (de: 9.6 ‰ a 12.4 ‰, media 10.66 ‰ \pm 1.06) (Fig. 5A, B, C). Además, los sedimentos superficiales batiales muestran una baja dispersión de $\delta^{13}\text{C}_{\text{POC}}$ (de -22,9 ‰ a -21,8 ‰, media -22,21‰ \pm 0,36), y una alta dispersión de los valores de C/N (de 7,7 a 9,4, media 8,4 \pm 0,56) y $\delta^{15}\text{N}_{\text{PON}}$ (de 10 ‰ a 12,9 ‰, media 11,68 ‰ \pm 1,04) (Fig. 5A, B, C). A pesar de los miles de metros que separan los sedimentos hadales de los batiales, éstos presentan pequeñas diferencias entre sus medias ($\delta^{13}\text{C}_{\text{POC}} \sim -0,97$ ‰; $\delta^{15}\text{N}_{\text{PON}} 0,9$ ‰; y relación C/N 1,02). Esta similitud podría deberse a, a) un origen similar de la POM; b) transporte de sedimentos pendiente abajo desde la zona batial hacia la zona hadal; y c) organismos que implican un fraccionamiento isotópico similar. Cabe señalar que los mecanismos que subyacen a la diagénesis postdeposicional podrían explicar las ligeras diferencias isotópicas entre el sedimento batial y el hadal (Gearing et al., 1984, Fenton & Ritz, 1988, Meyers, 1994; Liu et al., 2022). Además, las señales elementales e isotópicas de los sedimentos superficiales recogidos previamente en zonas por encima del reino hadal (Hebbeln et al., 2000) muestran diferencias de $\delta^{13}\text{C}_{\text{POC}} \sim 3$ ‰ en comparación con el sedimento bathyal y hadal de este estudio (ver Fig. S3, manuscrito 2). Estudios previos en el reino hadal sugieren que la alta presión y la baja temperatura características de este entorno promueven un mayor fraccionamiento isotópico del carbono en bacterias piezófilas heterótrofas en comparación con las bacterias heterótrofas de sedimentos superficiales menos profundos (Fang et al., 2006, Xu et al., 2018). Estos procesos combinados podrían explicar en parte por qué el sedimento hadal es isotópicamente más ligero en $\delta^{13}\text{C}$ y $\delta^{15}\text{N}$ que los sedimentos batiales. Sin embargo, otros modos de nutrición (p. ej., quimioorganótrofos y/o quimiolitioautótrofos) que pueden llevarse a cabo para el fraccionamiento isotópico en estos ambientes son menos conocidos.

Un estudio geoquímico reciente de los sedimentos de la fosa de las Marianas concluyó que las algas marinas son la principal fuente de MO en este sistema, como se refleja en los valores de C/N y $\delta^{13}\text{C}$ (Luo et al., 2017). Este resultado es coherente con estudios anteriores en

las fosas de Japón y Atacama (Nakatsuka et al., 1997; Danovaro et al., 2003). Sin embargo, los sedimentos profundamente enterrados de la Fosa de Atacama han revelado fases de sedimentación pelágica lenta en el pasado que se alternan con rápidos eventos de pérdida de masa, que alimentan el recambio de carbono microbiano a tasas notablemente altas (Glud et al., 2013; Zabel et al., 2022). Por lo tanto, esperamos que el reciclaje por bacterias piezofílicas en la región hadal de materia orgánica originada a partir de la producción primaria en el océano superficial y/o el transporte pendiente abajo altere la composición isotópica del carbono y el nitrógeno sedimentarios (Xu et al., 2018 y referencias en el mismo). De hecho, la relación de C/N y $\delta^{13}\text{C}$ para todos los datos de nuestro estudio refleja la presencia de una firma distinguible en los sedimentos hadales de la Fosa de Atacama que podría representar una mezcla de fuentes pelágicas, transporte descendente y actividad microbiana sedimentaria *in situ* (ver Fig. S4).

5.5 ¿Cuál es la contribución relativa de las fuentes autóctonas a los sedimentos de la Fosa de Atacama?

Se ha descrito de que las fosas marinas reciben diversas fuentes de materia orgánica (Glud et al., 2013; Luo et al., 2017; Xu et al., 2018). En general, la heterogeneidad intra e inter fosa en la composición de la materia orgánica sedimentaria, junto con las tasas de remineralización hadal bentónica, se han atribuido a diferencias en la productividad oceánica superficial regional (Jamieson, 2015; Wenzhöfer et al., 2016; Glud et al., 2021). Las partículas que se hunden, como mecanismos de transporte, son importantes para llevar el carbono a las profundidades oceánicas, donde puede almacenarse y eliminarse eficazmente del ciclo moderno del carbono (Williams y Giering, 2022). De hecho, se ha observado material fitodetrital fresco procedente de aguas superficiales en regiones hadales (Danovaro et al., 2003; Oguri et al., 2013; Guo et al., 2018). Consistentemente, dado que la Fosa de Atacama subyace a las aguas altamente productivas del HCS, es un sistema hadal más propenso a recibir partículas sintetizadas en aguas superficiales. Esto podría explicar, por ejemplo, por qué los sedimentos de la Fosa de Atacama contienen más carbono orgánico en comparación con las fosas situadas en el océano Pacífico occidental, que albergan aguas superficiales suprayacentes más oligotróficas y menos productivas (p. ej., Fosa de Kermadec, Yunping Xu et al., 2021; Fosa de las Marianas, Li et al., 2020; Fosa de Japón, Oguri et al., 2013). Sin embargo, un estudio reciente sobre perfiles sedimentarios de ^{210}Pb y TOC en la Fosa de Atacama no demostró una relación aparente entre

la productividad primaria neta en la superficie del océano y la tasa de acumulación de carbono en masa (Oguri et al., 2022). Estas observaciones sugieren que la dinámica deposicional y la batimetría local son más importantes que la cantidad de MO producida en la superficie. Sin embargo, en la Fosa de Atacama también se ha demostrado una elevada remineralización debida a una intensa actividad heterótrofa (Glud et al., 2013, Glud et al., 2021). Por lo tanto, aunque estudios previos han sugerido una importante contribución de MO procedente de material acumulado en sedimentos de la plataforma continental, a la zona bentónica hadal (Flores et al., 2022; Oguri et al., 2022; Zabel et al., 2022), la contribución de MO procedente de la zona eufótica a la zona hadalpelágica podría ser mayor de lo esperado.

Evaluamos los cambios en la productividad primaria superficial a través de los datos disponibles de POCsat y modelamos los flujos de POC en la Fosa de Atacama. POCsat muestra altas concentraciones y un alto grado de heterogeneidad espacial en las aguas superficiales sobre la región de la Fosa de Atacama (Fig. 6a, manuscrito 2). Esta tendencia está modulada por las aguas mar adentro, donde se produce el máximo de clorofila en invierno (Yuras et al., 2005) y está relacionada con la propagación de remolinos de mesoescala que expanden el área de alta concentración de clorofila más allá del centro de afloramiento costero (Correa-Ramírez et al., 2007). Observamos patrones similares de aumento estacional de POCsat en otoño e invierno en el área de estudio (Fig. S1, manuscrito 2). Además, los datos de POCsat por debajo de la zona epipelágica muestran una heterogeneidad espacial más atenuada, que se mantiene hasta el límite inferior de la zona mesopelágica (~16-27% POC; Fig. 6C). Nuestras mediciones discretas a la misma profundidad (~16.3% POC; Fig. 7B) confirman y validan los resultados del POCsat. Porcentajes similares de POC en la zona mesopelágica han sido reportados en otros sistemas de alta productividad, lo que se ha atribuido a la presencia de aguas ODZ que podrían reducir la tasa de descomposición de POC y aumentar su hundimiento en aguas más profundas (Weber & Bianchi, 2020; Ma et al., 2021).

Las mediciones discretas de la composición de la materia orgánica desde las zonas batipelágicas hasta las hadalpelágicas son escasas. Dado que las concentraciones de POC en las zonas batipelágica y abisopelágica superior (es decir, 1.000-5.000 m; Fig. 7B) son bajas y estables, especulamos que esto podría reflejar una capa profunda bien mezclada, como se sugirió

anteriormente en la fosa de Izu-Ogasawara (Kawagucci et al., 2018). Sin embargo, dado que observamos un ligero aumento de POC en la zona hadalpelágica en las estaciones A2 y A4 (ver Fig. 7B, manuscrito 2), debemos invocar un aporte adicional de POC en esta región. Las fuentes potenciales incluyen la acumulación de POC debido al sedimento resuspendido o una contribución lateral a través de capas nefeloides desde la pendiente menos profunda (Nakatsuka et al., 1997; Xu et al., 2018; Gardner et al., 2022). En estudios realizados en mar abierto y en el Golfo de México se ha observado que las zonas de elevada energía cinética superficial de los remolinos suelen estar relacionadas con zonas en las que las capas nefeloides son comunes (Gardner et al., 2022). Sin embargo, se desconoce si la capa nefeloide puede alcanzar profundidades hadales (6,000-11,000 m). Para investigar si la producción de POC en las zonas epipelágica y mesopelágica afecta a su comportamiento a mayores profundidades, comparamos los flujos verticales de POC calculados a partir de modelos teóricos (véanse los parámetros del modelo en la tabla S1) con las mediciones publicadas de flujo de POC *in situ* derivadas de trampas de sedimentos en la región (Fig. 7a, ver manuscrito 2). Los cálculos teóricos que mejor se ajustan a los datos de trampas de sedimentos profundos sugieren un bajo flujo de POC ($3.96 \text{ mg C m}^{-2} \text{ d}^{-1}$, $\sim 3.3\%$, ver Fig. 7a, ver manuscrito 2) desde la zona eufótica a los sedimentos superficiales de la Fosa de Atacama. Dadas las múltiples fuentes posibles de POC al océano profundo, aplicamos un modelo de contribución porcentual multifuente de Stock et al. (2018) a nuestro conjunto de datos isotópicos. Cuando sólo se utilizan fuentes de MO pelágicas, observamos que la zona epipelágica es la fuente dominante de POM a los sedimentos superficiales hadales (Figs. 8A, B). Sin embargo, cuando incluimos los sedimentos batiales como fuente adicional, la contribución a los sedimentos hadales de las regiones combinadas de la columna de agua es $<25\%$ (Figs. 8C,D, ver manuscrito 2). Por lo tanto, estos resultados indican que la MO puede alcanzar rápidamente la zona hadal, probablemente a través de una combinación de partículas de hundimiento rápido y transporte descendente y/o lateral, como se ha sugerido en estudios previos para la Fosa de Atacama (Fernandez-Urruzola et al., 2021; Zabel et al., 2022; Oguri et al., 2022). Especulamos que, además de los procesos descritos anteriormente, la pendiente del relieve batimétrico ($\alpha = 6,5^\circ$) en la fosa de Atacama (calculada a partir de GEBCO 2020 Grid; Kioka & Strasser, 2021), puede ser un factor adicional que contribuya a la materia orgánica sedimentaria a través del transporte pendiente abajo en esta región.

No obstante, reconocemos que no podemos inferir procesos biogeoquímicos o microbianos en la zona hadalpelágica simplemente extrapolando los flujos de POC de las aguas superficiales mediante modelos isotópicos y sin tener en cuenta otras fuentes alóctonas así como fuentes autóctonas. En consecuencia, debemos profundizar en la complejidad de los procesos que influyen en los modelos de flujo de POC, como la velocidad de hundimiento (Williams & Giering, 2022) y el efecto "embudo de fuentes" propuesto por Sigel et al. (2008) y ampliamente discutido por Fernández-Urruzola et al. (2021). Futuras mediciones de los flujos de las trampas de sedimentos del fondo de la fosa de Atacama nos permitirían cuantificar la contribución y composición de las diferentes fuentes de MO, y comprender su variabilidad temporal.

5.6 Implicaciones

En esta sección, nos proponemos detallar las implicaciones de nuestros hallazgos sobre la diversidad lipídica y potenciales adaptaciones para ahondar en la comprensión de la comunidad microbiana en el entorno hadal. En primer lugar, las estructuras de IPL más dominantes unidas a ésteres que se encuentran en los sedimentos batiales y hadales muestran una gran variedad de fosfolípidos con diversos grados de insaturación, la mayoría de ellos aún por describir, que probablemente proceden de fuentes bacterianas y/o eucariotas aún poco caracterizadas. En segundo lugar, los sedimentos hadales presentan estructuras de glicolípidos únicas, que hasta donde sabemos no se han descrito en otros entornos. Sin embargo, estos lípidos están presentes en baja abundancia y representan una pequeña fracción del conjunto total de IPL. En tercer lugar, mediante la integración de nuevos resultados sobre los lípidos de la membrana celular e información biogeoquímicos de fosas marinas que experimenten grados contrastados de productividad del agua superficial y fuentes de materia orgánica, podremos clarificar la relación entre la productividad primaria superficial y la concentración de carbono orgánico en los sedimentos superficiales hadales.

Además, reconocemos la necesidad de profundizar en algunos aspectos clave para ampliar nuestra comprensión de los ecosistemas hadales. En particular, es importante: a) establecer correlaciones biogeoquímicas del entorno con las distribuciones de las clases más abundantes de IPLs; b) investigar las fuentes biológicas específicas de IPLs; c) analizar los isótopos estables de compuestos específicos de IPLs para distinguir los efectos de la presión sobre los procesos de fraccionamiento isotópico; d) dilucidar los cambios estructurales que

evidencien las adaptaciones homeoviscosas en el entorno hadal; y finalmente, e) investigar la variabilidad temporal de los flujos de carbono al océano profundo y cuantificar su contribución. Abordar estos aspectos mencionados anteriormente podría contribuir significativamente a mejorar nuestra comprensión de los ecosistemas hadales.

6. CONCLUSIONES

- Los sedimentos hadales superficiales en la Fosa de Atacama contienen IPLs bacterianos y eucariotas similares a los encontrados en los sedimentos batiales, pero difieren de los hallados en las partículas orgánicas de los primeros 750 metros de la columna de agua, incluyendo la zona deficiente de oxígeno. Además, los isótopos estables analizados en los sedimentos superficiales de la Fosa de Atacama están estrechamente relacionados con los sedimentos batiales, ambos indican la presencia de un reservorio de materia orgánica isotópicamente más pesada en comparación con la columna de agua. Esta evidencia apoya parcialmente la hipótesis 1, ya que la alta similitud entre los sedimentos batiales y hadales, bajo estas dos aproximaciones, podría explicarse por un transporte lateral desde las pendientes menos profundas hacia los sedimentos hadales.
- El modelo de mezcla basado en las señales isotópicas del carbono y nitrógeno en la materia orgánica particulada pelágica y sedimentaria indican que aproximadamente el 75% de la materia orgánica presente en los sedimentos superficiales de la Fosa de Atacama podría provenir de sedimentos batiales. Sin embargo, al excluir la fuente batial en nuestro modelo de mezcla isotópico y utilizar sólo fuentes pelágicas, se observó una mayor contribución de la zona epipelágica. Esto sugiere que la materia orgánica podría distribuirse de manera diferente en la zona hadopelágica y la zona hadobentónica. Estos hallazgos respaldan parcialmente las hipótesis 2 y 3, que sugieren que la zona epipelágica no difiere significativamente de la zona hadalpelágica debido al rápido hundimiento de partículas desde el océano superficial y que la señal isotópica del sedimento hadal de la Fosa de Atacama difiere significativamente de toda la columna de agua debido a que recibe diferentes fuentes de materia orgánica.

7. REFERENCIAS

- Angel, M. V. (1982). Ocean trench conservation. *The Environmentalist*, 2, 1–17.
- Amstutz, A. (1951). Sur l'évolution des structures alpines. *Archives Des Science* , 4, 323–329.
- Argus, D.F., Gordon R.G. & DeMets, C. (2011). Geologically current motion of 56 plates relative to the no-net rotation reference frame. *Geochemistry, Geophysics, Geosystems*, 12(11), Q11001.
- Arts, M.T., Ackman, R.G., Holub, B.J. (2001). "Essential fatty acids" in aquatic ecosystems, a crucial link between diet and human health and evolution. *Can. J. Fish. Aquat. Sci.* 58, 122–137.
- Bergauer, K., Fernandez-Guerra, A., Garcia, A., Sprenger, R., Stepanauskas, R., Pachiadaki, M., Jensen O. & Herndl G. (2017). Organic matter processing by microbial communities throughout the Atlantic water column as revealed by metaproteomics. *PNAS* January 16, 2018 115 (3) E400-E408; first published December 18, 2017.
- Belyaev, G.M. (1989). Deep Sea Ocean Trenches and their Fauna. Nauka, Moscow, 255p (in Russian, translation courtesy of Scripps Institution of Oceanography Library).
- Bühning, S.I., Christiansen, B. (2001). Lipids in selected abyssal benthopelagic animals: links to the epipelagic zone? *Prog. Oceanogr.* 50, 369–382.
- Bligh, E.G., & Dyer, W. J. (1959). A rapid method of total lipid extraction and purification. *Can. J. Biochem. Physiol.* 37(8): 911–917.
- Briones, E., Rice, J. & Ardrón J. (2009). Global Open Oceans and Deep Seabed (GOODS) biogeographic classification. *IOC Tech. Ser.*, p. 84.
- Britton, J.C. & Morton, B. (1994). Marine carrion and scavengers. *Oceanogr. Mar. Biol.: Ann. Rev.* 32, 369–434.
- Chen, S. (2010). The earth dynamic system: the earth rotation vs mantle convection. *Natural Science*, 2, 1333-1340.
- Delong, E.F., Franks D.G. & Alldredge, A.L. (1993) Phylogenetic diversity of aggregate-attached vs free-living marine bacterial assemblages. *Limnol Oceanogr* 38:924–934.
- Danovaro, R., Gambi, C. & Della Croce, N. (2002). Meiofauna hotspot in the Atacama Trench, eastern South Pacific Ocean. *Deep-Sea Res. I* 49, 843–857.
- Danovaro, R., Della Croce, N., Dell'Anno, A. & Pusceddu, A. (2003). A depocenter of organic matter at 7800m depth in SE Pacific Ocean. *Deep-Sea Res. I* 50, 1411–1420.
- Danovaro, R., Snelgrove, P.V. & Tyler, P. (2014). Challenging the paradigms of deep-sea ecology. *Trends Ecol. Evol.* 29 (8), 465–475.

Dávila, Paola M., Díaz, S.H. & Valdés, J. (2014). Obtención de perfiles de biomasa fitoplanctónica en bahía San Jorge (Antofagasta, Chile) a partir de imágenes en color. *Ciencias marinas*, 40(1), 59-73.

Emerson, S. & Hedges, J. (1988). Processes controlling the organic carbon content of open ocean sediments. *Paleoceanography* 3 (5), 621–634’.

Eppley, R.W. & Peterson, B.J. (1979). Particulate organic matter flux and planktonic new production in the deep ocean. *Nature* 282: 677-680.

Ewing, M. & Heezen B.C. (1956). Mid-Atlantic Ridge seismic belt, *Trans. Am. Geophys. Un.*, 37,343.

Fisher, R. L. (1958). DOWNWIND investigation of the Nasca Ridge, p. 20--23 ht Fisher R. L. (Editor), Preliminary report on Expedition DOWNWIND, I G Y General Report Ser., IGY World Data Center A, Washington 2, 58 p.

Fisher, R. L., & Raitt, R. W. (1962). Topography and structure of the Peru-Chile trench: Deep-Sea Research, v. 9, p. 424-443.

Fossing, H., Gallardo, V.A., Jørgensen, B.B., Hüttel, M., Nielsen, L.P., Schulz, H., Canfield, D.E., Foster, S., Glud, R.N., Gundersen, J.K., Ramsing, N.B. Teske, A., Thamdrup, B. & Ulloa, O. (1995). Concentration and transport of nitrate by the mat-forming sulphur bacterium *Thioploca*. *Nature* 374:713-5.

Fujikura, K., Kojima, S., Tamaki, K., Maki, Y., Hunt, J. & Okutani, T. (1999). The deepest chemosynthesis-based community yet discovered from the hadal zone, 7326m deep, in the Japan Trench. *Mar. Ecol. Press Series* 190, 17–26.

Gašparović, B., Penezić, A., Frka, S., Kazazić, S., Lampitt, R.S., Holguin, F. O., Sudasinghe, N. & Schaub T. (2018). Particulate sulfur-containing lipids: Production and cycling from the epipelagic to the abyssopelagic zone. *Deep Sea Res Part I Oceanogr. Res. Pap.*,134 (2018), pp.12-22.

George, R.Y., & Higgins, R.P. (1979). Eutrophic hadal benthic community in the Puerto Rico Trench. *Ambio Special Report* 6, 51–58.

Guan, H.X., Chen, L.Y., Luo M., Liu, L.H., Mao, S.Y., Ge, H.M., Zhang, M., Fang, J.S. & Chen, D.F. (2018). Composition and origin of lipid biomarkers in the surface sediments from the southern Challenger Deep, Mariana Trench. *Geosci Front.* 2019; 10:351–60.

Glud, R.N., Wenzhöfer, F., Middelboe, M., Oguri, K., Turnewitsch, R., Canfield, D.E. & Kitazato, H. (2013). High rates of microbial carbon turnover in sediments in the deepest oceanic trench on Earth. *Nature Geoscience* 6, 284–288.

Handa, N. & H. Tominaga (1969): A detailed analysis of carbohydrates in marine particulate matter. *Mar. Biol.*, 2, 223-235.

Harvey, G.R., Boran, D.A., Chesal, L.A. & Tokar, J.M. (1983). The structure of marine fulvic and humic acids. *Mar. Chem.*, 12: 119-132.

Hedges, J.I. (1978). The formation and clay mineral reactions of melanoidins. *Geochim. Cosmochim. Acta*, 42: 69-76.

Hedges, J.I., Baldock, J.A., Gelin, Y., Lee, C., Peterson, M. & Wakeham, S.G., (2001). Evidence for non-selective preservation of organic matter in sinking marine particles. *Nature* 409, 801–804.

Herndl, G.J. & Reinthaler, T. (2013). Microbial control of the dark end of the biological pump. *Nat Geosci* 6:718–724.

Ichino, M. C. Clark, M.R., Drazen, J., Jamieson, A.J., Jones B., Martin, A., Rowden, A., Shank, T., Yancey & P., Ruhl, H. (2015). The distribution of benthic biomass in hadal trenches, a modelling approach to investigate the effect of vertical and lateral organic matter transport to the seafloor. *Deep-Sea Res. Part I Oceanogr. Res. Pap.*, 3, pp 1-49.

Itou, M., Matsumura, I. & Noriki, S. (2000). A large flux of particulate matter in the deep Japan Trench observed just after the 1994 Sanriku-Oki earthquake. *Deep-Sea Res. I* 47, 1987–1998.

Jahnke, R.A. & Jahnke, D.B. (2000). Rates of C, N, P and Si recycling and denitrification at the US Mid-Atlantic continental slope depocenter. *Deep-Sea Research I* 47, 1405–1428.

Jahnke, R.A., Reimers, C.E. & Craven, D.B. (1990). Organic matter recycling at the seafloor: Intensification near ocean margins. *Nature* 348, 50–54.

Jamieson, A. (2015). *The Hadal Zone: Life in the Deepest Ocean*. Cambridge University Press, United Kingdom.

Jamieson, A.J., Fujii, T., Mayor, D.J., Solan, M. & Priede, I.G. (2010). Hadal trenches: the ecology of the deepest places on Earth. *Trends Ecol. Evol.*, 25, pp.190-197

Lallemant, S. E., Collot, J. Y., Pelletier, B., Rangin, C., & Cadet, J. P. (1990). Impact of oceanic asperities on the tectogenesis of modern convergent margins. *Oceanologica Acta*, 10, 17–30.

Lallemant, S. E., Malavieille, J., & Calassou, S. (1992). Effects of oceanic ridge subduction on accretionary wedges: Experimental modelling and marine observation. *Tectonics*, 11, 1301–1313.

Leduc, D., Rowden A.A., Glud R.N., Wenzhofer F., Kitazato H. & Clark M.R. (2016b) Comparison between infaunal communities of the deep floor and edge of the Tonga Trench: Possible effects of differences in organic matter supply. *Deep-Sea Res Part I-Oceanogr Res Pap* 116:264–275.

Lee, C. & Cronin, C. (1984). Particulate amino acids in the sea: effects of primary productivity and biological decomposition. *J. Mar. Res.* 42, 1075-1097.

- Lee, C., Wakeham, S., & Arnosti, C., (2004). Particulate organic matter in the sea: the composition conundrum. *Ambio* 33, 565–575.
- Liu, R., Wang, L., Wei, Y., and Fang, J., (2017). The hadal biosphere: recent insights and new directions. *Deep-Sea Res Part II*.
- Liu, R., Wang, L., Liu, Q., Wang, Z., Li, Z., Fang, J., Zhang L. & Luo, M. (2018). Depth-resolved distribution of particle-attached and free-living bacterial communities in the water column of the New Britain Trench. *Frontiers in Microbiology*, 9.
- Lovenduski, N.S., Gruber N. & Doney S.C. (2008). Toward a mechanistic understanding of the decadal trends in the Southern Ocean carbon sink. *Glob. Biogeochem. Cycles* 22, GB3016.
- Lutz, M.J., Caldeira, K., Dunbar, R.B. & Behrenfeld, M.J. (2007). Seasonal rhythms of net primary production and particulate organic carbon flux to depth describe the efficiency of biological pump in the global ocean. *Journal of Geophysical Research: Oceans*, 112, C10.
- McCune B. & Grace J.B. (2002). *Analysis of ecological communities*. MjM Software Design, Gleneden Beach, Orlando.
- McKenzie, D., & Parker, R. L. (1967). The north pacific: an example of tectonics on a sphere. *Nature*, 216, 1276- 1280.
- Menzies, R. J. (1963a). General results of biological investigations on the deep sea fauna made on the U.S.N.S. Eltanin (U.S.A.R.P.) during Cruise 3 between Panama and Valparaiso, Chile in 1962. *Int. Revue ges. Hydrobiol. Hydrogr.*, 48 (2), 185-200.
- Menzies, R.J., Ewing, M., Worzel, J.L. & Clarke, A.H. (1959). Ecology of the Recent Monoplacophora. *Internationale Revue der gesamten Hydrobiologie und Hydrographie*, 48(4), 529–545.
- Menzies, R.J., George R. Y. & Rowe, G.T. (1973). *Abyssal Environment and Ecology of the World Ocean*. New York: John Wiley and Sons.
- Menzies, R.J. & George, R.Y. (1967). A re-evaluation of the concept of hadal or ultra- abyssal fauna. *Deep Sea Res. Oceanogr. Abstr.* 14, 703–723.
- Meyers, P.A. (1997). Organic geochemical proxies of paleoceanographic, paleolimnological, paleoclimatic processes. *Org. Geochem.* 27, 213-250.
- Miquel, J.-C., S. W. Fowler, J. La Rosa & P. Buat-Menard. (1994). Dynamics of the downward flux of particles and carbon in the open northwestern Mediterranean Sea. *Deep-Sea Res. I*, 41, 243-261.
- Morgan, W. J. (1968). Rises, trenches, great faults, and crustal blocks. *Journal of Geophysics Research*, 73, 8275-8291.

Nunoura, T., Takaki, Y., Hirai, M., Shimamura, S., Makabe, A., Koide, O., Kikuchi, T., Miyazaki, J., Koba, K., Yoshida, N., Sunamura, M., & Takai, K. (2015). Hadal biosphere: insight into the microbial ecosystem in the deepest ocean on Earth *Proc. Natl. Acad. Sci.*, 112 (11) pp. E1230-E1236.

Nunoura, T., Hirai, M., Yoshida-Takashima, Y., Nishizawa, M., Kawagucci, S., Yokokawa, T., Miyazaki, J., Koide, O., Makita, H., Takaki, Y., Sunamura, M., & Takai, K. (2016). Distribution and niche separation of planktonic microbial communities in the water columns from the surface to the hadal waters of the Japan trench under the eutrophic ocean *Front. Microbiol.*, 7:1261.

Oguri, K., Kawamura, K., Sakaguchi, A., Toyofuku, T., Kasaya, T., Murayama, M., Fujikura, K., Glud, R.N & Kitazato, H. (2013) Hadal disturbance in the Japan Trench induced by the 2011 Tohoku-Oki Earthquake *Science Reports*, 3.

Pantoja, S., Lee, C. (1999a). Molecular weight distribution of protein in Long Island Sound sediments. *Limnology and Oceanography* 44, 1323–1330.

Parrish, C. C. (2018). Nutritional and biomarker lipids in marine food webs. *Lipids in the ocean: structure, function, ecological role and applications*. Nov. 2018, Brest France.

Peoples, L.M., Donaldson, S., Osuntokun, O., Xia, Q., Nelson, A., Blanton, J., Allen, E.E., Church, M. J. & Bartlett, D.H. (2018). Vertically distinct microbial communities in the Mariana and Kermadec trenches. *PLoS One*. 2018;13:0195102.

Perrone, F. M., Della Croce, N. & Dell'anno, A. (2003). Biochemical composition and trophic strategies of the amphipod *Eurythenes gryllus* at hadal depths (Atacama trench, South Pacific). *Chemistry and Ecology*, 19, pp. 441-449.

Rathburn, A.E., Levin, L.A., Tryon, M., Gieskes, J.M., Martin, J.B., Pérez, M.E., Fodrie, F.J., Neira, C., Fryer, G.J., Mendoza, G., McMillan, P.A., Kluesner, J., Adamic, J. & Ziebis, W. (2009). Geological and biological heterogeneity of the Aleutian margin (1965–4822m). *Prog. Oceanogr.* 80, 22–50.

Rontani, J.-F., Zabeti, N. & Wakeham, S.G., (2011). Degradation of particulate organic matter in the equatorial Pacific Ocean: biotic or abiotic? *Limnol. Oceanogr.* 56, 333–349.

Romankevich, E.A. (1984). *Geochemistry of Organic Matter in the Ocean*. Springer, Heidelberg, 334 pp.

Salot, A., Laureillard, J., Scribeand, P. & Sicre, M.A. (1991). Evolutionary trends in the lipid biomarker approach for investigating the biogeochemistry of organic matter in the marine environment. *Marine Chemistry*, 36, 233-248.

Schippers, P., Vermaat, J.E., de Klein, J. & Mooij, W.M. (2004). The effect of atmospheric carbon dioxide elevation on plant growth in freshwater ecosystems. *Ecosystems*, 7, 63–74.

Schlunz, B., R. R. Schneider, P. J. Muller, W. J. Showers, & G. Wefer (1999). Terrestrial organic carbon accumulation on the Amazon deep sea fan during the last glacial sea level low stand. *Chem. Geol.*, 159, 263–281.

Sievers, H. A., Ceradini, S., Petrillo, M., Danovaro, R., Della Croce, N. (1999). A note on the thermal structure in South Eastern Pacific waters off Antofagasta, Chile. *Atacama Trench International Expedition (ATIE), Second Report*, University of Genoa Press, Genoa, Italy, p. 83.

Smith, K.J., Ruhl H., Bett B., Billett D., Lampitt R., Kaufmann, R. (2009). Climate, carbon cycling, and deep-ocean ecosystems. *Proc. Natl. Acad. Sci. USA* 106: 19211–18.

Stern, R.J. (2002). Subduction zones, *Reviews of Geophysics*, 40(4), 1012.

Stockton, W.L. & Delaca, T.E. (1982). Food falls in the deep sea: occurrence, quality, and significance. *Deep-Sea Res.* 29 (2A), 157–169.

Suess, E. (1980). Particulate organic carbon flux in the oceans?— surface productivity and oxygen utilization. *Nature* 288, 260-263.

Tamburini, C., Boutrif, M., Garel, M., Colwell, R.R. & Deming, J.W. (2013). Prokaryotic responses to hydrostatic pressure in the ocean – a review. *Environ. Microbiol.* 15(5), 1262-1274.

Tietjen, J.H., Deming, J.W., Rowe, G.T., Macko, S. & Wilke, R.J. (1989). Meiobenthos of the Hatteras abyssal-plain and Puerto-Rico trench - abundance, biomass and association with bacteria and particulate fluxes. *Deep-Sea Res. Part A* 36 (10), 1567-1577.

Tortell, P.D., Rau, G.H. & Morel, F.M. (2000). Inorganic carbon acquisition in coastal Pacific phytoplankton communities. *Limnol. Oceanogr.*, 45, 1485–1500.

Turnewitsch, R. Falahat, S., Stehlikova, J., Oguri, K., Glud, R.N., Middelboe, M., Kitazato, H., Wenzhöfer, F., Ando, K., Fujio, S., Yanagimoto, D. (2014). Recent sediment dynamics in hadal trenches: evidence for the influence of higher-frequency (tidal, near-inertial) fluid dynamics. *Deep-Sea Research I* 90, 125-138.

Urrère, M.A. & Knauer, G.A. (1981). Zooplankton fecal pellet fluxes and vertical transport of particulate organic material in the pelagic environment. *Journal of Plankton Research*, 3, pp.369-387.

Van Mooy, B. & Fredricks. H. F. (2010). "Bacterial and eukaryotic intact polar lipids in the eastern subtropical South Pacific: water-column distribution, planktonic sources, and fatty acid composition." *Geochimica et Cosmochimica Acta* 74.22: 6499-6516.

Vigny, C., Rudloff A., Ruegg, J.C., Madariaga, R., Campos, J. & Álvarez, M. (2009). Upper plate deformation measured by GPS in the Coquimbo Gap, Chile. *Phys. Earth Planet. In.*, 175(1–2), 86-95.

Vinogradova, N.G. (1979). The geographical distribution of the abyssal and hadal (ultra-abyssal) fauna in relation to the vertical zonation of the ocean. *Sarsia* 64, 41–49.

Wakeham S. G. & Canuel E. A. (1988) Organic geochemistry of particulate matter in the eastern tropical North Pacific Ocean: implications for particle dynamics. *J. Mar. Res.* 46, 183–213.

Wakeham, S.G., Hedges, J.I., Lee, C., Peterson, M.L. & Hernes, P.J., (1997a). Compositions and transport of lipid biomarkers through the water column and surficial sediments of the equatorial Pacific Ocean. *Deep-Sea Research II* 44, 2131–2162.

Wakeham, S. G., & Lee, C. (1989). Organic geochemistry of particulate matter in the ocean: The role of particles in oceanic sedimentary cycles. *Organic Geochemistry*, 14(I), 83–96.

Wakeham, S.G., Lee, C., Hedges, J.I., Hernes, P.J., Peterson, M.L., (1997b). Molecular indicators of diagenetic status in marine organic matter. *Geochimica Cosmochimica Acta* 61, 5363–5369.

Wakeham, S.G., Lee, C., Farrington, J.W. & Gagosian, R.B. (1984). Biogeochemistry of particulate organic matter in the oceans: results from sediment trap experiments. *Deep-Sea Research A*, 31, 509–528.

Watling, L., Guinotte J.M., Clark M. & Smith C. (2013). A proposed biogeography of the deep ocean floor. *Progress in Oceanography* 111: 91–112.

Wenzhöfer, F., Oguri, K., Middelboe, M., Turnewitsch, R., Toyofuku, T., Kitazato, H. & Glud, R.N. (2016). Benthic carbon mineralization in hadal trenches: assessment by in situ O₂ microprofile measurements. *Deep-Sea Res. I*, 116, pp.276-286.

Wolff, T. (1959). *La faune hadale ou faune des profondeurs supérieures à 6000-7000 mètres La Terre et la Vie*, Paris, 106.

Yunping, X., Huangmin, G. & Jiasong F. (2018). Biogeochemistry of Hadal Trenches: Recent developments and future perspectives. *Deep-Sea Research Part II: Topical Studies in Oceanography* (in press).

Zenkevich, L.A. (1969). Deep-Sea Bottom Fauna, Pleuston, in *The Pacific Ocean, the biology of the Pacific Ocean*, edited by V. G. Kort, vol. 7, part 2, 1-353.

Zenkevich, L. A., Filatova Z. A., Belyaev G. M., Lukyanova T. S., Suetova A. (1971). *Byull. Mosk. O. Ispyt. Prir.*, 76, 27-34.

Zeigler, J.M., Athearn, W.D. and Small, H. (1957). Profiles across the Peru–Chile Trench. *Deep-Sea Research*, 4, 238–249.